~~CONFIDENTIAL~~
~~RESTRICTED DATA~~
~~Atomic Energy Act - 1954~~

MASTER

SNPO-C

WANL-TNR-193

March, 1965

Record Copy

NOTICE
This report was prepared as an account of work sponsored by the United States Government. Neither the United States nor the United States Energy Research and Development Administration, nor any of their employees, nor any of their contractors, subcontractors, or their employees, makes any warranty, express or implied, or assumes any legal liability or responsibility for the accuracy, completeness or usefulness of any information, apparatus, product or process disclosed, or represents that its use would not infringe privately owned rights.

Classification cancelled [illegible]

by authority of

by [illegible] SEP [illegible]

Prepared By:

Test Engineering

Approved By:

J. B. McGuffin, Manager

Test Engineering, WANL

DISTRIBUTION OF THIS DOCUMENT IS UNLIMITED

Approved By:

W. H. Arnold, Manager

Test Systems And

Operations, WANL

NERVA Program

NRX-A2 Test

Final Report

(Title Unclassified)

NOTICE

PORTIONS OF THIS REPORT ARE ILLEGIBLE. It has been reproduced from the best available copy to permit the broadest possible availability.

~~CONFIDENTIAL~~
~~RESTRICTED DATA~~
~~Atomic Energy Act - 1954~~

~~CONFIDENTIAL~~
~~RESTRICTED DATA~~
~~Atomic Energy Act - 1954~~

Astronuclear

NRX-A2 TEST FINAL REPORT

TABLE OF CONTENTS

	Title	Page No.
1.0	SUMMARY	1-1
2.0	INTRODUCTION	2-1
	2.1 Background	2-1
	2.2 Test Objectives	2-2
	2.2.1 Major Objectives and Goals	2-2
	2.2.2 Specific Objectives	2-4
	2.3 Test Assembly, Disassembly and Facility Description	2-7
3.0	DESCRIPTION OF RUNS AND TEST HIGHLIGHTS	3-1
	3.1 Overall Sequence of Testing	3-1
	3.2 Summary of Pre-Power Tests	3-1
	3.2.1 Experimental Plan I-A - Initial Criticality	3-1
	3.2.2 Experimental Plan I-B - Flow Tests	3-2
	3.2.3 Experimental Plan II - Neutronics Calibration	3-5
	3.2.4 Experimental Plan III - Scaled-Down Power Test	3-5
	3.3 Summary of Experimental Plan IV - Power Test	3-6
	3.4 Summary of Experimental Plan V - Low Flow-Low Power Mapping	3-10
4.0	TEST RESULTS AND DISCUSSION	4.1-1
	4.1 Thermal and Fluid Flow Performance	4.1-2
	4.1.1 General	4.1-2
	4.1.2 EP-IV Test Description and Chronology	4.1-11
	4.1.3 Prechill	4.1-19
	4.1.4 High Power Holds	4.1-30
	4.1.5 EP-IV Startup and Shutdown	4.1-91
	4.1.6 EP-IV Cooldown	4.1-112
	4.1.7 Experimental Plan V - Low Power Mapping Test	4.1-117

~~CONFIDENTIAL~~
~~RESTRICTED DATA~~
~~Atomic Energy Act - 1954~~

CONFIDENTIAL
RESTRICTED DATA
Atomic Energy Act - 1954

TABLE OF CONTENTS (Cont)

	Title	Page No.
4.2	Fuel and Other Material Behavior	4.2-1
4.2.1	General	4.2-1
4.2.2	Surface Corrosion	4.2-3
4.2.3	Bore Corrosion (Pinholing, Channel Examinations)	4.2-25
4.2.4	Weight Changes in NRX-A2 Fuel Elements	4.2-28
4.2.5	Dimensional Change in NRX-A2 Fuel Elements	4.2-31
4.2.6	Incremental Electrical Resistance Changes	4.2-32
4.2.7	Special Element Behavior	4.2-33
4.2.8	Deposits	4.2-40
4.2.9	Non-Fuel Reactor Materials	4.2-43
4.3	Mechanical Evaluation	4.3-1
4.3.1	General	4.3-1
4.3.2	Analysis of Data	4.3-2
4.3.3	Analysis of Component Damage	4.3-45
4.4	Nuclear Analysis	4.4-1
4.4.1	General	4.4-1
4.4.2	Criticality and Control Drum Calibrations	4.4-1
4.4.3	Reactivity Effects	4.4-7
4.4.4	Power Distribution	4.4-19
4.4.5	Radiation Heating	4.4-21
4.4.6	Radiation Environment	4.4-23
4.5	Instrumentation, Control, and Data System Performance	4.5-1
4.5.1	Temperature Measurements	4.5-4
4.5.2	Pressure Measurements	4.5-15
4.5.3	Strain Measurements	4.5-16
4.5.4	Nuclear Heating Measurements	4.5-17
4.5.5	Control System Performance During EP-4	4.5-19
4.5.6	Data System Performance	4.5-21A
5.0	CONCLUSIONS	5-1
6.0	APPENDIX	6-1
6.1	Bibliography	6.1-1

CONFIDENTIAL
RESTRICTED DATA
Atomic Energy Act - 1954

TABLE OF CONTENTS (Cont)

	Title	Page No.
6.2	Post Operative Examination Summary Tables	6.2-1
6.3	Pre-Operational Preparation and Special Tests	6.3-1
	6.3.1 NRX-A2 Assembly and Pre-Test Operations	6.3-1
	6.3.2 NRX-A2 Vibration Tests	6.3-10

LIST OF ILLUSTRATIONS

Figure No.	Title	Page No.
2.3-1	Schematic - Flow Diagram Test Cell "A"	2-8
3.2-1	EP-IB Planned and Actual Flow Profiles - Ambient Gas	3-3
3.2-2	EP-IB Planned and Actual Flow Profiles - Liquid Hydrogen	3-4
3.3-1	EP-IV Planned and Actual Flow Profiles	3-9
3.4-1	EP-V Planned and Actual Power vs Flow	3-14
3.4-2	EP-V Low Flow-Low Power Map	3-15
4.1-0	Cycle Design Point Conditions	4.1-4
4.1-1	Power, Flow, and Temperature EP-IV	4.1-15
4.1-2	Typical Core Temperatures vs Time (Prechill)	4.1-22
4.1-3	Core Inlet and Dome End Temperatures vs Azimuthal Position at End of Prechill (CRT 13693)	4.1-23
4.1-4	Reflector Inlet and Outlet Temperature vs Azimuth at End of Prechill (CRT 13693)	4.1-24
4.1-5	NRX-A2 EP-IV Control Drum, Vane, and Sector Temperatures at End of Prechill (CRT 13693)	4.1-26
4.1-6	NRX-A2 EP-IV Inner Reflector Material and Seal Chamber Temperatures at End of Prechill (CRT 13693)	4.1-27
4.1-7	NRX-A2 EP-IV Prechill and Startup Typical Reflector Inlet and Outlet Temperature Time Histories	4.1-29

LIST OF ILLUSTRATIONS (Cont)

Figure No.	Title	Page No.
4.1-8	NRX-A2 EP-IV Core Material Temperature Histories	4.1-43
4.1-9	NRX-A2 Thermal Capsule Data Preliminary 18 Radial Positions in Core Central Region	4.1-45
4.1-10	NRX-A2 Thermal Capsule Data Preliminary 7 Radial Positions in Core Periphery	4.1-46
4.1-11	Radial Plot of Station 45 Thermal Capsule Readings	4.1-47
4.1-12	NRX-A2 Core Periphery Filler Strip Temperature Thermal Capsule Test Data	4.1-48
4.1-13	Axial Temperature Profile in Average Fueled and Unfueled Element CRT 13790 (581 MW)	4.1-51
4.1-14	Axial Temperature Profile in Average Fueled and Unfueled Element CRT 13900 (953 MW)	4.1-52
4.1-15	Axial Temperature Profile in Average Fueled and Unfueled Element CRT 13985 (1051 MW)	4.1-53
4.1-16	Axial Temperature Profile in Average Fueled and Unfueled Element CRT 14085 (1110 MW)	4.1-54
4.1-17	NRX-A2 EP-IV Calculated and Measured Radial Temperature Profile CRT 13900 (953 MW)	4.1-56
4.1-18	Comparison of NRX-A2 Thermal Capsule Results with Post Run Calculations at High Power Hold Station 45	4.1-57
4.1-19	Tie Rod Exit Gas Temperature Profile EP-IV	4.1-60
4.1-20	Reflector System Fluid Temperatures and Pressures for NRX-A2 EP-IV at CRT 14085	4.1-69

LIST OF ILLUSTRATIONS (Cont)

Figure No.	Title	Page No.
4.1-21	Temperatures, Flows, and Radiation Heating Rates in Shield and Support Plate at CRT 14085 (1110 MW)	4.1-70
4.1-22	NRX-A2 EP-IV Inner Reflector Temperatures at CRT 14085	4.1-71
4.1-23	Outer Reflector Sector Material Temperature vs Axial Position	4.1-78
4.1-24	Azimuthal Sector Temperature Variation in NRX-A2 EP-IV at CRT 14085	4.1-80
4.1-25	Control Drum and Boral Vane Temperatures for NRX-A2 EP-IV	4.1-82
4.1-26	Calculated and Measured Temperatures of Inner Reflector Material	4.1-83
4.1-27	Comparison of Measured and Calculated Inner Reflector Temperature	4.1-86
4.1-28	NRX-A2 EP-IV Lateral Support Hydrogen and Material Temperatures (Measured and Calculated)	4.1-88
4.1-29	Comparison of Measured and Predicted Seal Chamber Pressure Distribution	4.1-89
4.1-30	Startup LH_2 Flow Log	4.1-92
4.1-31	NRX-A2 EP-IV Startup Power and Nozzle Chamber Temperature	4.1-93
4.1-32	Core Material Temperatures and Tie Rod Exit Temperatures During Startup	4.1-95
4.1-33	Core Inlet Pressure and Core ΔP vs Time	4.1-98

LIST OF ILLUSTRATIONS (Cont)

Figure No.	Title	Page No.
4.1-34	NRX-A2 EP-IV Prechill and Startup Reflector Inlet, Outlet and Differential Pressure Time Histories	4.1-103
4.1-35	Pressure and Temperature to Illustrate Asymmetry at Reflector Inlet	4.1-100
4.1-36	Core Inlet Azimuthal Temperature Variation at CRT 13720 and 13780	4.1-101
4.1-37	NRX-A2 EP-IV Prechill and Startup Selected Inner Reflector and Control Drum Material Temperature Time Histories	4.1-105
4.1-38	NRX-A2 EP-IV Prechill and Startup Selected Outer Reflector Material Temperature-Time Histories	4.1-106
4.1-39	NRX-A2 Shutdown Nozzle Chamber Temperature	4.1-108
4.1-40	Comparison of the Shutdown Demands to Measured Parameters	4.1-109
4.1-41	Reactor Shutdown History	4.1-111
4.1-42	NRX-A2 Test Series: EP-IV Cooldown Predicted and Actual Coolant Flow Rates	4.1-113
4.1-43	NRX-A2 Test Series: EP-IV Cooldown Predicted and Actual Coolant Usage	4.1-114
4.1-44	Comparison Between Measured and Calculated Decay Power During Cooldown Following EP-IV	4.1-118
4.1-45	EP-V Low Power Mapping Test Low Power Performance Map	4.1-119
4.1-46	EP-V Low Power Mapping Test Power Flow, and Control Drum Position vs Time	4.1-121

LIST OF ILLUSTRATIONS (Cont)

Figure No.	Title	Page No.
4.1-47	EP-V Low Power Mapping Test: Fixed Control Drums, Power and Flow	4.1-132
4.1-48	EP-V Low Power Mapping Test: Fixed Control Drums, Nozzle Chamber and Tie Rod Temperatures	4.1-134
4.1-49	EP-V Low Power Mapping Test: Fixed Control Control Drums, Reactor Plenum Pressures	4.1-135
4.2-1	Tile Pattern Corrosion Bands on Peripheral Elements Located Between θ = 350° and 75°	4.2-5
4.2-2	Peripheral Element with NbC Coating on Peripheral Flats, 39-C7639, Position 6J8D	4.2-6
4.2-3	Liner Exposure Produced by Tile Pattern Corrosion at Station 51 on D Flat on Element 32-11765 Position 1J7J	4.2-8
4.2-4	Heavy Corrosion Effect Produced at Station 31 on the C and D Flats of Fuel Element 89-C8407 Position 4J6B Adjacent to a Station 32 Thermocouple Installation	4.2-10
4.2-5	Black Streaks on the C and D Flats Element 89-11877 Position 1J5G at Station 28	4.2-12
4.2-6	Corrosion Band at the Shoulder on Element with Very Little End Corrosion, Element 39-11671 Position 1J3U at A and F Flats	4.2-13
4.2-7	Corrosion Band at the Shoulder on Element 39-11864 Position 4J3U on D, E, and F Flats	4.2-14
4.2-8	Better Than Typical End Flats and Exit Face on Element 39-C7575 C/P 4J4N	4.2-16
4.2-9	Worse Than Typical Exit Face Conditions and Typical End Flat Condition on Element 79-11932 C/P 3J9B	4.2-17

LIST OF ILLUSTRATIONS (Cont)

Figure No.	Title	Page No.
4.2-10	Typical End Flat Conditions with Corrosion Band at the Shoulder on Element 99-07086 C/P 2A1G	4.2-18
4.2-11	Typical Exit Face Condition on Element 99-09313 C/P 4A1D	4.2-19
4.2-12	Worse Than Typical End Flat on Element 39-11681 C/P 6J3F	4.2-20
4.2-13	Comparison of the Coated End on Element 39-11629 C/P 1J9H Before and After Reactor Test	4.2-21
4.2-14	Comparison of the Coated End on Element 99-07100 C/P 1F1F Before and After Reactor Test	4.2-22
4.2-15	Pinholes on the "A" Flat on Element 99-07089 C/P 4E4E at Stations 45 to 48	4.2-27
4.2-16	View of Channels 8, 9, 10, 11, and 12 at Stations 47 to 49 on Element 99-07089, C/P 4E4E Showing Corrosion Pockets and Typical Pinhole Formation in the Channels and the Graphite Matrix	4.2-29
4.2-17	Comparison of Changes in Electrical Resistance Profiles of Elements from Same Run Tested in WANL H_2 Corrosion Facility and in NRX-A2	4.2-34
4.2-18	View of the Exit Face of a Recoated Element 32-11735 C/P 6J5L	4.2-38
4.2-19	Core Periphery Showing Elements with Tile Pattern Corrosion and White Deposit, θ = 315° - 75°	4.2-41
4.2-20	View of Shiny Pyro Carbon Deposits in Corroded Area of Element 39-07575, Core Position 4J4M, at Axial Station 44 to 45	4.2-42

LIST OF ILLUSTRATIONS (Cont)

Figure No.	Title	Page No.
4.3-1	Schematic of Strain Gage Transducers Measuring Core/Reflector Cylinder Gap Changes	4.3-3
4.3-2	Typical Signal Profiles of Core/Reflector Cylinder Gap Change and Related Parameters During NRX-A2 EP-IV Power Run	4.3-5
4.3-3	Predicted Average Decrease in Radial Gap Between Core and Inner Reflector at the Aft End	4.3-7
4.3-4	Calculated and Measured Change in Radial Gap Between Core and Inner Reflector	4.3-8
4.3-5	Calculated and Estimated Core Growths	4.3-13
4.3-6	Schematic of Core Periphery and Inner Inner Reflector Clearances at the Aft End	4.3-17
4.3-7	Free Body of Filler Strips When Gap Exists	4.3-18
4.3-8	Continuous Playback of Wide Band Data from Channels M 416, M 420, and M 424 During Shutdown of NRX-A2 EP-IV	4.3-20
4.3-9	Relative Radially Inward Plunger Pin Movement from Maximum Outward Position and Related Parameters During NRX-A2 EP-IV Shutdown	4.3-21
4.3-10	Location of Instrumented Tie Rods in Cluster J9, Sector 5, NRX-A2 Power Test	4.3-24
4.3-11	Typical Wide Band Playback of Control Drum Position and Torque During Shutdown of NRX-A2 EP-IV Power Run	4.3-29
4.3-12	Continuous Signal of 60 cps with Some 17.7 cps on Inner Reflector Spring Strain Gage	4.3-37

LIST OF ILLUSTRATIONS (Cont)

Figure No.	Title	Page No.
4.3-13	High Speed Playback (40"/sec) of Unreal Signal on Tie Rod Strain Gage	4.3-37
4.3-14	Nozzle Flange Accelerometer Drift, Seconds Prior to Initial Power Increase	4.3-38
4.3-15	Nozzle Flange (H151) and Feedline (H101) Accelerometers Displaying Unreal Signals at 3rd Power Hold	4.3-38
4.3-16	Forward Flange (H261) and Nozzle (H111) Accelerometer Signals at 3rd Power Hold	4.3-39
4.3-17	Forward Flange (H262) and Nozzle (H112) Accelerometer Signals at Cooldown	4.3-39
4.3-18	Inner Deflector Spring Strain Gage Output During Initial Power Ramp	4.3-40
4.3-19	Various Channel Outputs at Full Power Scram	4.3-40
4.3-20	Tie Rod Strain Signal Observed at Start of 2nd Power Hold	4.3-41
4.3-21	Nozzle Flange Accelerometer Signal Observed During Low Power Mapping of Restart Test	4.3-41
4.3-22	Nozzle Flange Accelerometer Signal Observed During Low Power Mapping of Restart Test	4.3-41
4.3-23	Various Pressure Profiles at Full Power Scram	4.3-42
4.3-24	NRX-A2 Barrel and Support Cone Showing Bent Tabs at Forward End of Barrel	4.3-46
4.3-25	Schematic of Core Support Structure	4.3-47
4.3-26	Exploded View of Cluster Retention Hardware, NRX-A2	4.3-50

LIST OF ILLUSTRATIONS (Cont)

Figure No.	Title	Page No.
4.3-27	Typical Cross Sections of Cluster Retention Hardware, NRX-A2	4.3-51
4.3-28	Tensile Crack in Element 4A1A	4.3-55
4.3-29	Tensile Crack in Element 4J5A	4.3-56
4.3-30	Location of Station 32 Thermocouples	4.3-57
4.3-31	Temperature Distribution in Cooled Unfueled Element	4.3-58
4.3-32	Schematic of Station 45 Thermocouple, NRX-A2	4.3-60
4.3-33	Sketch of Typical Tie Rod Exit Gas Thermocouple Installation, NRX-A2	4.3-62
4.3-34	Typical Buckled Tie Rod Exit Gas Thermocouple Probe, NRX-A2	4.3-64
4.4-1	NRX-A2 Fuel Loading Distribution	4.4-2
4.4-2	NRX-A2 EP-1A Integral and Differential Bank Worth	4.4-5
4.4-3	NRX-A2 EP-1A Control Drum Worth Uniformity	4.4-6
4.4-4	NRX-A2 Reactivity Equations	4.4-8
4.4-5	NRX-A2, EP-1B Drum Bank Rotation vs GH_2 Mass Flow Rate	4.4-10
4.4-6	NRX-A2, EP-II Measured Nuclear Average Temperature for Major Components	4.4-11
4.4-7	NRX-A2, EP-II Control Drum Bank Rotation During Temperature Coefficient Tests	4.4-12
4.4-8	NRX-A2 EP-IV Power, Flow, Chamber Temperature and Drum Position vs Time	4.4-14

LIST OF ILLUSTRATIONS (Cont)

Figure No.	Title	Page No.
4.4-9	NRX-A2 EP-IV Control Drum Bank Position During the High Power Test, Measured Calculated	4.4-15
4.4-10	NRX-A2 EP-V Low Power Mapping Test	4.4-17
4.4-11	NRX-A2 Operating Reactivity Map	4.4-18
4.4-12	Comparison of the Measured and Predicted Axial Power Distributions	4.4-20
4.4-13	Experimental and Calculated Gamma Ray Dose Rate (Rads-tissue/hr.-watt) as a Function of Distance from Reactor (Feet)	4.4-24
4.4-14	Experimental and Calculated Gamma Ray Dose Rate (Rads-Tissue/hr-watt) on the Meridian Ring as a Function of Reactor Polar Angle	4.4-25
4.4-15	NRX-A2 Region Description Showing Major Components	4.4-28
4.5-1	Pertentage of the Valid [illegible] During Each Phase of Testing	4.5-2
4.5-2	Thermocouple Calibration Curve - Station 32	4.5-9
4.5-3	Thermocouple Calibration Curve - Station 45	4.5-11
4.5-4	Indication of Temperature Peaking EP-IV	4.5-12
4.5-4A	Simplified Narrow Band Data Acquisition	4.5-22
4.5-5	Simplified Narrow Band Data Processing	4.5-25
4.5-6	Simplified Wide Band Data Acquisition	4.5-27
4.5-7	Simplified Wide Band Data Reduction	4.5-28
4.5-8	NRX-A2 Channel Anomaly Analysis	4.5-30
4.5-9	NRX-A2 Channel Anomaly Analysis - Parameters	4.5-32

LIST OF ILLUSTRATIONS (Cont)

Figure No.	Title	Page No.
6.3-1	NRX-A2 Test Assembly on Way to Test Cell "A"	6.3-8
6.3-2	NRX-A2 Vibration Test Excitation Point and Accelerometer Locations Plan View	6.3-13
6.3-3	NRX-A2 Vibration Test Excitation Points and Accelerometer Locations Elevation	6.3-14

LIST OF TABLES

Table No.	Title	Page No.
4.1-1	NRX-A2 EP-IV Chronology	4.1-12
4.1-2	Limits Established for NRX-A2 Operation	4.1-14
4.1-3	NRX-A2 Operating Conditions	4.1-18
4.1-4	Reactor Conditions at the End of Prechill (CRT 13690) Predicted and Measured	4.1-20
4.1-5	EP-IV High Power Test LH_2 Flow Rates and Nozzle Chamber Temperature	4.1-31
4.1-6	Details of Heat Balance Calculations, EP-IV	4.1-35
4.1-7	EP-IV Reactor Thermal Power at Steady-State Holds	4.1-36
4.1-8	Test Values and Post Test Calculations at Four Steady-State Holds	4.1-41
4.1-9	Maximum Fuel Temperatures at High Power Hold CRT 14085 (1096 MW)	4.1-59
4.1-10	Tie Rod Exit Gas Temperature Uncertainty Analysis, EP-IV Full Power Hold	4.1-62
4.1-11	Comparison of Experimental and Calculated Pressures and Differential Pressures in the Reflector System	4.1-74
4.1-12	Calculated Reflector Heating Rates from ΔH and Flow Rate and Comparison to Nuclear Heating Rates	4.1-76
4.1-13	NRX-A2 EP-IV Control Drum and Control Vane Temperatures	4.1-84
4.1-14	Comparison of Test and Post Test Calculated Nozzle Tube Pressures and Temperatures at Holds	4.1-65

LIST OF TABLES (Cont)

Table No.	Title	Page No.
4.1-15	Comparison of KIWI-B4E and NRX-A2 Cooldown Data	4.1-116
4.1-16	NRX-A2 EP-V Low Power Mapping: Steady-State Test Data	4.1-124
4.1-17	EP-V Low Power Mapping Test Comparison Between TNT Predictions and Test Data	4.1-129
4.2-1	Characteristics of High Performance Recoated Elements	4.2-35
4.3-1	Radial Change in Gap Between Core and Reflector Cylinder During NRX-A2 EP-IV Power Run Holds	4.3-10
4.3-2	Estimated Radial Core Growths During NRX-A2 EP-IV Power Run Holds	4.3-12
4.3-3	Estimated Displacement of Core Center, EP-IV Power Run	4.3-15
4.3-4	Measured and Computed Tie Rod Loading NRX-A2 EP-V Power Run	4.3-25
4.3-5	Tie Rod Load Distribution in Cluster - J9, Sector 5	4.3-27
4.3-6	Dynamic Measurements and Comments for NRX-A2 Run EP-IB	4.3-30
4.3-7	Dynamic Measurements and Comments for NRX-A2 Run EP-IV	4.3-32
4.3-8	Dynamic Measurements and Comments for NRX-A2 EP-V	4.3-35

LIST OF TABLES (Cont)

Table No.	Title	Page No.
4.4-1	NRX-A2 Reactor Characteristics	4.4-3
4.4-2	Comparison of Measured and Calculated Heating in NRX-A2 Reflector Expressed as a Per Cent of Reactor Total Power (NRX-A2, EP-IV, Power Run)	4.4-22
4.4-3	NRX-A2 Major Component Neutron and Gamma Radiation Exposure as a Result of EP-IV-A and EP-V	4.4-27
6.2-1	Sensors with Questionable Design Performance	6.2-2
6.2-2	Post-Operative Examination Summary, Outer Reflector Assembly, Dome End, and Core Support Components	6.2-10
6.2-3	Post-Operative Examination Summary, Non-Nuclear Hardware	6.2-11
6.2-4	Post-Operative Examination Summary, Core Region Components	6.2-13

1.0 SUMMARY

The NRX-A2 test was the first integral reactor in the NRX-A series in which nuclear power generation and radiation environment were major factors. All of the NRX-A reactors are based on KIWI-B-4 design and are part of the ground testing and development of the nuclear reactor to be used in the NERVA engine. At design power, 1120 MW are generated, with the hydrogen entering the nozzle chamber at a mixed mean temperature of 4090°R and 560 psia at the design flow of 71.3 lb/sec.

On the basis of a critical review and analysis of the NRX-A2 test data and observations, it is concluded that the test was successful in meeting its objectives as well as confirming the nuclear, thermal, flow, and mechanical design analysis methods. The reactor operated at sufficient power levels and duration to demonstrate mechanical and thermal performance.

The NRX-A2 series consisted of several Experimental Plans (EP's), each one consisting of a test or group of tests closely related to each other. The tests conducted from August 12 to October 15, 1964, on NRX-A2 were grouped as follows:

Pre-Power Tests

EP-IA - Initial Criticality	(August 12)
EP-IB - Flow Tests	(September 4)
EP-II - Neutronics Calibration	(September 16)
EP-III - Scaled Down Power Test	(September 18)

EP-IV - Power Test (September 24)

EP-V - Low Flow-Low Power Mapping (October 15)

The design adequacy of the reactor assembly for the test conditions was ascertained during the following analyses and inspections:

1. Preliminary analysis of data and visual observation of the reactor and films during and between testing.
2. Detailed post-test data analysis and interpretation.
3. Systematic, thorough post-operative examination of all reactor assembly components and subassemblies.

The information obtained from the NRX-A1 test and the modifications resulting from that test all contributed to the success of NRX-A2*. These items included:

1. Increased clearance between the control drum and outer reflector sector.
2. Design changes in the nozzle end spigot of the outer reflector sector.
3. Increased clearance between the pressure vessel and nozzle end support ring.

---

*NRX-A1 Test Final Report, WANL-TNR-176, September, 1964 - CRD.

4. Flow profile modification for the power test because of identification of flow lag.

During the high power test, an average of 813 MW was produced during a 7 minute period. At the 40 second maximum power hold, the following conditions existed:

Total Thermal Power	1096 ±50 MW
Coolant Flow	75.6 ±1.5 lb/sec
Nozzle Chamber Temperature	3815 ±215°R
Maximum Measured Fuel Temperature	4400 ±180°R

The most accurate estimate of the power level is believed to be that based on a calculated nozzle chamber temperature and reactor enthalpy balance using observed nozzle constants, nozzle chamber pressure, and flow rate in the calculations. This method is preferred to the direct measurement since it is reasonably certain that the nozzle chamber thermocouples were not measuring the mixed mean chamber temperature.

A post-test calculation of the reactor operating conditions using actual power and flow profiles was performed with the TNT code and the reactor model used for pre-test predictions. Comparison of this calculation to the test data demonstrates the general adequacy of the TNT transient startup representation and pointed the way to necessary modifications to the model in several regions to allow it to predict more closely operating parameters at steady state.

The duration of the run and power level presented an opportunity to observe the fuel element behavior under realistic conditions approaching an endurance test, permitting extrapolation to NRX-A3 conditions. The general fuel behavior and weight losses observed were as expected, based on out of reactor corrosion tests and KIWI experience. The fuel manufacturing process and element design therefore were demonstrated as adequate for the conditions of the NRX-A2 test.

The most serious corrosion problem occurred along the fuel element flats at the core periphery towards the hot end of the core. This corrosion was the result of hydrogen leaking in through filler strips and pyro-tiles, and contacting fuel at elevated temperature producing a characteristic striated pattern on the flats. In the few points where NbC coating was present on the periphery, corrosion was largely inhibited. It was decided, therefore, to coat the periphery of the NRX-A3 core with NbC. In addition, the periphery fuel will be kept cooler by increased flow of coolant using appropriate orificing.

Also related to the power level were anomalies observed for station 32 core material thermocouples, which were used for control. These thermocouples generally were indicating temperatures below that of the actual fuel (as confirmed by thermal capsule data) because of failure of the potting compound used. This failure, which was confirmed in the post-operational examination, permitted flow of cool gas around the thermocouple and explains the low temperature indication.

In NRX-A3, it is planned to use station 26 thermocouples for power control. In addition to running cooler, these thermocouples will use a redesigned installation not requiring potting compound and utilizing multiple graphite blocks in the channel for flow blockage. For the nozzle chamber temperatures mentioned earlier, one thermocouple will be inserted deeper into the flow stream to see if the probability of obtaining a mixed mean temperature can be improved.

In the area of mechanical design evaluation, the following results and conclusions were obtained:

1. Structural performance of NRX-A2 reactor was excellent.
2. Measured tie rod loads agreed reasonably well with predictions.
3. Absence of high vibration levels of the reactor or its components was noted.
4. Specification of larger clearance for plunger pins in the inner reflector cylinder to eliminate sticking was necessary.
5. Redesign of tie rod coolant gas thermocouple probes to prevent buckling was necessary.

The possible buckling of the tie rod coolant gas thermocouples and contact with a hot solid surface appears to explain the high readings obtained on these sensors.

Turning from the high power test to the low power-low flow mapping tests, a number of important characteristics of the reactor were demonstrated. The mapping tests were run at constant power and at fixed drum position.

In the constant power runs (3.4% of design), stability was demonstrated for the flow range of 8.3 to 13.5 lb/sec on Dewar pressure. During these runs, a maximum positive reactivity feedback condition of $0.43 was produced. At this reactivity feedback condition, two phases of coolant were present at the core inlet, without instability. On the basis of these results, the core inlet temperature limitation of 90°R can be modified and replaced by a more general reactivity criterion. This change increases the area of permissible reactor operation and simplifies the control requirements.

During the fixed control drum position runs, stable operation was demonstrated in the flow range of 5.2 to 13.5 lb/sec. The corresponding power range was 2 to 4.7% of design power. These fixed control drum position runs demonstrated operation with little or no reactivity feedback compensation. The successful attainment of the effective and timely future planning of NRX, NRX/EST, and NERVA engine testing.

The NRX-A2 power test has thus provided a sound basis and increased confidence for proceeding to the more stringent endurance and transient testing in NRX-A3.

2.0 INTRODUCTION

2.1 BACKGROUND

The NRX-A program is conceived as a series of evolving nuclear rocket reactor designs, with the evolution of the design based on analytical results, component test results, and integral reactor test results. Tested in the NRX-A program are integral reactors equivalent to those to be used eventually in the NERVA engine.

The NRX-A1 reactor contained an unfueled core mechanically equivalent to the nuclear power reactors to be tested. The major objectives of the NRX-A1 series were accomplished. These tests confirmed the dynamic stability of the core and the adequacy of the components under cold flow test conditions.* The information obtained from the NRX-A1 tests provided a sound basis for proceeding to NRX-A2, the first of the nuclear power tests in this series.

The NRX-A2 was the logical next step in the NRX-A series. In NRX-A2 power generation and radiation environment were the major factors introduced to the test program. The flow path was identical to the NRX-A1 test. This path consisted of coolant entering the plenum beneath the outer reflector from the nozzle tubes, continuing up the outer reflector housing the control drums, then through the simulated

---

* NRX-A1 Test, Final Report, WANL-TNR-176, September, 1964, CRD.

shield, turning, passing through the fueled core, and discharging out the nozzle. Parallel flow paths cool the pressure vessel, dome, graphite reflector cylinder, lateral support parts, and the aluminum barrel surrounding the graphite reflector. A more detailed description of the NRX-A2 reactor as well as the test facilities are given in a test specification and test plan.*

The design power of NRX-A2 is 1120 MW with a mixed mean reactor coolant exit temperature of 4090°R. The design flow rate of hydrogen is 71.3 lb/sec with a design nozzle chamber pressure of 560 psia. The design conditions result in a vacuum specific impulse of 760 sec.

In addition to making similar evaluations as in NRX-A1 of the mechanical stability and adequacy of components, NRX-A2 provided the initial opportunity in the NRX-A program of evaluating the integrity of the nuclear fuel elements and the nuclear design of the core.

2.2 TEST OBJECTIVES

2.2.1 Major Objectives and Goals

The major objectives of the NRX-A2 power test were:

1 To provide significant information for verifying the steady-state design analysis for power operation.

---

* NRX-A2 Test Specification, WANL-TNR-153, May, 1964, CRD.
NRX-A2 Test Plan, WANL-TNR-146, February, 1964, CRD.

2. To provide significant information which will aid in assessing the suitability of the reactor to operate at the steady-state power level and temperatures required for the reactor to be a component of an experimental engine system.

The information required to achieve the above objectives were obtained by measurements made during the test and post-operative examinations. Post-operative examination of the reactor is an essential feature of the test and yields information which cannot be obtained in any other way. Since uncontrolled damage to the reactor may obscure the interpretation of the post-operative data, the test conditions imposed on the NRX-A2 reactor were set and controlled to develop the required information with a minimum risk to the integrity of the reactor.

To achieve the major objectives of the NRX-A2 power test, two major power operating goals were established. The first and principal goal of the NRX-A2 test was to operate the reactor at steady-state power and temperature levels pre-selected on the basis that these will provide significant data for verifying the design analysis, while at the same time providing a high probability of reactor survival. The secondary goal of the NRX-A2 test was to operate the reactor at as high a steady-state power and temperature level that pre-test analyses and test data indicate will not compromise the

structural integrity of the reactor. The second goal depended on the evaluation of the test data accumulated during the initial power operation. The test conditions ultimately selected for the NRX-A2 test were consistent with the latest information available from prior full-scale tests and the concurrent component test and analytical programs.

For the low-power, low-flow test the major objectives were to demonstrate stable operation in the region of interest at transient startup and cooldown with liquid hydrogen.

2.2.2 Specific Objectives

The objectives for the power test were categorized by two levels to clarify their relative importance. Level one meant top priority for achievement during NRX-A2, while the second level indicates that the accomplishment of this objective is less urgent. These objectives are listed in Table 2.2-1.

TABLE 2.2-1

NRX-A2 POWER TEST OBJECTIVES

LEVEL I - IMPORTANCE CATEGORY

1. To evaluate the effects of the environmental conditions on the structural integrity of the test assembly and its components.
2. To evaluate the performance of the core assembly.
3. To evaluate the performance of the lateral support and seal system.
4. To evaluate the performance of the core axial support system.
5. To evaluate the performance of the outer reflector assembly.
6. To evaluate the performance of the control drum and actuation system.
7. To evaluate the overall reactivity characteristics.

LEVEL II - IMPORTANCE CATEGORY

1. To evaluate the performance of the nozzle assembly.
2. To evaluate the performance of the pressure vessel assembly.
3. To evaluate the performance of the shield assembly design.
4. To evaluate the performance of the test assembly instrumentation.
5. To evaluate the performance of the nucleonic power control system.
6. To evaluate the performance of the propellant feed and control systems.
7. To evaluate the performance of the nozzle chamber temperature control loop.
8. To evaluate the performance of the test car systems.

TABLE 2.2-1 (Cont'd)

9. To evaluate the radiological hazards associated with operation of the reactor.
10. To evaluate the thermal and nuclear environments surrounding the reactor.
11. To evaluate the performance of advanced NRX power control system components.
12. To evaluate the performance of a single range control system.
13. To evaluate transfer function of components and systems under various operating conditions.
14. To evaluate the performance of the in-core temperature control loop.
15. To evaluate the transient characteristics of the overall test systems.

For the low-power, low-flow test the following specific objectives were set for the test:

1. Demonstration of stability at low liquid H_2 flow using dewar pressure.
2. Demonstration of suitability at constant power with flow variation.
3. Demonstration of stability at fixed control drum position with flow variation and resulting power change.

4. Achievement of a reactivity feedback value associated with liquid hydrogen at the core entrance.

The test results in relation to the specific objectives are discussed in detail in Section 4.

2.3 TEST ASSEMBLY, DISASSEMBLY AND FACILITY DESCRIPTION

Detailed descriptions of the test assembly and test facilities appear in a number of documents and are not repeated here. However, a flow diagram for Test Cell "A" (Figure 2.3-1) is included for reference. The NRX-A2 hardware configuration tested was in accordance with WANL Drawing 936J446, NRX-A2 Test Assembly Parts List.

The following documents are suggested for detailed descriptions:

1. Test Assembly and Instrumentation - NRX-A2 Test Specification, WANL-TMR-153, May, 1964, CRD.
2. Test Facility - Safety Analysis Report-NRX Testing, WANL-TMR-148, April 27, 1964, CRD.
3. Test Car - NRX-A1 Test Specification, WANL-TMR-121, November, 1963, CRD.
4. Reactor Disassembly - NRX-A2 Post-Test Report, NTO-R-0018, February 5, 1965, CRD.

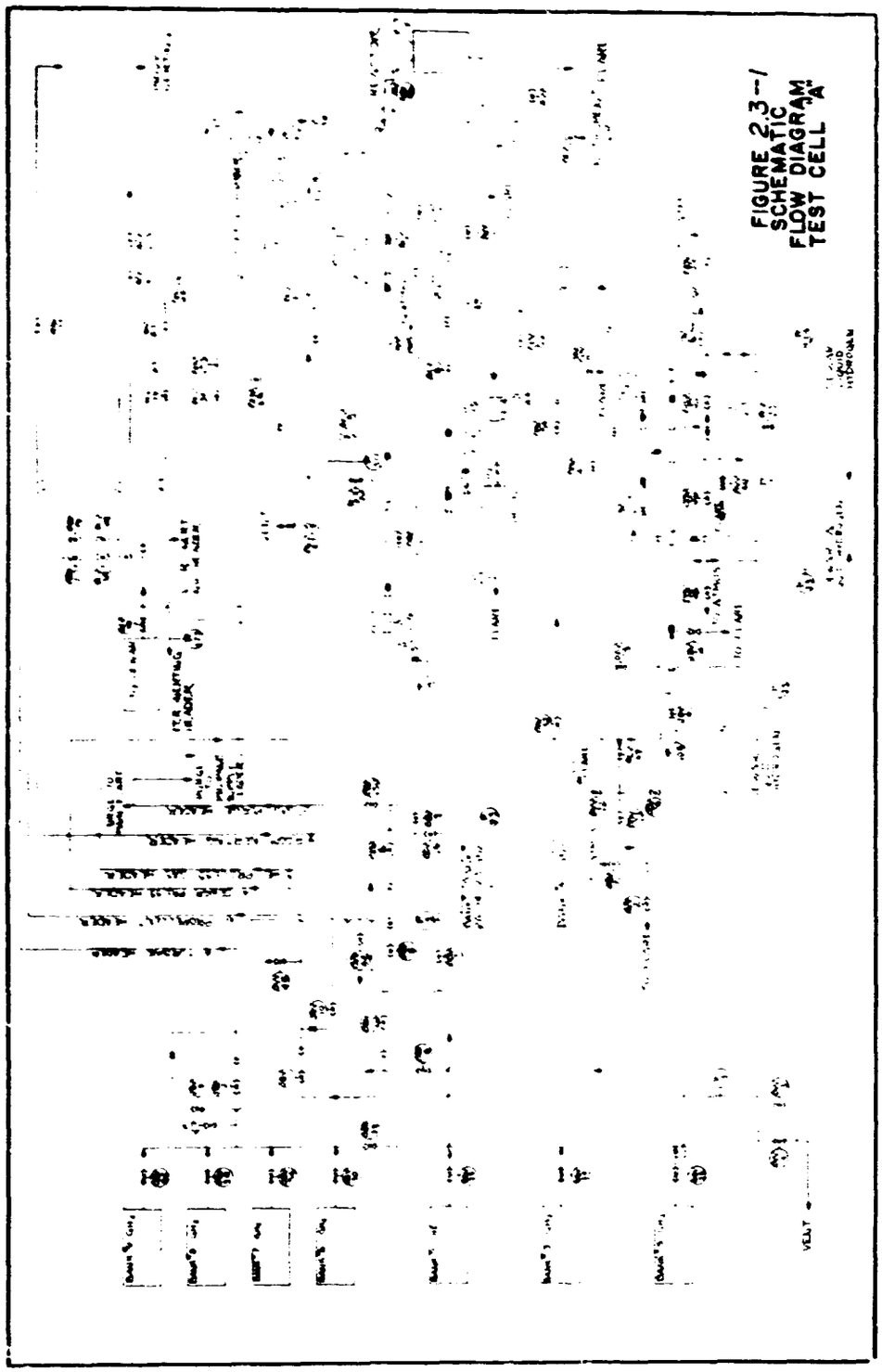

FIGURE 2.3-1
SCHEMATIC
FLOW DIAGRAM
TEST CELL "A"

3.0 DESCRIPTION OF RUNS AND TEST HIGHLIGHTS

3.1 OVERALL SEQUENCE OF TESTING

In order to accomplish the major objectives of the NRX-A2 test series, a series of six separate tests were planned. The first four were designed to verify basic reactor operational characteristics in preparation for the power test. The power test was the fifth in the series and was followed by a sixth test which explored the behavior of the reactor system in the low-power, low-flow region of its operating range. A more detailed description of the tests is given in a sit test report.*

3.2 SUMMARY OF PRE-POWER TESTS

3.2.1 Experimental Plan I-A - Initial Criticality

This Experimental Plan was completed on August 12, 1964. During central poison wire removal operations, data was obtained to permit determination of the control drum span and the shape of the control drum bank differential worth curve. Initial criticality was achieved with 336 wires remaining in the core. A preliminary power calibration and preliminary evaluation of the power control system were obtained. In addition, control drum #2 was calibrated. The reactor was operated at ambient temperature and at a maximum indicated log power level of 500 watts.

* NRX-A2 Site Test Report, NTO-R-0008, November 20, 1965, CRD.

3.2.2 Experimental Plan I-B - Flow Tests

This Experimental Plan, completed on September 1, 1964, included the initial automatic reactor startups. An ambient gaseous hydrogen flow test and two LH_2 startup flow tests were completed to verify the operability of the Test Assembly and Test Assembly Instrumentation, to obtain hydrogen reactivity worth data, and to verify the chilldown characteristics of the assembly. Operation in accordance with the planned profiles did not indicate any evidence of abnormalities. During this test, the reactor was operated at a maximum indicated power level of 1 KW with an indicated integrated power generation of 0.7 MW-sec.

The ambient GH_2 flow profile, Figure 3.2-1, was a programmed ramp to a maximum flow of 12 lb/sec, similar to those completed during NRX-A1 testing. Good agreement is shown between the planned and actual flow profiles. The slight difference shown was the result of a minor scaling error introduced to the programmers.

The LH_2 runs are compared to the planned on Figure 3.2-2. The higher than planned ramp rate and the initial delay appear to be the result of a one to two second lag between the ACW-3 program demand and the start of valve motion. A rerun of the LH_2 run is also shown on Figure 3.2-2. This rerun was done mainly because the observed control drum motion in the first LH_2 run was less than predicted. This reactivity variation was observed in both LH_2 profiles and is attributed

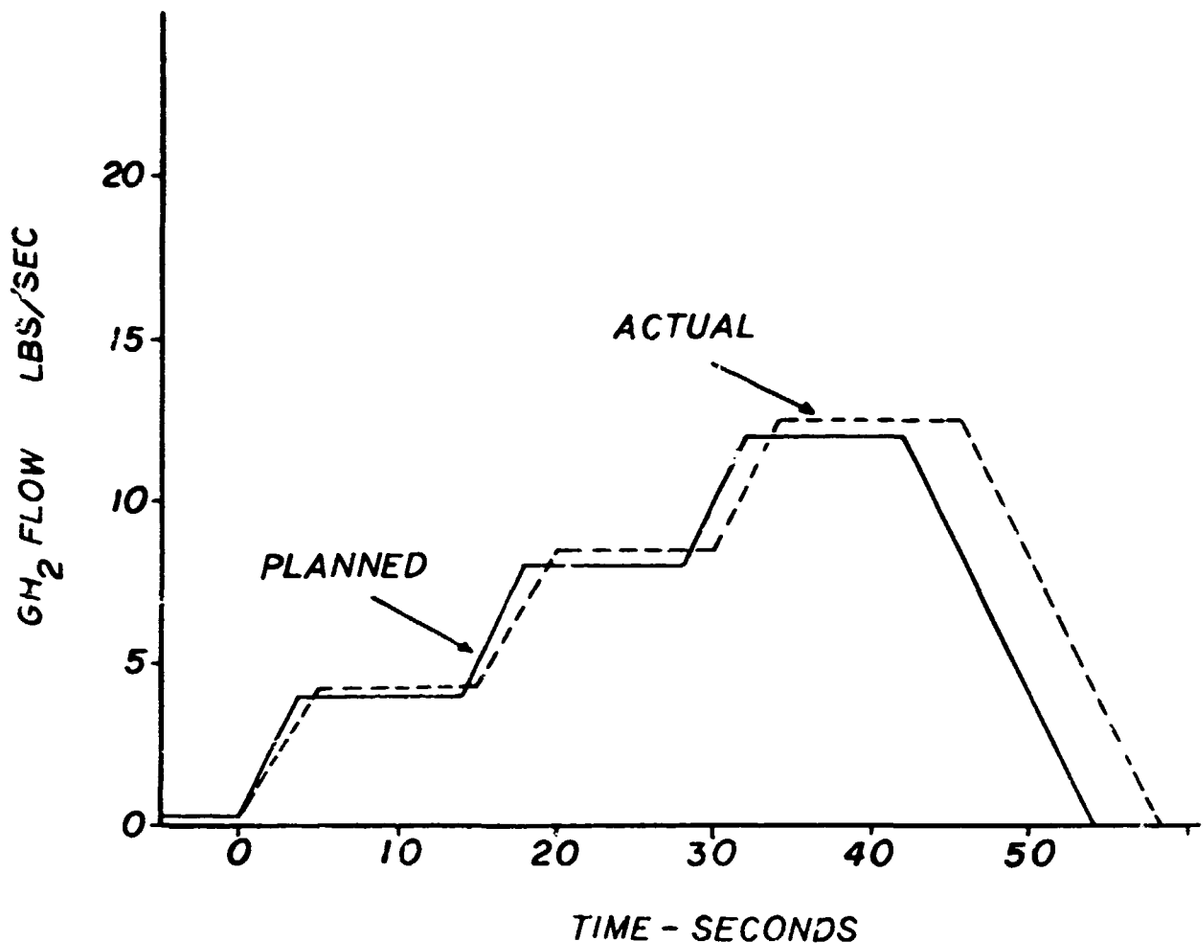
20
15
10
5
0
GH_2 FLOW LBS/SEC
ACTUAL
PLANNED
0
10
20
30
40
50
TIME - SECONDS

FIGURE 3.2-1 - [illegible]

CONFIDENTIAL
RESTRICTED DATA
Atomic Energy Act - 1954

Astronuclear

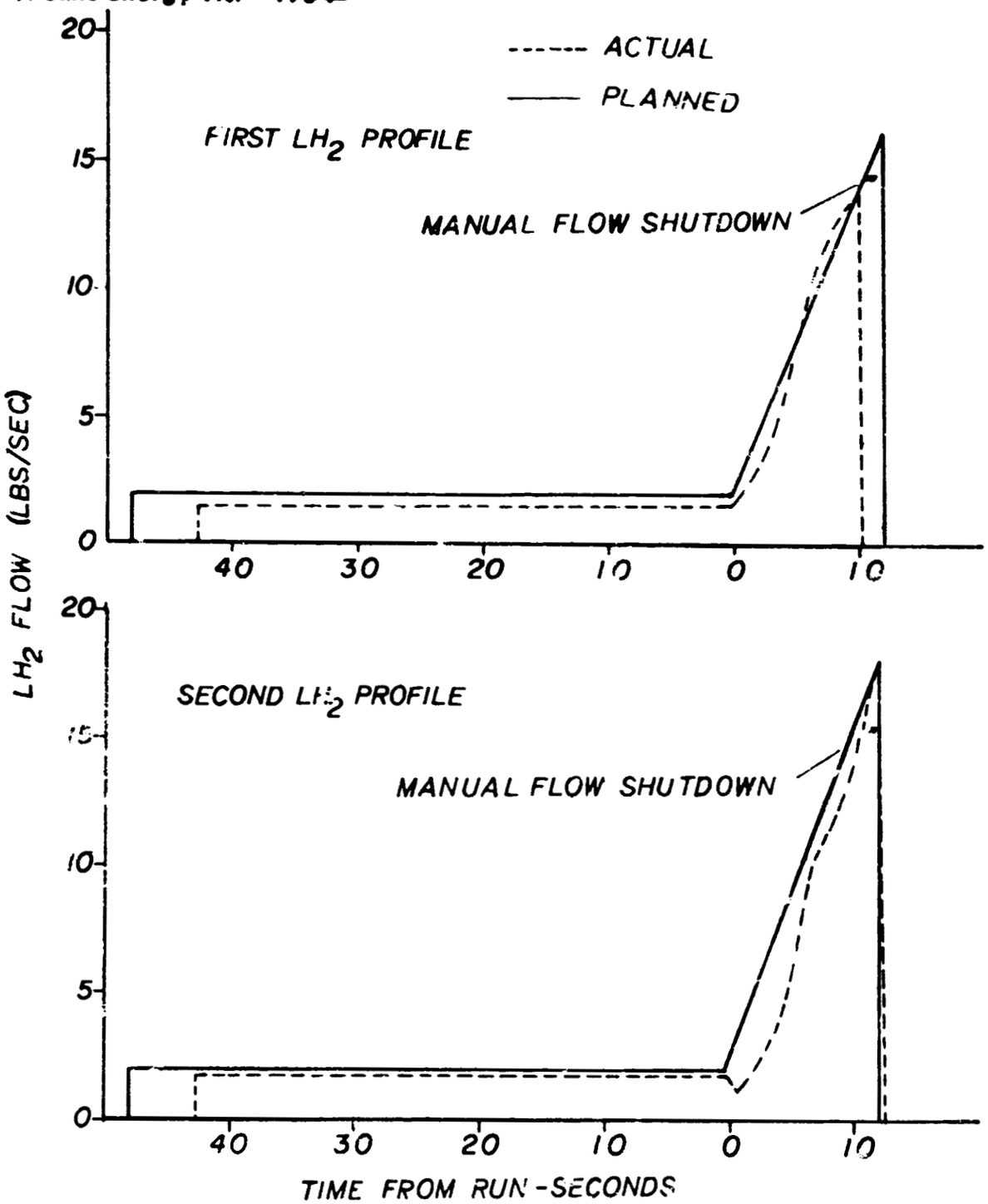

FIGURE 3.2-2 - RP-1B PLANNED AND ACTUAL FLOW PROFILES - LIQUID HYDROGEN

CONFIDENTIAL
RESTRICTED DATA
Atomic Energy Act - 1954

to the flow lag between actual reactor flow and indicated flow through FE-7. This flow lag condition was considered in planning the profile for the power test. It is also significant to note that the control drum torques observed during the LH_2 runs were normal, and therefore the modifications initiated as a result of the NRX-A1 test were successful.

3.2.3 Experimental Plan II - Neutronics Calibration

Experimental Plan II, completed on September 16, 1964, incorporated additional automatic reactor startups and neutronics instrumentation calibration. Calibration data was obtained by irradiating U-Al wires for approximately 130 KW-min. The reactor was then operated at temperatures up to 1000°R to obtain data relevant to material temperature coefficients of reactivity and to verify the proper operation of the power control system temperature trim loop. Integrated power during this run was measured as 700 MW-sec with a maximum indicated power level of 1 MW.

3.2.4 Experimental Plan III - Scaled-Down Power Test

The final test in preparation for the Power Test was completed on September 18, 1964, and was an integrated dry run operation to insure that the required systems, programs, procedures and personnel were thoroughly checked out for the power test. The reactor was operated using the power test profile reduced by a factor of approximately 1000. Feed system operation was simulated using the power test programs. The only coolant available for use during this test was helium. Power generated was indicated as 400 MW-sec.

3.3 SUMMARY OF EXPERIMENTAL PLAN IV - POWER TEST

The fifth test of the NRX-A2 series was completed on September 24, 1964, after being postponed from the previous day due to adverse meteorological conditions. The major objectives of the power test were:

a. To obtain experimental verifications of the steady-state design analysis for power operation.

b. To obtain experimental data for assessing the suitability of the reactor to operate at the steady-state power level and temperature required of a component of an experimental engine system.

c. To confirm that the reactor can start, operate at steady-state, and shut down using liquid hydrogen.

In preparation for the power test profile for EP-IVA an automatic reactor startup to 2 MW was performed. In completing this startup the control drums were programmed out to angle θ_{cc} (cold critical drum position) on an exponential ramp with a time constant of 2 seconds at which time a drum linear ramp rate of 0.11 deg/sec was initiated. The period scram was set at 0.3 second during this startup and no anomalies were noted. The cryogenic system chilldown was then completed and initial conditions established for the power profile. The temperature trim control loop was controlling on station 32 in-core thermocouples throughout the run.

The as-run power profile consisted of a reactor pre-chill corresponding to a 90°R drop in core inlet temperature at a flow rate of 2 lb/sec LH_2. Upon reaching this temperature the programmed run was initiated. This run consisted of a power and flow rise corresponding to a 50°R/sec change in exit gas temperature to a nominal one minute 50% power hold. The floating power and period inputs to the scram chain were automatically deactivated at 100 MW. During the 50% power hold the Chief Test Operator applied a power correction to the power controller using the power correction factor throttle. This correction changed the throttle setting from 1.15 to 0.6*. Transfer function measurements were also completed at this hold. This hold was terminated at the end of 60 seconds when the programmers were switched to RUN.

During the planned 76% power hold additional transfer function measurements were made. This hold was terminated at the end of 132 seconds based on the reduction of tank farm pressure to 1700 psig. This tank farm pressure criteria had been pre-determined to permit obtaining the necessary hold duration at the planned 83% power. The reactor was maintained at the 83% power hold for approximately 138 seconds. During this hold the Chief Test Operator applied a positive correction of approximately 10% with the power correction factor throttle to maintain the desired exit gas temperature. The shutdown was initiated

---

* This large change is discussed in detail on pp. 7-46 and 7-47 of the Site Report (NTO-R-0008).

by a retreat upon reaching a tank farm pressure of 1100 psig. A manual flow shutdown, upon command from the Test Director, terminated the retreat when PCV-33 opened wide. The PCV-41 pressure control loop operated satisfactorily and normal cooldown operations were completed.

As can be seen in Figure 4.1-1, Section 4.1, the actual powers reached were 51% for the planned 50% hold, 84% for the planned 76% hold, and 93-98% for the planned 83% hold. Figure 3.3-1 presents the planned vs. actual flow rates. The actual flows at the higher power holds were somewhat higher than planned because of compressibility effects and the precision of the Venturi flowmeters.

Early in the power profile, at about the 50% power hold, a number of small fires were noted on the test assembly. These were located in the vicinity of the dosimetry belly-band and the dome end closure. The fires were of a short duration and based upon post-run observations, appeared to be the result of partial melting of the belly-band and dosimeters and burning of pressure transducer insulation and epoxy potting compound. The inspection did not show any indication of significant hydrogen leakage. During the 83% (nominal) power hold the dewar deluge system was automatically activated due to thermal radiation heating in the dewar area. Following the initiation of retreat, there was a loss of dewar pressure indication on dewars A and B and loss of pressure feedback to PCV-33 (dewar pressurization valve)

FIGURE 3.3-1 · SP-IV PLANNED AND ACTUAL FLOW PROFILES

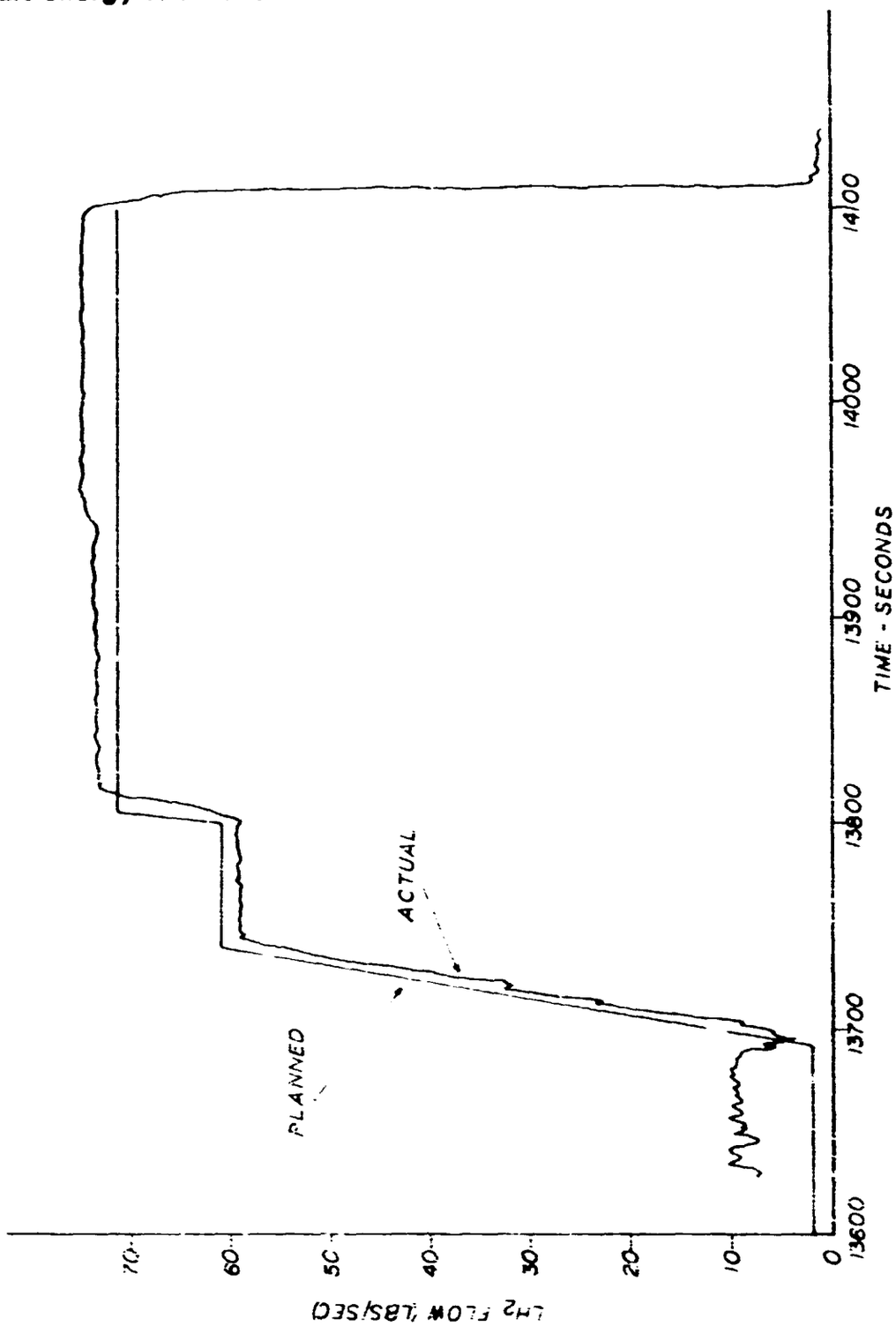

causing the valve to open wide. The dewar safety valves opened to prevent over-pressurizing of the dewars. A post-test inspection showed that the dewar pressure transducers were burned. These anomalies were not considered to be of undue importance.

From the standpoint of observations during the tests and early analysis of data all the objectives of the Power Test were met. The nuclear, thermal, flow and mechanical design analysis, all predicted test parameters which were generally observed during the test.

As was pointed out in the power profiles, the power obtained was higher than planned. This pointed out certain shortcomings in the instrumentation system. These shortcomings occurred mainly in the station 32 in-core thermocouples which were reading low and demanding increased power.

3.4 SUMMARY OF EXPERIMENTAL PLAN V - LOW FLOW-LOW POWER MAPPING

Since the power levels attained during the Power Test were in the vicinity of full power, the restart was planned to obtain the following major objectives in the low-flow, low-power region:

a. To verify that the reactor operation is stable at steady-state in this region using power control while varying the liquid hydrogen flow rate.

b. To verify the predicted power response of the reactor to changes in liquid hydrogen flow rate and density while maintaining a fixed drum position.

Prior to this experimental plan a number of data channels were rescaled and low range differential pressure transducers were installed on the turbo-pump inlet and discharge Venturis. At 10 lb/sec LH_2 flow rate, the precision of the devices with the new range was approximately 3%.

During this experimental plan on October 15, 1964, LH_2 flow rate was controlled by varying ACV-3 stem position with constant dewar pressure. Since the turbo-pump was not used, the turbine header blank (BV-1) was left in place, thereby preventing powering of the turbo-pump. In order to prevent the uncontrolled addition of LH_2 to the reactor by a failure of PCV-41 causing the rapid addition of the stored LH_2 inventory, PCV-41 was switched to SAFE.

During the scram check phase the reactor was brought critical in POSITION control. The critical drum position was found to be 96.0° at a power level of 50 watts with a minimum helium flow through the reactor.

After establishing initial conditions for the run, (i.e., completion of the pre-operational, drum unlocking, scram check, and system chilldown phases) an automatic startup was initiated to 1 MW. During this startup the system failed to lock into power control and the control drums were programmed in, as would be expected. The Chief Test Operator switched into POSITION Control as soon as the inward motion of the drums was observed. The Chief Test Operator then rejected the auto-startup and switched into power control, and established the initial 1 MW condition.

At this point a 2 lb/sec LH_2 flow rate was initiated to pre-chill the core inlet temperature to 300°R. At the completion of the pre-chill operation, the reactor was switched into POWER Control to establish the first point on the flow-power map, 33 MW and 7 lb/sec LH_2 flow. Power increased to 33 MW on a 3 second period, but the manual flow rate increase, as seen by the reactor, lagged the power increase and the tie-rod exit gas test parameter limit of 1200°R appeared to be reached. At this point, a flow shutdown and scram was initiated.

Following an evaluation of the quick-look data, the run was resumed. A modified approach to the first point on the flow-power map was used. In this case power was first increased to 19 MW, on a 10 second period, with a simultaneous LH_2 flow rate increase to 7.3 lb/sec.

Steady-state data was obtained at this point (Figure 3.4-1). It was [illegible] necessary to increase the [illegible] flow rate to 8.2 lb/sec (~[illegible]) in order to maintain the tie rod exit gas temperature below 1000°R. After obtaining steady-state data at this point, the LH_2 flow rate was increased to 13.3 lb/sec. With the reactor in POWER Control at 40-45 MW, steady-state data was obtained at flow rates of 13.3, 7.7, 8.3, and 10.3 lb/sec. The 10.3 lb/sec point (point 6 of Figure 3.4-1) was chosen since it was approximately midway between the minimum and maximum flow rate points.

At the 45.1 MW and 10.3 lb/sec point the reactor was switched into POSITION Control (thereby holding a constant drum position) and flow increased to 13.3 lb/sec and then reduced to 5.1 lb/sec, steady-state data being obtained at each point. The power swing associated with this mode of operation was from 60 to [illegible] MW. The parameters covered are shown on Figure 3.4-2, the NRX-A2 Low Power Map. The run was terminated from the final point by initiating a flow shutdown and scram. A reactor restart was completed to determine post-test critical bank position, 97.6°.

Over the full range of operations completed, in both POWER and POSITION Control, the reactor was completely stable. During these operations the core inlet plenum temperatures reached the low point of their range (40°R) which was indicative of LH_2 entering the core. The demonstration of stability under this condition is considered a major program milestone.

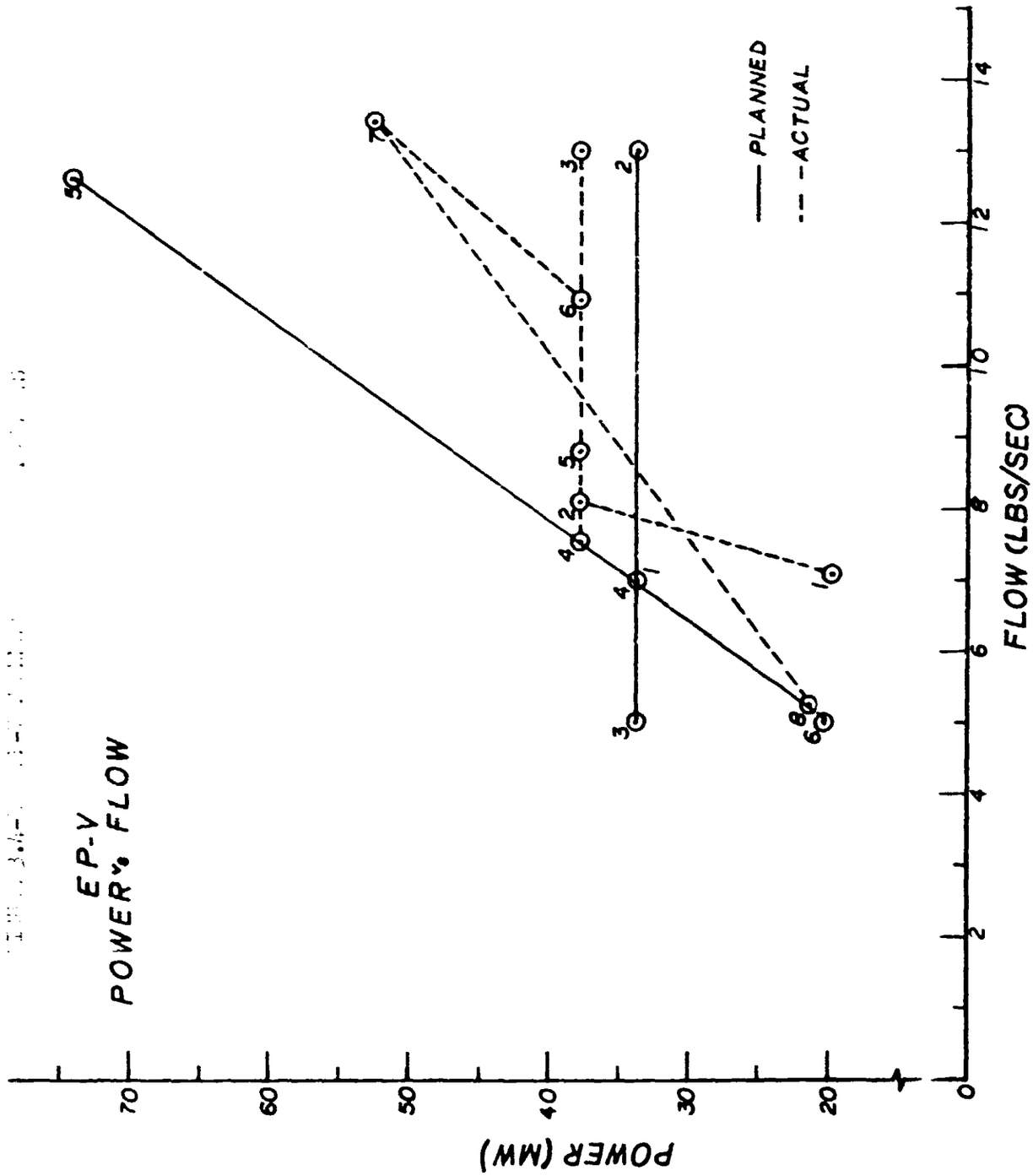
EP-V
POWER vs FLOW
PLANNED
ACTUAL
POWER (MW)
FLOW (LBS/SEC)
70
60
50
40
30
20
0
2
4
6
8
10
12
14

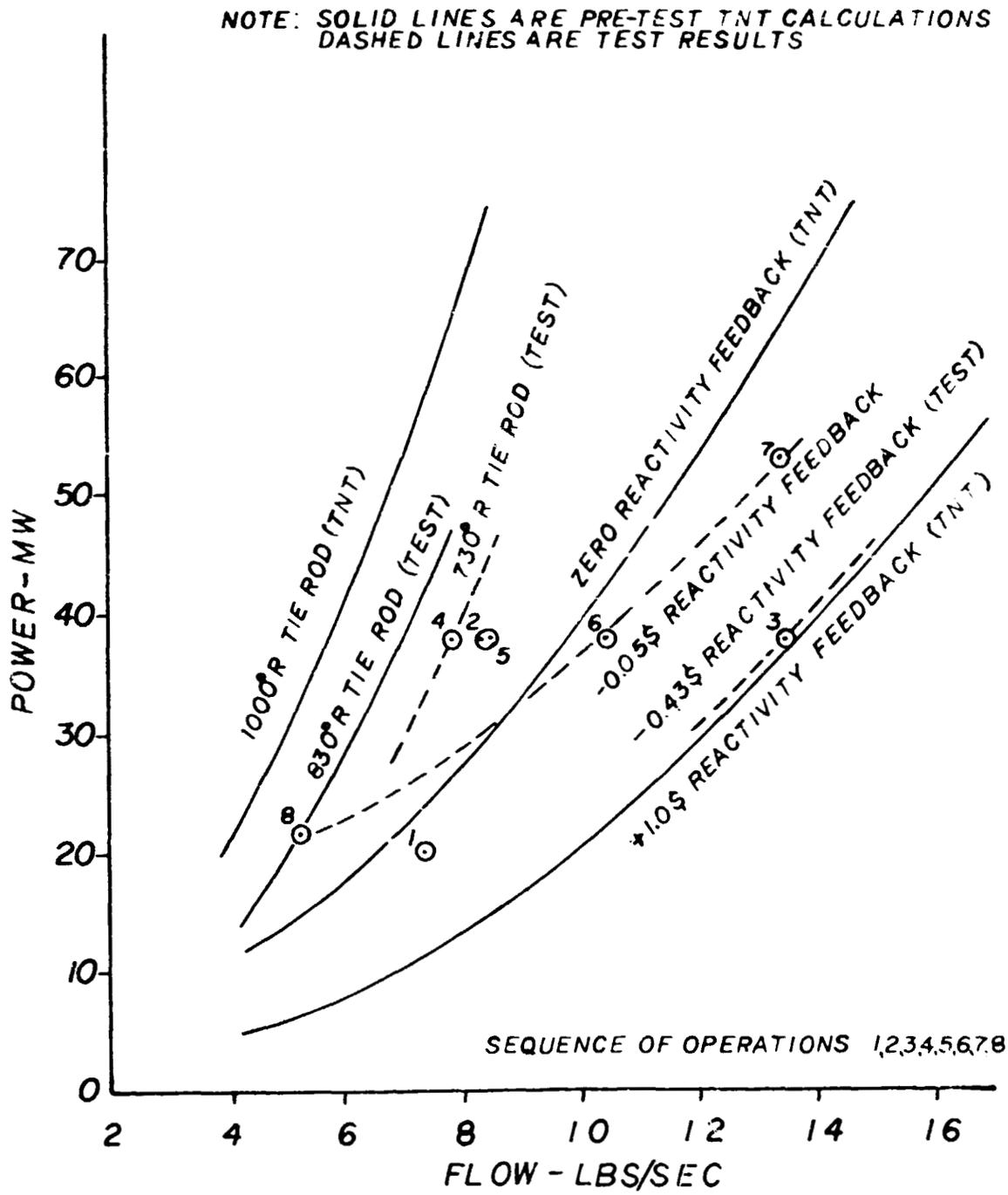

FIGURE 3.4-2 - EP-V LOW FLOW - LOW POWER MAP

4.0 TEST RESULTS AND DISCUSSION

This section presents the test results, data analyses, and correlation of the analyses with design and pre- and post-test observations. Analytical considerations are applied to the data and observations, leading to the development of the conclusions.

The presentation in Section 4 is divided into the following portions:

4.1 Thermal and Fluid Flow Performance

4.2 Fuel and Other Material Behavior

4.3 Mechanical Evaluation

4.4 Nuclear Analysis

4.5 Instrumentation, Control and Data Processing Performance

4.1 THERMAL AND FLUID FLOW PERFORMANCE

4.1.1 General

In this section emphasis is placed on EP-IV and EP-V, the power test and low power mapping test. Reference is made to other NRX-A2 tests as they apply to the results of these major tests. EP-I, II and III, the pre-power tests are discussed in detail elsewhere.*

A. Performance Summary

1. EP-IV

The reactor operated successfully during all phases including the startup, shutdown, and at steady-state operation during EP-IV. Maximum nozzle chamber temperature rate of change was +125°R/sec during startup and -350°R/sec during shutdown. Operating conditions during the test series are listed in Table 4.1-3. Nozzle chamber thermocouples did not indicate average chamber temperature, therefore power was calculated from an energy balance using calculated nozzle chamber temperatures. At the 40 second maximum reactor power hold, the flow was 75.6 ± 1.5** lb/sec H_2 flow, the calculated values were 3815 ± 215°R for nozzle chamber temperature and 1096 ± 50 MW for total thermal power.

---

* NRX-A2 Reactor Performance, WANL-TME-___, January, 1965, CRD.

** All accuracies given in this section are 2σ (95% confidence) range.

The reactor power given above was confirmed within the calculated accuracy by rabbit measured power, and linear neutronic channel number 2 power. The peak power level was also indirectly confirmed by comparable quantities of total energy release during the test series obtained from integrated thermal power and from post-operative radiochemistry. Maximum reactor power implied from core thermal capsule material temperature measurements agrees within the accuracy of the measurements, however, this comparison is not completely satisfying because core temperatures imply a power level 5% higher than 1096 MW. During ZP-IV the power averaged 313 MW over the 7 minute test, while total energy release was 3.81 x 10" watt-seconds for the test series. Best values of steady-state system operating conditions are given in the cycle diagram of Figure 4.1-0.

A post-test calculation of the reactor operating conditions using measured power and flow profiles was performed with the TNT code and the reactor model used for pretest predictions given in WANL-TME-887. Comparison of this calculation to test data demonstrated the adequacy of the TNT transient startup representation and the necessity for adjustments to the model in several regions to more closely represent operating conditions at steady state.

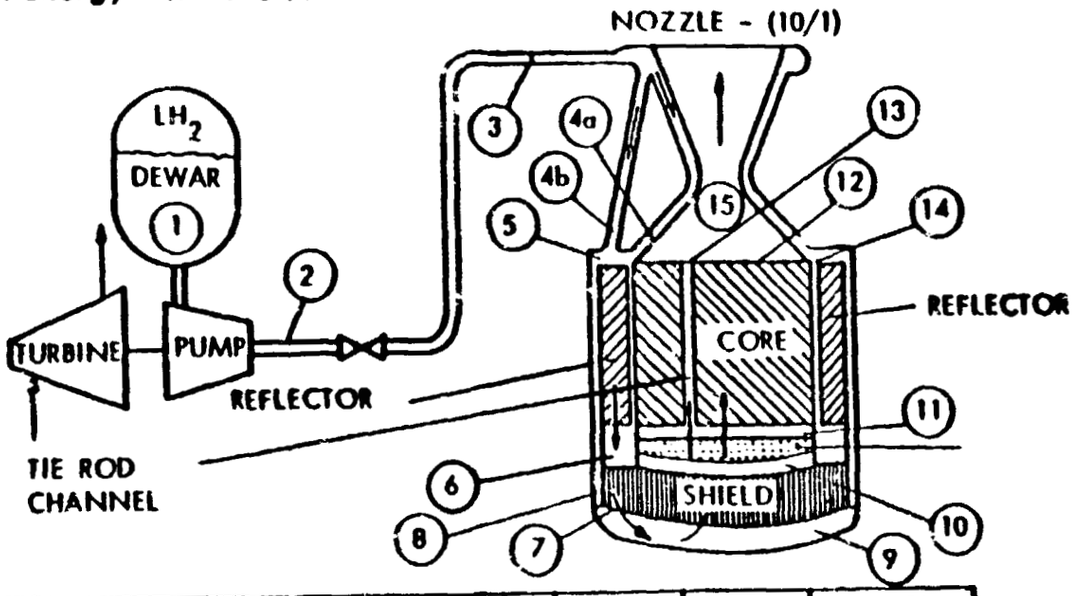

STATION	DESCRIPTION	W - lb/sec	P - psia	T - °R	ENERGY INPUT BTU/SEC
1	Dewar Conditions	75.6	88	38	
2	Pump Outlet	75.6	932		
3	Nozzle Inlet	75.6	860	50	
4a	Nozzle Tubes Outlet	75.6	751	136	32.0 (noz.)
4b	Flange Coolant Outlet				
5	Reflector Inlet	75.6	751	136	
6	Reflector Outlet	62.9*	713	233	
7	First Pass Shield Outlet	75.6	707	216	
8	P.V. Annulus Outlet	12.7*	748	155	
9	Second Pass Shield Inlet	75.6	707	216	22.7(Refl.)
10	Second Pass Shield Outlet				
11	Support Plate Outlet	75.6	702	245(226)*	0.2*
12	Fuel Outlet	70.64*	581	4033*	1056*(Fuel)
13	Tie Rod Outlet	4.60*	581	674(503)*	5.2*
14	Reflector Seal Leakage	0.36*	581	1815*	
15	Nozzle Chamber	75.6	581	3420(3819)*	1096*

* Calculated

605020A

FIGURE 4.1-6 - CYCLE DESIGN POINT CONDITIONS

Preliminary cold flow tests performed in EP-1B demonstrated that it was necessary to take the LH_2 storage between the LH_2 venturi meter and the reactor into account for the power test startup.

2. EP-V

The reactor was operated for approximately 20 minutes with 5 to 13 lb/sec LH_2 flow, 21 to 53 MW reactor power, and nozzle chamber temperature up to 1300°R. The objectives of the test were achieved. A considerable portion of the test was performed with two-phase conditions in the reflector region and at the core inlet. Comparison of the measured data with TNT calculated conditions was reasonable considering the inaccuracy of the test results since most transducers were operating near the low end of their scale.

B. Core Parameters Summary

1. Core Material Temperatures

Station 32 thermocouples indicated temperatures to 1200°R less than core material temperatures because of lost potting compound and bypass flow through the thermocouple lead channel. The best indication of maximum core temperatures were obtained from the thermal capsules located in the central elements which indicated temperatures from 4000°R to 4400°R at station 45. A multiple regression fit of the thermal capsule data was performed in order to correlate the temperatures with core radius. This data fit shows that the average

temperature of the entire central region* of the core was 4276 ± 109°R and there was no significant radial variation. At the core periphery the data fit reveals a linear radial variation rising to a maximum of 4360 ± 179°R at the core periphery. Families of thermal capsules in four clusters indicated the maximum temperature of 4400°R in the J row.

Core fuel element temperatures at maximum power were calculated for the test conditions of core inlet temperature, operating control drum angle and measured reactor flow rate and power (1096 MW). Correlating the results of this calculation as a function of radius gives a reasonably flat radial profile in the central region of the core at a nominal level of 4080 ± 215°R and an increasing temperature toward the core periphery to a maximum of 4327 ± 215°R at the core periphery. The maximum calculated temperature occurs in element J-5-J which was also one of the 4 highest thermal capsule indications. The high peripheral temperatures result from the core orificing which was based on an operating drum angle of 90° and an inlet hydrogen temperature of 250°R while the maximum operating condition was 103° drum angle and 225°R core inlet temperature.

The calculated values are almost 200°R lower in the central region. Possible reasons for this variation which are being investigated include: temperature sensors indicating high due to

---

* Central region of the core is defined as all clusters except the J row.

internal heating, calculational model used to treat central element and fuel element heat interchange, core bypass flow in excess of 0.36 lb/sec, higher reactor power, or lower reactor flow.

2. Core Pressure Drop

Calculated core pressure drop was about 5% lower than measured core pressure drop. This may be due to the friction factor correlation used for calculations. It is noted that arbitrarily decreasing fuel element flow rate 5% would lead to calculational confirmation of both the core material temperature and the core ΔP.

3. Tie Rod Exit Gas Temperatures

Measured tie rod temperatures were 130 to 260°R higher than calculated during EP-IV and EP-V tests. Also the indicated temperatures were erratic, T-755 was about 100°R lower than T-760 and T-765 during EP-IV, while T-760 was up to 465°R higher than the other two operative thermocouples during EP-V. The erratic behavior and high indications have been attributed to the T/C contacting the hotter molybdenum cone during the test, as evidenced by the bent thermocouples observed during disassembly.

C. Reflector, Shield and Lateral Support Parameters Summary

The power picked up in the reflector system calculated from measured LH_2 flow rate and measured temperatures at the four power holds was (2.15 ± 10) % of total reactor thermal power while calculated nuclear heating rates give a reflector power equal to $(1.76\ ^{+0.6}_{-0.5})$% of

reactor power. A comparison of these values indicates that the measured reflector heating rate was about 20% higher than the calculated heating rate but was within the error range of the calculated rate. This measurement provides more accurate reflector heating than was previously available.

Comparisons of measured conditions and pretest calculated conditions were not meaningful because (a) the test was considerably different than planned; (b) nozzle tube exit temperature (reflector inlet) was higher than pretest calculations indicated; (c) the support ring temperatures, which affect the inner-outer reflector gap size and thereby overall reflector impedance, were lower than had been expected; and (d) reflector heating rate was high, as mentioned above. On the basis of the measured test power and flow rate, measured reflector inlet temperature, measured reflector heating rate and measured support ring temperature, the reflector, shield and lateral support system conditions were calculated at the highest power hold. These calculated pressures, fluid temperatures and material temperatures were compared to measured values in order to confirm the calculational method and to discover any anomalies in operation of these components during the test. Generally there was reasonable agreement between the measured and calculated values. Items of interest obtained from this comparison are:

1. All calculated pressures including the lateral support pressure distribution were in good agreement with measurements.
2. All calculated plenum fluid temperatures were in good agreement with measured temperatures. Single thermocouple temperature indications for the hydrogen exiting from individual major reflector coolant passages were in reasonable agreement with calculations.
3. Lateral support seal chamber fluid temperature measurements were about 800°R lower than calculated. Reviewing other temperature measurements in the lateral support region and reviewing the thermocouple installation lead to the conclusion that these T/C's were most likely indicating inner reflector material temperature, rather than the average seal fluid temperature.
4. Material temperature measurements in the shield, support plate, filler strips, inner reflector, control drums, and boral vane were all reasonably close to calculated values. However, the graphite

inner reflector material temperatures increased with time throughout the test, even at the steady state holds. This increase is believed to be due to a decrease in graphite thermal conductivity with irradiation, although experimental data on the effect of irradiation on H4LM graphite conductivity is not presently available.

5. Temperature symmetry was evident at steady-state operation during EP-IV in reflector inlet, reflector outlet, dome end, and core inlet plenums. During EP-V azimuthal temperature asymmetries are evident. These asymmetries and their cause are being studied in detail.

D. Nozzle

The nozzle tube inlet pressure drop calculated with the TNT Reactor Model agreed well with test measurements. However, heat pickup of the nozzle coolant was about 30% greater than calculated.

Temperature distribution at the nozzle tube exit was symmetrical throughout the high power test after hydrogen asymmetry exceeded critical pressure during the startup. An azimuthal temperature asymmetry during prechill and the first portion of startup was apparently oriented with the nozzle feedline, but had no significant effect on operation.

4.1.2 EP-IV Test Description and Chronology

The high power test was performed on September 24, 1964. The planned profile consisted of a reactor prechill corresponding to a 90°R drop in core inlet temperature followed by a power and flow rise corresponding to a 50°R/sec increase in exit gas temperature at a 50%* power hold. A 76% and 83% power hold were planned followed by a retreat to 2200°R chamber temperature and a scram and simultaneous switch to ambient hydrogen coolant. All power and flow changes were planned to be in a manner to correspond to a nozzle chamber temperature change of 50°R/sec, excepting for a 135°R/sec nozzle chamber temperature decrease rate following the scram. Table 4.1-1 presents a selected chronology.

Planned duration of the 50% hold was one minute while the 76% hold was to be terminated when turbine supply pressure decreased to 1700 psig or after a five-minute interval. The supply pressure hold termination criteria had been established prior to the test as that turbine pressure which would allow for a reasonable final hold duration. The final hold was to be terminated after a three-minute interval or at a 1200 psig turbine supply pressure whichever occurred first. 1200 psig was the minimum tank farm pressure for turbine requirements.

---

* Percent of 1120 MW, design power.

TABLE 4.1-1

CHRONOLOGY NRX-A2 EP IV

Reference to Figures	Event	Control Room Time
	Automatic power startup	13268
A	Open OBV 86 for prechill	13642
B	Power starts up, end of prechill	13693
	Nozzle pressure exceed critical pressure	13711
	Temperature control trim starts	13713
C	Start of first hold	13743
	Switch to run	13804
D	Start of second hold	13816
	Switch to run	13946
E	Start of third hold	13953
F	Increase power to maximum hold	14065
G	Retreat starts	14101
H	Flow shutdown and power scram	14109
	Nozzle inlet temperature starts to rise as GH_2 flow is established	14113
	Cooldown	

Planned steady-state operating conditions were as follows:

Power MW	Power % of 1120 MW	Flow Rate lb/sec	Nozzle Chamber Temperature °R	Duration
560	50	61	2650	1 min.
855	76	71.3	3200	5 min. max.
930	83	71.3	3450	3 min. max.

Operating limits established prior to the test are given in Table 4.1-2.

Figure 4.1-1 graphically presents the three major parameters - nozzle chamber gas temperature, reactor thermal power, and coolant mass flow rate - as they varied in time during the higher power test of the NRX-A2. The calculated nozzle chamber temperatures given at four times during the test are considered to be the best estimate of true chamber temperature during the test.

With the reactor in power control at a constant power of 2 MW and a hard chill of the LH_2 feed system, the main coolant valve OBV-86 was opened at the time designated by "A" on the Figure 4.1-1. A 50 second reactor prechill corresponding to a 90°R drop in core inlet at a flow rate of approximately 2 lb/sec LH_2 followed, and at time "B" on the figure the programmed run was initiated. The planned power holds are designated on the figure as the time intervals from C to D, D to E, and E to G with an unprogrammed manual power adjustment at time F.

CONFIDENTIAL
RESTRICTED DATA
Atomic Energy Act - 1954

TABLE 4.1-2

LIMITS ESTABLISHED FOR LH-A2 OPERATION

Parameter	Limit	Qualification
Nozzle chamber temperature, max.	3620°R	Set 5% above calculated value
(Expected start and retreat rate)	50°R/sec	
(Expected shutdown rate)	135°R/sec	
Tie Rod Temperature, max.	1000°R	Steady-state
	1200°R	Transient
Fuel Element Temperature, max.	800°R	Air exposed
	1[illegible]00°R	Nitrogen exposed
Station 45 fuel element temperature, max.	39[illegible]0°R	Set 5% above calculated value
Station 32 fuel element temperature, max.	3450°R	Set 5% above calculated value
Core inlet temperature, min.	90°R	
	250°R	LH_2 flow test only
Nozzle inlet pressure, max.	1000 psia	
Nozzle chamber pressure, max.	600 psia	
Graphite barrel ΔP, max.	200 psid	
Core ΔP, max.	150 psid	
Reactor period, min.	1 second	
Shutdown reactivity, min.	2 $	
Cooldown Limits		
Core orifice	900°R	
Core support plate temperature, max.	850°R	
Replacement shield	950°R	
Inner reflector	750°R	
Outer reflector	750°R	
Pressure vessel	850°R	
Core fuel (with Nitrogen)	1200°R	200°R low to provide margin for core hot spot

CONFIDENTIAL
RESTRICTED DATA
Atomic Energy Act - 1954

Astronuclear

CONFIDENTIAL
RESTRICTED DATA
Atomic Energy Act - 1954

Astronuclear

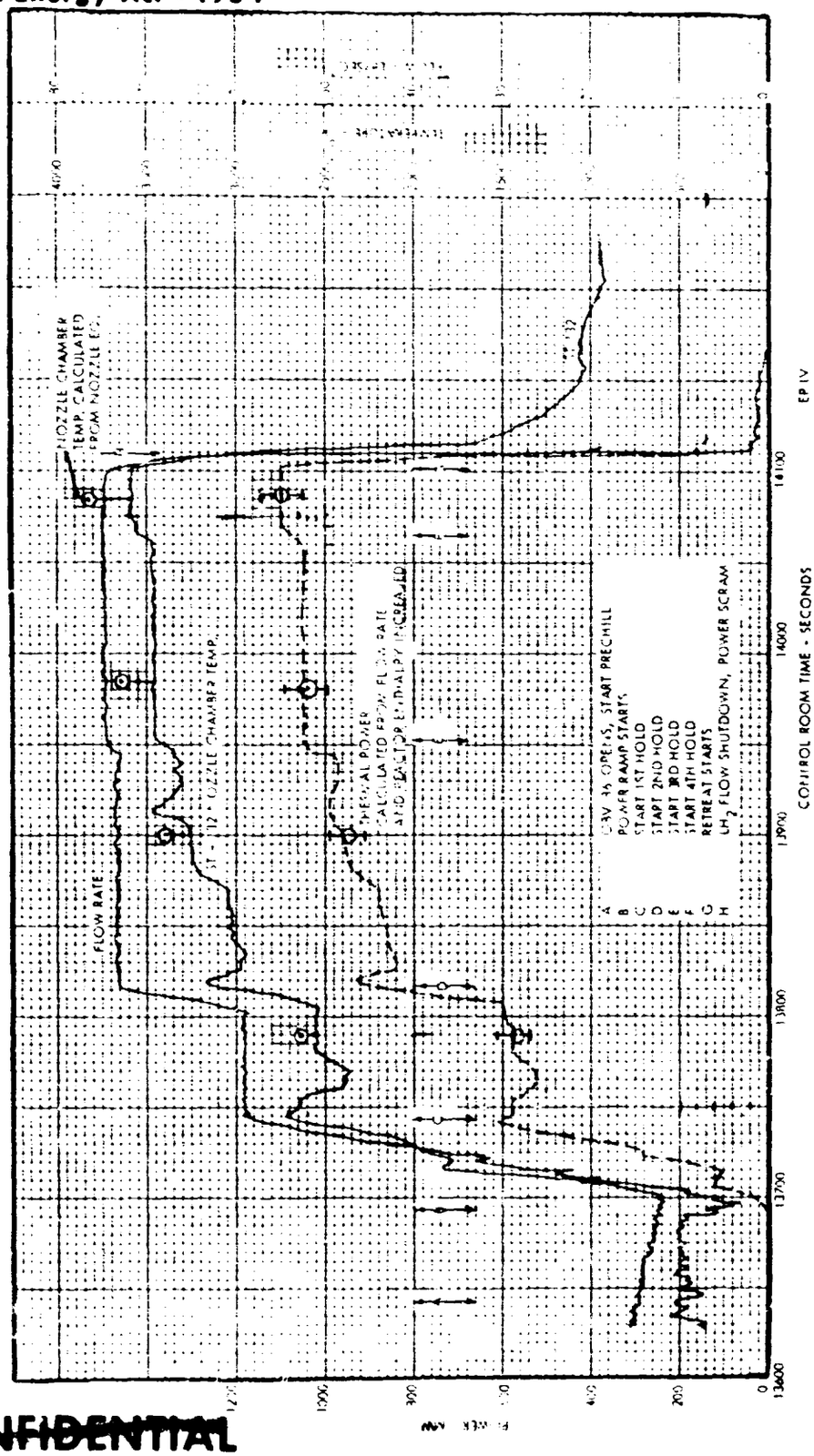

CONFIDENTIAL
RESTRICTED DATA
Atomic Energy Act - 1954

Power level was higher than planned during the early portion of the startup resulting in nozzle chamber and fuel element temperature increase rates higher than expected. However, when station 32 material temperature exceeded 1450°R the temperature trim loop became operative and the remaining portion of the power ramp was as planned. The 50% power hold was close to planned power and temperature levels, with a duration of approximately one minute. The programmers were switched to run at the end of this hold and power and flow increased to the approximate conditions planned for the 76% power hold. During the power rise and the hold, station 32 core material temperature thermocouple indications began to decrease, due to failure of the thermocouple potting and attendant bypass flow cooling the thermocouple. The temperature control loop trimmed reactor power to the maximum allowable increase of +15% during this programmed hold. Thus the power drifted upward during this hold of about 2 minutes. When turbine supply pressure reached 1700 psig the hold was ended and the programmers increased power to the final planned 83% power hold. Power during this hold was approximately 1040 MW for about 2 minutes compared to a planned 930 MW. The station 32 core material thermocouples were indicating approximately 1000°R low at the end of this hold. In addition, the nozzle chamber thermocouples were indicating temperatures several hundred degrees lower than the true mixed mean chamber temperature. No useful information

could be obtained from the station 45 core material thermocouples because they saturated at about 3700°R as expected. On the basis of the available temperature indications, the Chief Test Operator manually increased the power to final level of 1096 MW for about 40 seconds.

At the predetermined turbine supply pressure, shutdown was initiated with the planned retreat ("G" on Figure 4.1-1). Eight seconds later a flow shutdown and scram, upon command of the Test Director, terminated the retreat. The shutdown, due to loss of the dewar pressure signal, was from a chamber temperature of 3380°R rather than the planned 2200°R and was consequently more severe.

A restart and post-run critical rod position test was performed approximately 2 hours after shutdown. Following the power test there was a 32 hour cooldown period with ambient hydrogen, ambient nitrogen and cold nitrogen to remove the decay heat from the reactor.

In summary, EP-IV was of 7 minutes duration from the end of the prechill to the scram with an average power of 825 MW and maximum operating conditions of 1096 MW with 75.6 lb/sec LH_2 coolant and 3815°R nozzle chamber temperature.* Operating conditions, more severe than planned, were successfully sustained by the reactor during the startup, at high power holds and during the reactor shutdown. These operating conditions of power, temperature, pressure and flow are tabulated in Table 4.1-3.

* Power and nozzle chamber temperatures quoted are determined from a reactor heat balance described in the following section.

TABLE 4.1-3

NRX-A2 EXTREME OPERATING CONDITIONS

Parameter	Value Observed	When Observed	
Power			
Integrated	6500 MW-Min.	All EP's	
Instantaneous	1096	EP IV	For 40 seconds
Temperatures			
Chamber Rate, Max.	+125°F/sec	EP IV	Startup
Min.	-350°F/sec	EP IV	Shutdown
Unfueled Core Mod., Max.	4350°R	EP IV	Measured thermal capsule
Avg. Min.	200°R	EP IV	Cooldown
Nozzle Chamber, Max.	3815°R	EP IV	Calculated
Tie Rod Exit Gas, Max.	1670°R	EP V	Abort, Transient(negligible core ΔP)
Time above 3250°R	355 sec	EP IV	
Core Orifice Adhesive	1050°R	EP IV	Cooldown prior to first GN_2 pulse (inferred from Station 8)
Inner Reflector, Max.	850°R	EP IV	Cooldown
	1400°R	EP IV	$T_{max.}$
Outer Reflector, Max.	750°R	EP IV	Cooldown
Core Inlet, Min.	47°R	EP V	H_2 Quality estimated between 70 to 90%
Pressures			
Nozzle Chamber Rate, Max.	36 psi/sec	EP IV	Startup
Nozzle Chamber, Max.	581 psia	EP IV	
Feed Line, Max.	855 psia	EP IV	
Core ΔP, Max.	121 psid	EP IV	
Ref. Inlet/Noz. Chamb. ΔP, Max.	172 psid	EP IV	
Nozzle Tube ΔP, Max.	109 psid	EP IV	
Flow			
Rate of change	6 lb/sec^2	EP IV	Startup
LH_2	75.6 lb/sec	EP IV	

Detailed test data and analysis of the high power test described above follow in this section. The EP-IV test is considered in the following order.

Subsection	Contents	Control Room Time Interval
4.1.3	Prechill	13642 to 13693
4.1.4	High Power Holds	13743 to 14101
4.1.8	Startup and Shutdown	13693 to 13743 and 14101 to 14130
4.1.6	Cooldown	14101 on

4.1.3 Prechill

A. Reactor

Predicted reactor system temperatures at the end of prechill given in WANL-TME-787 are compared to the measured test temperatures at the end of the prechill period in Table 4.1-4. The pretest calculated values were based on the entire reactor being at ambient temperature of 540°R when the prechill was initiated. The reactor had been at 2 MW for over 5 minutes prior to the prechill and the reactor and core temperatures were above ambient temperature when OBV-86 was opened. During the prechill interval the core inlet temperature was reduced from 588°R to 455°R, somewhat more than the planned 90°R reduction. T-781 which was used to determine when the 90°R quench had been obtained decreased 114°R during this interval. Although the initial test temperatures were considerably higher than those on which the calculations were based, the temperatures at the end of prechill were very close to expectations as shown in the table.

TABLE 4.1-4

REACTOR CONDITIONS AT THE END OF PRECHILL
(CRT 13693) PREDICTED AND MEASURED

	Measured	Predicted*
Reflector Inlet (Average of 7 T/C)	43°R	38°R
Reflector outlet (Average of 5 T/C)	331°R	351°R
Core Inlet (Average of 11 T/C)	455°R	443°R
T/C T-781	473°R	---
Nozzle Chamber (Average of 4 T/C)	565°R	506°R
Tie Rod Exit Gas (Average of 4 T/C)	641°R	570°R
Time for 90°R reduction at core inlet	44 sec	48 sec
Actual time of prechill	51 sec	48 sec

*Calculated with pre-run TNT

Similar to EP 1-B LH_2 test, actual flow rate could not be obtained during EP-IV from the LH_2 flow meter FE-7, because part of the flow was bypassed through AVV-2. However, there are several indications that 2 lb/sec was close to the actual flow during the prechill. First, the time for the 90°R temperature reduction at the core inlet, measured and predicted, were in reasonable agreement (48 sec predicted vs. 44 seconds measured). Also the reflector inlet and exit temperatures (measured and predicted) are in fair agreement.

B. Core

Figure 4.1-2 has four time histories of selected core fluid and material temperatures to illustrate typical conditions in the core region during the prechill and startup. Core inlet thermocouple T-781 decreased during the prechill and continued to decrease at about the same rate after startup was initiated (CRT 13693) until about CRT 13710. At this time the flow increased rapidly with a resulting rapid decrease in core inlet temperature, tie rod exit gas temperature, and station 8 core material temperature. During the prechill and startup the core inlet temperature decreased continually to a minimum at the steady-state power hold.

The azimuthal asymmetry at the end of prechill is shown on Figures 4.1-3 and 4.1-4. This asymmetry is similar to that observed in EP-I-B with an indication of minimums at 120° and 300° locations. The variation is somewhat attenuated from an 85°R azimuthal variation

CONFIDENTIAL
RESTRICTED DATA
Atomic Energy Act 1954

Astronuclear

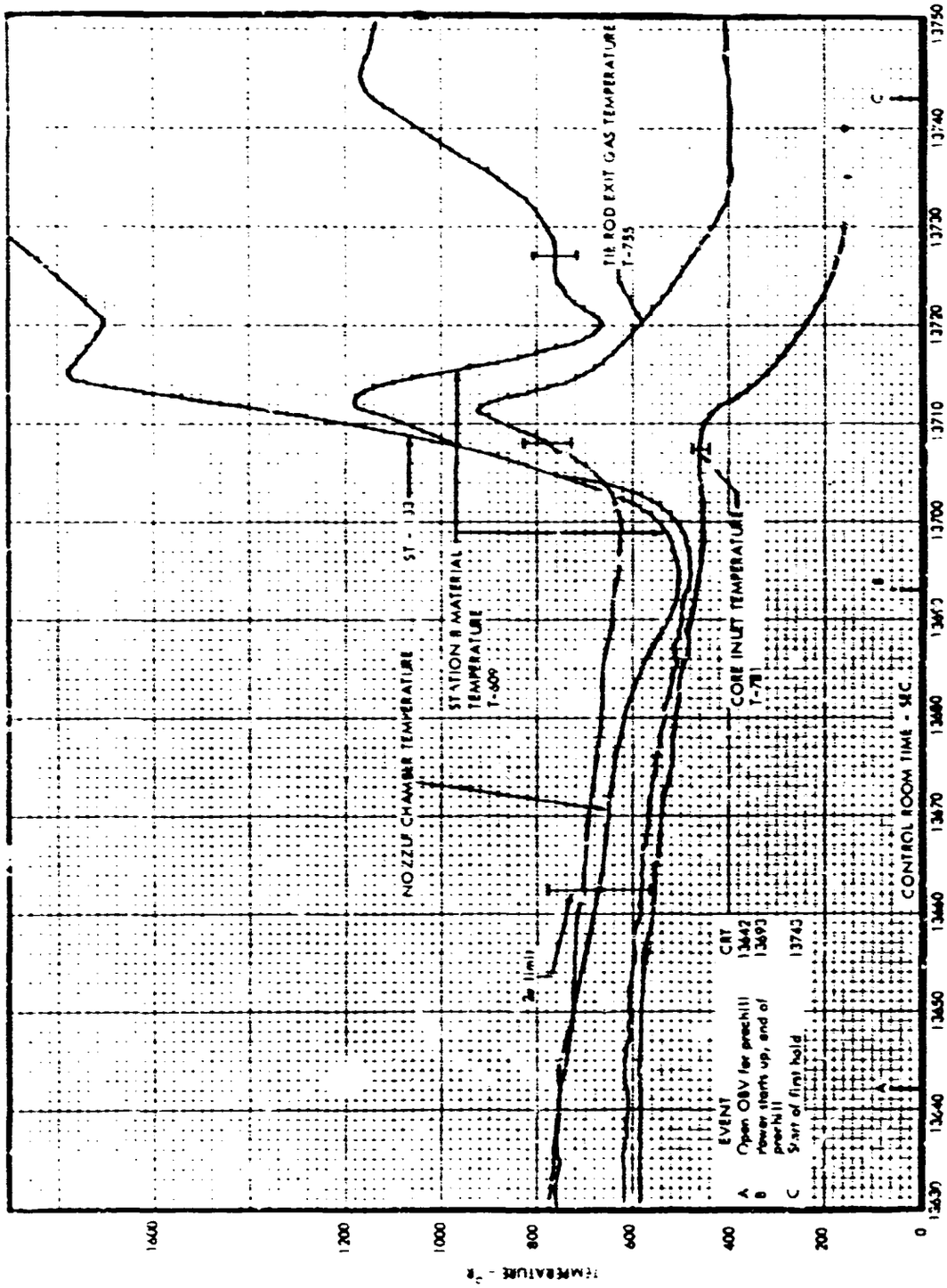

FIGURE 4.1-2 TYPICAL CORE TEMPERATURES VS. TIME (PRECHILL)

CONFIDENTIAL
RESTRICTED DATA

Astronuclear

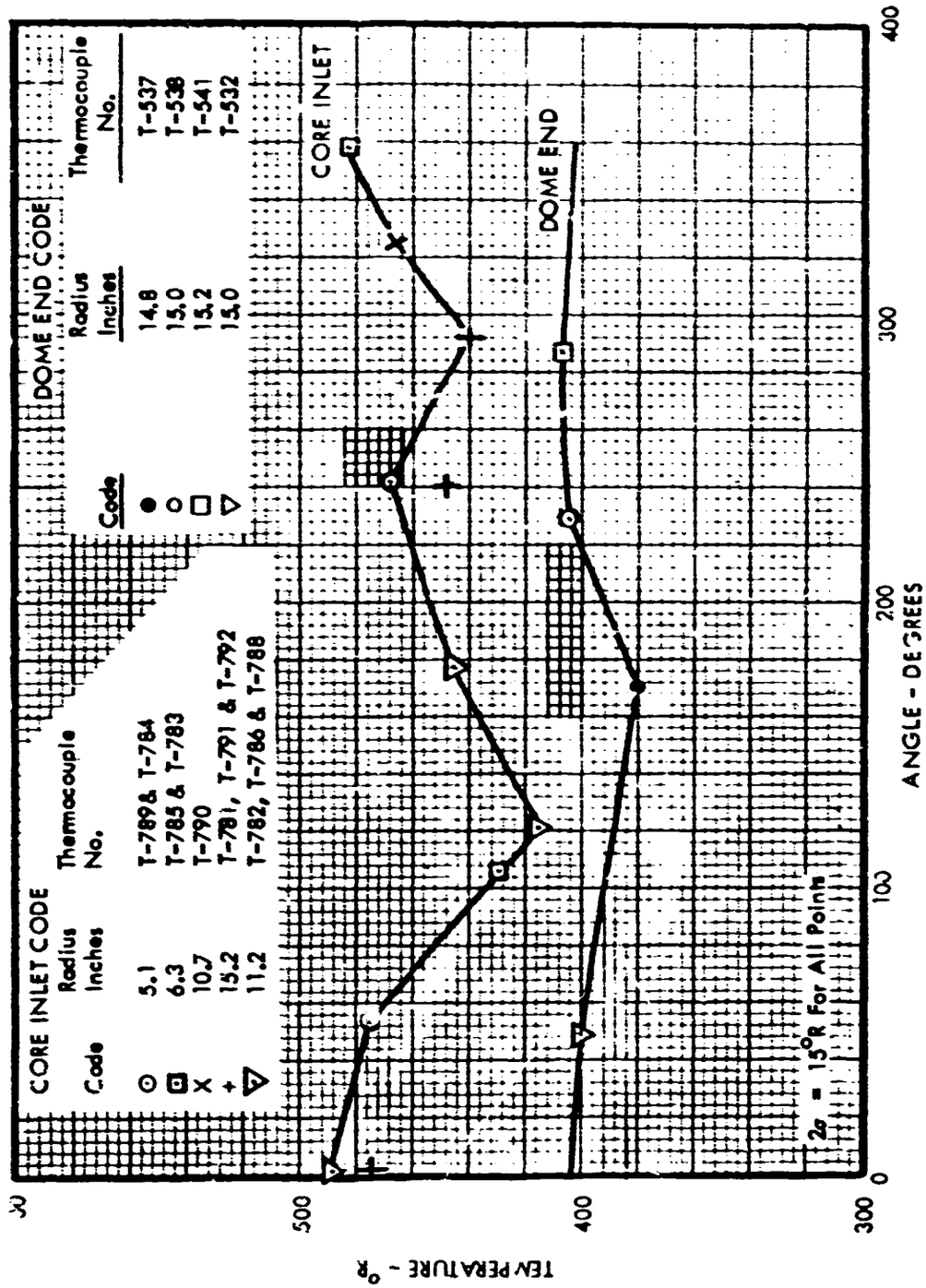

FIGURE 4.1-3 CORE INLET AND DOME END TEMPERATURES VS. AZIMUTHAL POSITION AT END OF MacCHILL (CRT 13693)

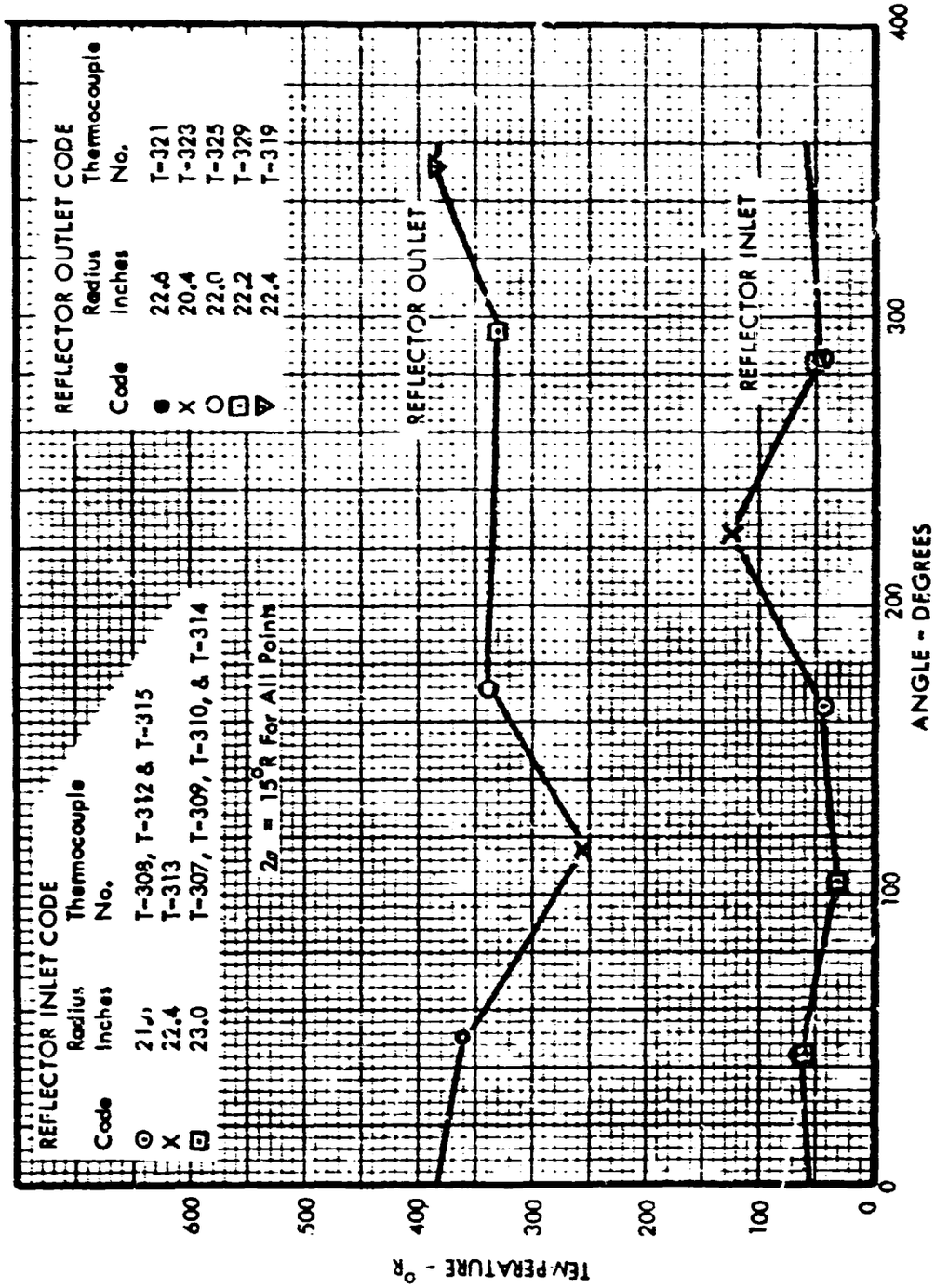

FIGURE 4.1-4 REFLECTOR INLET AND OUTLET TEMPERATURE VS. AZIMUTH AT END OF PRECHILL (CRT 13693)

at reflector inlet to 68°R at the core inlet. However, the maximum variation occurs at the reflector outlet and is 130°R. This asymmetry disappears during the power run, and is discussed more fully in the startup section.

C. Reflector

The axial distribution of material temperatures at the end of pre-chill (CRT 13693) for the reactor, control drum, and control vane are shown on Figure 4.1-5. As may be expected, the nozzle end of the reflector system where the low temperature nozzle exit fluid enters the reflector system is colder than at the dome end. The bulk fluid temperature increases as it passes through the reflector due to the sensible heat pickup from the reflector materials. Also, it is noticed that the control vane which has a low heat capacity is coolest. The control drum and the sectors are less effectively cooled during the transient, and thus show correspondingly higher material temperatures.

Inner reflector material and seal chamber fluid temperatures are shown on Figure 4.1-6. The seal chamber temperatures shown decreasing temperatures from the dome end to the nozzle end, with the exception of T/C T-442 at station 35.3. The cause of this single higher temperature is not known. The other temperature measurements appear to be as might be expected considering the low temperature pin leakage entering the system without high power generatin at this time. The axial distribution and temperature level of the

~~CONFIDENTIAL~~
~~RESTRICTED DATA~~
~~Atomic Energy Act - 1954~~

Astronuclear

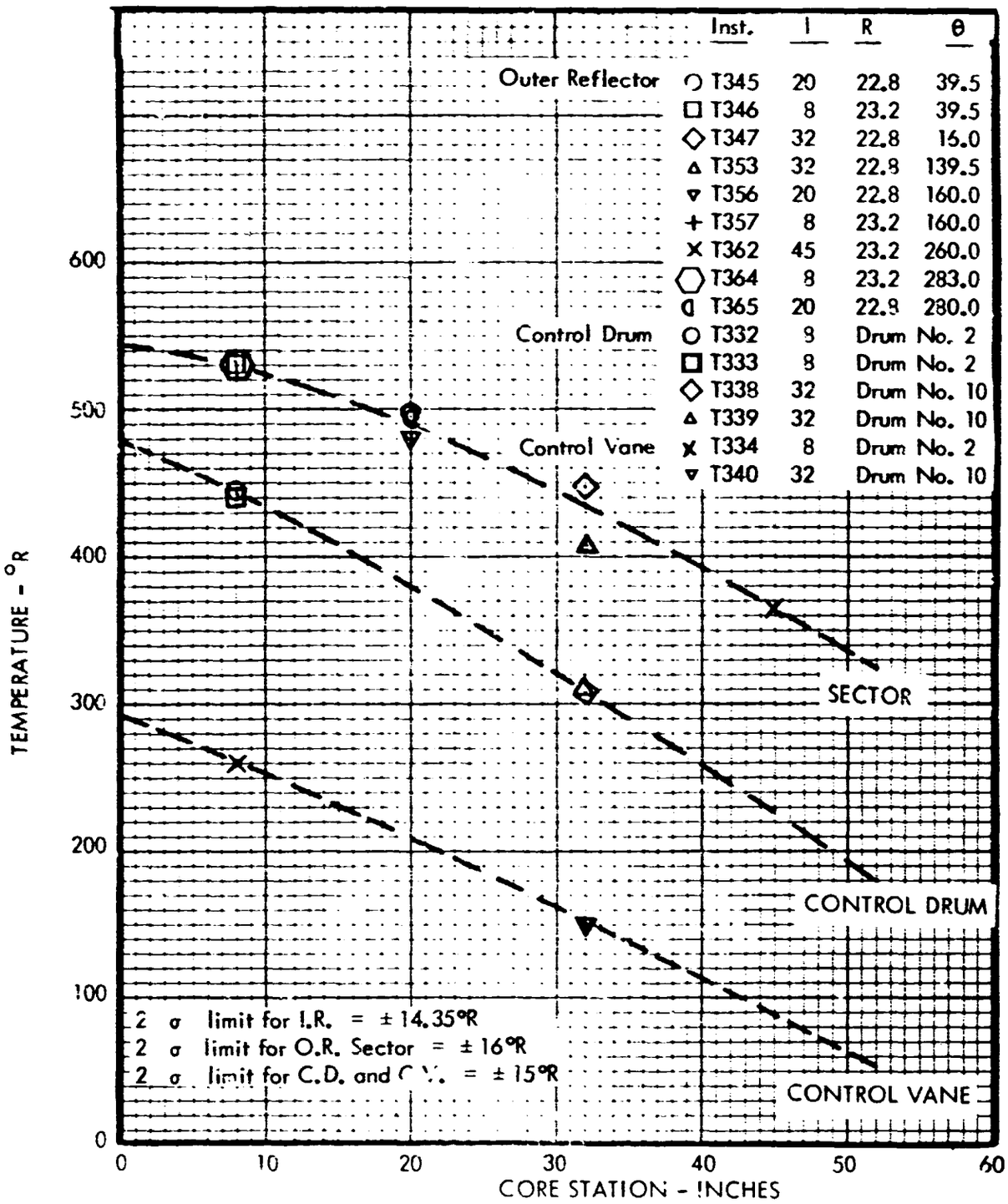

FIGURE [illegible] [illegible] CONTROL DRUM, VANE AND SECTOR TEMPERATURES AT [illegible] OF [illegible] HILL (ORT 13693)

~~CONFIDENTIAL~~
~~RESTRICTED DATA~~
~~Atomic Energy Act - 1954~~

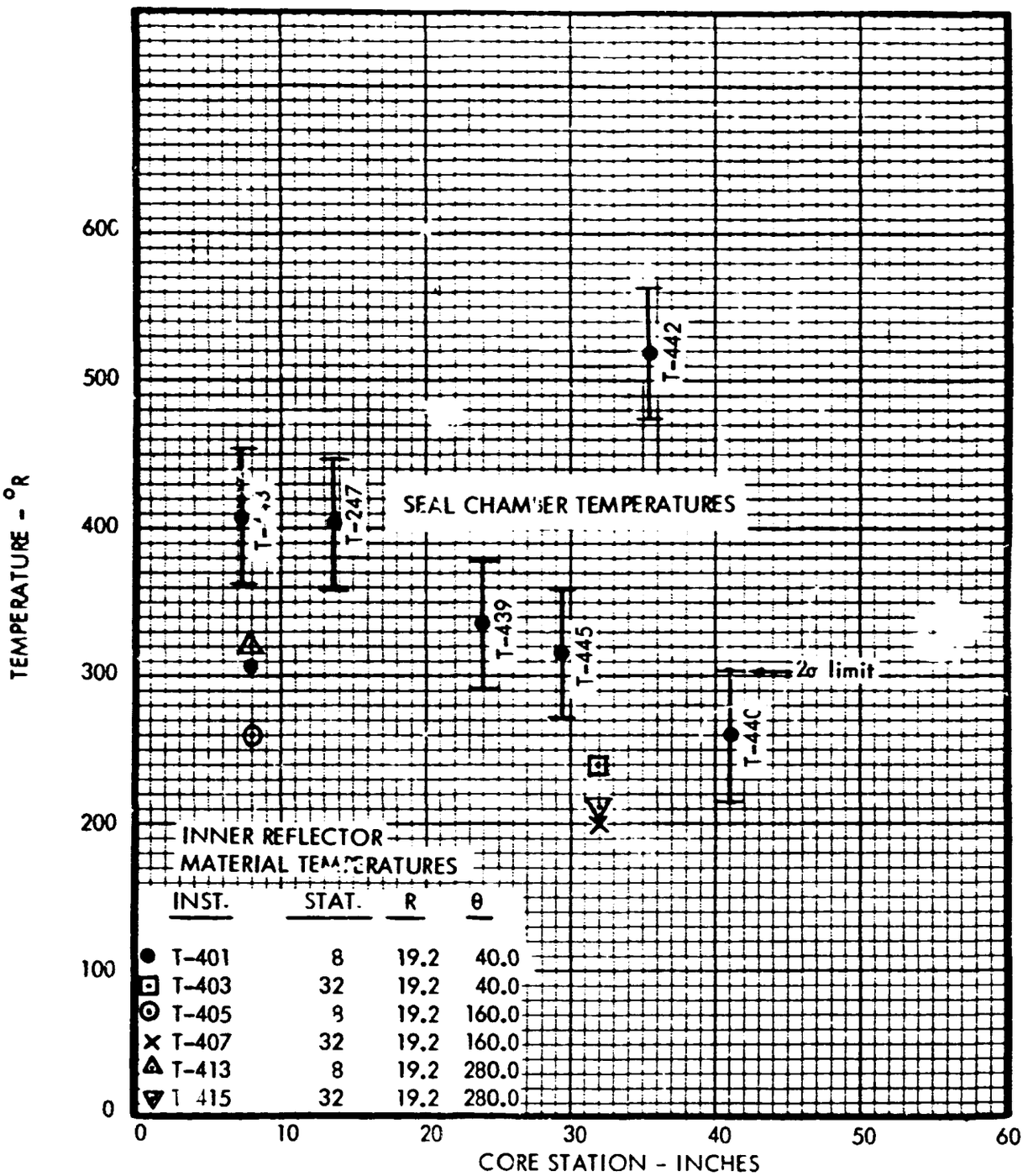

FIGURE 4.1-6 NRX-A2 EP-IV INNER REFLECTOR MATERIAL AND SEAL CHAMBER TEMPERATURES AT END OF PRECHILL (CRT 13692)

inner reflector material temperature as shown in Figure 4.1-5 is similar to the other reflector components shown in Figure 4.1-4. During the transient prechill, as expected, the inner reflector cylinder cooled more rapidly than did the drum and sector reaching a lower temperature at the end of the prechill.

A comparison between the measured values of reflector inlet and outlet plenum conditions with those predicted is shown in Figure 4.1-7 for the prechill interval. The calculated values for the startup period (after 13693 second) are based on a post-run TNT calculation.

Only the traces for the maximum and minimum temperature are shown for both the reflector inlet and outlet on Figure 4.1-7. The linear average of these bulk temperatures is shown by the 2 limit error band (95% confidence level) at the end of the prechill (CRT 13693) and start of the first power hold (CRT 13743). The reflector inlet temperature is the average of seven thermocouples and the reflector outlet temperature is an average of five thermocouples.

At the start of prechill the temperatures of the reflector inlet plenum dropped rapidly to a steady-state value of 43°R. The temperature of the outer reflector exit plenum decreased at a slower rate because of the heat pickup in the reflector system. At CRT 13693 the prechill ends and the startup begins. During the startup period the reflector inlet plenum temperature rises, and levels off at 90°R at the start of the first power hold (CRT 13742).

Astronuclear

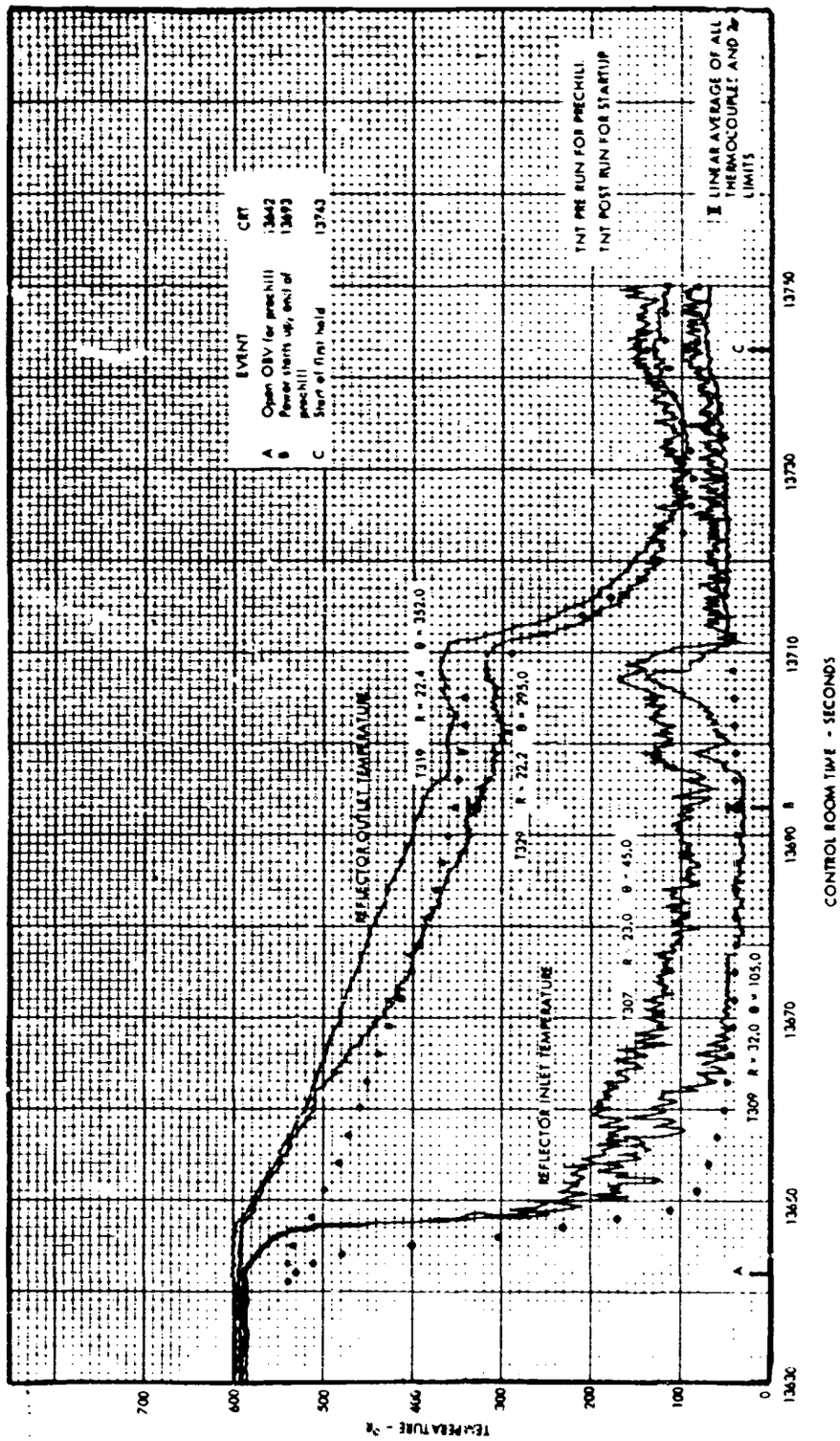

The reflector outlet temperature decreases after the initiation of prechill, and holds constant between CRT 13695 and CRT 13710. After CRT 13710, when the flow increased rapidly, the temperature decreased rapidly to a minimum value of about 100°R and there increased to its steady value of 140°R at the first power hold. The increase in temperature was the result of change in power to flow ratio of the reactor.

4.1.4 High Power Holds

In this section reactor performance and reactor component performance at the steady-state power holds are considered. Transient operation during the startup and shutdown are considered in the next section. Four operating times were chosen for examination of the experimental data and analyses which were required. These control room times (13790, 13900, 13985, and 14085 seconds), were selected as representative of steady-state operations during each of the four high power holds. The run profile on Figure 4.1-1 gives calculated thermal power, measured flow rate and measured nozzle chamber temperature. At the four steady-state times nozzle chamber temperature calculated from the nozzle equation are included.

A. Power Determination

The liquid hydrogen flow rates were calculated at the selected EP-IV hold times. Results of the calculations for the venturi meter upstream of the pump (FE-4) and the venturi downstream of the pump (FE-7) are used in Table 4.1-5.

TABLE 4.1-5

EP IV HIGH POWER TEST LH_2 FLOW RATES AND NOZZLE CHAMBER TEMPERATURE

Control Room Time (seconds)	13790	13900	13985	14085
Reactor Flow (lb/sec.)				
Inlet venturi (FE-4)	60.1	74.0	75.4	75.4
Discharge venturi (FE-7)	60.2	74.2	75.9	75.8
Average Flow Rate	60.1	74.1	75.6	75.6
2σ Error of Average Flow Rate	$\pm$ 1.6	$\pm$ 1.5	$\pm$ 1.5	$\pm$ 1.5
Tie Rod Channel Flow (lb/sec)	3.64	4.44	4.54	4.57
Lateral Support Flow (lb/sec)	0.28	0.35	0.36	0.36
Nozzle Chamber Temperature	2603°R	3390°R	3544°R	3815°R
2σ Error (°R)	$\pm$ 200	$\pm$ 210	$\pm$ 210	$\pm$ 215
Nozzle Chamber Pressure (psia) Average of p-122 and p-124	382	537.5	568.5	581.5

The tie rod flow rates given in the table were calculated for the experimental reactor operating conditions using the MCAP program. The lateral support system flow rates in the table were obtained by extending Data Book calculations* to A2 operating conditions. An experimental verification of these flow rates could not be made, primarily because of the questionable seal chamber temperature indications. Analyses in this report are based on the flow rates in Table 4.1-5, using the average FE-7 and FE-4 for reactor flow. Nozzle chamber temperature and reactor power is calculated from a heat balance using this average venturi flow rate. The two venturis are in good agreement, however, any systematic error in the LH_2 flow rate which was 6% higher than planned, would effect the reactor power levels calculated in this section.

Nozzle chamber temperature measurements were found to be considerably lower than the mixed mean nozzle chamber temperature calculated. The principle cause of this low indication by the chamber thermocouples is believed to be the proximity of the thermocouples to the nozzle wall, as discussed later in this section. The most accurate mixed mean nozzle chamber temperature was calculated from the nozzle flow equation.

---

* Reactor Analysis Data Book, WANL-TME-840.

$$W = KA\,P/\sqrt{T}$$

where

W = flow rate, lb/sec

P = nozzle chamber pressure, psia

T = nozzle chamber temperature, °R

A = nozzle throat area, 59.0 in.^{2} at operating temperature

K = flow coefficient, 0.138°R/sec average theoretical value x .985.

Test values of the chamber pressure and flow rate, a nozzle flow coefficient 1 1/2% less than theoretical, and measured nozzle throat area corrected to operating nozzle temperature were used in the chamber temperature calculation. The resulting nozzle chamber temperatures at the four steady state times and the 2 error based on flow and pressure accuracy and a ± 1% 2 error on the flow coefficient are given in Table 4.1-5. Chamber pressures used in this calculation which are an average of the two nozzle chamber pressure transducer indications are also included in the table. On Figure 4.1-1 the calculated values are compared to a typical nozzle chamber thermocouple indication.

A heat-balance was performed from the reflector inlet to the nozzle chamber to obtain reactor thermal power. Test pressure and temperature conditions at the reflector inlet gave the inlet enthalpy while nozzle chamber pressure and calculated temperature gave the nozzle chamber enthalpy. Thus, the thermal power in MW was calculated from the expression.

$$PWR = W\,(h_c - h_r)\,10^{-6}\,1055 + C$$

where PWR = total reactor thermal power in MW

W = reactor flow rate, lb/sec

h_c = nozzle chamber enthalpy, BTU/lb

h_r = reflector inlet enthalpy, BTU/lb

C = nuclear heating in the nozzle and radiation from core to nozzle, MW

The regenerative heat transfer between the hot and cold side hydrogen in the nozzle do not appear in the power expression because the hot side heat loss is cancelled by the cold side heat gain; however, nuclear heating in the nozzle and radiation heat transfer from the core to the nozzle are accounted for by "C" in the above expression. The value of C was calculated and found to be approximately 2 MW at design conditions. At part power operation the "C" was assumed to be directly proportioned to the power. The factors in the power calculation and the calculated power are given in Table 4.1-6.

Independent methods of obtaining the reactor power include "rabbits" which were irradiated for specific time intervals during the test, and neutronics tank detectors. Reactor thermal power evaluated by the rabbits, the neutronics tank linear number 2, and the heat balance are tabulated in Table 4.1-7 for the four steady state hold times. The agreement of these power measurements is well within the expected accuracy of these measurements.

TABLE 4.1-6

DETAILS OF HEAT BALANCE REACTOR POWER CALCULATION, EP IV

Control Room Time	13890	13900	13925	14085
Average Reflector inlet temp. (°R)	92	115	136	136
Reflector inlet pressure (psia)	636	687	731	751
Reflector inlet enthalpy (Btu/lb)	149	217	288	287
Nozzle chamber temperature from table 4-5 (°R)	2603	3390	3644	3815
Nozzle chamber pressure, from table 4-5 (psia)	362	537.5	568.5	581.5
Nozzle chamber enthalpy (Btu/lb)	9183	12259	13280	13991
Enthalpy rise (Btu/lb)	9034	12042	12992	13704
Average flow rate, from table 4-5 (lb/sec)	60.1	74.1	75.6	75.6
C (MW)	1.0	1.7	1.9	2
Reactor thermal power (MW)	574	943	1038	1096

TABLE 4.1-7

EP IV REACTOR THERMAL POWER AT STEADY STATE HOLDS

Control Room Time, Seconds	Heat Balance, MW	Rabbit MW	Neutronics Tank (Linear No. 2) MW
13790	574 ± 38	537^{+32}_{-72}	527^{+32}_{-72}
13900	943 ± 45	895^{+54}_{-120}	902^{+54}_{-120}
13985	1038 ± 49	979^{+59}_{-131}	983^{+59}_{-131}
14085	1096 ± 50	1059^{+63}_{-142}	1047^{+63}_{-140}

A2 TEST TOTAL REACTOR ENERGY COMPARISON

Detector	Energy release (watt-sec)
Linear neutronics	3.67×10^{11}
Rabbit	3.59×10^{11}
Thermal	3.81×10^{11}
Post Test Radiochemistry	$3.68 \times 10^{11} \pm 0.157 \times 10^{11}$

Also an indirect indication of the adequacy of the power level measurements can be made from another independent source, the total integrated A2 power obtained from post-test radiochemistry. The integrated power from this source and from integrating the linear neutronics power, the rabbit power and the heat balance power are given at the bottom of Table 4.1-7. The total energy obtained from radiochemistry* with the assigned accuracy is indicated in the table. Accuracy on three energies obtained from integrating the power data are not given because of the unknown error associated with the integration. The agreement of the total energy release is very good, with a total variation of less than 6% for all four sources. Thus, the radiochemistry results provide an added confirmation of the maximum power level. Heat balance calculated power is used for all calculations described in this report. This power level was selected because its precision is the best of all the methods used.

A power level could also have been calculated from the measured core temperatures using measured flow rate and core inlet conditions. Rather than make this additional power comparison, core temperatures were calculated from reactor flow rate and reactor power (from heat balance) and compared to measured core temperatures. These comparisons are made later in Section 4.1.

---

* Radiochemistry Measurements on NRX-A2, NTO-M-1671, December 14, 1964.

B. Reactor and Feed System Conditions

For control room time 14085 at the maximum power hold operating cycle point conditions are given in Figure 4.1-0. All values in the cycle diagram are test data or follow directly from test data unless denoted by an asterisk. These asterisked values were calculated using the best available data and are the best estimate of actual operating conditions. In cases where both a test and calculated value is included, the test data is considered to be unreliable.

The steady operation was at an off-design condition of about 98% power and 105% flow (1096 MW and 75.6 lb/sec). The notable variations from cycle conditions which would be expected at this operating condition, all of which are considered in detail in the following portion of this section were:

1. Reflector inlet temperature 15°R high due to about 30% more heat pickup in nozzle.
2. Core inlet temperatures 35°R high due to 15% more heat generation in reflector and high nozzle coolant heat pickup.
e. Core P 5% low.

C. High Power Holds, Core

1. Core Inlet Temperatures

The core is designed and orificed to run with a flat radial temperature profile (within a tolerance band due to the use of finite orifice sizes). To achieve this profile the core must operate at the design inlet temperature and control drum angle. The inlet temperature is important because the orifice pressure drops depend on the hydrogen properties. With other conditions held constant, a reduction in inlet temperature from the design value will cause a reduction in the impedance across every orifice. The core pressure drop will be reduced as a result, but the more important effect is a redistribution of flow between the fuel element channels. The result is an excess of flow in the low power factor channels and starving of the high power factor channels.

Orificing of the NRX-A2 core took place well in advance of final determination of sufficient information to make a firm prediction of the core inlet temperature. Orificing was based on 250°R core inlet temperature and a 90° hot drum angle. Subsequently, the nozzle change caused a reduction in pre-run calculated core inlet temperature at full power design conditions to 210°R. This occurred too late to make a change in the orificing but the effects of off-design inlet temperature were included in the calculation of expected core temperatures and hot channel factors. Using the pre-run method based on maximum test conditions of 1096 MW and 75.6 lb/sec flow, the core inlet temperature was calculated to be 190°R. However, the measured average inlet temperature was 245°R at maximum power (CRT 14085).

There were three reasons for the high measured values of core inlet temperature:

(1) The measured nozzle tube exit temperature was 20°R higher than calculated.

(2) The measured heat pickup in the reflector region was high by about 15%.

(3) There was high measured heat pickup from the dome end plenum to the core inlet.

These factors were investigated in detail*.

[illegible]. Core Pressure Measurements

Two sensors, P-122 and P-124, that were located in the nozzle chamber operated reliably during the high power holds. There was one pressure measurement in the core inlet plenum, P-604. The core pressure drop was measured by one instrument, DP-603. The core pressure drop agreement between DP-603 and the difference between absolute pressure measurements at the core inlet and exit was within 1-1/2 psid or less.

The measured core inlet pressure is on line 4, Table 4.1-8. Line 10 contains measured core exit (nozzle chamber) pressures and line 12 the measured core pressure drop. The maximum measured core pressure drop of 121.2 psid occurs [illegible] CRT 14085 during the highest power hold.

[illegible]. Core Temperature Measurements

Thermocouples

During the four high power holds, the thermocouple

[illegible] Performance, NAML-TMR-199, January 1965, CRD

TABLE 4.1-8

TEST VALUES AND POST TEST CALCULATIONS AT FOUR STEADY STATE HOLDS

Control Room Time Power in watts (thermal)	13790 (574 MW)	13900 (943 MW)	13985 (1038 MW)	14085 (1096 MW)
Core Inlet Temperature, °R				
Calculated	153 ± 9	204 ± 9	220 ± 9	225 ± 9
Measured*	172	219	233	245
Core Inlet Pressure, Psia				
Calculated	462 ± 12.9	652 ± 12.8	691 ± 12.7	707 ± 12.7
Measured	460 ± 13	648 ± 13	686 ± 13	701 ± 13
Fuel Element Gas Exit Temp., °R				
Calculated	2753 ± 200	3579 ± 210	3839 ± 210	4013 ± 215
Maximum Fuel Temp., °R				
Calculated	2937 ± 200	3751 ± 210	4016 ± 210	4327 ± 215
Highest Measured	3180 ± 105	4000 ± 105	4050 ± 105	4400 ± 200**
Tie Rod Exit Temperature, °R				
Calculated	374	453	485	499
Measured	513 ± 26	611 ± 26	657 ± 26	690 ± 26
Core Exit Pressure, Psia				
Measured	381 ± 10	536 ± 10	567 ± 10	580 ± 10
Core Pressure Drop, Psid				
Calculated	81 ± 8.1	116 ± 8.0	124 ± 7.8	127 ± 7.8
Measured	78.7 ± 3	111.7 ± 3.6	118.7 ± 3.6	121.2 ± 3.6
Shield Dome End Temperature, °R				
Measured	148 ± 7.5	196 ± 7.5	211 ± 7.5	216 ± 7.5
Total Flow, lb/sec				
Measured	60.1 ± 1.6	74.1 ± 1.5	75.6 ± 1.5	75.6 ± 1.5
Nozzle Chamber Temp., °R				
Measured	2603 ± 200	3300 ± 210	3644 ± 210	3815 ± 215

*Core Inlet Temperature Thermocouple Readings Uncorrected for Internal Heat Generation - The Correction is Approximately a 20 - 30°R reduction.

**Highest Thermal Capsule reading at Station 45 Inches.

measurement of core material temperatures showed the expected pre-test trends, except for the station 32 thermocouples. Figure 4.1-8 contains the time history of one station 45 core material thermocouple and two station 32 core material thermocouples. The trace of the station 45 thermocouple, T-632, was typical of all station 45 T/C's and was as expected. When the temperature exceeded about 3700°R, the thermocouple degraded and gave an approximately constant indication regardless of temperature. This saturation is the reason station 45 T/C's were not selected for reactor control. The station 32 thermocouple, T-647, indicated temperatures very close to the expected trend at this location, however, this T/C was the only station 32 T/C which indicated the expected temperature. T-643 on Figure 4.1-8 is typical of the behavior of the rest of the station 32 T/C's. They diverged from the expected material temperature during the rise to the second hold and indicated temperatures up to 1200°R low. Section 4.5 discusses thermocouple results in detail.

The 2σ error in a single thermocouple reading during all high power holds at station 20, 32, or 45 is ± 105°R. This is based only on the data acquisition system, instrument error, and reading error. The 2σ error in the calculated temperature at station 45 will be discussed along with the method of post-test calculations.

b. Thermal Capsule Temperature Measurement Description

The utilization of thermal capsule temperature measurement, contrasted to the thermocouple, does not provide a temperature time history. Thermal capsule temperatures are determined during post-operative inspection and define maximum temperatues experienced for each specific

Astronuclear

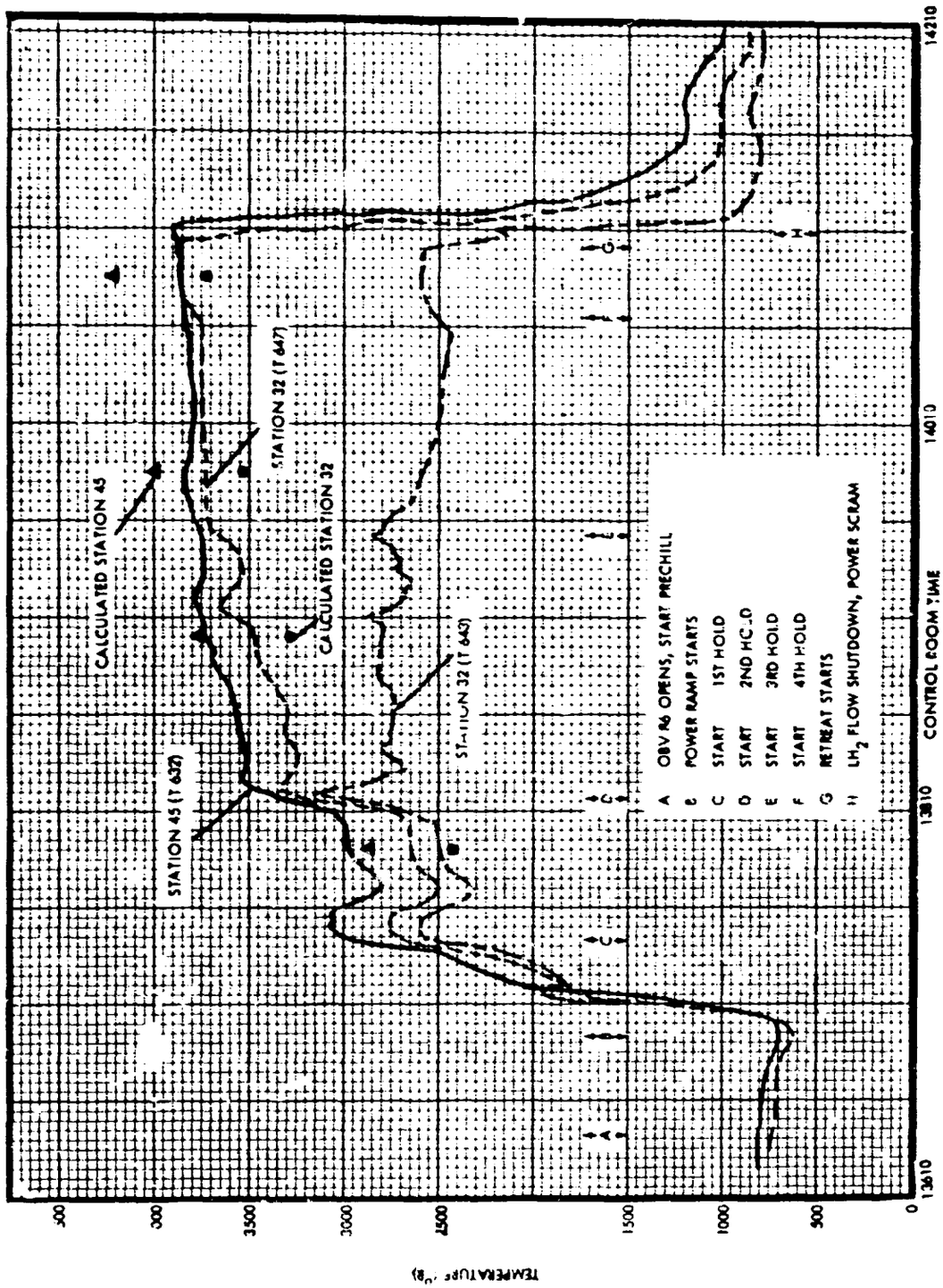

placement. Two inherent advantages of the thermal capsule over the thermocouple are, (1) determination of an axial temperature profile for each thermal capsule placement and (2) no instrumentation leads. When installed, these units are potted in permanently and do not perturb the design geometry.

Evaluation of NRX-A2 thermal capsule results of in-core temperature distribution are presented for the central region which essentially define a radial condition whereas the peripheral region reflects radial and small measured azimuthal effects. Figure 4.1-9 shows thermal capsule results of axial temperatures in the central region in which the radial temperature at the hot end of the core was within 400°R. Two shaded areas are identified in Figure 4.1-9. Area I bounds 11 axial profiles which indicate temperatures at station 45 in the range of 4300°R to 4350°R inclusive. Area II covers 8 profiles with temperatures at station 45 in the range inclusive of 4150°R to 4250°R. Because of control drum effects, the temperature distribution in the periphery was wider. Figure 4.1-10 shows a maximum spread of 500°R in the peripheral region. Area I of Figure 4.1-10 covers profiles in the range of 4350°R - 4400°R; area II has 19 at 4200°R - 4300°R, and area III covers 8 in the range including 4000°R to 4150°R. Figure 4.1-11 is a radial plot of the station 45 thermal capsule readings.

Thermal capsule temperature measurement in the core filler strips consisted of three placements. Figure 4.1-12 shows the thermal capsule family distribution as well as the calculated axial temperature distribution The test results indicate that the temperatures in these instrumented filler strips were greater than 2678°R at the mid-core plane as well as at

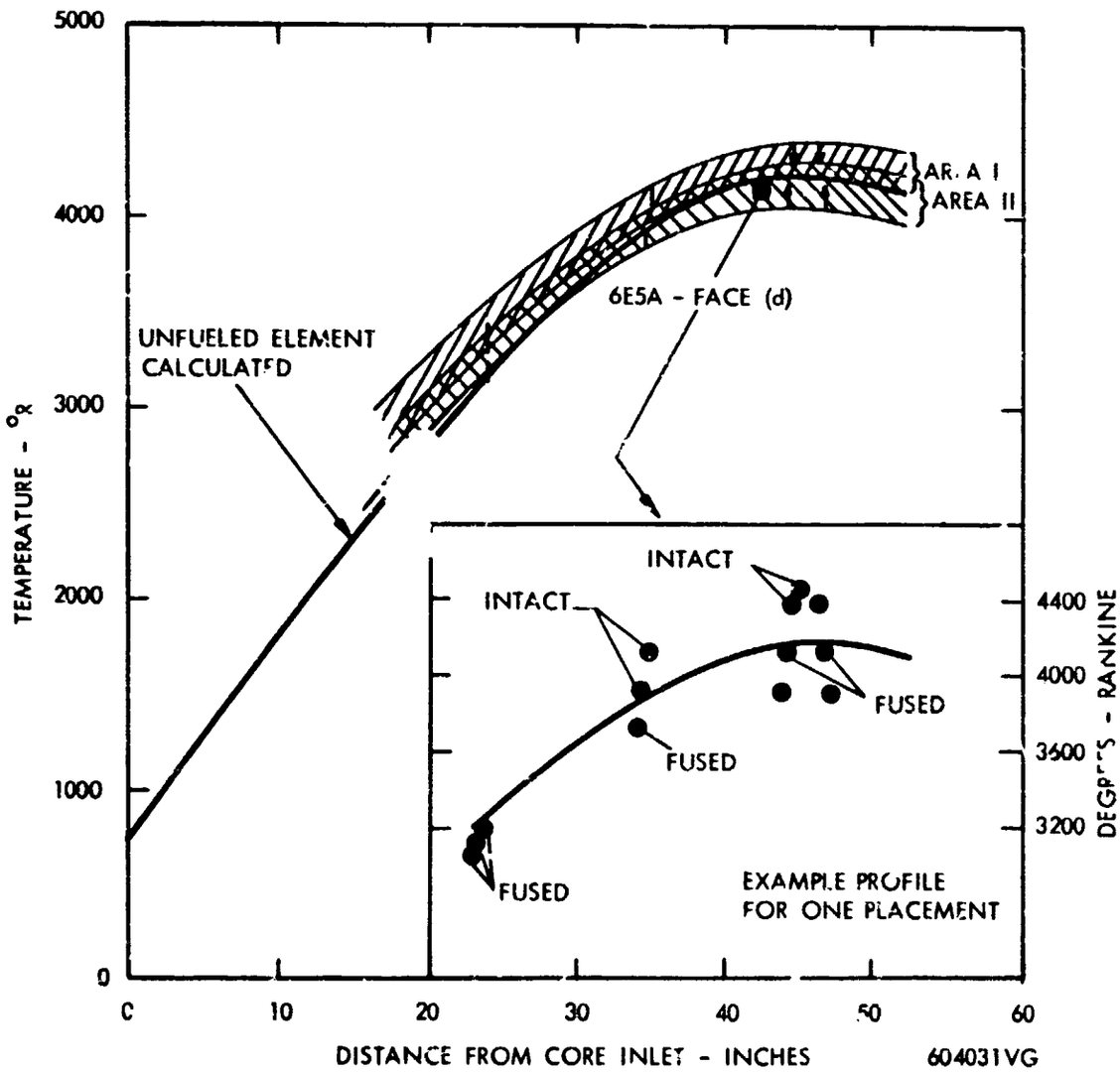

FIGURE 4.1-9 - NRX-A2 THERMAL CAPSULE DATE PRELIMINARY
19 RADIAL POSITIONS IN CORE CENTRAL
REGION

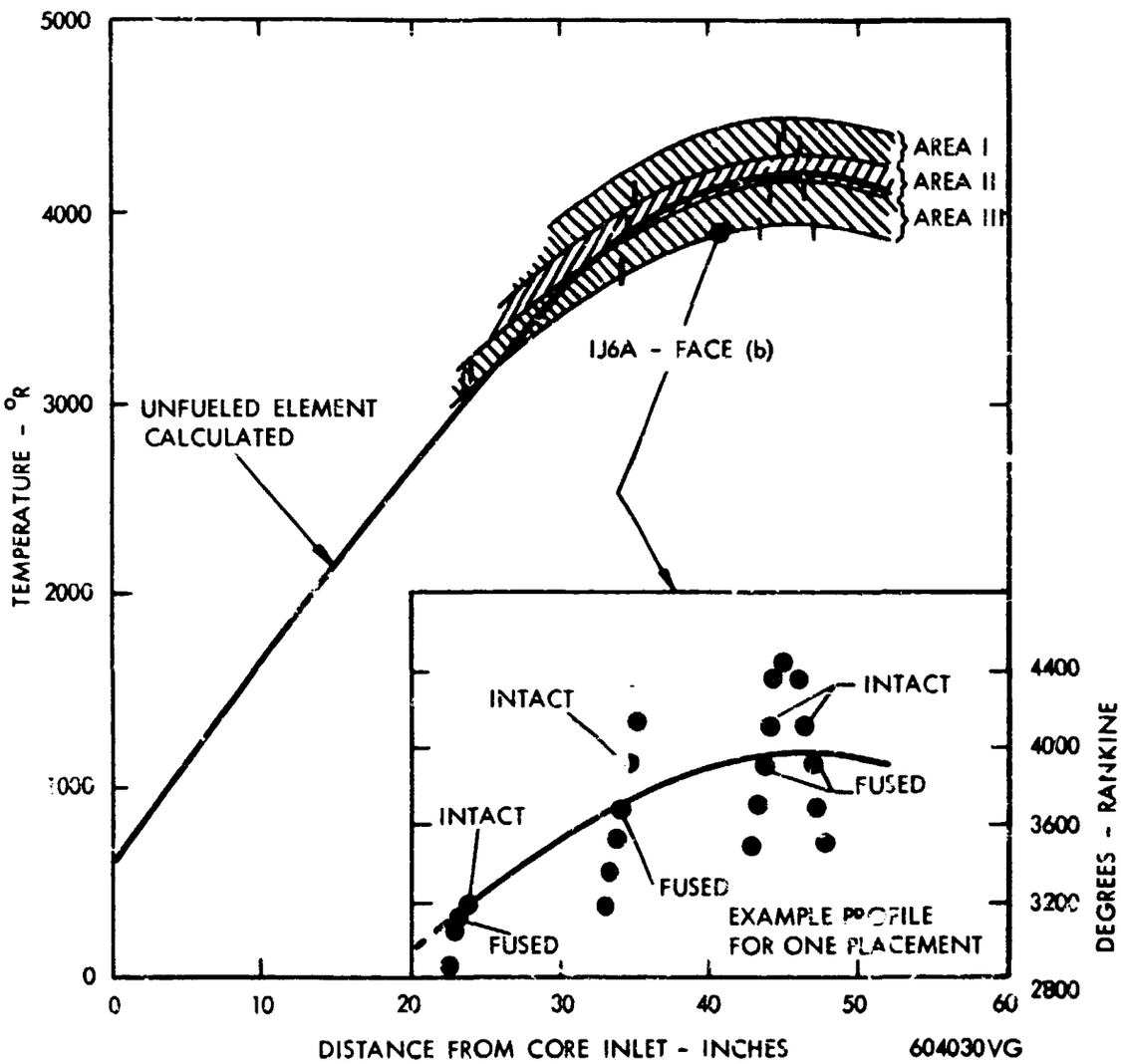

FIGURE 4.1-10 - NRX-A2 THERMAL CAPSULE DATA PRELIMINARY
34 RADIAL POSITIONS IN CORE PERIPHERY

CONFIDENTIAL
RESTRICTED DATA
Atomic Energy Act — 1954

Astronuclear

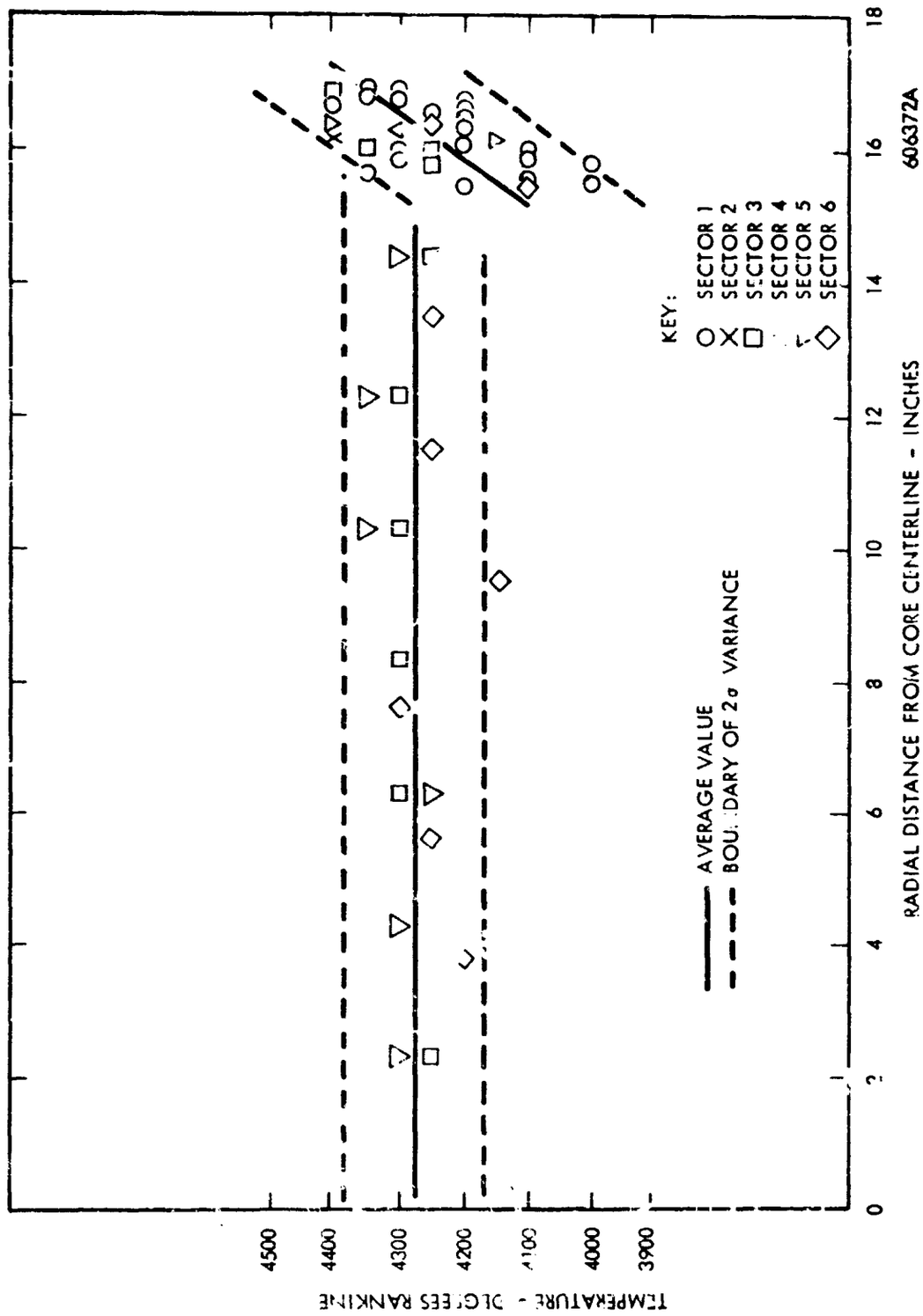

FIGURE 4.1-11 - RADIAL PLOT OF STATION 45 THERMAL CAPSULE READINGS

CONFIDENTIAL
RESTRICTED DATA
Atomic Energy Act — 1954

CONFIDENTIAL
RESTRICTED DATA
Atomic Energy Act - 1954

RESTRICTED DATA
ATOMIC ENERGY ACT
OF 1954

FIGURE 4.1-12
NRX-A2 CORE PERIPHERY FILLER STRIP TEMPERATURE
THERMAL CAPSULE TEST DATA

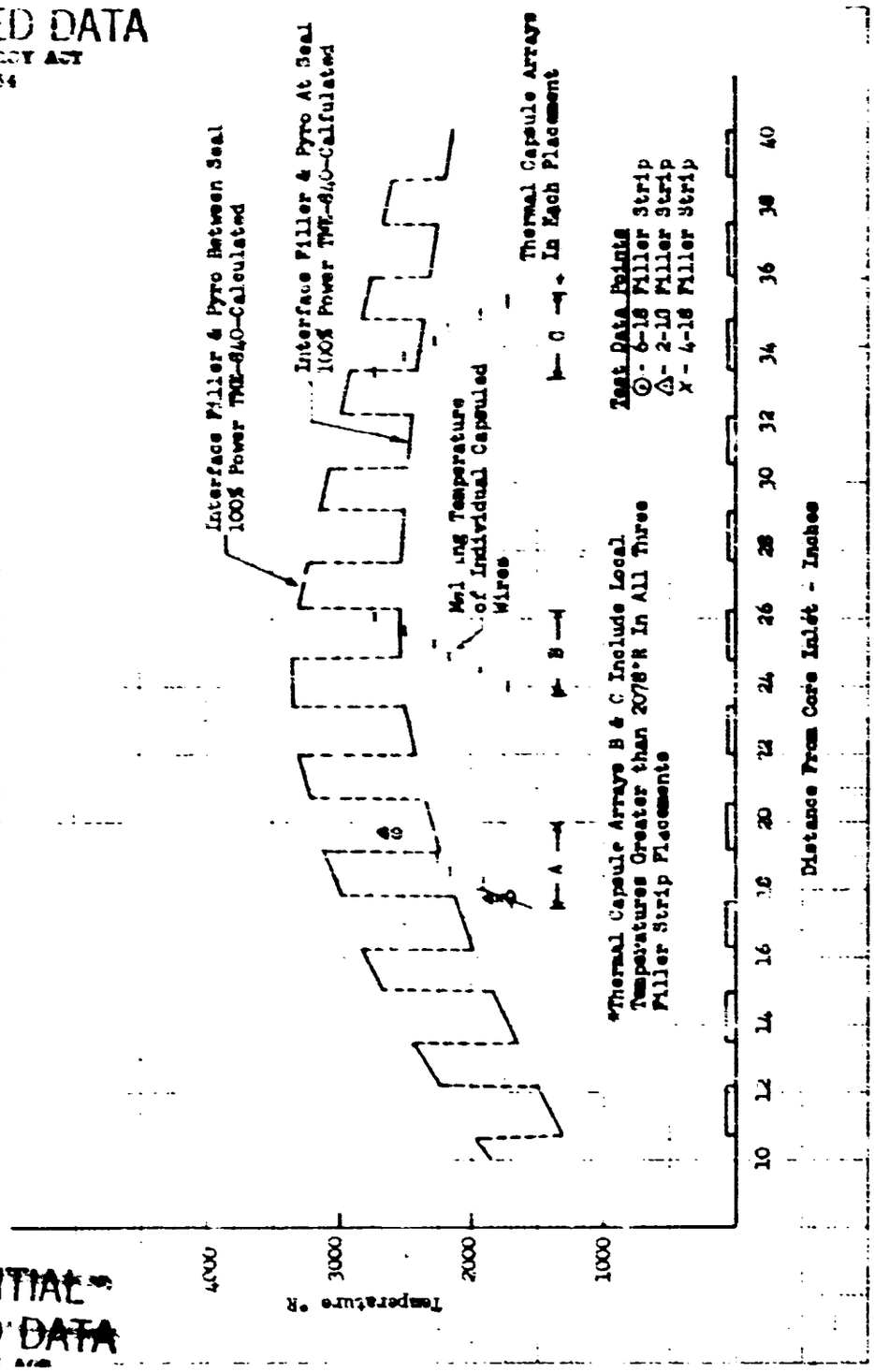

NFIDENTIAL
RICTED DATA
ATOMIC ENERGY ACT

CONFIDENTIAL
RESTRICTED DATA
Atomic Energy Act - 1954

station 33. At stations 18-21, however, the measured temperatures tend to complement the predicted calculated values.

Temperature levels of these three filler strips when compared circumferentially reflect a similar trend of temperature levels that were measured in the core periphery.

4. Post Test Calculation of Core Operating Conditions

a. Pressure Drop and Average Axial Temperature Distribution Calculation

Post-test calculations with NCAP and the tie rod program were performed utilizing measured input parameters at the four hold times. The purpose of these calculations was to obtain core P and nominal axial temperature distributions. The procedure adopted closely followed the method used for core design.

There was sufficient data redundancy to make possible a choice of alternate procedures, for example, specifying the flow and calculating the pressure drop or vice versa. The measured values having the highest accuracy which were chosen as input for post-test calculations are core exit (or nozzle chamber) pressure, shield dome end plenum temperature (used in Section (1) to calculate core inlet temperature), total reactor flow, and nozzle chamber temperature. The measured values which were used as input at the four high power holds are summarized in Table 4.1-8, lines 10, 13, 14, and 15, respectively. A summary of the post-test calculated and measured core parameters at each of the four power holds is also given in that table. The calculated values for core pressure drop are within 5% of measured and are consistently on the high side. This suggests a possible systematic difference in

friction factor, channel roughness, additional leakage, or an error in total reactor flow rate or power. Details of these calculations are present elsewhere .

Figures 4.1-13, 14, 15, and 16 show the calculated axial temperature distribution for the average power factor at each of the four high power holds. Also shown is the average and spread of all thermocouple and thermocapsule measurements. There is a 2σ error in each calculated temperature caused by the errors in measured reactor flow, inlet temperature, and nozzle chamber temperature. These are directly applicable to determine the agreement between measured and calculated values to a 95% confidence level.

The consistently low calculated temperatures indicate that a systematic error is in the analysis, even though agreement at station 45 is within the 2σ limits. There are several possible reasons measured temperatures could be higher than calculated including an error in measured total reactor flow and/or power.

An analysis** of the effect of gamma heating on thermocouple installed at station 45 showed that the thermocouple readings operate about 72°R above the shim hole wall temperature. Investigation is continuing into the effects of gamma heating at the other core stations.

b. Radial Temperature Variations

Since the control drum angle and core inlet temperature

* NRX-A2 Reactor Performance, WANL-TMR-199, January 1965, CRD
** Effect of Gamma Heating on a High Temperature Thermocouple, WANL-TME-1076, January 1965, CRD

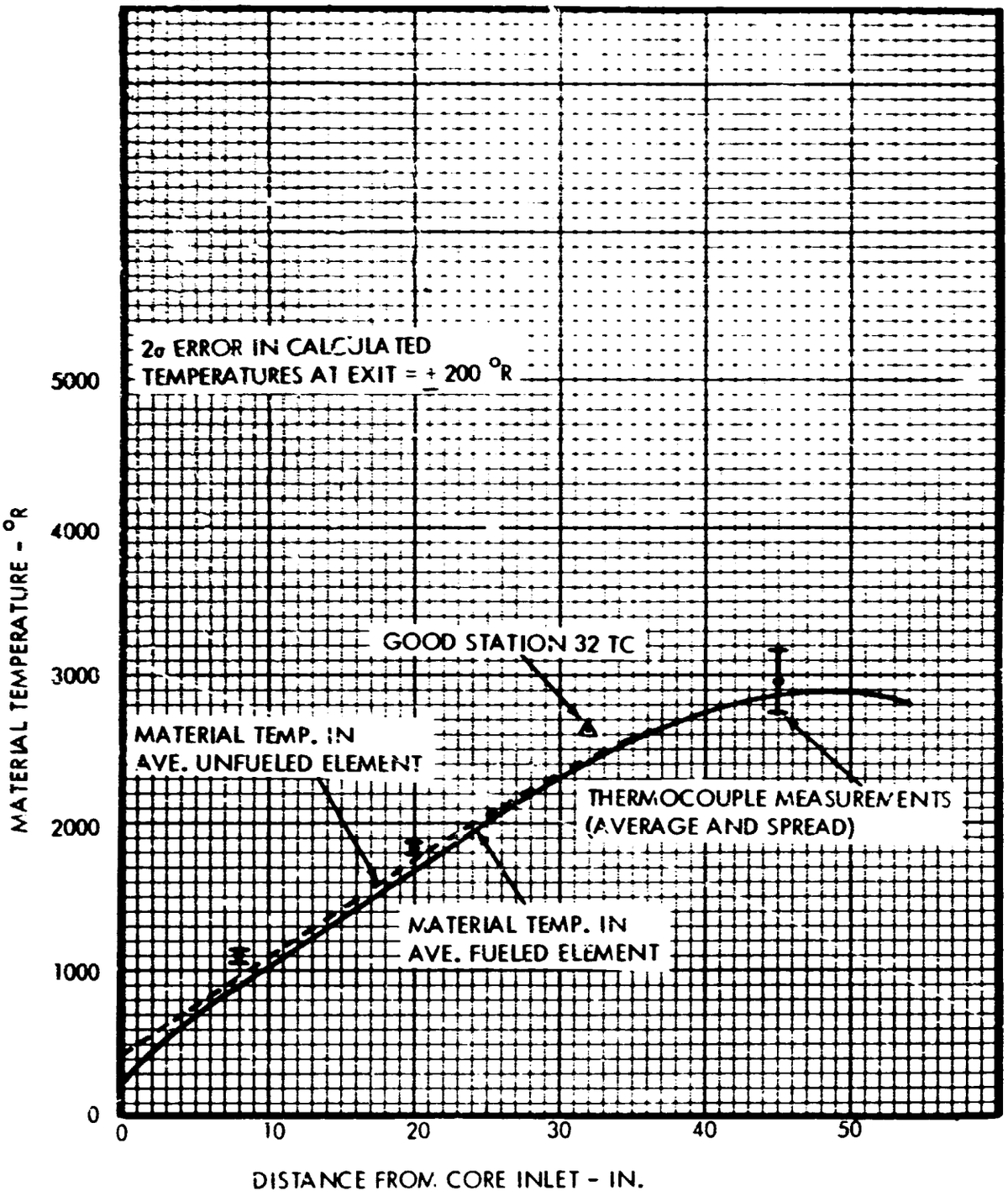

FIGURE 4.1-13 - AXIAL TEMPERATURE PROFILE IN AVERAGE FUELED AND UNFUELED ELEMENT CRT-13790 (581 MW)

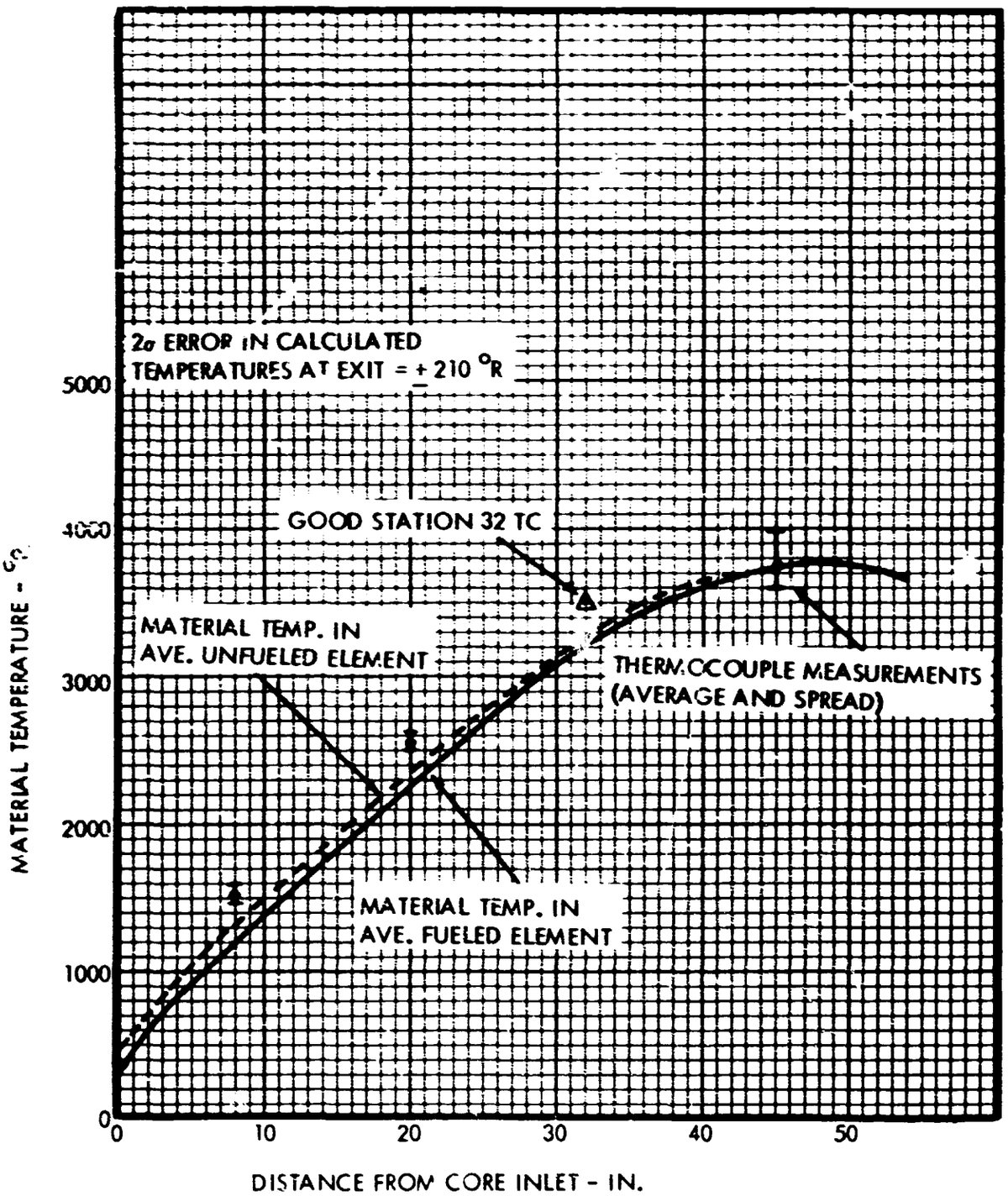

FIGURE 4.1-14 AXIAL TEMPERATURE PROFILE IN AVERAGE FUELED AND UNFUELED ELEMENT CRT-13900 (953 MW)

CONFIDENTIAL
RESTRICTED DATA
Atomic Energy Act - 1954

Astronuclear

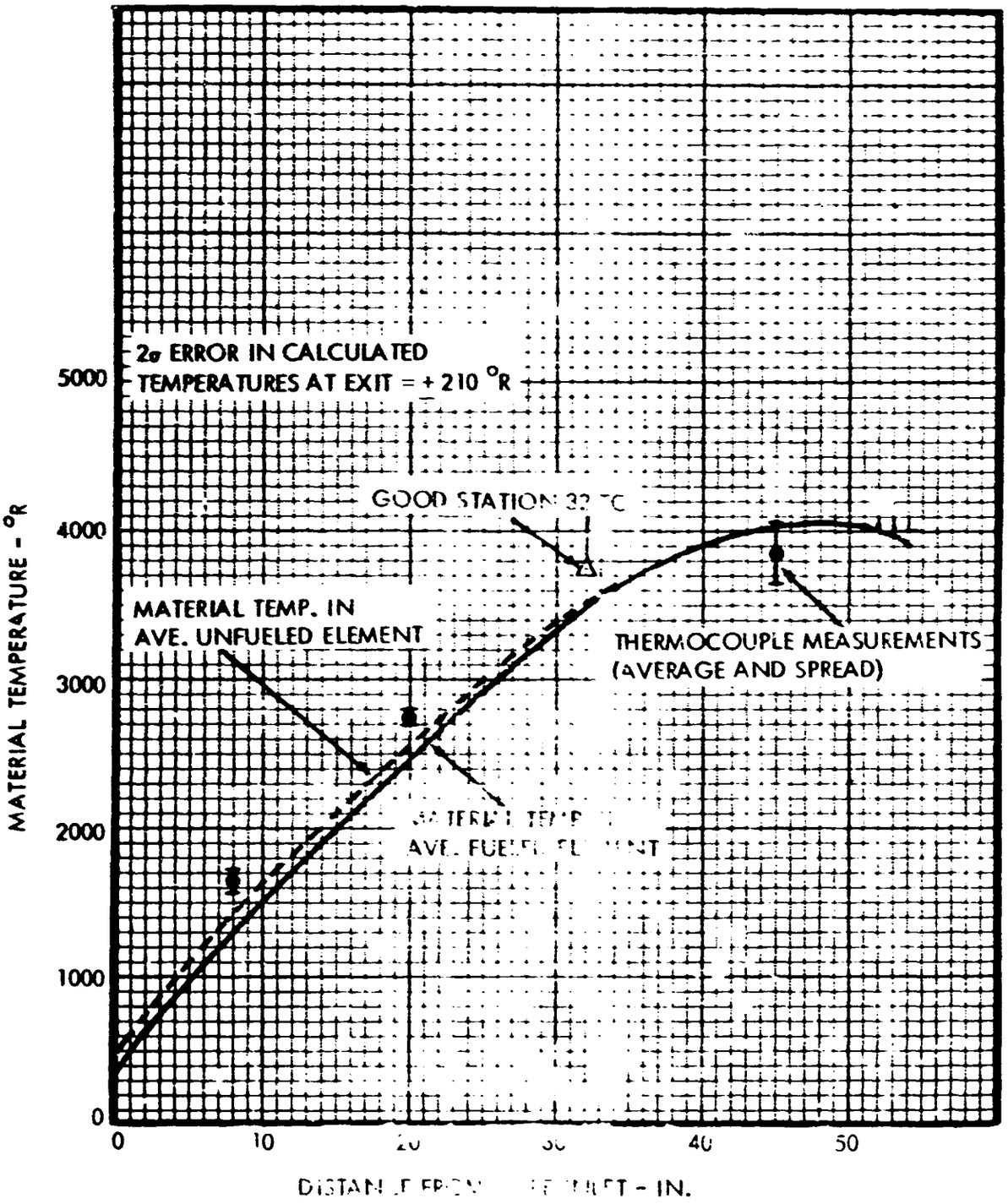

FIGURE 4.1-15 AXIAL TEMPERATURE PROFILE IN AVERAGE FUELED AND UNFUELED ELEMENT SRT-13983 (1951 MW)

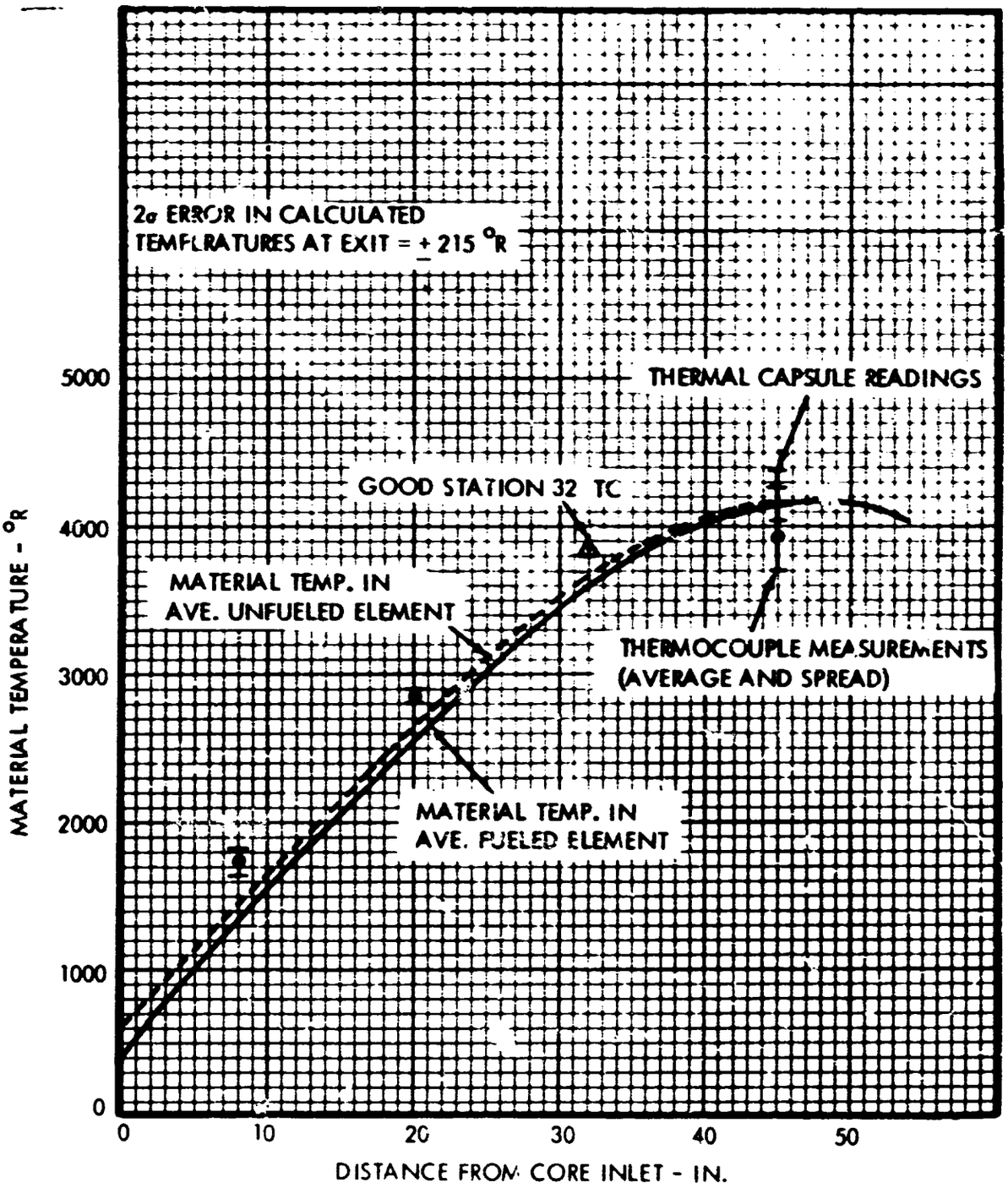

FIGURE 4.1-16 AXIAL TEMPERATURE PROFILE IN AVERAGE FUELED AND UNFUELED ELEMENT CRT-14085 (1096 MW)

during all four high power holds in IP-IV were off-design, the radial temperature distribution is not flat. The 90° control drum angle was used to calculate the pressure drop and the average fuel temperature, since these are not significantly affected by the drum angle. The effects of the off-design inlet temperature can be seen in the radial temperature profile for the 90° drum angle in Figures 4.1-17 and 4.1-18. The high power factor channels, which are starved by a lower than design inlet temperature are located near the core centerline and at the outer edge of each peripheral loading zone (approximate radius 14.6, 15.4, and 17 inches). The highest temperatures are seen to occur in these locations.

The radial temperature profile at the operating drum angle was obtained by adjusting the prediction results from the 90° angle. The per cent change in power factor with drum angle is known at each core location and the change in gas exit temperature with per cent change in power factor is known from parametric data. The gas exit temperatures at 90° drum angle were then adjusted at each radial location according to the drum position.

The off-design drum angles will cause the power to be suppressed near the core centerline and increased near the core periphery. The comparison for drum angle 99.6° versus 90° in Figure 4.1-17 and 103° versus 90° in Figure 4.1-18 should be noted. It is seen that the off-design drum angle tends to flatten the radial temperature distribution in the core central region and amplify the temperature increase with radius in the core periphery. These qualitative results were observed in a statistical treatment of the thermal capsule measurements. The 2 random element-to-element variation in

CONFIDENTIAL
RESTRICTED DATA

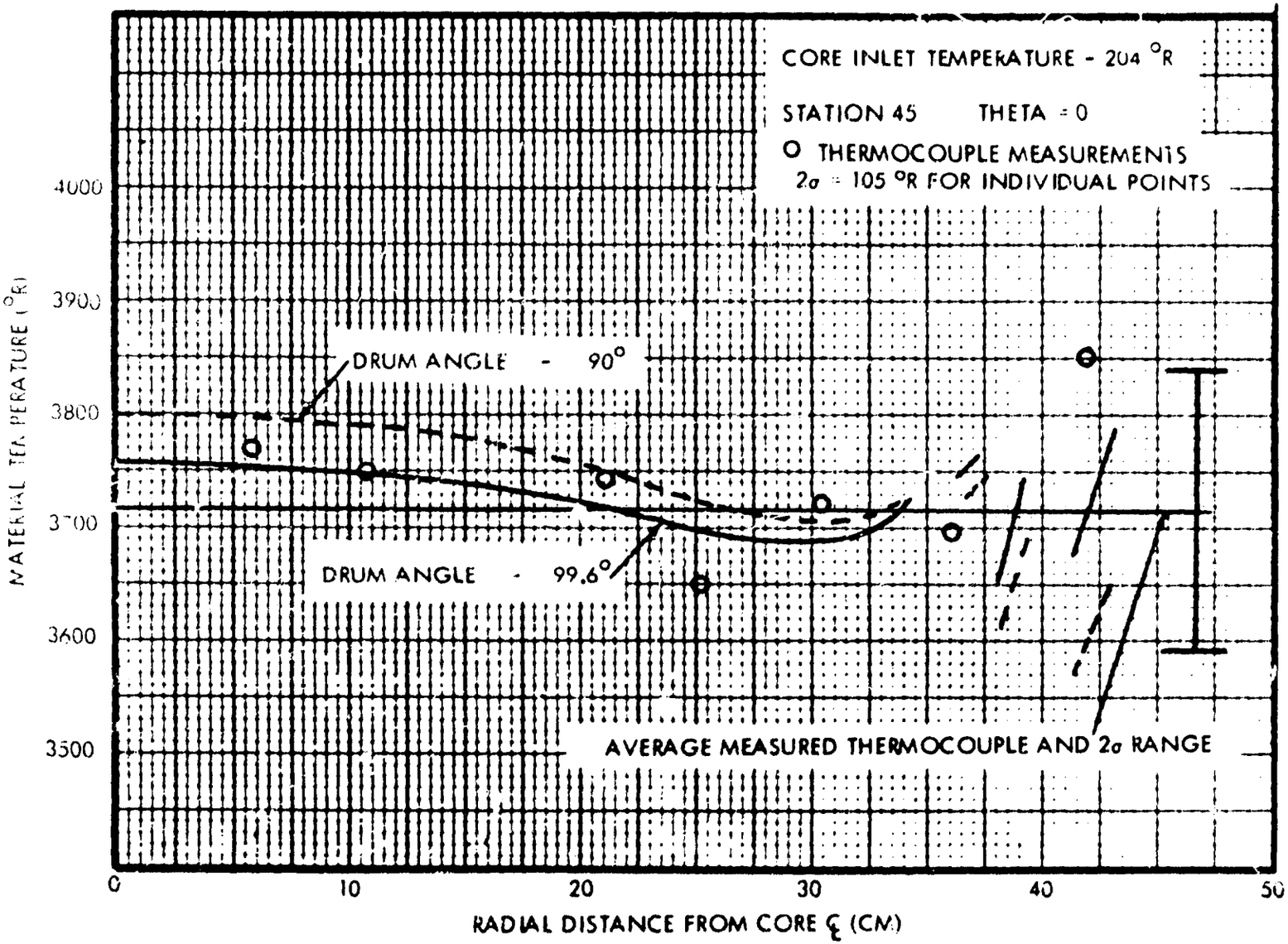

FIGURE 4.1-17 NRX-A2 EP-IV CALCULATED AND MEASURED RADIAL TEMPERATURE PROFILE CRT-15900 (953MW)

CONFIDENTIAL
RESTRICTED DATA

Astronuclear

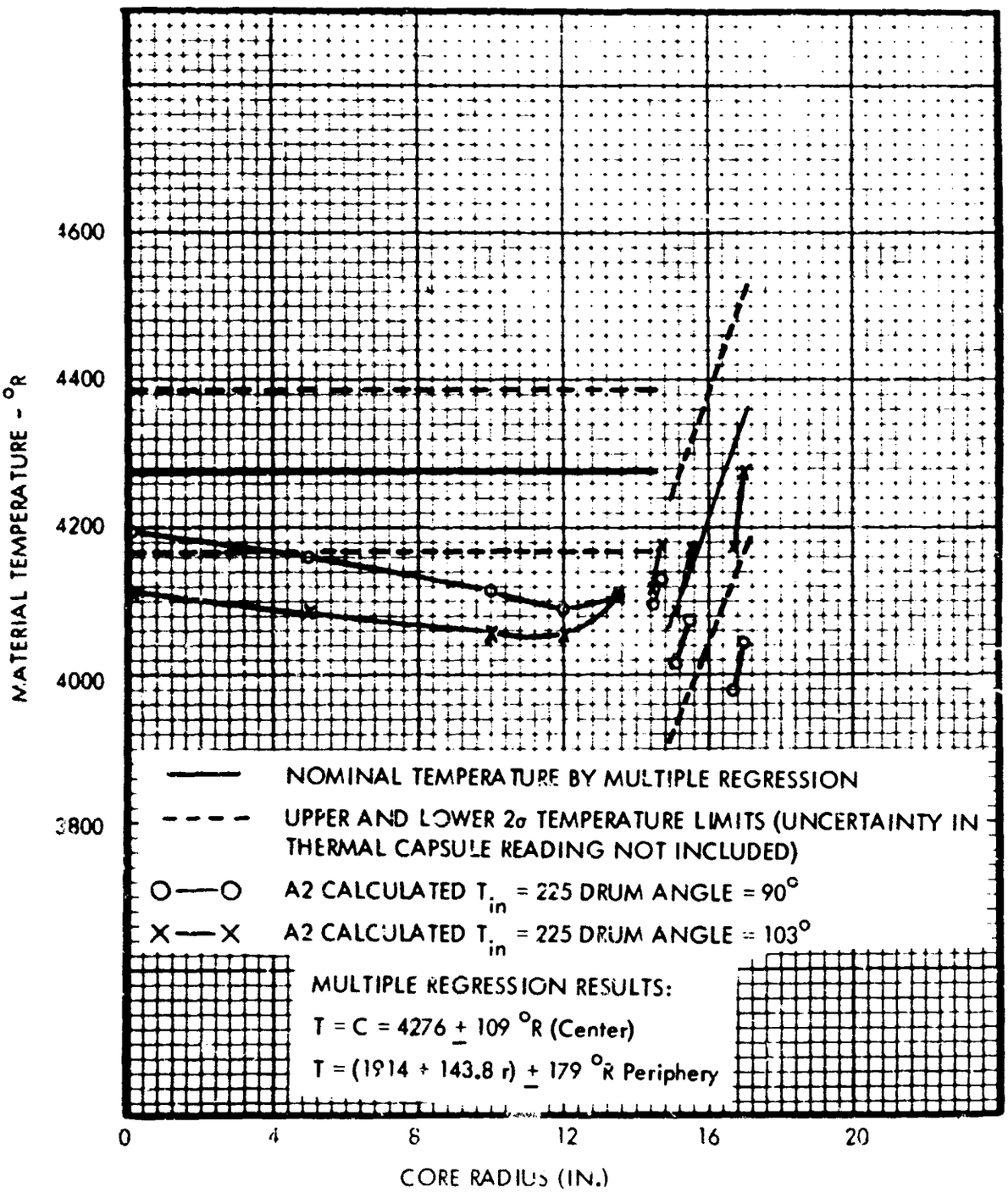

FIGURE 4.1-18 COMPARISON OF NRX-A2 THERMAL CAPSULE RESULTS WITH POST-RUN CALCULATIONS AT HIGH POWER HOLD STATION 45

temperature in the core central region was ± 109°R and in the peripheral region it was ± 179°R. No statistically significant variation in temperature with radius was measured in the core central region.

In the core periphery, the measured temperature is a significant function of radius. The calculated temperature is also a function of radius, although the calculated fine structure was not picked up in the thermal capsule data. In order to accomplish such an analysis, more measurements are required.

c. Maximum Calculated Fuel Temperatures

The maximum calculated nominal fuel temperature at CRT 14085 is found at the core periphery in fuel element J5J. This element because of its location is strongly affected by the control drum position. The average power in the element increases by 6.2 per cent due to a drum angle change from 90° to 103°. Using the previously described results for a control drum at 90° with the average element power factor, the maximum fuel temperature was 4048°R and after increasing the power due to drum angle effects, the maximum fuel temperature is 4327°R. This temperature carries a ± 215°R tolerance due to errors in the measured input parameters of inlet temperature, flow, and nozzle chamber temperature as indicated in Table 4.1-8. The maximum measured temperature in the core periphery was 4400°R using thermal capsule data. These temperatures and other statistical data are summarized in Table 4.1-9.

d. Tie Rod Temperature

Measured tie rod exit gas temperatures are higher than predicted as indicated on Figure 4.1-19. In an attempt to resolve the differences between measured and predicted values, an uncertainty analysis was

TABLE 4.1-9

MAXIMUM FUEL TEMPERATURES AT HIGH POWER HOLD CRT 14085 (1096 MW)

Maximum nominal fuel element temperature (calculated station 45)	4327°R ± 215
Calculated 2σ hot spot fule temperature	4734°R
Calculated 2σ element to element temperature variation	
Central region	155°R
Peripheral region	179°R
Maximum indicated temperature (thermal capsule)	4400°R
Element to element temperature variation based on thermal capsules	
Central region	109°R
Peripheral region	179°R

Astronuclear

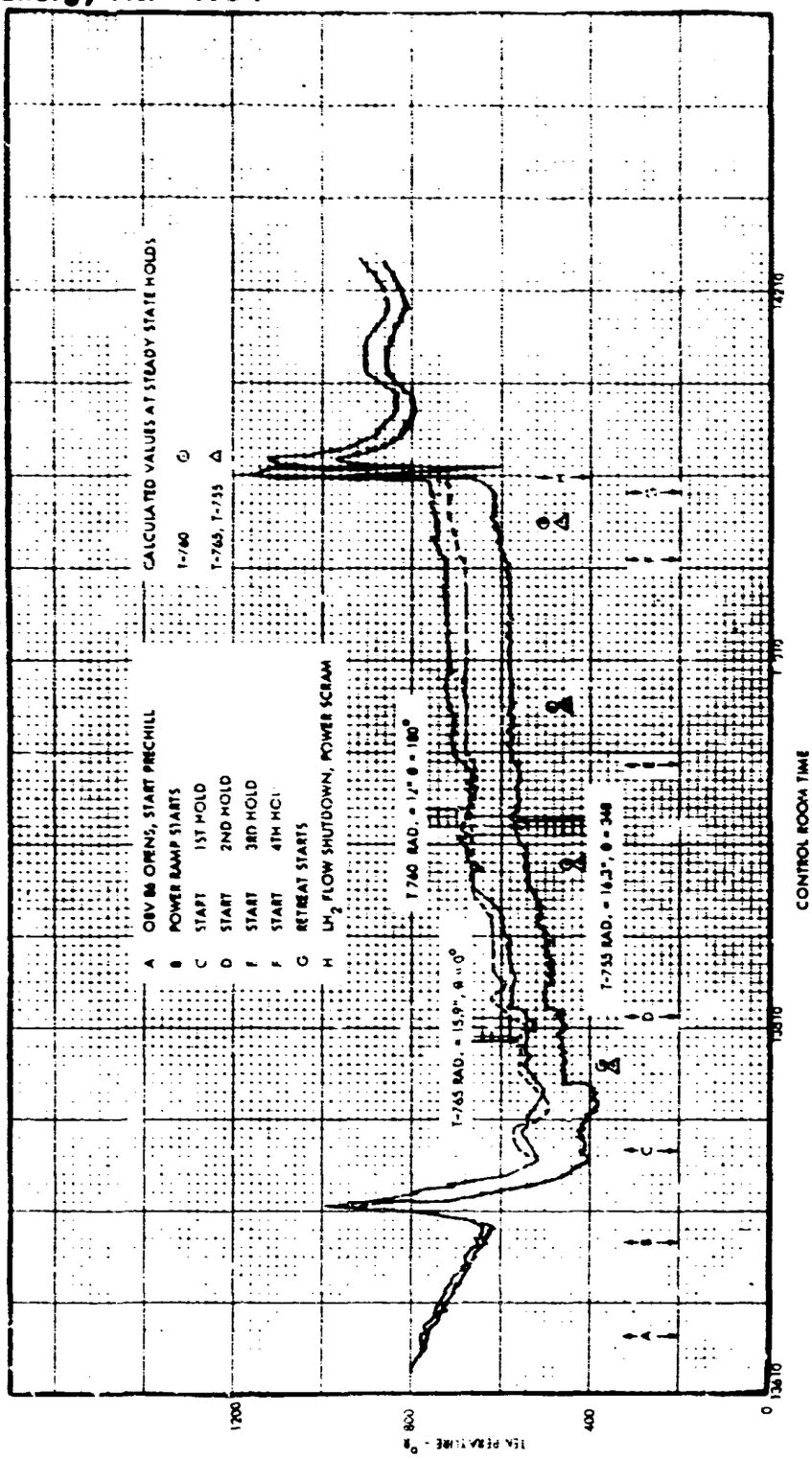

FIGURE 4.1-19 TIE ROD EXIT GAS TEMPERATURE PROFILE RP-IV

performed on the variation in the tie rod centering bushing loss coefficient, variations in the heating in the unfueled graphite, variations in core inlet temperature, variations in the thermal conductivity of the pyrographite insulating sleeves, variations in the hydrogen gap thickness between the stainless steel liner and the pyrographite insulating sleeve, and variations in thermocouple readout. These variations were considered to be the major contributors to the increase in the tie rod exit gas temperatures.

Tie rod exit gas temperatures from four unfueled elements, 000 (T-750), 4F1A (T-760), 6J9Q (T-765), and 6J8 (T-755), were measured. The thermocouple in unfueled element 000 (T-750) operated intermittently during the test series and indicated questionable temperatures and has been neglected in the data reduction analysis.

Table 4.1-10 tabulates the uncertainties, deviations, and 3σ temperature increases used for the uncertainty analysis. The temperature variations were combined statistically to determine the 3σ maximum tie rod exit gas temperature for full power and flow EP-IV test conditions. The temperature variance is the square of the difference of the deviated temperature minus the same temperature under nominal conditions. These temperature variances were then summed for all considered deviations. Since all deviations considered were input on a 3σ confidence level, the square root of the total variance is the 3σ maximum temperature. At the bottom of Table 4.1-10 is a summary of the measured, calculated, and 3σ maximum tie rod exit gas temperatures for the EP-IV full power hold.

Astronuclear

TABLE 4.1-16

TIE ROD EXIT GAS TEMPERATURE UNCERTAINTY ANALYSIS
EP IV FULL POWER HOLD

UNCERTAINTY	DEVIATION	3σ TEMPERATURE INCREASE
Pyro Sleeve Conductivity	1σ = ± 30%	
T-760		126
T-765		117
T-755		117
Unfueled Graphite Heating	2σ = ± 30%	
T-760		59
T-765		41
T-755		41
Inlet Loss Coefficient	3σ = ± 50%	
T-760		56
T-765		50
T-755		49
Core Inlet Temperature	2σ = ± 15°R	
T-760		38
T-765		35
T-755		36
Hydrogen Gap Between Liner and Pyro	2σ = ± 0.001 in.	
T-760		16
T-765		16
T-755		16
Thermocouple Readout	2σ = ± 45°R	
T-760		68
T-765		68
T-755		68

SUMMARY

	Measured - °R	Calculated - °R	3σ Temp. increase - °R	3σ Max. Temp. - °R
T-760	733	508	169	677
T-765	693	476	154	630
T-755	597	471	154	625

Table 4.1-1[illegible] indicates that the 3 maximum temperatures for T-76[illegible] and T-765 are below the measured values. The 3 maximum temperature in T-755 is above the measured value. The large temperature differences between the measured exit gas temperatures T-765 and T-755 were not expected due to the proximity of each unfueled element to the core periphery. A temperature difference of 32°R was calculated between thermocouples T-76[illegible] and T-765 which resulted in good agreement with the measured value, 4[illegible]°.

Based on a review of EP-IV test data, there is reason to believe that the thermocouples located at the exit end of the tie rod element are not sensing the correct exit gas temperature. This could be substantiated by the fact that the 3 maximum temperatures for T-76[illegible] and T-76[illegible] are lower than the measured values. The exact position of the thermocouples cannot be verified. The probability of contact of the thermocouples with the molybdenum cone which is 200-300° hotter than the coolant is a possible explanation for the data. This possibility is discussed in detail in Section 4.3.

D. High Power Holds, Nozzle

Information on nozzle geometry and heat transfer coefficients which were based on the results of Aerojet chemical firing tests, were furnished by AGC in July of 1964. This information was used in conjunction with the TNT code to calculate nozzle operating characteristics prior to the NRX-A2 test. It was necessary to repeat the TNT calculation after the test to obtain results comparable to actual test conditions rather than planned conditions. More details of the rerun TNT are given elsewhere*. Nozzle tube conditions at the four steady-state times from the TNT calculation are compared to the test values in Table 4.1-14.

Nozzle tube inlet pressure and differential pressure agree reasonably well with calculated values. Nozzle tube exit temperatures and enthalpy increase did not agree with the calculated values, the actual nozzle heat pickup being about 30% more than calculated. These nozzle heat transfer test results are quite useful and will lead to improved heat transfer correlation for use in the TNT U-tube nozzle model. The ability to properly calculate nozzle coolant heating is of importance because of its effect on downstream fluid conditions. The core inlet temperature higher than calculated was partially due to the higher than expected heat pickup in the nozzle and partially due to reflector heating rates higher than predicted (although within the assigned uncertainty).

---

* NRX-A2 Reactor Performance, WANL-TNR-199, January, 1965, CRD.

CONFIDENTIAL
RESTRICTED DATA
Atomic Energy Act - 1954

TABLE 4.1-14

COMPARISON OF TEST AND POST TEST CALCULATED
NOZZLE TUBE PRESSURES AND TEMPERATURES AT HOLDS

Control Room Time (seconds)	13790		13900		13985		14085	
	TNT	TEST	TNT	TEST	TNT	TEST	TNT	TEST
Nozzle tube inlet pressure (psia)	539	547	783	788	835	833	858	855
Nozzle tube exit pressure (psia)	481	490	686	687	729	731	748	752
Nozzle tube ΔP (psid)	58	57	97	101	106	102	110	103
Nozzle tube inlet temperature (°R)	46	45 ± 5	49	45 ± 5	49	45 ± 5	50	45 ± 5
Nozzle tube exit temperature (°R)	81	90	104	113	111	129	116	128
Nozzle tube inlet enthalpy (Btu/lb)	-72	(-72)*	-57	(-57)*	-55	(-55)*	-54	(-54)*
Nozzle tube exit enthalpy (Btu/lb)	98	149	172	217	197	288	216	287
Nozzle tube Δh (Btu/lb)	170	221	229	274	252	343	270	342
Nozzle tube $\Delta h_{test}/\Delta h_{TNT}$	1.30		1.20		1.36		1.27	

*Assumed to be the same as for the TNT calculation because nozzle inlet enthalpy could not be accurately determined from test data.

CONFIDENTIAL
RESTRICTED DATA
Atomic Energy Act - 1954

Astronuclear

Nozzle chamber thermocouples indicated temperatures which were several 100°R less than the actual mixed mean nozzle chamber temperatures during EP-IV high power operation. These low temperatures have been primarily attributed to gas temperature at the T/C location being lower than the average nozzle chamber gas temperature. The nozzle chamber thermocouples extend approximately 1.3 inches from the nozzle tubes into the gas stream at a location approximately 15 inches downstream of the core. The gas at the T/C location could be at a reduced temperature for two reasons, 1) impingement by lower temperature hydrogen from the lateral support system not fully mixed with the core flow, and 2) heat transferred to the 15-inch length of nozzle wall which the peripheral flow follows. Calculations have been performed which show that these effects plus thermal radiation from the T/C to the nozzle could account for the lower temperatures observed.

E. High Power Holds, Reflector

In this section the shield, reflector and lateral support system thermal and hydraulic test results at steady state conditions are presented and compared to calculated values. The pretest predicted values* of reflector system temperatures and pressures did not give a meaningful comparison for several reasons: 1) operating conditions were not as planned; 2) nozzle tube heat pickup was higher than calculated, therefore, reflector inlet conditions were

---

* NRX-A2 Test Prediction Report, WANL-TME-887.

considerably different from those given by the pretest calculations; 3) the support ring temperatures were lower than had been expected. These support ring temperatures affect the gap size of the inner-outer reflector annulus under power operating condition. This gap size in turn has a major influence on the reflector system overall pressure drop and flow distribution.

In order to obtain a useful evaluation of the analytical model used for the reflector system analysis and the calculation methods, post-test calculations of reflector system temperatures and pressures were performed and compared to test values. Results of these comparisons are given in this section. In particular, comparisons of coolant temperatures and pressures and material temperatures at the highest power hold at CRT 14085 seconds (1096 MW thermal power) are presented in more detail. For these calculations at the steady-state hold, the measured reactor flow rates given in Table 4.1-5 and the measured reflector inlet temperatures and pressures were used. Based on the test measurements of the reflector pressure distribution and temperatures at full power, the inner-outer reflector annulus was recalculated to be 0.092" as compared to the pretest value of 0.108". This smaller gap annulus clearance was used in the reflector system analytical model for the post-test calculations. In addition, some minor changes in flow impedances of several flow channels in the reflector system were incorporated into the reflector analytical model.

These changes were made because additional component test data became available and there were some hardware changes since the pretest calculations were performed.

In addition to the comparisons of fluid temperatures and pressures the total reflector system heat pickup was calculated from experimental data and is summarized in this section, and the lateral support system performance is compared to calculated performance.

1. Reflector System Coolant Temperatures and Pressures at the Highest Power Hold, CRT 14035

The parallel flow path in the reflector system is shown in Figures 4.1-20 and 21. Included in these figures are the measured and calculated fluid temperatures and pressures at the highest power hold, CRT 14085. The reflector inlet plenum temperature of 136°R is the average of 7 thermocouple measurements. The reflector exit plenum temperature of 233°R is the average of 5 thermocouple measurements. The inlet and outlet plenum pressures are each an average of two pressure measurements. The measured temperature of the coolant exiting from the individual major reflector coolant passage is a single thermocouple reading at specific location in the outlet plenum. Therefore, these temperatures should be considered only as representative of specific channel exit temperatures and do not represent the average which may be expected from all similar channels.

CONFIDENTIAL
RESTRICTED DATA

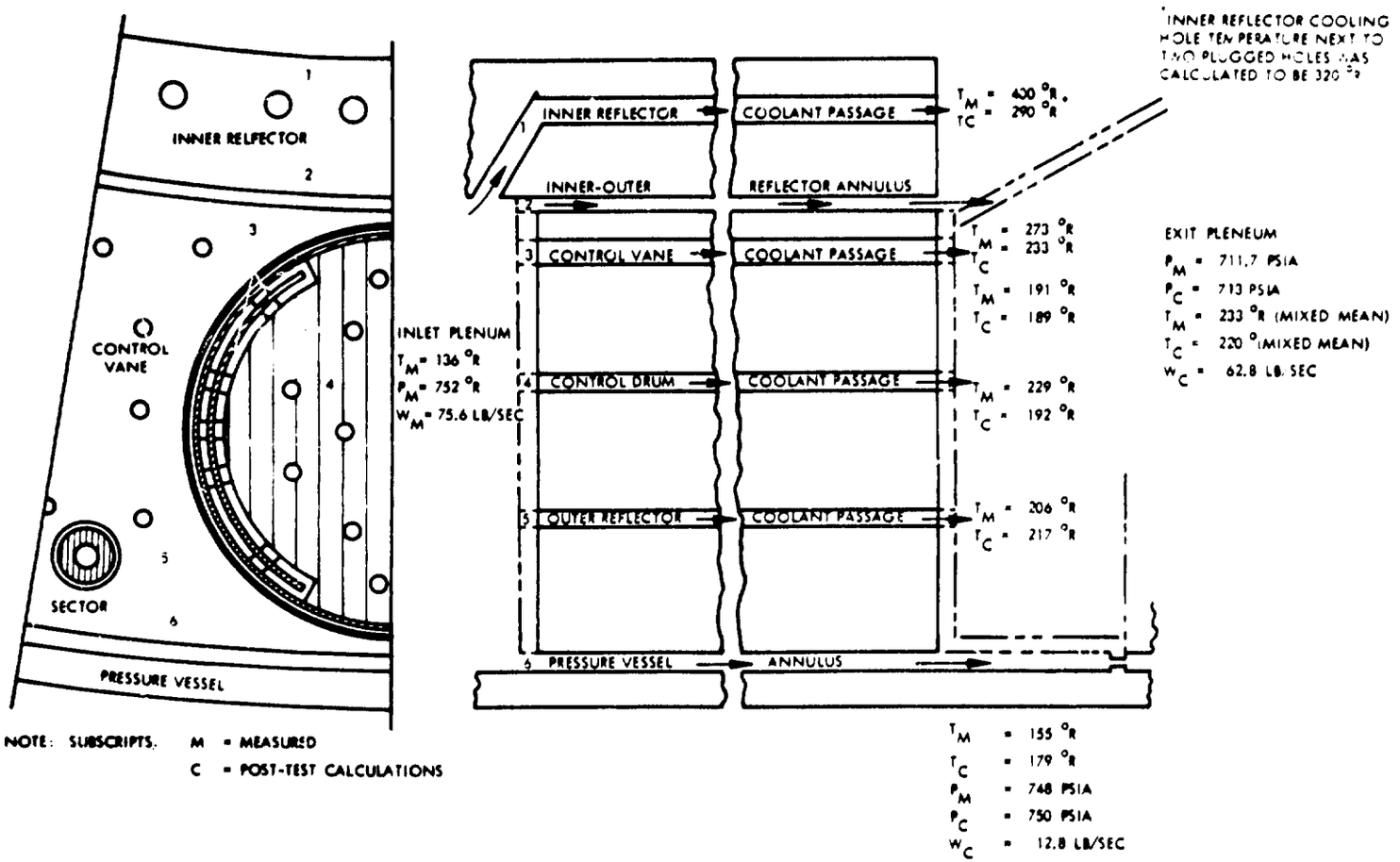

FIGURE 4.1-20 REFLECTOR SYSTEM FLUID TEMPERATURES AND PRESSURES FOR NRX-A2 EP-IV AT CRT 1408.5

Astronuclear

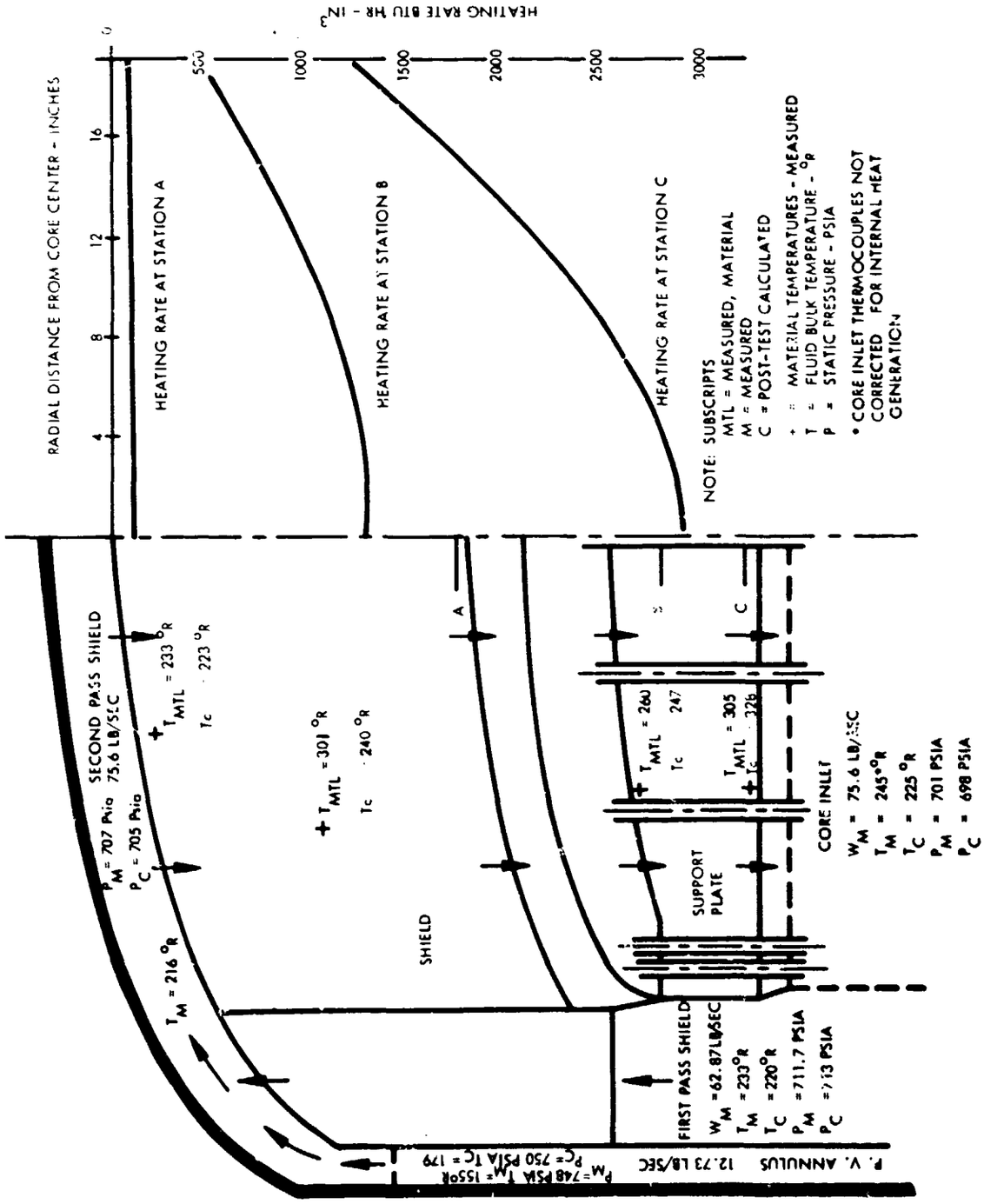

FIGURE 4.1-21 TEMPERATURES, FLOWS, AND RADIATION HEATING RATES IN SHIELD AND SUPPORT PLATE AT CRT 14085

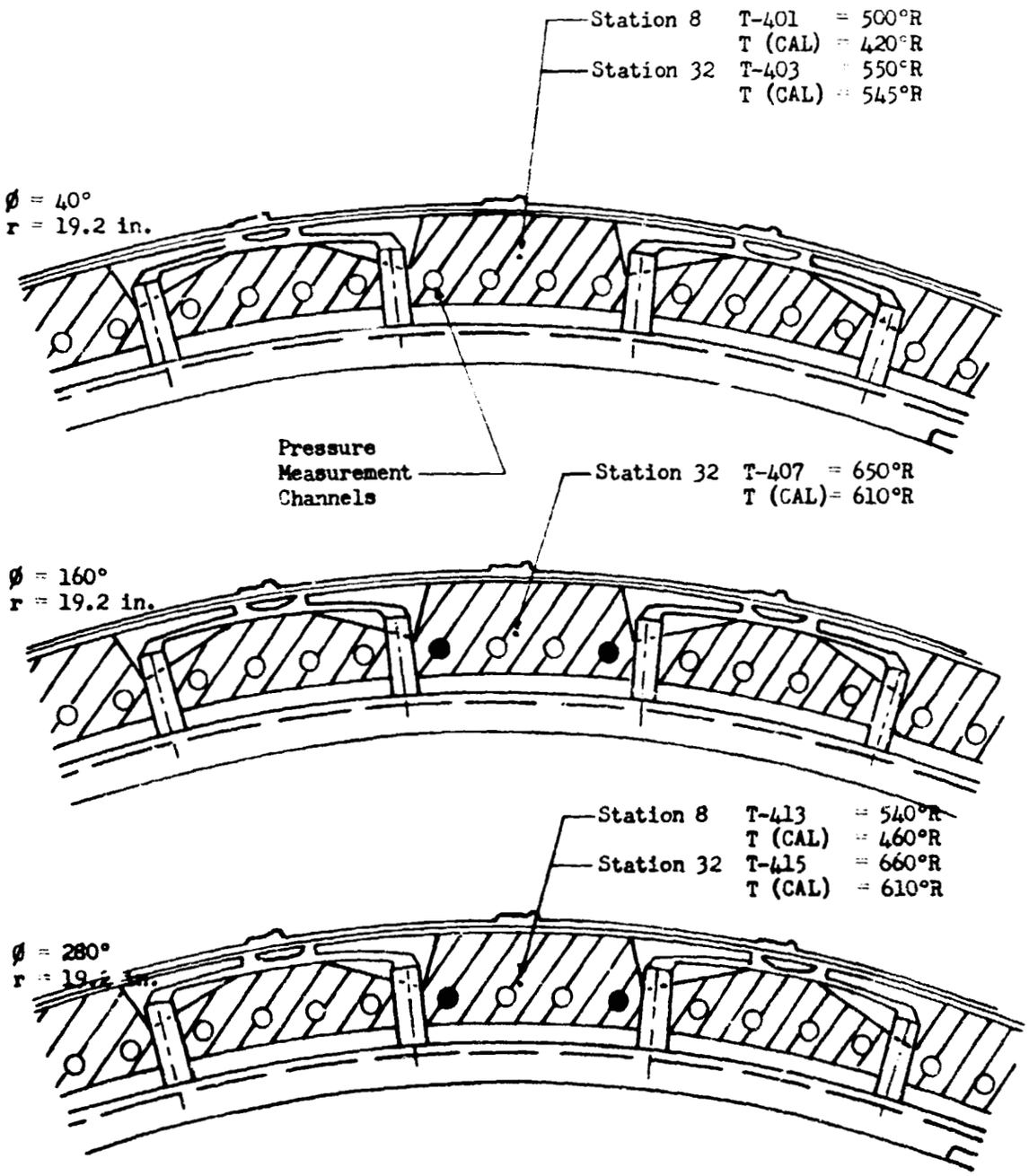

FIGURE 4.1-22 - NRX-A2 EP-IV INNER REFLECTOR
TEMPERATURES AT CRT 14085

The post-test calculation at the highest power hold was performed by using the computer code MCAP-TOSS.* The calculation used the test reflector inlet temperature of 136°R, inlet pressure of 752 psia and flow rate of 75.6 lb/sec. The other parameter specified in the calculation was the total power pickup of the reflector system which was determined by energy balance between reflector inlet and the first pass shield exit (shield dome end plenum). The power shapes for the various materials are the ones reported in Reactor Analysis Data Book (WANL-TME-840) in the Radiation and Shielding Section for NRX-A2. The total power pickup in the reflector is discussed later.

Figure 4.1-20 shows the major flow passages in the outer and inner reflectors. The fluid temperatures and pressures at the exit plenum, pressure vessel annulus, sector cooling holes and control drum cooling passages agree reasonably well. In the inner reflector cooling passage, the exit fluid temperature thermocouple was located between two open holes which in turn were between two plugged holes as shown in Figure 4.1-22. The measurement indicated only the local coolant temperature. Fifteen of the 144 inner reflector cooling holes were plugged in the NRX-A2 reactor for pressure measurements of the seal chamber pressure. In the post-test calculation the inner reflector analytical heat conduction model includes some plugged and some open holes. These holes are arranged in the same relative positions

*A. Y. Lee, A Program for Steady State Fluid Flow and Heat Conduction Coupled Calculations of Heat Generating Solids Cooled by Parallel Channels - Using MCAP and TOSS Codes, WANL-TME-867, October, 1964.

as in the NRX-A2 so that the effect of the plugged holes on the coolant exit temperature in the vicinity of the plugges holes can be studied. The calculated exit temperature is 320°R as compared to the measured value of 400°R. This shows that the plugged hole does increase the coolant temperature at the holes near to the plugged ones. The calculated nominal reflector coolant exit temperature is 290°R as shown in the figure.

Figure 4.1-21 shows the fluid temperatures and pressures at the shield and core support plate region of the coolant flow. Using the calculated reflector outlet plenum pressure of 713 psia, the pressure drop through the first pass of the shield was calculated to be 8.0 psi, giving a dome plenum pressure of 705 psia. This compares with the measured value of 707 psia. The pressure drop across the second pass of the shield and the screen was calculated to be seven psi and the pressure drop across the support plate was calculated to be 0.5 psi. These give a calculated core inlet pressure of 698 psia to the nearest psi. This compares with the measured value of 701 psia. Table 4.1-11 summarizes the pressures and pressure drops throughout the reflector system.

TABLE 4.1-11

COMPARISON OF EXPERIMENTAL AND CALCULATED PRESSURES AND DIFFERENTIAL PRESSURES IN THE REFLECTOR SYSTEM

Reflector and Shield System at CRT 14085

	Measured	Calculated
P (Reflector Inlet)*	752 Psia	752 Psia
P (Reflector Exit)	711.3 Psia	713 Psia
P (Dome End Shield)	707 Psia	705 Psia
P (Core Inlet)	701 Psia	698 Psia
P (PV Annulus-Dome End)	748 Psia	750 Psia
ΔP (Outer Reflector)	70.7 Psi	39 Psi
ΔP (Inner Reflector)	38 Psi	35 Psi
ΔP (Shield)		15 Psi

*For post calculation of reflector and shield fluid systems, the measured values of the conditions at the reflector inlet were used.

The comparisons of the calculated and measured shield and core support plate material temperatures are also shown in Figure 4.1-21. The calculated dome end shield material temperature of 223°R was based on the dome plenum temperature of 216°R; this confirms the dome plenum fluid temperature reasonably well. Using this dome plenum temperature of 216°R and the internal heat generation rates of the shield and the support plate as shown in the figure, the calculated core inlet temperature is 226°R as compared to the measured value of 245°R. From the comparison of the support plate calculated and measured temperatures, it is believed that the calculated core inlet temperature of 226°R is consistent with the measured support plate temperature.

2. Reflector System Power Comparison at Various Power Holds

Table 4.1-12 shows a summary of the power picked up in the reflector system calculated from the hydrogen flow rate and the temperature rise across the reflector and first pass of the shield. The power picked up in the reflector system arrived by this method averaged over the four power holds, was 2.15% of the total reactor power. Also tabulated on this table is the power which wouldhave been calculated under test flow conditions and inlet temperature using the nuclear heating rated reported in Reactor Analysis Data Book under Radiation and Shielding Section for NRX-A2. Using the calculated reflected heating

CONFIDENTIAL
RESTRICTED DATA
Atomic Energy Act - 1954

Astronuclear

TABLE 4.1-12

CALCULATED REFLECTOR HEATING RATES FROM ΔH AND FLOW RATE AND COMPARISON TO NUCLEAR HEATING RATES

	EP IV POWER HOLD CONTROL ROOM TIME				
	13790	13900	13985	14085	Average
Reactor Power	574	941	1038	1096	--
Power of Reflector System plus first pass of shield from test (Calculated by energy balance between reflector inlet and first pass shield exit).	13.6	22.0	20.9	22.7	--
Estimated power deposited in first pass shield	0.3	0.5	0.5	0.5	--
Power of reflector system from test	13.3	21.5	20.4	22.2	--
Power of reflector system using calculated heating rates (Ref: TME-840) (1.76 x Reactor Power)				19.3	--
Reflector system power (test)/reactor power	2.32%	2.29%	1.97%	2.03%	2.15%
Reflector system power (cal)/reactor power	1.76%	1.76%	1.76%	1.76%	1.76%
Reflector system power (test)/reflector system power (cal)				1.15%	1.22%

CONFIDENTIAL
RESTRICTED DATA
Atomic Energy Act - 1954

rates shows the reflector system absorbs 1.76% of the total reactor power at full power conditions. Comparison of these two powers, one reflecting calculated conditions, one reflecting test conditions, it appears that the heating rates as tested are about 15% higher than expected from calculation for high power hold, and about 22% if the average of the four power holds is considered.

3. Reflector Inlet and Outlet Plenum Temperature Azimuthal Measurements

The average azimuthal thermocouple measurements at the reflector inlet and outlet plenums at the various power holds were investigated. The maximum variation in a reading is ± 6°R. From this study, it was seen that there were no detectable azimuthal variation in the coolant temperature in the reflector inlet and outlet plenum during the four power holds. However, there was asymmetry during chilldown and the early stage of startup. These are discussed in the startup and the shutdown section of the report.

4. Material Temperatures

The measured outer reflector sector material temperatures at the locations of the thermocouples at the four power holds are shown in Figure 4.1-23. The calculated material temperature at the vicinity of the thermocouple locations at the highest power hold, CRT 14085, is also plotted in the figure for comparison. The axial shape of these curves are as expected. The maximum temperature level occurred

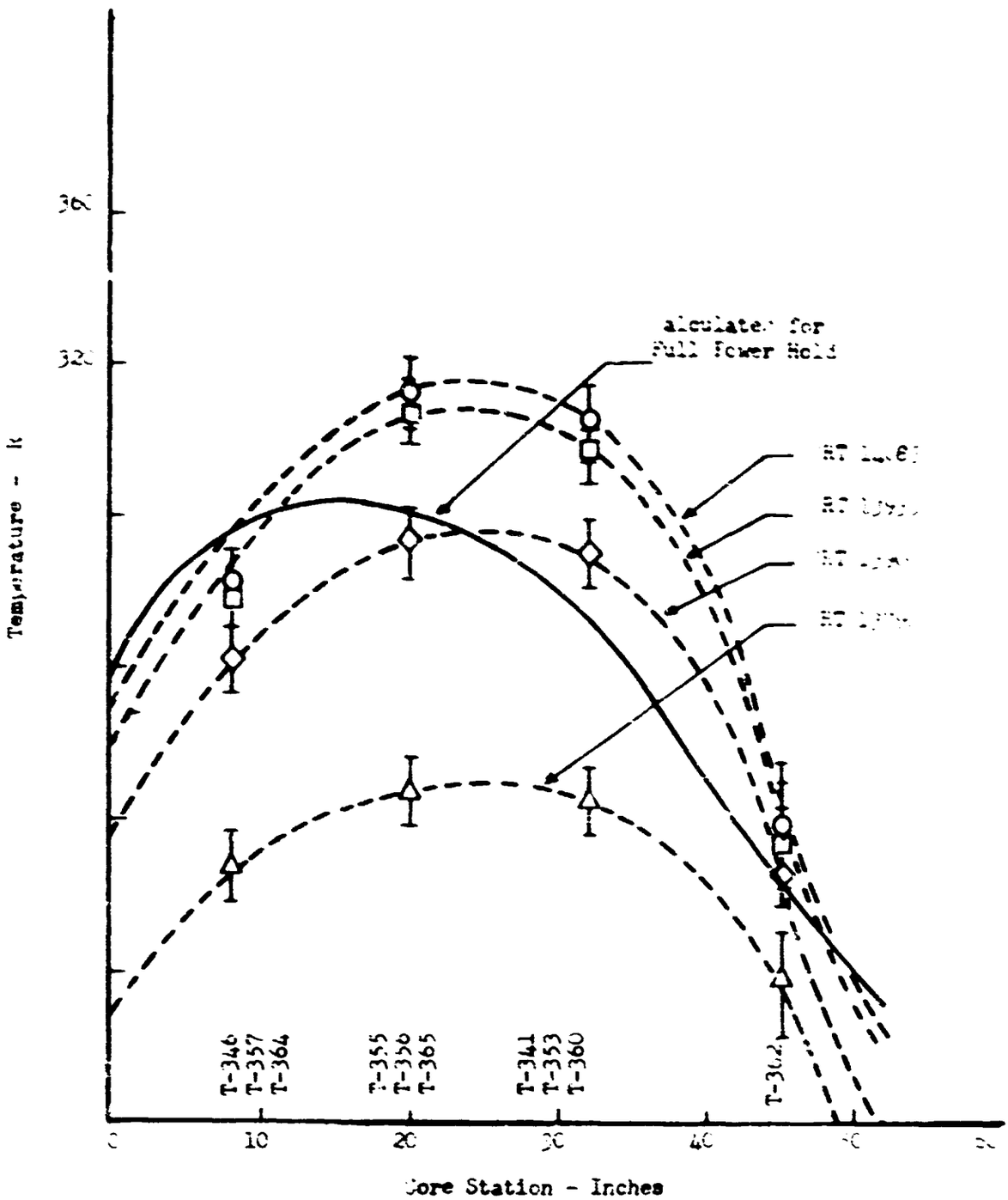

FIGURE 4.1-23 OUTER REFLECTOR SECTOR MATERIAL TEMPERATURE VS. AXIAL POSITION

around the central portion of the reactor where the internal heat generation is maximum. The experimental curve peaks are nearer the center of the core than the calculated curve. The maximum deviation of the calculated value from test value at CRT 14085 is about 50°R. The measured temperatures shown in the figure for the various power holds do not represent the average reflector sector material temperatures. The thermocouples were located in the region where the maximum material temperatures might occur. The maximum calculated sector temperature at CRT 14085 is 310°R at core station 20", and at approximately R = 21.8" and one inch from the radial edge of the sector. At CRT 14085 the calculated maximum sector average temperature is 265°R and the maximum sector average to inner wall temperature difference is 50°R.

Figure 4.1-24 shows the sector material temperatures at core station 8, 20, and 32 plotted as a function of azimuthal position. This curve is typical of the steady-state operation observed at the other lower power holds. There appears to be little, if any, azimuthal variation apparent in the sector temperatures. The maximum range of variation of the individual thermocouple readings is ± 18°R and the range of the average values is ± 12°R.

CONFIDENTIAL
RESTRICTED DATA
Atomic Energy Act - 1954

Astronuclear

RESTRICTED DATA
ATOMIC ENERGY ACT
OF 1954

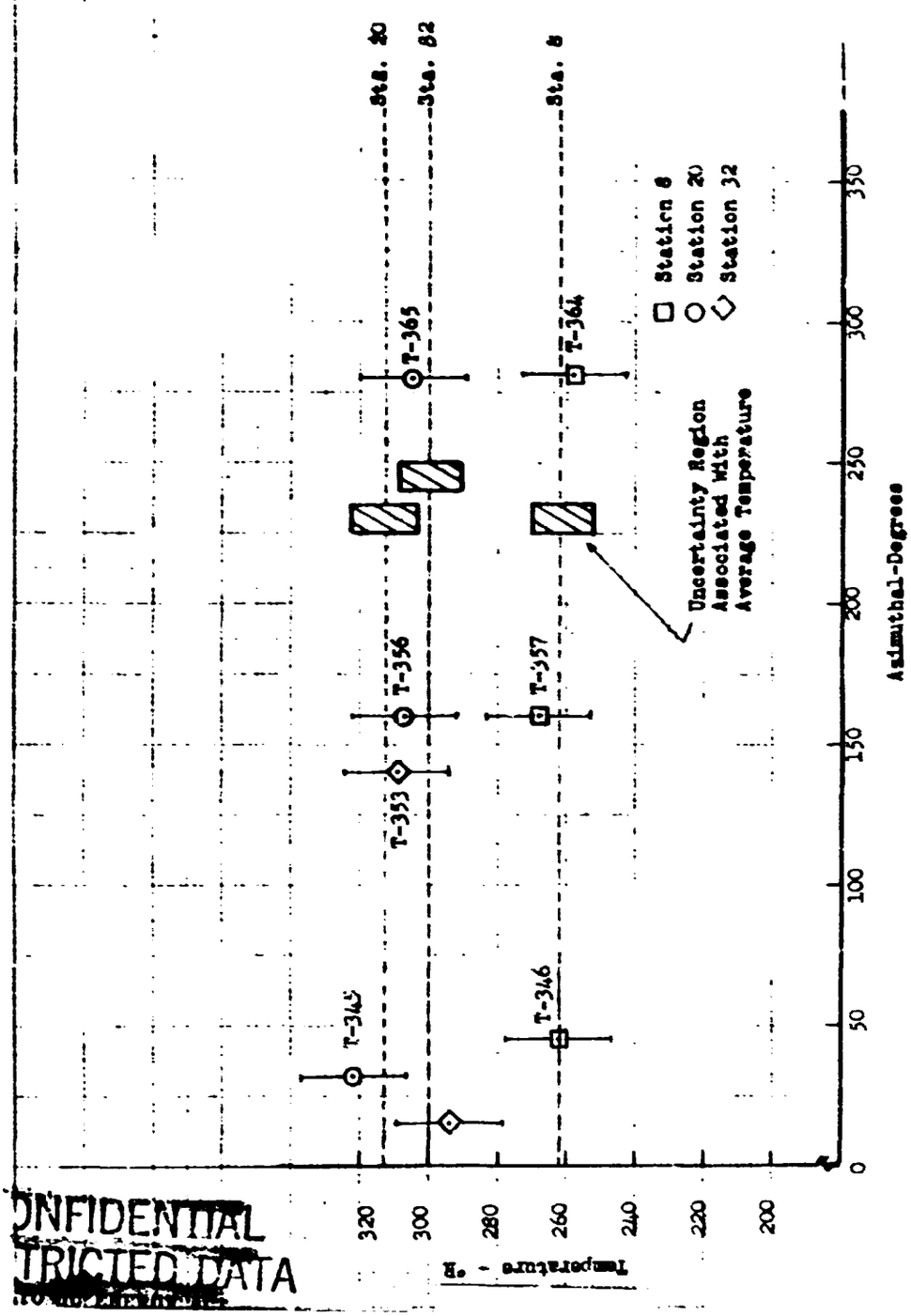

FIGURE 4.1-24 AZIMUTHAL SECTOR TEMPERATURE VARIATION IN NRX-A2 EP-IV AT CRT L4085

CONFIDENTIAL
RESTRICTED DATA

CONFIDENTIAL
RESTRICTED DATA
Atomic Energy Act - 1954

Figure 4.1-25 shows the measured control drum and control vane temperatures at the highest power hold, CRT 14085. Included in this figure are the calculated local nodal temperatures at the vicinity of the thermocouples. The calculated values agree very well with the measured values. The temperature difference across the control drum at station 8 with the drum operating at an average temperature slightly above 226°R was measured to be 42°R; the comparable value was calculated to be 37°R.

Table 4.1-13 tabulates the measured control drum and control vane temperatures at the four power holds and the calculated values at the highest power hold. The experimental temperatures of the inner reflector material at the three power holds, CRT 13790, 13900, and 14085, are shown in Figure 4.1-26. A sketch of the inner reflector and the thermocouple locations is shown in Figure 4.1-22. The thermocouples T-412, T-407, T-415 are located between two open and plugged holes whereas T-401 and T-403 are near one plugged hole. With the effect of the plugged holes taken into consideration in the post-test analysis, the calculated material temperature at the vicinity of the thermocouples at the highest power hold, CRT 14085, are shown in the figures. The upper curve in Figure 4.1-26 is the calculated temperature at the location between two plugged holes and the lower curve near one plugged hole. It is seen in Figure 4.1-22 that the maximum deviation

CONFIDENTIAL
RESTRICTED DATA
Atomic Energy Act - 1954

Astronuclear

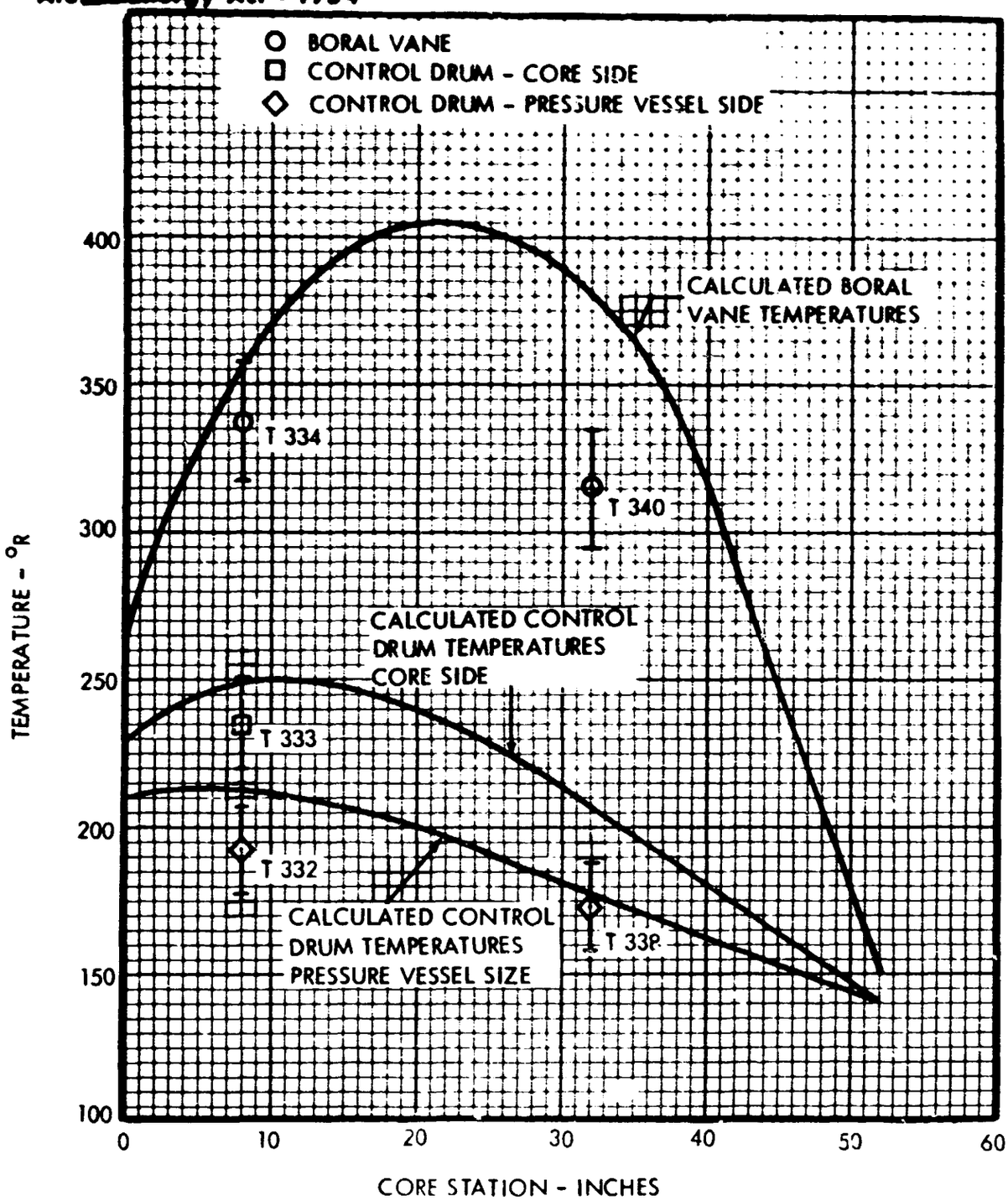

FIGURE 4.1-26 CONTROL DRUM AND BORAL VANE TEMPERATURES FOR NRX-A2 EP-IV

CONFIDENTIAL
RESTRICTED DATA
Atomic Energy Act - 1954

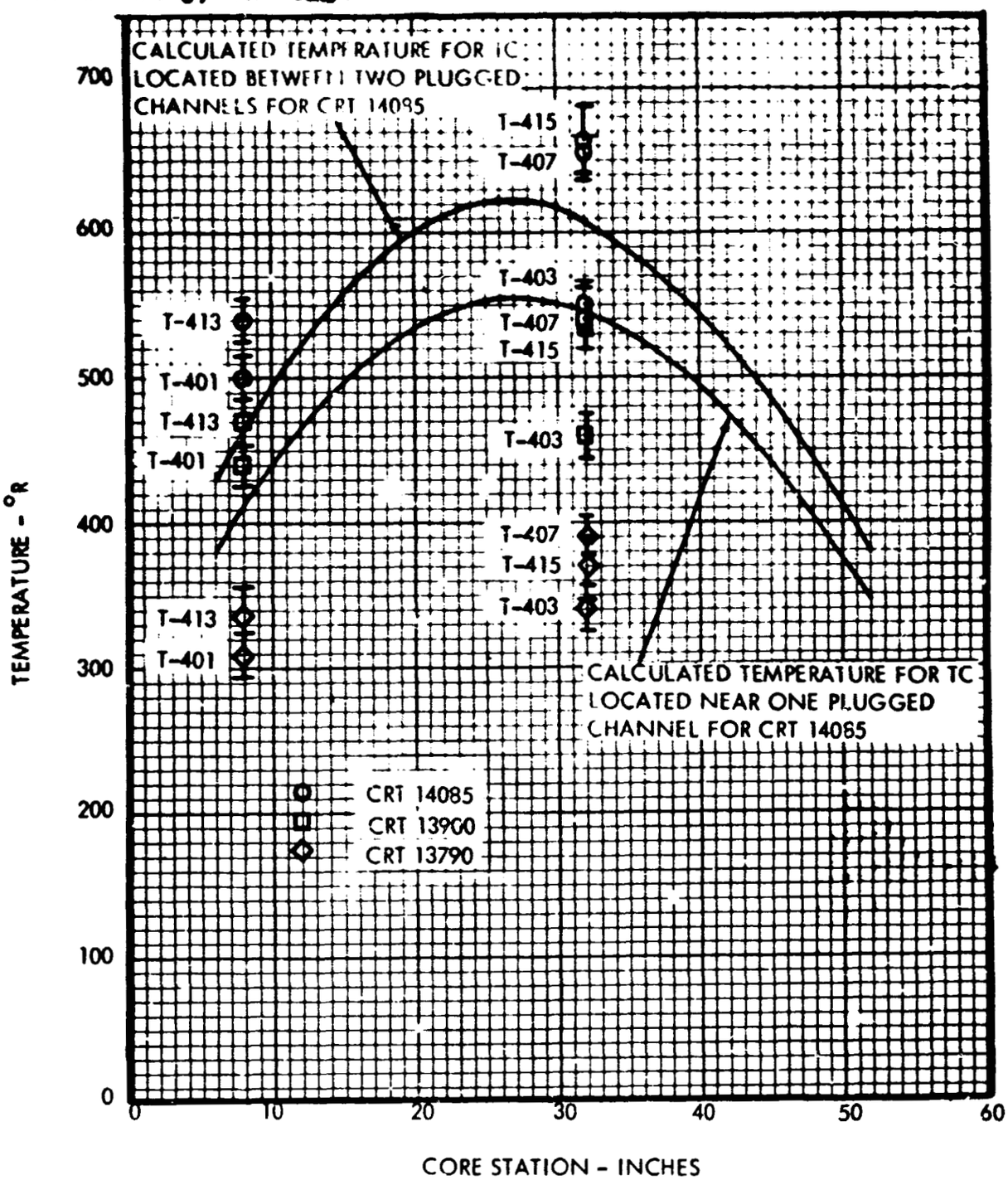

FIGURE 4.1-26 CALCULATED AND MEASURED TEMPERATURES OF INNER REFLECTOR MATERIAL

TABLE 4.1-13

NRX-A2 EP IV

CONTROL DRUM AND CONTROL VANE TEMPERATURES

CONTROL DRUM TEMPERATURES

Drum No.	Station	Temperatures at Specified Control Room Time				
		13790	13900	13985	14085	Calculated High Power
2	8.0	120	159	178	188	213
2	8.0	151	206	223	235	248
10	32.0	103	150	168	173	178
10	32.0		INOPERATIVE			

CONTROL VANE TEMPERATURES

Drum No.	Station	Temperatures at Specified Control Room Time				
		13790	13900	13985	14085	Calculated High Power
2	8	240	315	320	338	356
10	32	230	282	305	315	380

between the calculated and measured values is 80°R. At core station 32 and at the same radial location, but away from any plugged hole, the average material temperature was calculated to be 110°R lower than the temperature measured between two plugged holes.

Figure 4.1-27 shows the time trace of the inner reflector material temperature as measured by thermocouple T-415. It is seen that the material temperature continued to rise during the power holds. A similar result was also observed in Kiwi B-4E tests. This temperature increase is believed to result from the decrease in material thermal conductivity due to irradiation damage. The values of thermal conductivity used in these calculations are those on unirradiated graphite, not impregnated H4LM. Experimental data on thermal conductivity of H4LM and in particular, the effect of irradiation on H4LM thermal conductivity, are not available at this time. Preliminary investigation shows that a 7% decrease (linear) in the inner reflector material thermal conductivity over the same period of time as the third power hold (110 seconds) resulted in an increase in the material temperature with similar slope as shown by the trace of T-415. The dash line in Figure 4.1-27 indicates the calculated inner reflector average temperature at core station 32 considering the 7% decrease in thermal conductivity during the 110 seconds due to irradiation effect.

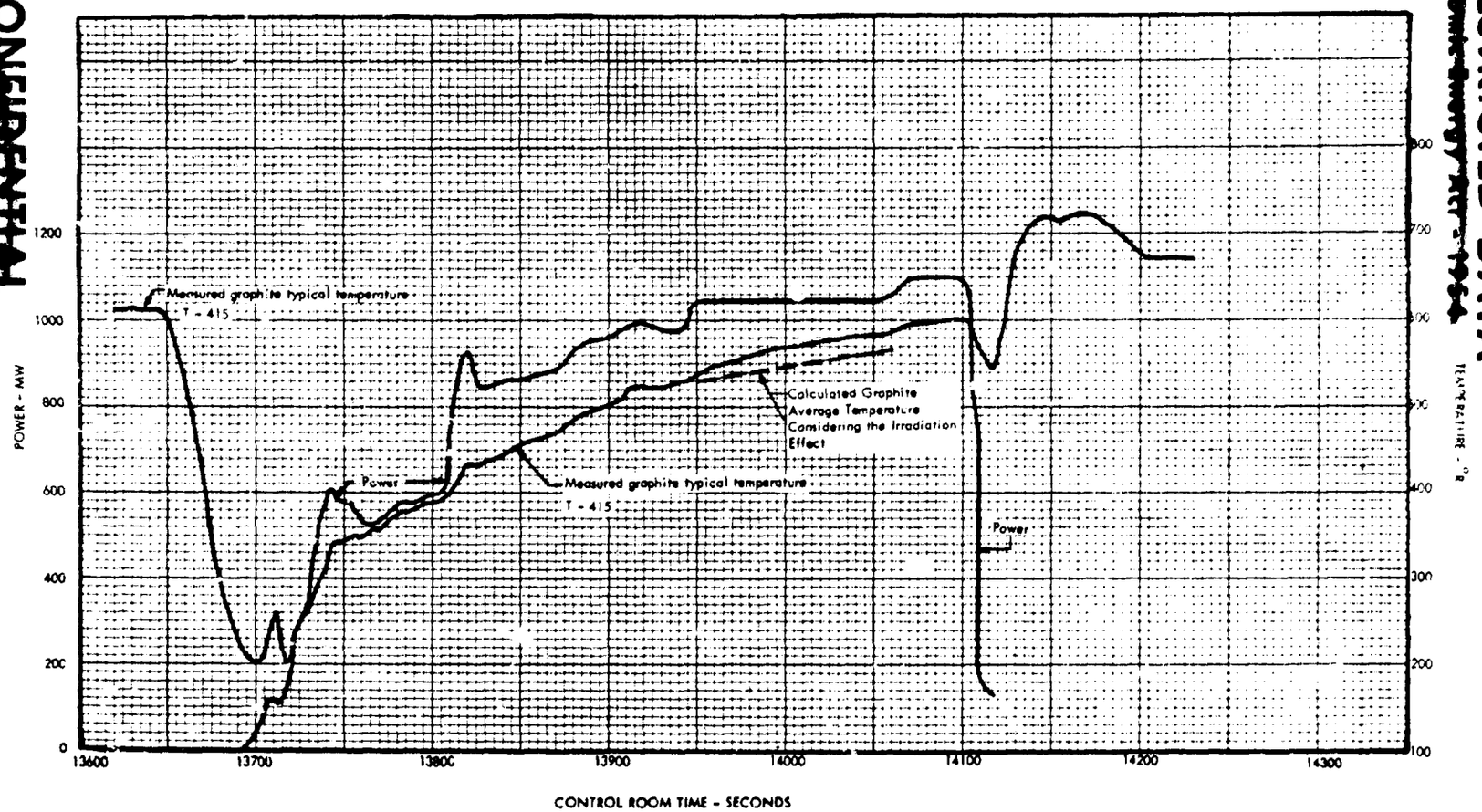

FIGURE 4.1-27 COMPARISON OF MEASURED AND CALCULATED INNER REFLECTOR TEMPERATURE

5. Lateral Support System

The lateral support system fluid flow path, fluid temperature and pressure and material temperatures during the high power hold, CRT 14085, are shown in Figures 4.1-28 and 29. In Figure 4.1-28, Curve A is the predicted filler strip temperature at the filler strip-pyro-tile interface at points on seals at full power. The axial average filler strip temperature along this interface is between these two curves. The thermal capsule measurements at the three filler strip pyro-tile interface locations are shown on the figure for comparison. At core station 19.2" (on seal) the thermal capsule indicated a temperature of 2450°R as compared to the predicted value of 2300°R. At the other two core stations the thermal capsules fused, indicating a temperature of the material above 2678°R which was the highest melting temperature of the capsule wires installed in the NRX-A2 filler strips. The coolant temperature in the seal system was measured by thermocouples at locations between seals. A typical thermocouple installation is shown at D and the detail of the installation is also shown in the figure. The measured fluid temperature is much lower than the predicted temperature (Curve C). If one compares the fluid temperature measurements with the predicted inner reflector material temperature at the surface of the seal chamber between seals (Curve E), it is evident that the thermocouples were measuring much closer to the inner reflector wall temperature than to the fluid bulk temperature.

CONFIDENTIAL
RESTRICTED DATA
Atomic Energy Act - 1954

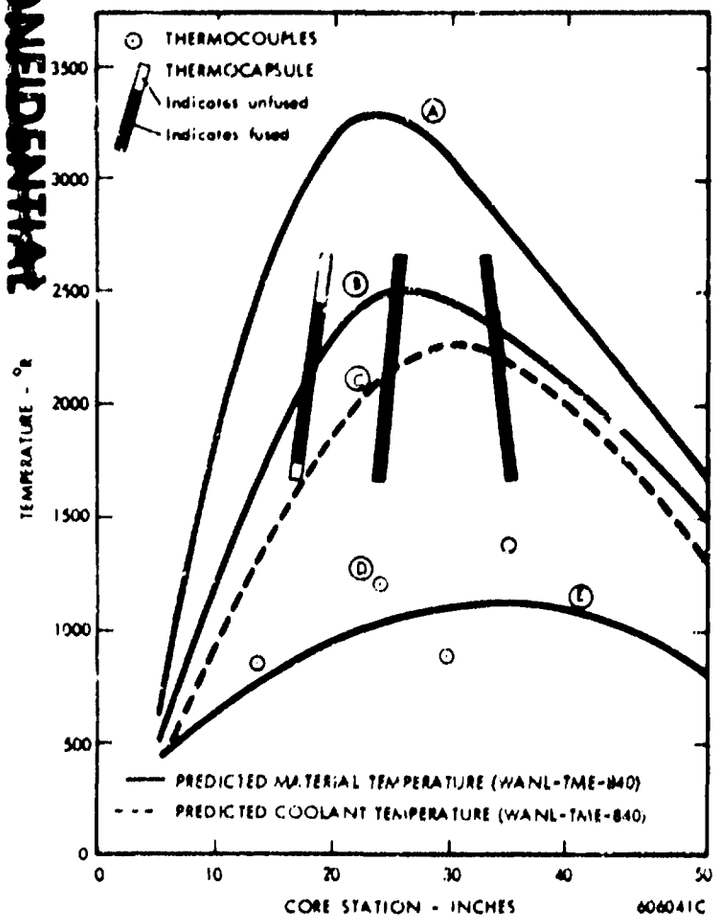

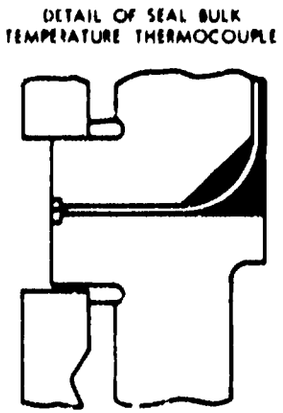

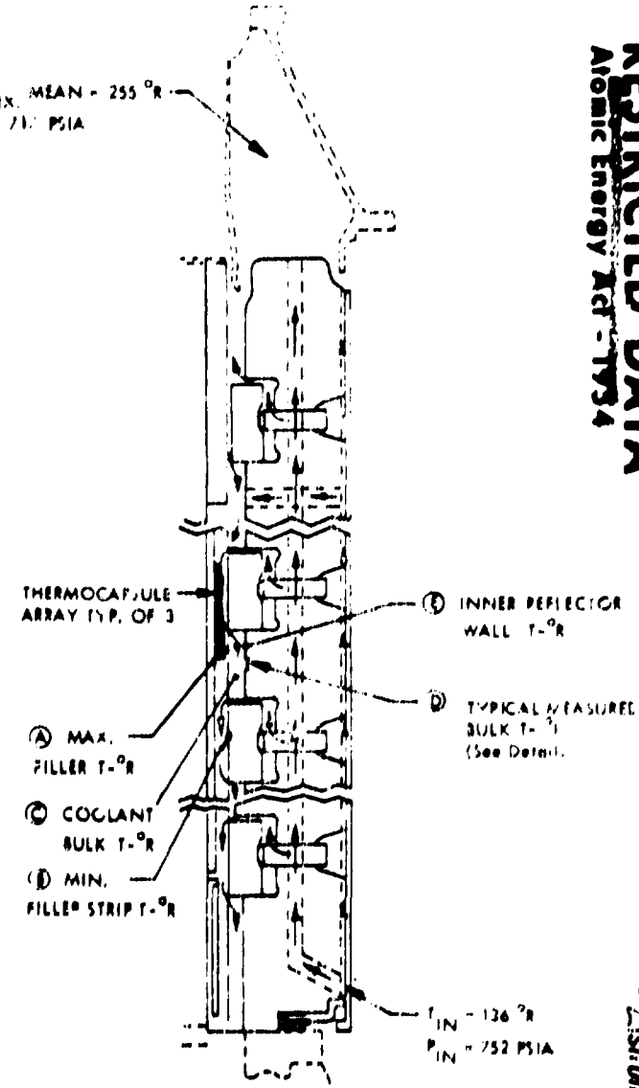

FIGURE 4.1-28 NRX-A2 EP-IV LATERAL SUPPORT HYDROGEN AND MATERIAL TEMPERATURES (MEASURED AND CALCULATED)

CONFIDENTIAL
RESTRICTED DATA
Atomic Energy Act - 1954

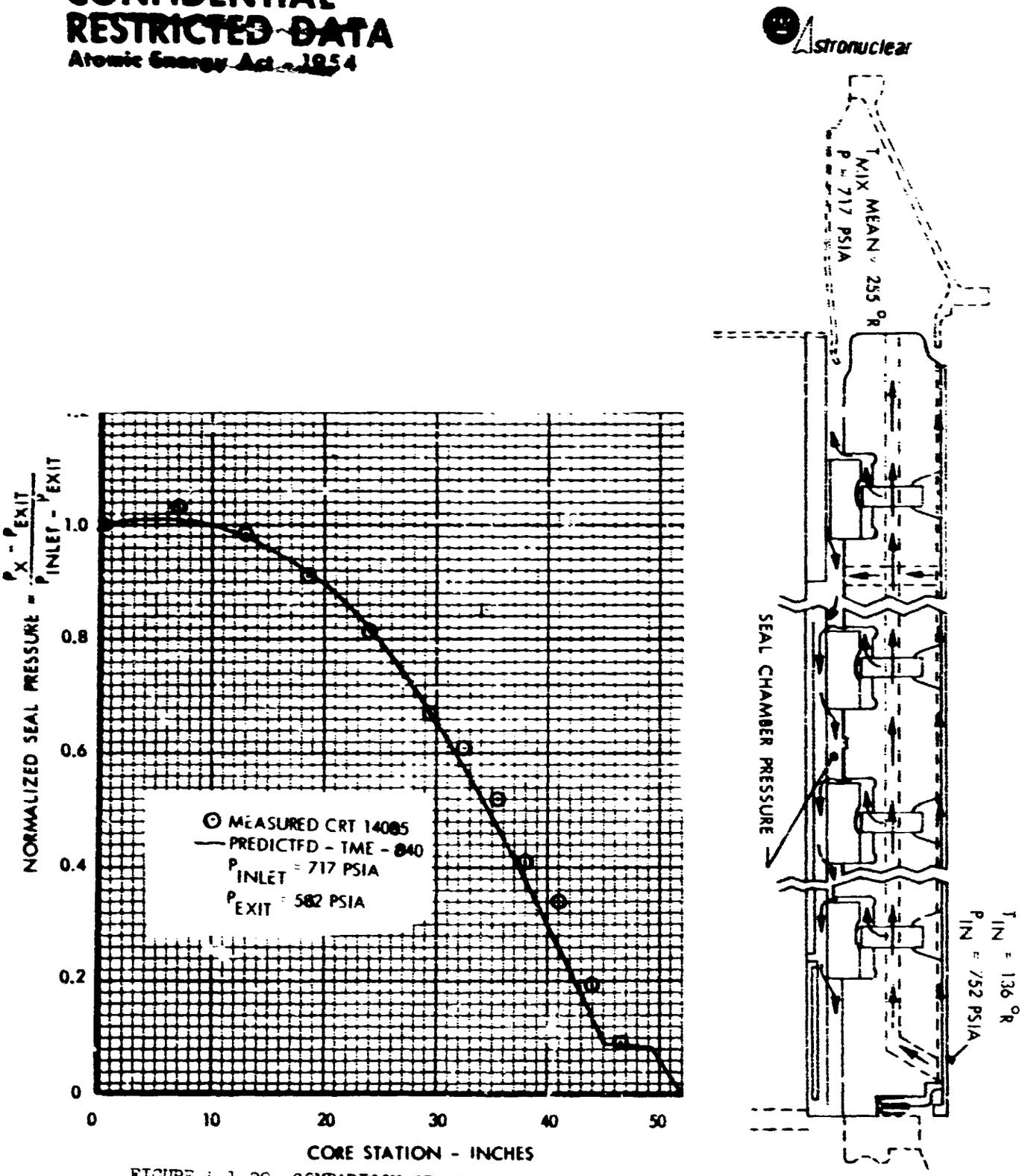

FIGURE 4.1-29 COMPARISON OF MEASURED AND PREDICTED SEAL CHAMBER PRESSURE DISTRIBUTION

Reviewing the thermocouple installation, this is entirely possible. The thermocouple is recessed back into the inner reflector and could be reasonably expected to measure the boundary temperature of the flow in that chamber. This type of installation was necessary to prevent damage to the filler strips, if the core should bottom out on the inner reflector either during shipping or during operation. The thermal growth of the core and the uncertainty in the relative inward movement of the inner reflector made it inadvisable to place a thermocouple inside the envelope of the I.D. of the inner reflector. Assuming the same heat input as used in the prediction, it was estimated that the coolant flow would have to increase 100% in order to get the chamber coolant temperature down to the measured values. This does not seem to be probable.

Figure 4.1-29 shows the comparison of the measured and the predicted normalized pressure distribution in the seal chamber at the high power hold, CRT 14085. The reason for comparing the normalized values is that the prediction did not have the same inlet and exit pressure as in the test. From this figure it is seen that the predicted pressure distribution shape agrees with the measured one. The normalized pressure distributions measured during the other three steady-state hold periods also agree with calculated values shown for the high power hold at CRT 14085 in Figure 4.1-29.

4.1.5 EP-IV Startup and Shutdown

A. Startup

1. Reactor

Based on the results of the EP-1B liquid hydrogen test, the reactor flow was expected to lag the venturi flow during the first 15 seconds of the startup. Reactor flow during this interval was obtained from NRX-A1 cold flow test results, and the power demand had been reprogrammed prior to the EP-IV to give the desired 50°R/sec nozzle chamber temperature startup. Given on Figure 4.1-30 are the NRX-A2 EP-IV flow demand profile, the LH_2 flow profile measured at the venturi meter downstream of the pump, FE-7, and the reactor flow rate which was calculated from measured nozzle chamber conditions. Superimposed on the same figure in the proper relation to the demand flow profile are the NRX-A1 and NRX-A2 EP-1B second LH_2 test reactor flow rates. These results show that the actual reactor flow rate during the startup was very similar to that which was expected. The flow lag was analyzed in detail for NRX-A2.*

The dotted curves on Figure 4.1-31 are the power demand ramp and planned nozzle chamber temperature ramp while the actual power and chamber temperature ramps are given by the solid curves. It can be seen that the power was higher than programmed during the early stage of the startup (CRT 13700 to 13720) and the nozzle chamber

---

* NRX-A2 Flow Lag, WANL-TME-1017, October 26, 1964.

CONFIDENTIAL
RESTRICTED DATA
Atomic Energy Act - 1954

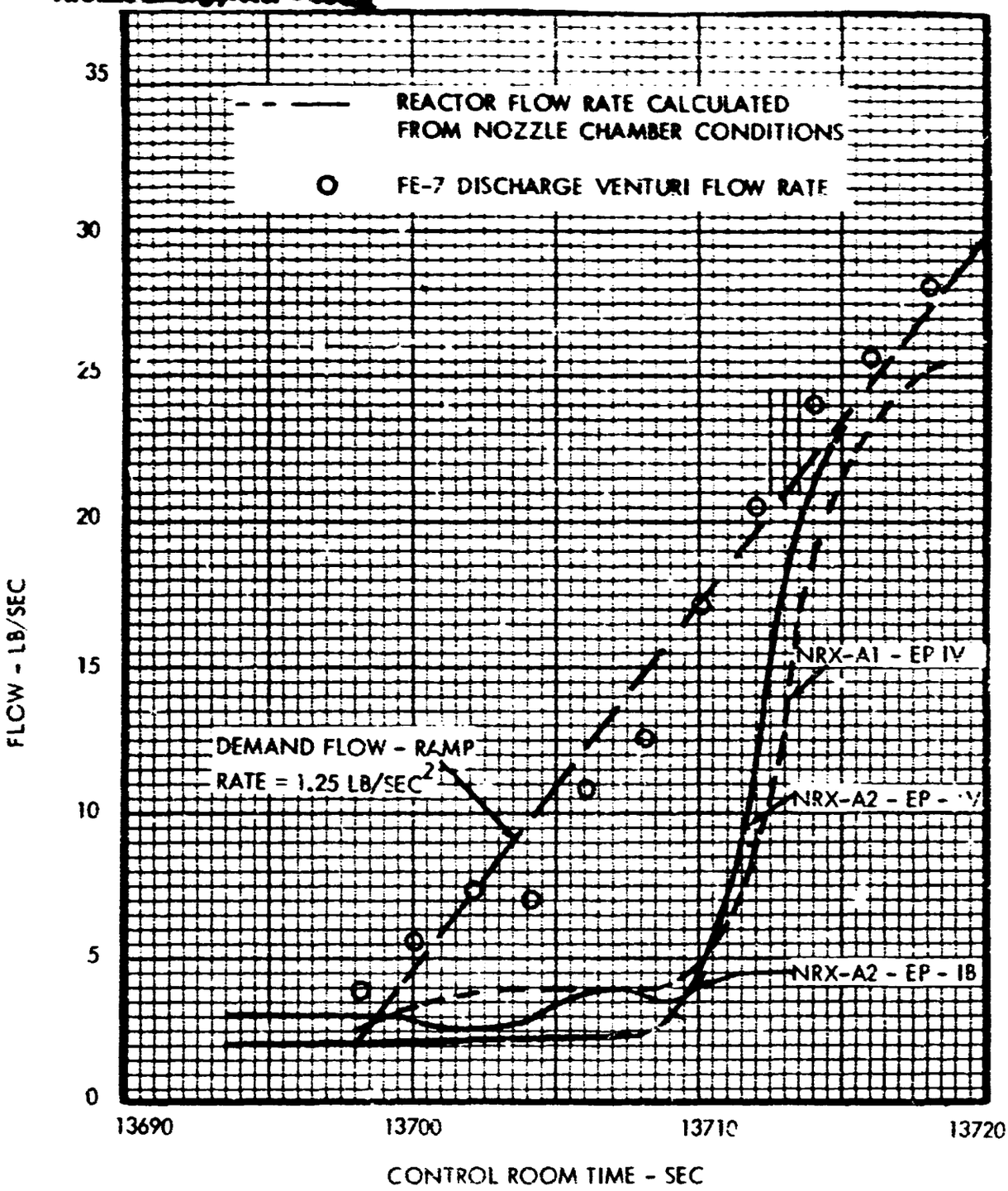

FIGURE 4.1-30 STARTUP LH_2 FLOW LAG

CONFIDENTIAL
RESTRICTED DATA
Atomic Energy Act - 1954

CONFIDENTIAL
RESTRICTED DATA
Atomic Energy Act - 1954

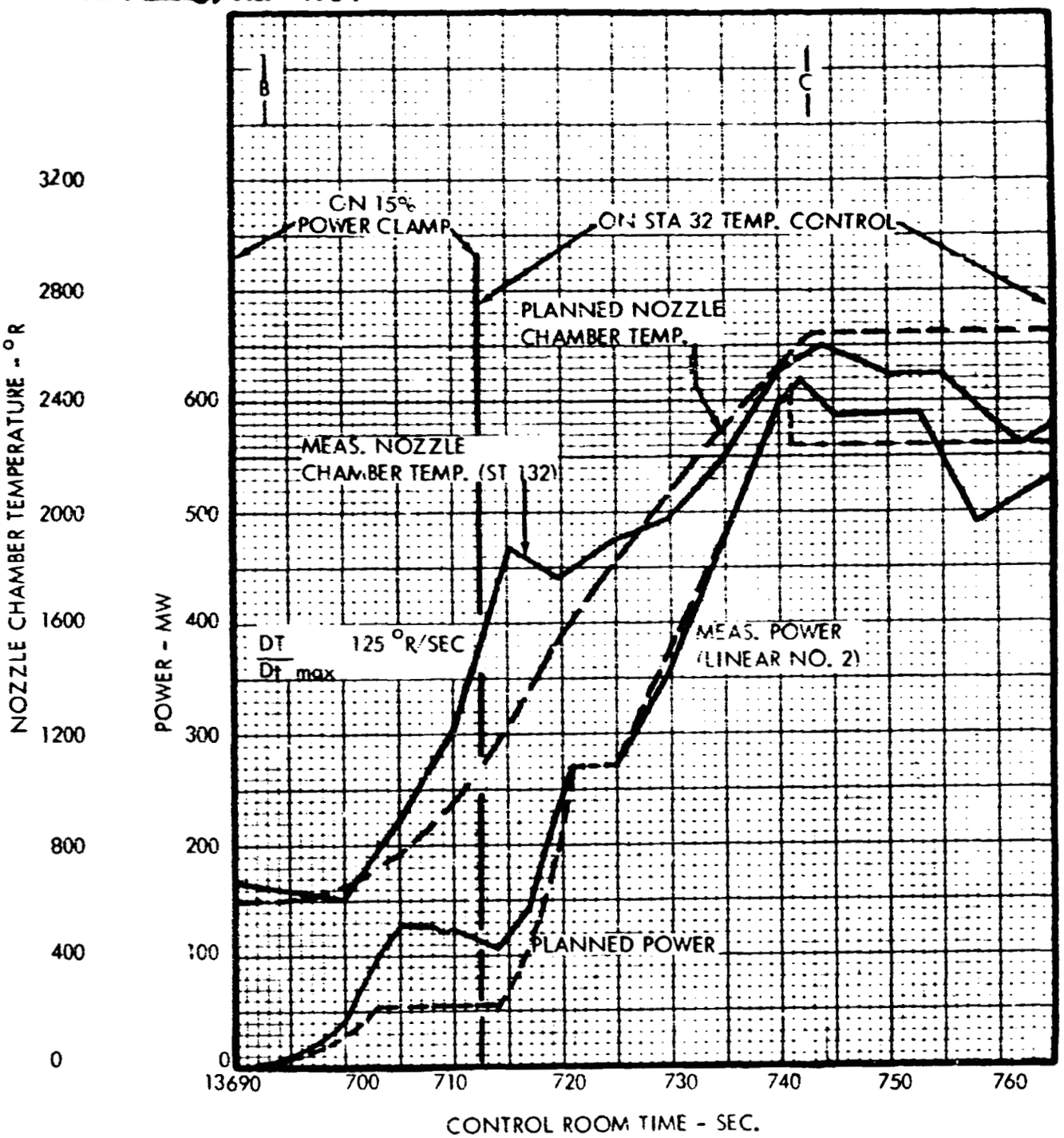

FIGURE 4.1-31 NRX-A2 EP-IV STARTUP POWER AND NOZZLE CHAMBER TEMPERATURE

CONFIDENTIAL
RESTRICTED DATA
Atomic Energy Act - 1954

temperature increased at about 125°R/sec, while 50°R/sec was the expected rate. The effect of the high power on core material temperatures for this same time interval are given on Figure 4.1-32. The higher power was due to an error in setting up the programmer.*

2. TNT Calculated and Measured Startup Conditions

Pre-test operating conditions for the NRX-A2 test were calculated with the TNT reactor model. Because the operating power and flow profiles during the test were considerably different from planned, the pre-test calculations were not applicable. To provide a better comparison of test data and calculations, operating conditions were recalculated using the TNT code and the test power and flow. There were no changes in the reactor model from that used in the pre-test calculations.

Flow rate used was that calculated from nozzle chamber conditions while power was obtained from linear number 2 neutronic power channel, increased by the appropriate ratio to coincide with thermal calculated power at the steady-state hold times. The calculation was performed from the beginning of startup through the entire test profile. Steady-state high power operation comparisons were in poor agreement because of the higher than expected nozzle heat pickup and reflector heating rate. A comparison of TNT and measured nozzle operating conditions was given in Table 4.1-14. On the basis

---

* NRX-A2 Site Test Report, NTO-R-0008, October 20, 1964, CRD.

CONFIDENTIAL
RESTRICTED DATA
Atomic Energy Act - 1954

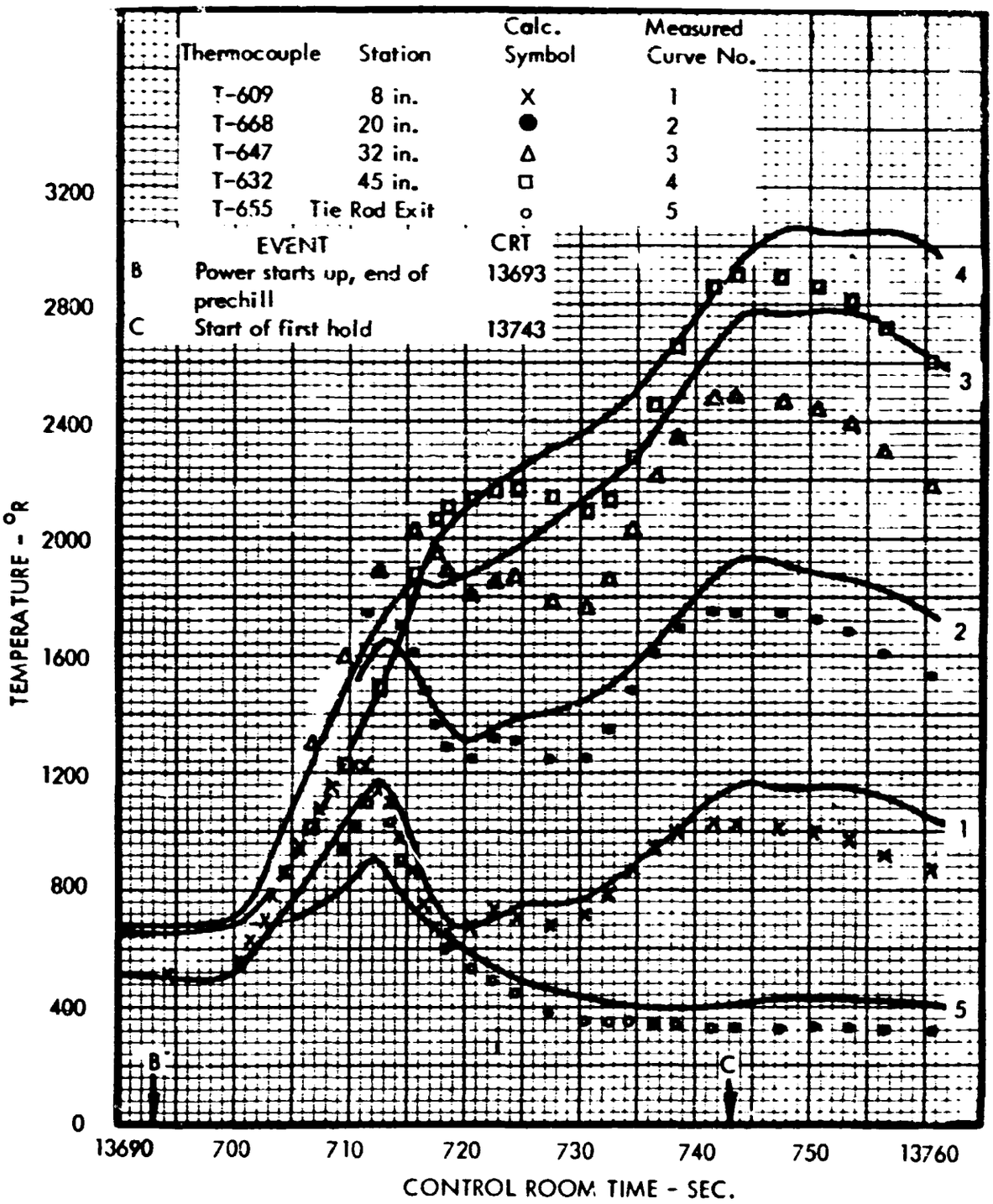

FIGURE 4.1-32 CORE MATERIAL TEMPERATURES AND TIE ROD EXIT TEMPERATURES DURING STARTUP

CONFIDENTIAL
RESTRICTED DATA
Atomic Energy Act - 1954

of these comparisons, the TNT reactor model is being adjusted. To measure the ability of the TNT calculation to reproduce transient reactor conditions, a comparison of measured and calculated temperatures and pressures during prechill* and startup are included in this section. These comparisons of TNT calculated and test results during prechill and startup show that the TNT model closely reproduced the reactor condition during this transient, the transient core temperature distribution agreement being exceptionally good.

The TNT comparisons are given on the figures listed below, and a discussion is included in the following pages.

TNT AND TEST STARTUP COMPARISONS

Figure Number	Comparison Of
4.1-32	Core Material Temperatures and Tie Rod Exit Temperature
4.1-7	Reflector Inlet and Outlet Temperatures
4.1-33	Core Inlet Pressure and Core P
4.1-34	Reflector Inlet and Outlet Pressure and Reflector P

* As noted above, the TNT was rerun from the beginning of startup. All TNT results for the prechill period (to time 13693) are from the pretest predictions.

3. Core Startup Period

Figure 4.1-32 shows a comparison of measured and TNT post-test calculated selected core material temperatures of the core region during the startup period (CRT 13693 to CRT 13743). This comparison shows that the core temperature distribution during the transient is very closely reproduced by the TNT code. However, the calculated temperatures are slightly low as steady-state is approached, possibly because the TNT model used for calculations did not account for the heat interchange between the tie rod unfueled element and the fuel elements. This is presently being investigated with an improved model.

Figure 4.1-33 is a comparison of measured and TNT post-test calculated values of core inlet pressure and core pressure drop. The measured values of core pressure drop and core inlet pressure agree very well with those calculated during this startup period.

4. Reflector - Startup

The azimuthal temperature variation at the reflector inlet, reflector outlet, dome end plenum, and core inlet at the end of prechill (CRT 13693) were given in Figures 4.1-3 and 4.1-4. These figures show a similar geometric temperature variation in all plenums with a minimum in the vicinity of the nozzle feed line ($\theta = 120°$ location), and in some cases an indication of a lesser temperature depression opposite the feed line ($\theta = 300°$). The flow rate and system

Astronuclear

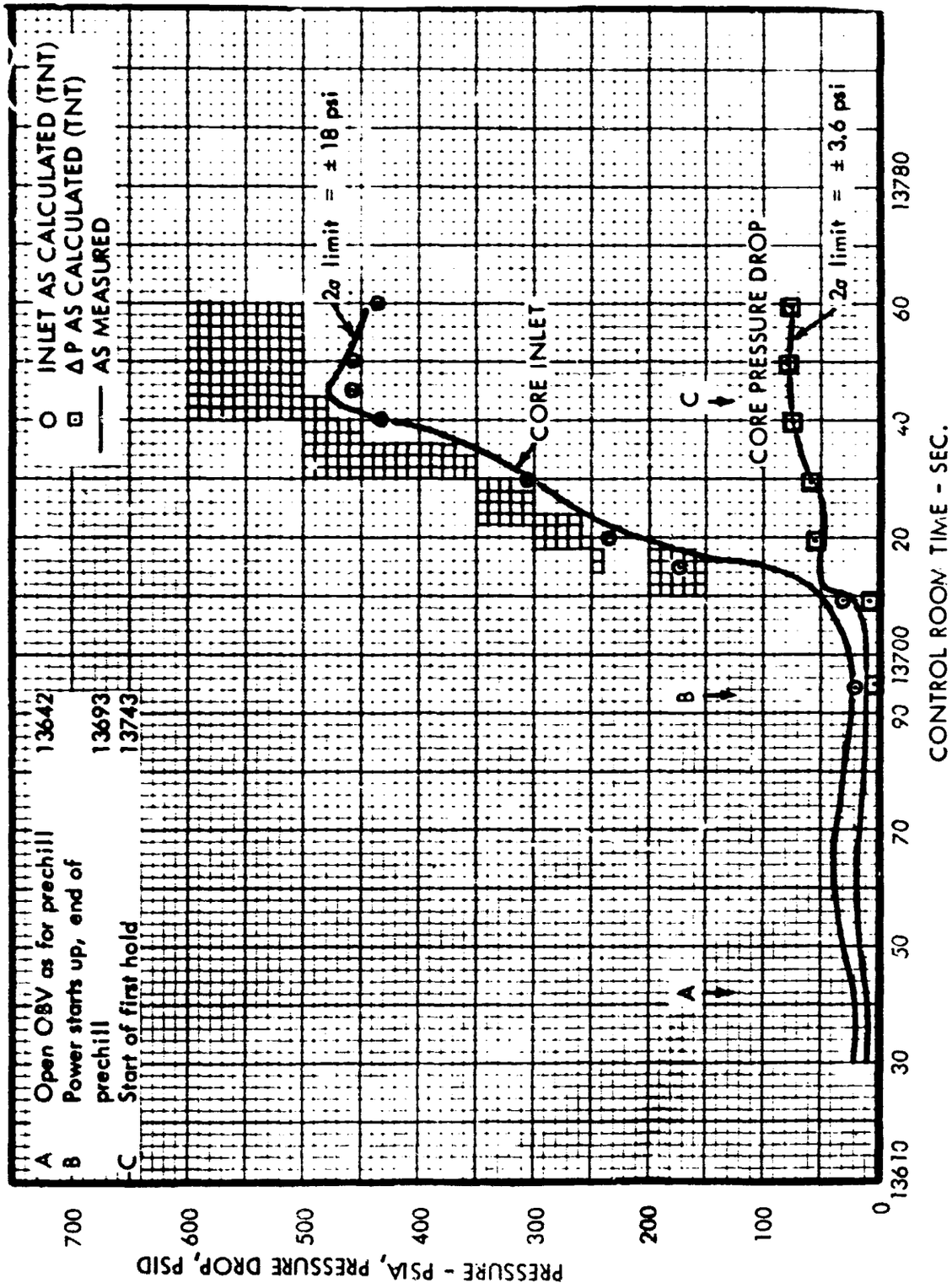

FIGURE 4.1-33 CORE INLET PRESSURE AND CORE ΔP VS. TIME

pressures began to increase rapidly at CRT 13709 and shortly thereafter the temperature asymmetry was gone. No adverse effect of this temperature asymmetry during the early stages of startup is evident.

In Figure 4.1-35 the two extreme fluid T/C indications at the reflector inlet plenum are shown with the pressure at the same location. In the upper part of the figure is the azimuthal temperature variations when the reflector inlet pressure is less than critical pressure and when it exceeds critical pressure. It is noted that the azimuthal temperature variation has been drastically reduced. At the core inlet the asymmetry persisted for a longer time, however, it disappeared on the ramp to the first power hold. Figure 4.1-36 shows that the asymmetry was still in evidence at CRT 13720 but not at CRT 13790, during the power hold. At this time the measured values are all within the 2 error limit. The azimuthal temperature variation is probably associated with two phase flow in the nozzle, but the times at which it reduces drastically cannot be directly correlated with exceeding hydrogen critical pressure, and as noted above, the asymmetry persists at the core inlet for 10 to 15 seconds longer than at the reflector inlet. It is concluded therefore that the thermal asymmetries cause no adverse effect during the startup and are not evident during the steady holds. The TNT calculated and test values of reflector inlet and reflector outlet fluid temperatures during the prechill and startup were given in Figure 4.1-7 and show excellent agreement.

Astronuclear

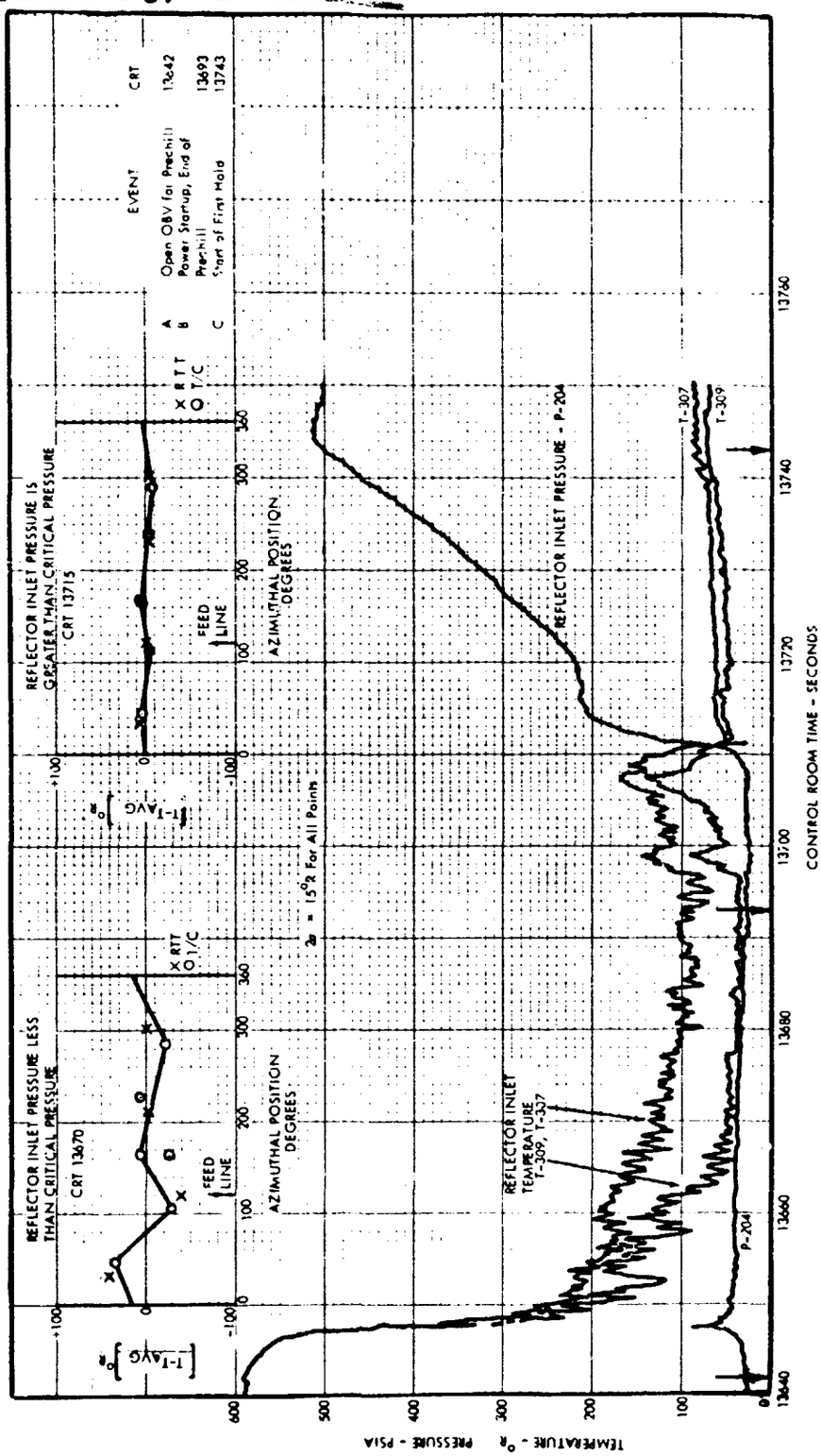

FIGURE 4.1-35 [illegible] TO ILLUSTRATE [illegible] FLUCTUATIONS

Astronuclear

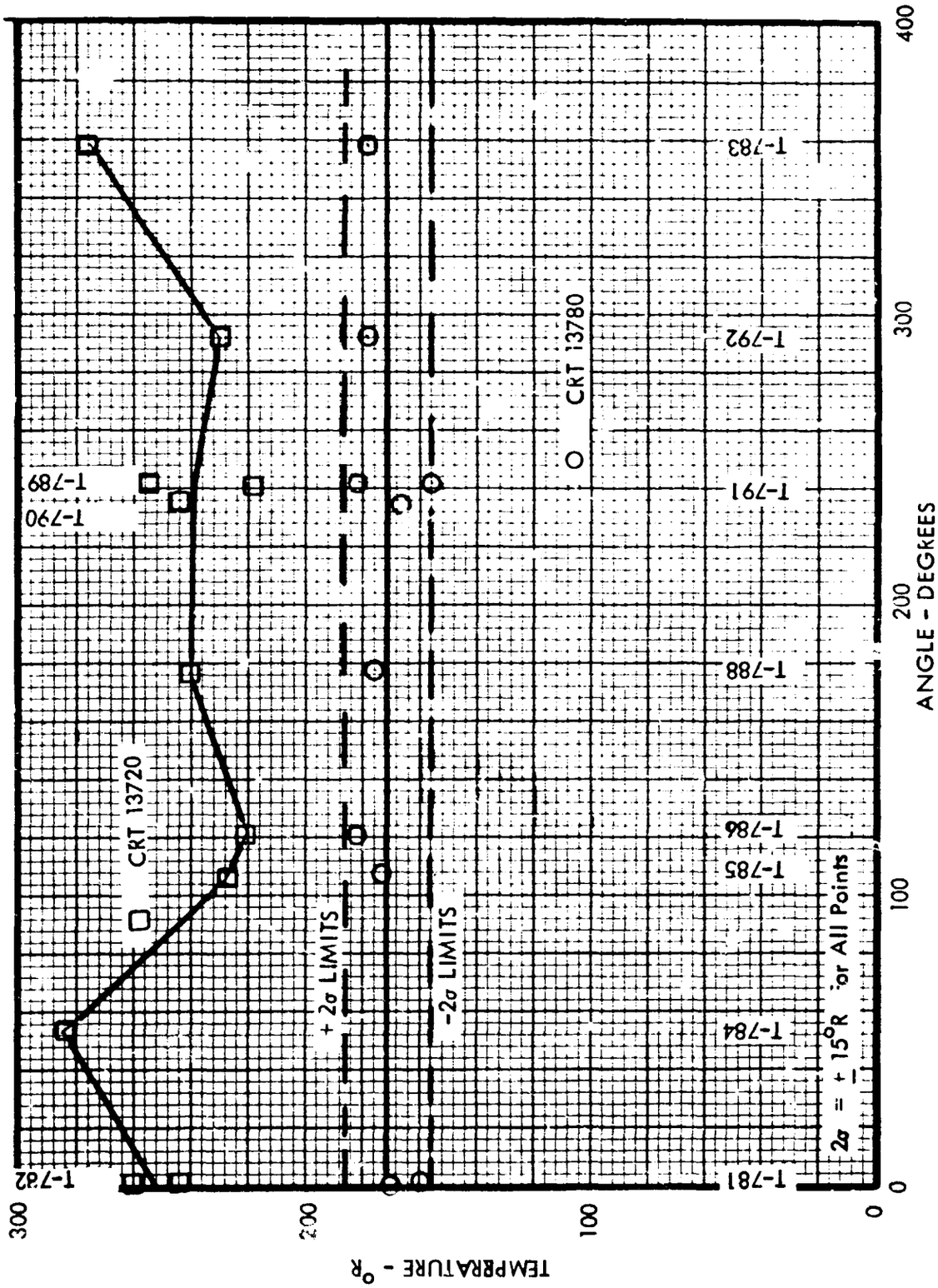

FIGURE 4.1-36 CORE INLET AZIMUTHAL TEMPERATURE VARIATION AT CRT 13720 AND CRT 13780

The lower curve of Figure 4.1-34 is a comparison of calculated (TNT post-run with test power and flow schedules input) and measured values he reflector inlet and exit pressure. During the prechill and startup, calculated values are within the 2 σ limit of the measured values. At the start of the first power hold (CRT 13743) the calculated values are about 10 psi below this 2 σ limit.

The upper curve in Figure 4.1-34 is a comparison of the calculated and measured pressure drops. As seen on the figure the calculated values are below the measured by about 8 psid. There are several reasons for this; first, the flow annulus between the inner and outer reflector has been calculated using measured temperature and pressure conditions in the reactor during the power run. A reevaluation showed the annulus width to be an average of 0.092", compared with the value of 0.108" used for the TNT model. This represents an increase in the total flow impedance of the reflector system. Secondly, the percent of total reactor power measured in the reflector region was 15% higher than that used for post-test TNT calculations. This increase in reflector power results in increased pressure drop across the reflector system. These two items and the measured reflector inlet temperature have been incorporated into the post-test reflector steady-state model, and the post-test values calculated at the high power hold (CRT 14085) give an outer reflector pressure drop which is 0.3 psid lower than the measured value and is well within the 2 σ limit of 1.8 psid for this measurement.

CONFIDENTIAL
RESTRICTED DATA
Atomic Energy Act - 1954

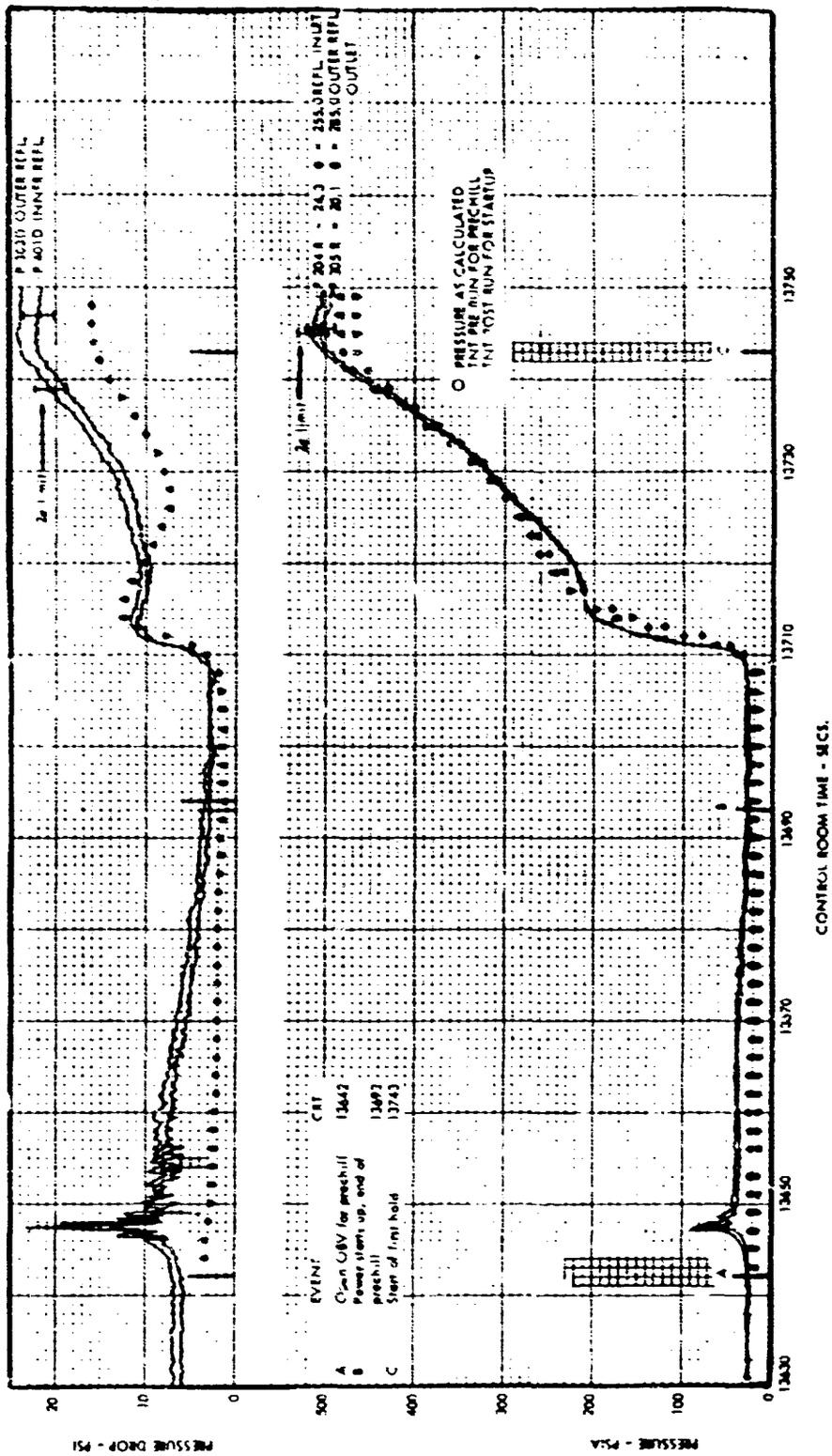

FIGURE 4.1-34 [illegible]

CONFIDENTIAL
RESTRICTED DATA
Atomic Energy Act - 1954

The small spikes in reflector pressure and pressure drop, shown on Figure 4.1-34 occurring at about CRT 13648 is most likely due to the closing of bypass valve AVV-11, resulting in a small surge and increase in flow at this time.

The upper and lower material temperature traces for both the inner reflector and the control drum are shown in Figure 4.1-37. The inner reflector chills at a faster rate than the control drum, however, during a power run these temperatures run higher than the control drum and therefore during the startup these temperatures cross and rise above the control drum temperatures.

Figure 4.1-38 shows selected material temperatures of the outer reflector during the pre-chill and startup. The temperatures continue to drop even after the startup has been initiated. Station 45 T/C reaches its minimum value at CRT 13716 and then begins to rise. Station 32 and 8 being further downstream reach their minimum values at the later times of CRT 13725 and CRT 13729 respectively.

CONFIDENTIAL
RESTRICTED DATA
Atomic Energy Act - 1954

Astronuclear

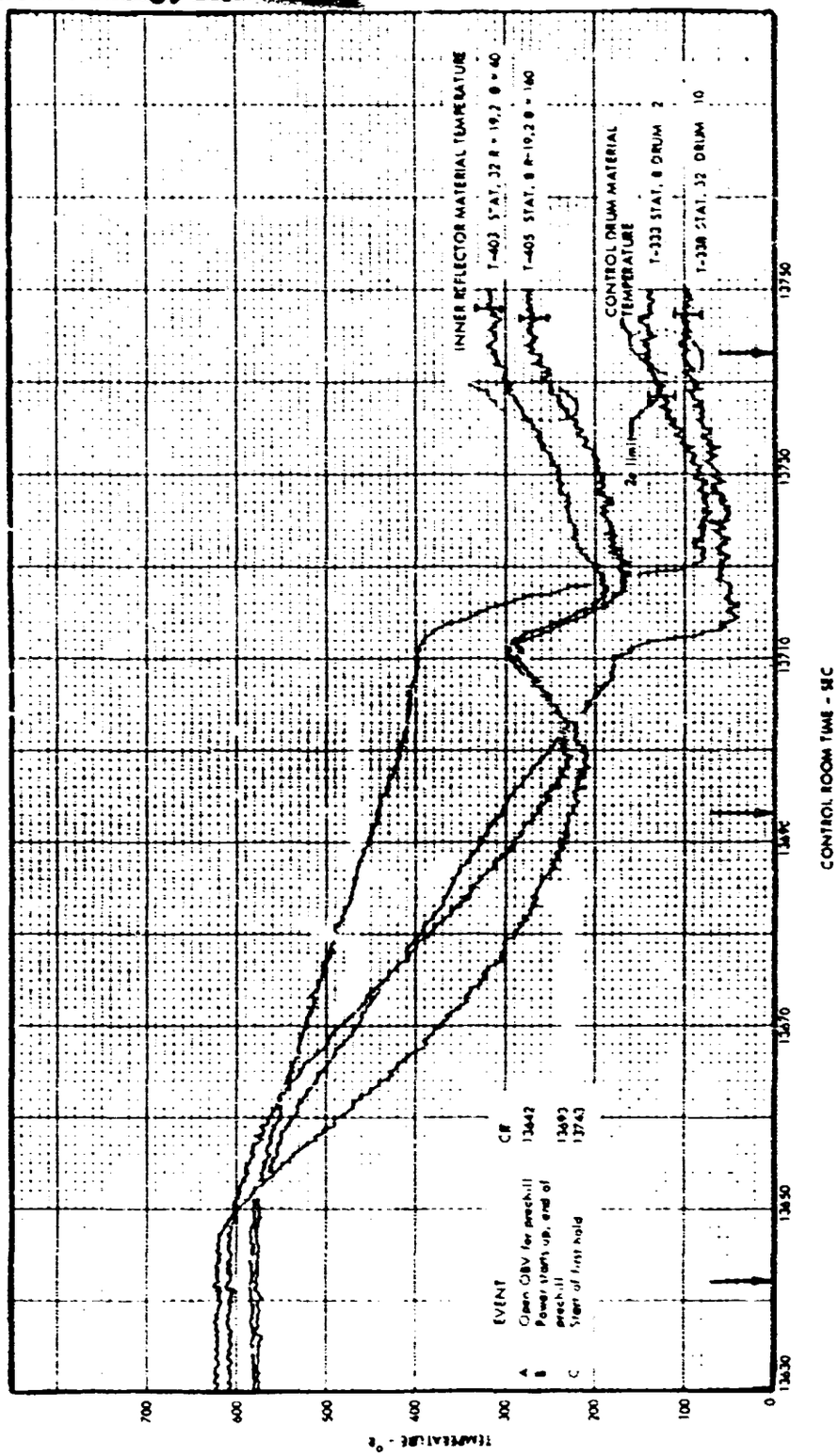

FIGURE 4.1-37 MRX-A2 SP-IV PRECHILL AND STARTUP SELECTED INNER REFLECTOR AND CONTROL DRUM MATERIAL TEMPERATURE TIME HISTORIES

CONFIDENTIAL
RESTRICTED DATA
Atomic Energy Act - 1954

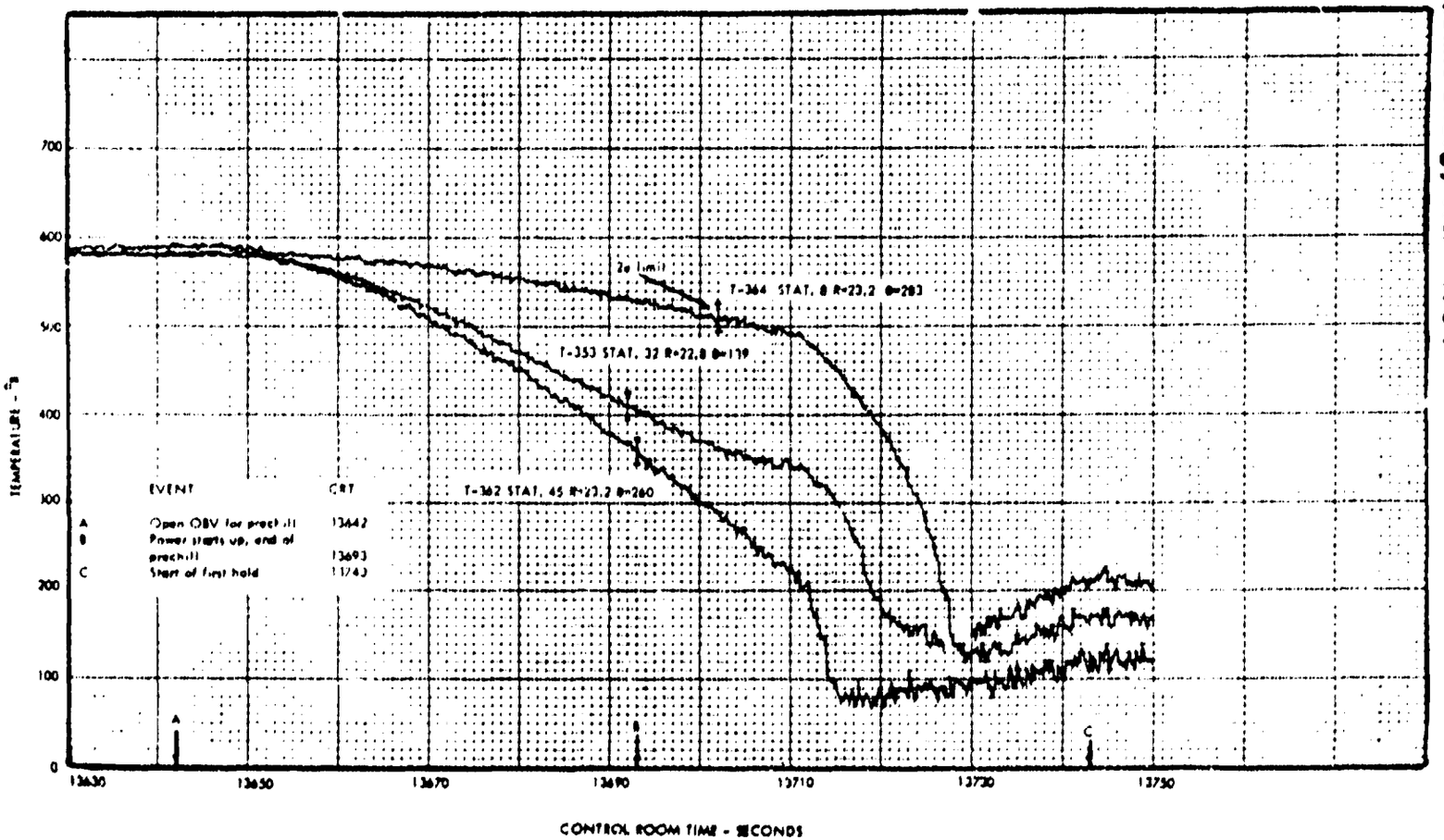

FIGURE 4.1-38 [illegible] PRECHILL AND STARTUP SELECTED OUTER EMPLACEMENT MATERIAL TEMPERATURE-TIME HISTORIES

B. Shutdown

At the completion of EP-IV, the programmers were switched to retreat. Power and flow began to decrease and nine seconds later a manual flow shutdown and power scram were initiated due to apparent loss of dewar pressure. The planned shutdown was to retreat with the nozzle chamber temperature decreasing at 50°R/sec until nozzle chamber temperature had been reduced to 2200°R, then to initiate a flow shutdown and power scram. Calculations indicated that the scram would result in a maximum nozzle chamber temperature decrease of 135°F/sec. The emergency scram occurred when nozzle chamber temperature had decreased only about 350°R from the maximum of 3815°R and was consequently more severe than the planned shutdown.

A comparison of the planned and test nozzle chamber temperatures for the shutdown interval is made in Figure 4.1-39. The maximum nozzle chamber temperature decrease rate was 350°R/sec compared with 135°R/sec planned. Although the nozzle chamber thermocouple was not giving the mixed mean nozzle chamber temperature, its rate of change is the best available indication of the reduction in chamber temperature. Initial chamber temperature decrease rates were greater than 50°R/sec preceeding the scram. This change resulted from a lag in the response of the reactor power to the demand and the problem with the station 32 thermocouples which were indicating low. This is illustrated by comparison of the shutdown demands to the measured variables in Figure 4.1-40. The bottom curve of this figure shows that

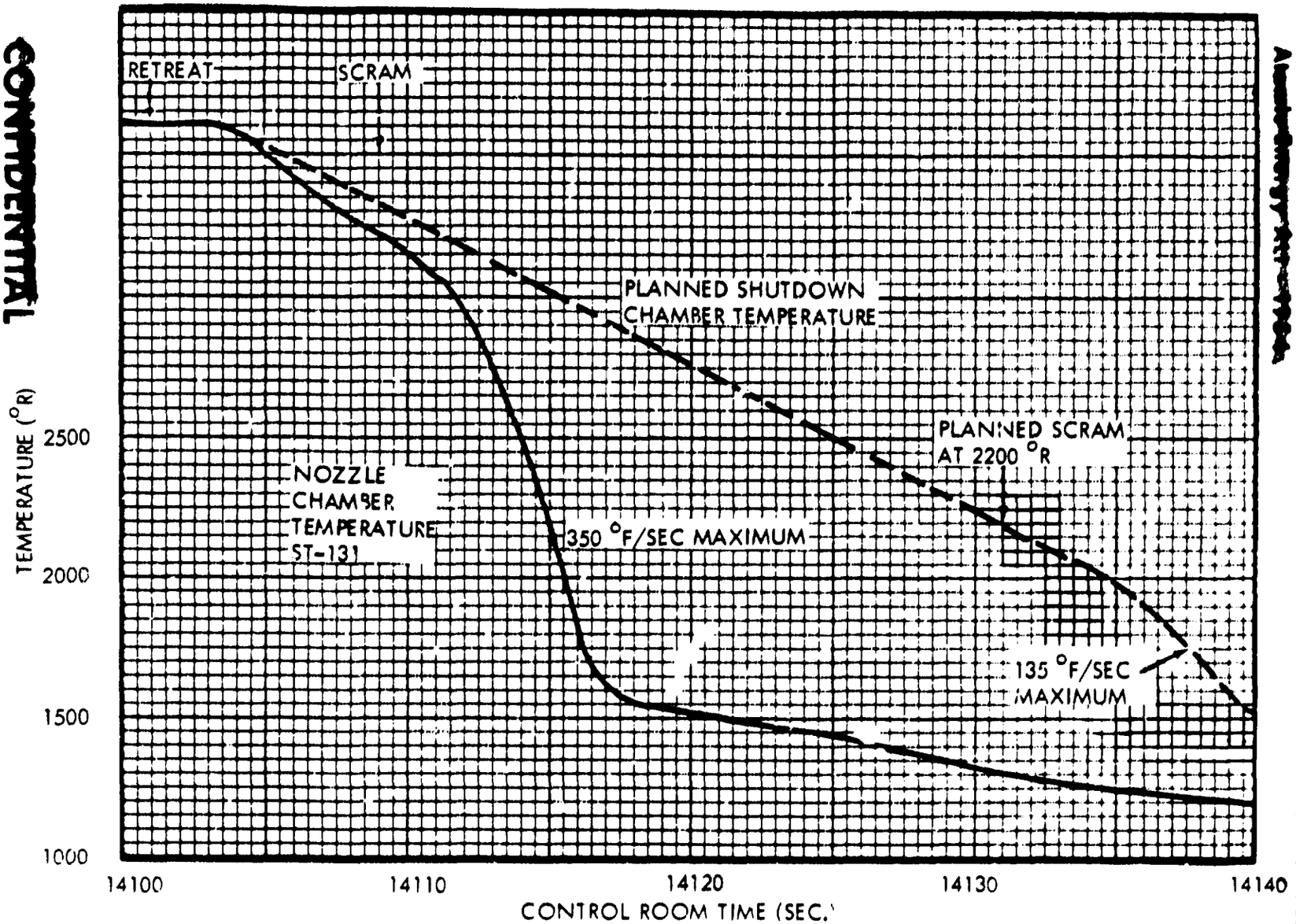

FIGURE 4.1-39 NRX-A2 SHUTDOWN NOZZLE CHAMBER TEMPERATURE

CONFIDENTIAL
RESTRICTED DATA
Atomic Energy Act - 1954

Astronuclear

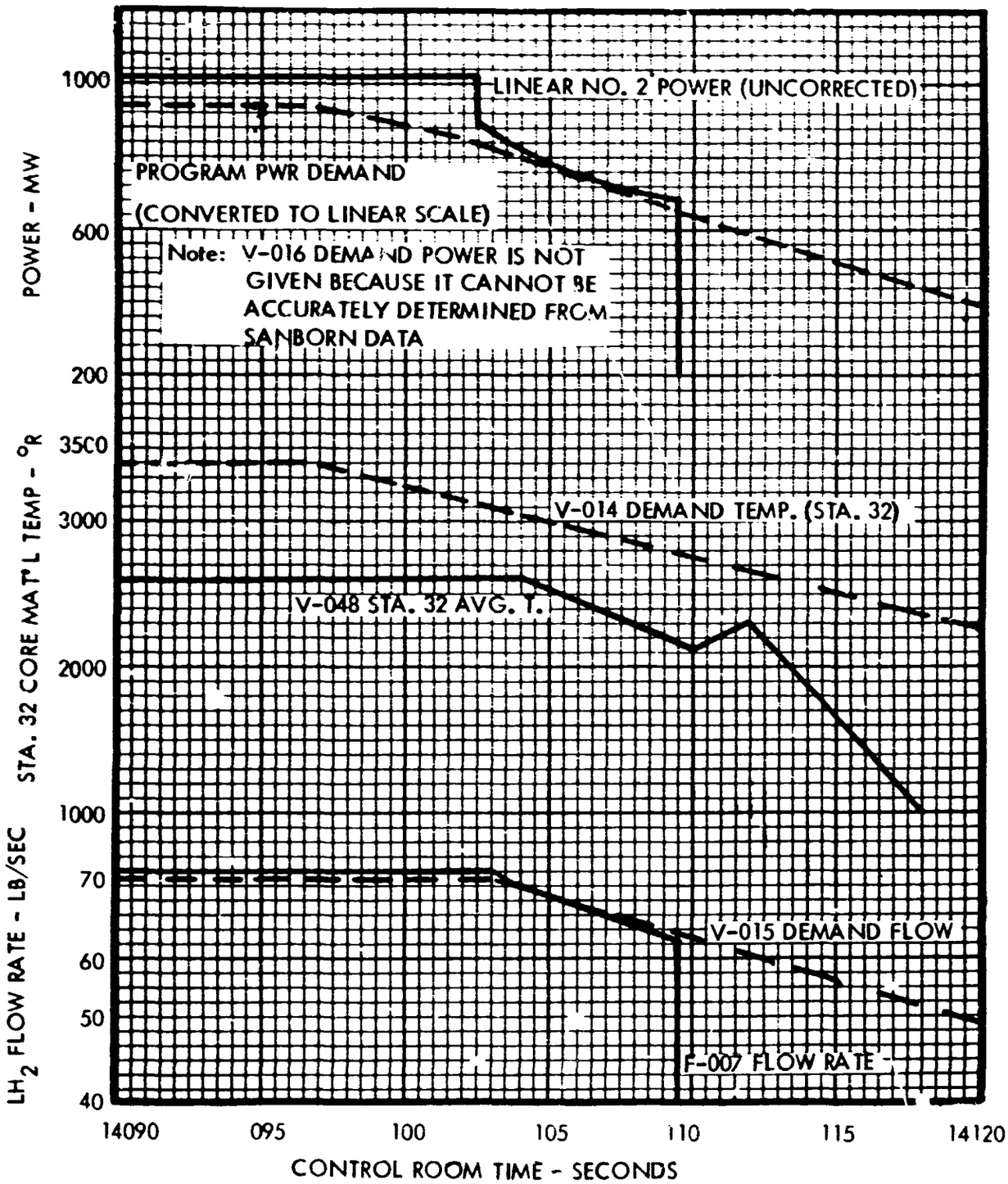

FIGURE 4.1-40 COMPARISON OF THE SHUTDOWN DEMANDS : MEASURED PARAMETERS

CONFIDENTIAL
RESTRICTED DATA
Atomic Energy Act - 1954

flow responded well to demand flow. The middle curves show that temperature demand had resulted in the maximum -15% power trim and had no control effect for the shutdown. The top curve of this figure indicates that there was a six second delay in response of the power to the power demand. When the power did respond to the demand there was a sudden decrease of over 100 MW just as the flow had began to decrease resulting in a cooldown rate in excess of 50°R/sec. If the flow shutdown had not occurred, the nozzle chamber temperature decrease rate would have approached 50°R/sec as the retreat continued.

Tie rod exit gas temperature peak at 1200°R, the exact limit for a transient during EP-IV. Tie rod time-temperature traces were given in Figure 4.1-19. The minimum core inlet temperature during the shutdown was 150°R.

Ambient GH_2 was introduced into the feedline upstream of the mixing chamber when the reactor scrammed. This gaseous hydrogen was to be introduced at about 50% of the LH_2 pressure which existed just prior to the scram. As indicated by the reactor flow rate in Figure 4.1-41, there were some oscillations as the GH_2 forced the 200 pounds of LH_2 out of the system piping and mixing chamber. These oscillations were evident in the nozzle inlet pressure also, as shown in the figure.

Immeidately following the reactor shutdown, sixteen station 45 material temperatures indicated a rise in temperature and four of these thermocouples failed. This effect is treated in Section 4.5.

CONFIDENTIAL
RESTRICTED DATA
Atomic Energy Act - 1954

Astronuclear

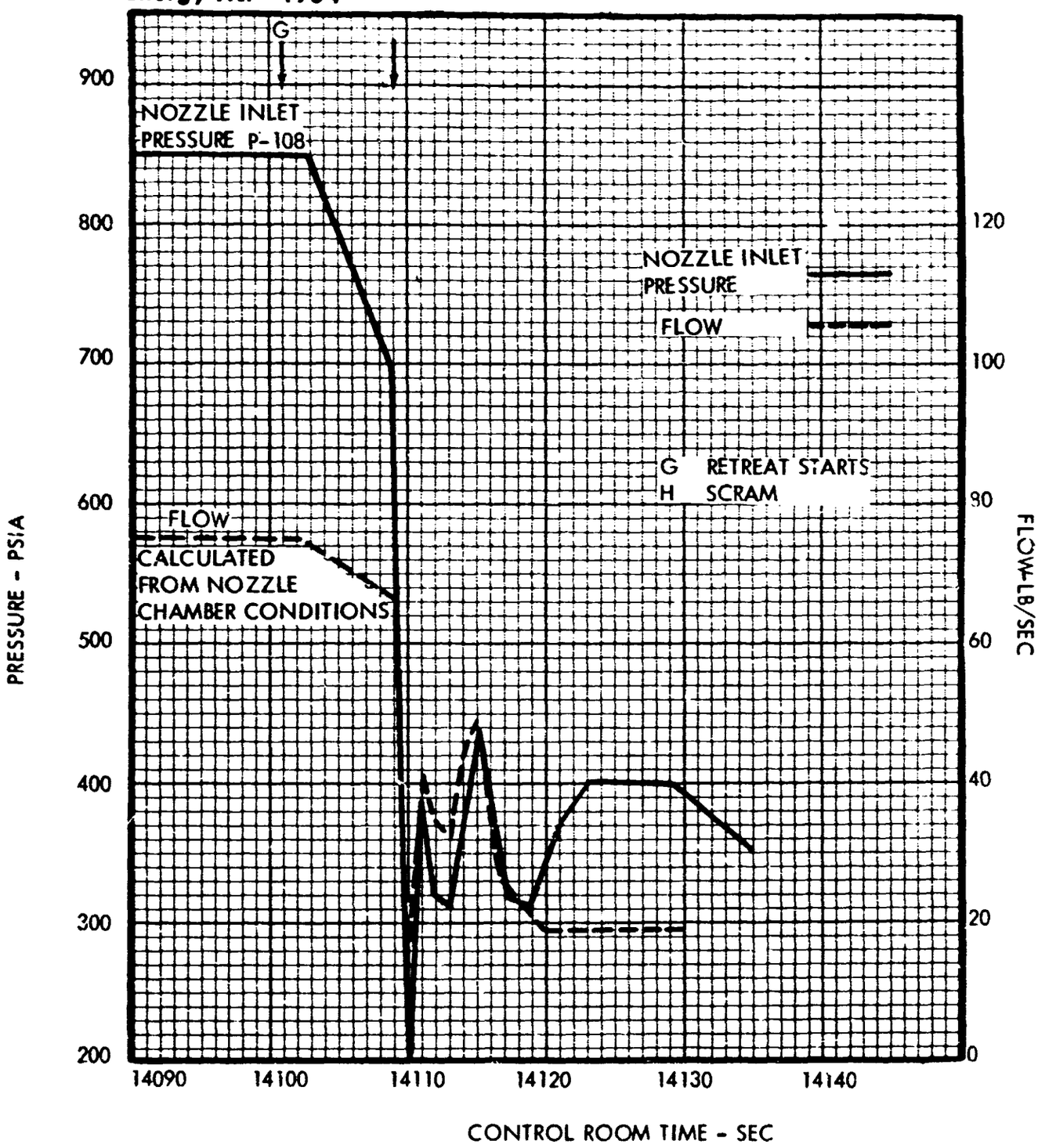

FIGURE 4.1-41 REACTOR SHUTDOWN HISTORY

CONFIDENTIAL
RESTRICTED DATA
Atomic Energy Act - 1954

4.1.6 EP-IV Cooldown

Figures 4.1-42 and 4.1-43 present the best available information on flow rates and coolant usage during cooldown. Time zero for the cooldown analysis is designated as control room time (CRT) 14109 seconds and corresponds to the time of reactor scram. The PCV-41 pressure control loop was activated simultaneously with reactor scram. About 11 seconds were required to exhaust the approximate 200 lb of LH_2 that is stored in the piping system and mixing chamber during operation. Continuous ambient GH_2 cooling between 20 and 6 lb/sec was maintained until 125 seconds after scram. At this time, the maximum core temperature was well below 1400°R and therefore ambient nitrogen cooling was initiated at a flow of approximately 30 lb/sec. The continuous ambient nitrogen flow was manually controlled between approximately 30 and 5 lb/sec. Pulse cooling with approximately 5 lb/sec of ambient nitrogen was initiated at about 1 hour after scram. Pulses were initiated by one of the following temperature limitations: 900°R core station 8, 850°R inner reflector, and 850°R support plate. The core station 8 temperature exceeded the 900°R limit by 150°R before the first ambient nitrogen pulse was initiated. The purpose of core station 8 temperature limit was to limit the orifice adhesive temperature. The orifice adhesive has been successfully tested under irradiation at 1200°R, however without gamma radiation effects. In addition, the orifice was undoubtedly at a lower temperature than core station 8. Thus, the orifice adhesive was probably not damaged during cooldown. After approximately 13,000 seconds (3.6 hours), 200°R GN_2 at about 5 lb/sec was used for pulse cooling. During this period an excessive amount of coolant was used because a faulty

Astronuclear

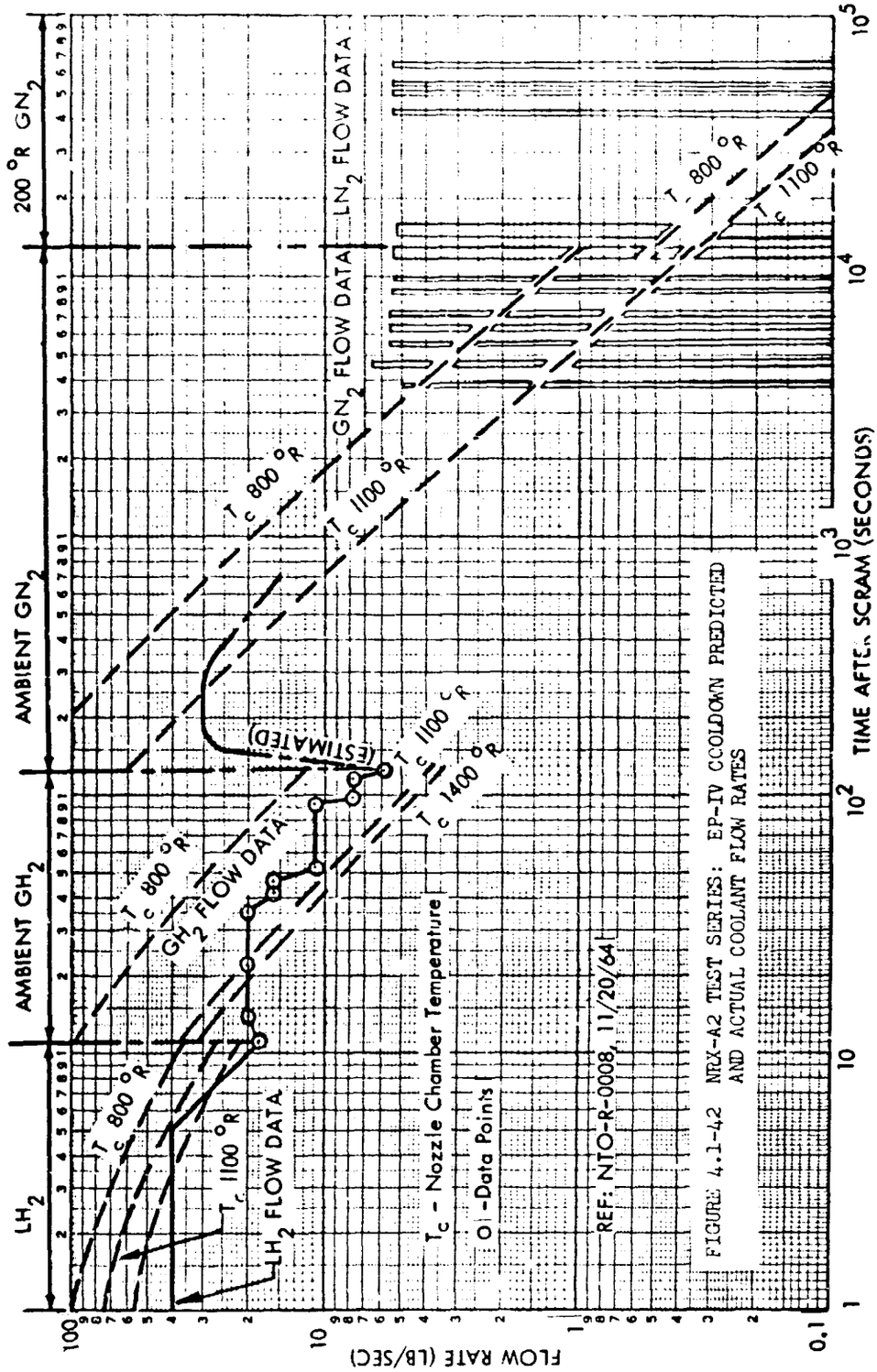

FIGURE 4.1-42 NRX-A2 TEST SERIES: EP-IV COOLDOWN PREDICTED AND ACTUAL COOLANT FLOW RATES

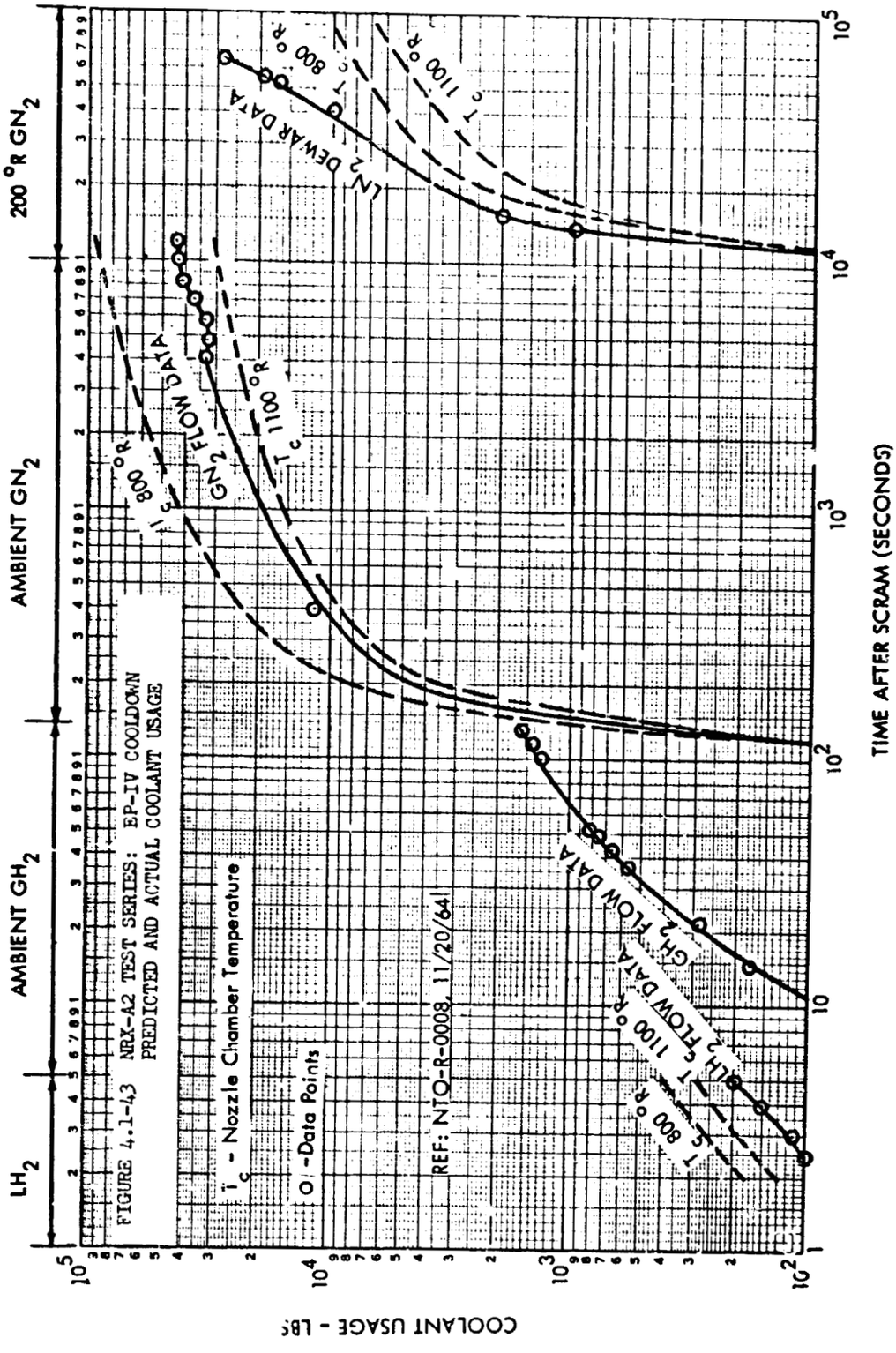

FIGURE 4.1-43 NRX-A2 TEST SERIES: EP-IV COOLDOWN PREDICTED AND ACTUAL COOLANT USAGE

core support plate thermocouple gave readings higher than the operating limit. As a result, the core was cooled inefficiently to approximately 200°R. Pulse cooling was ended at 32 hours after scram.

The total quantities of all fluids used during cooldown are shown on Figure 4.1-43. Figures 4.1-42 and 4.1-43 also show calculated coolant flow rates and coolant usage for constant chamber temperatures between 800°R and 1400°R. The following description* applies to the calculated data on these two figures: "The predicted (calculated) values shown are for an integrated power 3×10^5 MW-sec and a peak power of 102%. The reactor decay power was computed by the Way-Wigner fission product decay model and a summation of six delayed neutron groups to obtain the delayed neutron power decay. This model has been verified by using data obtained following the completion of KIWI B-4D and B-4E tests." Calculated flow rates and coolant usage are only shown to indicate the approximate coolant exit conditions that existed during cooldown. More detailed analysis was not deemed necessary in view of the uncertainties of the available cooldown data. A comparison of KIWI B-4E and NRX-A2 cooldown gas requirements is given in Table 4.1-15. To evaluate the efficiency of cooldown, the average exit gas temperature for all gases used during the cooldown has been calculated and is given in the table. These absolute temperatures on a relative basis are a good indication of the efficiency of the cooldowns.

The cooldown was not compared directly with the pre-test predictions primarily because the power profile was different than the one used for the predictions and the coolant usage and control was considerably different

* NRX-A2 Site Test Report, NTO-R-0008, November 20, 1964, CRD

TABLE 4.1-15

COMPARISON OF KIWI-B4E & NRX-A2 COOLDOWN DATA

		NRX-A2	KIWI-B4E	
		EP-IV	Power Test	Restart
Total Integrated Power	- MW sec	3.46×10^5	5×10^5	1.75×10^5
Total LH_2 Used	- lb	200	700	3540
Total GH_2 Used	- lb	1550	2530	1550
Total GN_2 Used	- lb	44,000	64,700	34,000
Total 200 N_2 Used	- lb	28,000		
Cooldown Time	- hrs	32	73.5	8
Average Exit Temperature of Gas Used	- °R	815	935	459
ΔT		425	448	190

than assumed. Figure 4.1-44 compares the predicted decay power during cooldown to the two experimental power values. The calculated power is based on the EP-IV power profile and decay power data. The experimental power values are based on heat storage in the core during intervals between ambient nitrogen coolant pulses. Since only relative changes in core temperature were required for this calculation, the results are not influenced by the considerable inaccuracies of the measured core temperatures at low temperatures. The experimental values were increased by 7% to convert core power to total reactor power. The agreement between the two experimental values and the predicted power is exceptionally good. Due to the limited cooldown data, only two experimental power values at approximately one and two hours after scram were calculated. However, these two points are sufficient to check the absolute value of the predicted decay power curve. As expected, the experimental values are below the calculated power since the heat loss from the core was neglected in the experimental power determination.

4.1.7 Experimental Plan V - Low Power Mapping Test

A. Description and Chronology

During the EP-V test, the reactor demonstrated stable operation at seven distinct steady state holds which covered a range of 21.3 - 52.6 MW in thermal power and 5.2 - 13.5 lb/sec. Power response as a result of variations in flow was completely stable.

Two figures, the low power performance map and the time variation of power, flow, and control drum bank position, describe the EP-V test chronology. Figure 4.1-45 illustrates the steady state low power performance

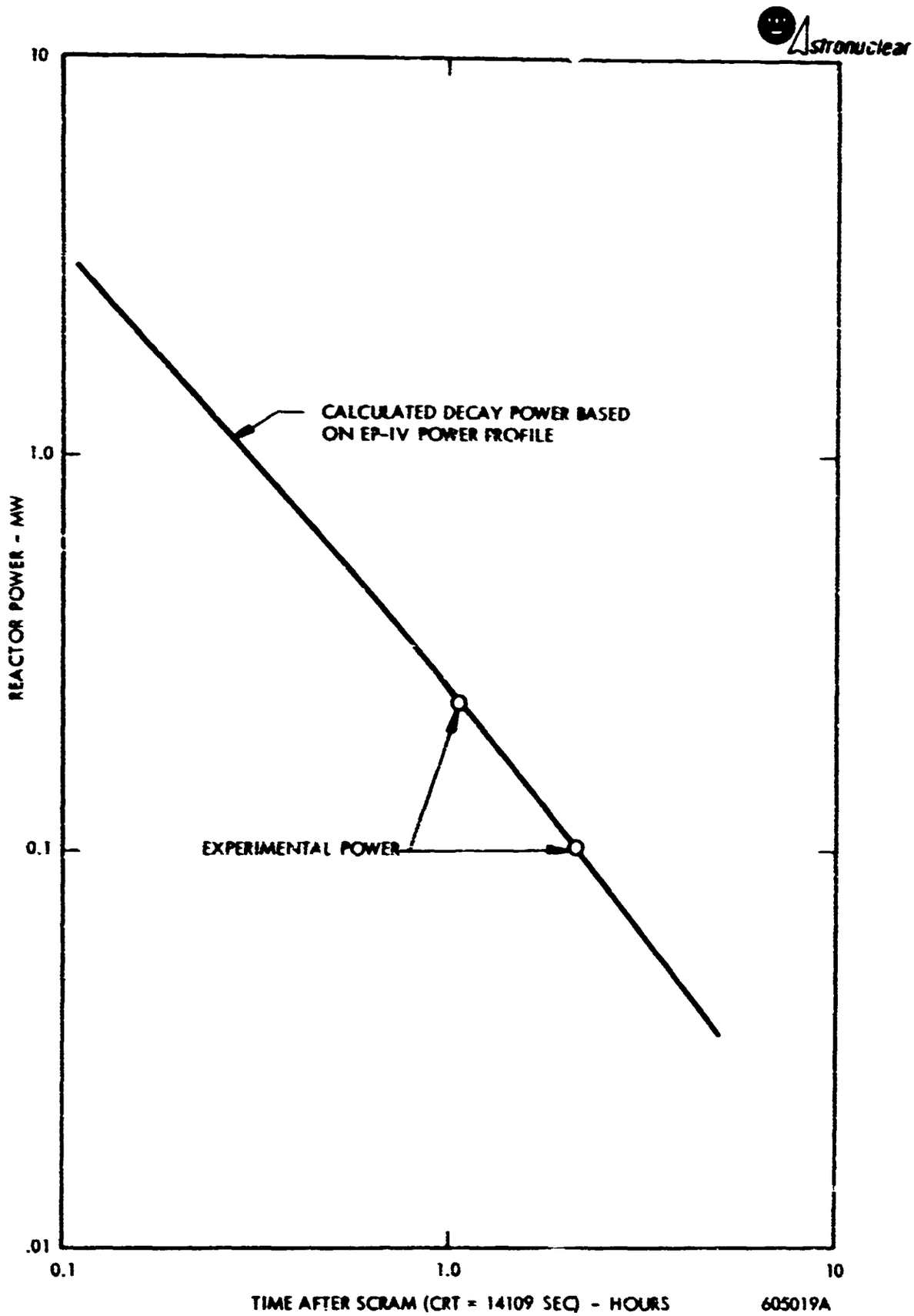

FIGURE 4.1-44 - COMPARISON BETWEEN EXPERIMENTAL AND CALCULATED DECAY POWER DURING COOLDOWN FOLLOWING EP-IV

CONFIDENTIAL
RESTRICTED DATA
Atomic Energy Act 1954

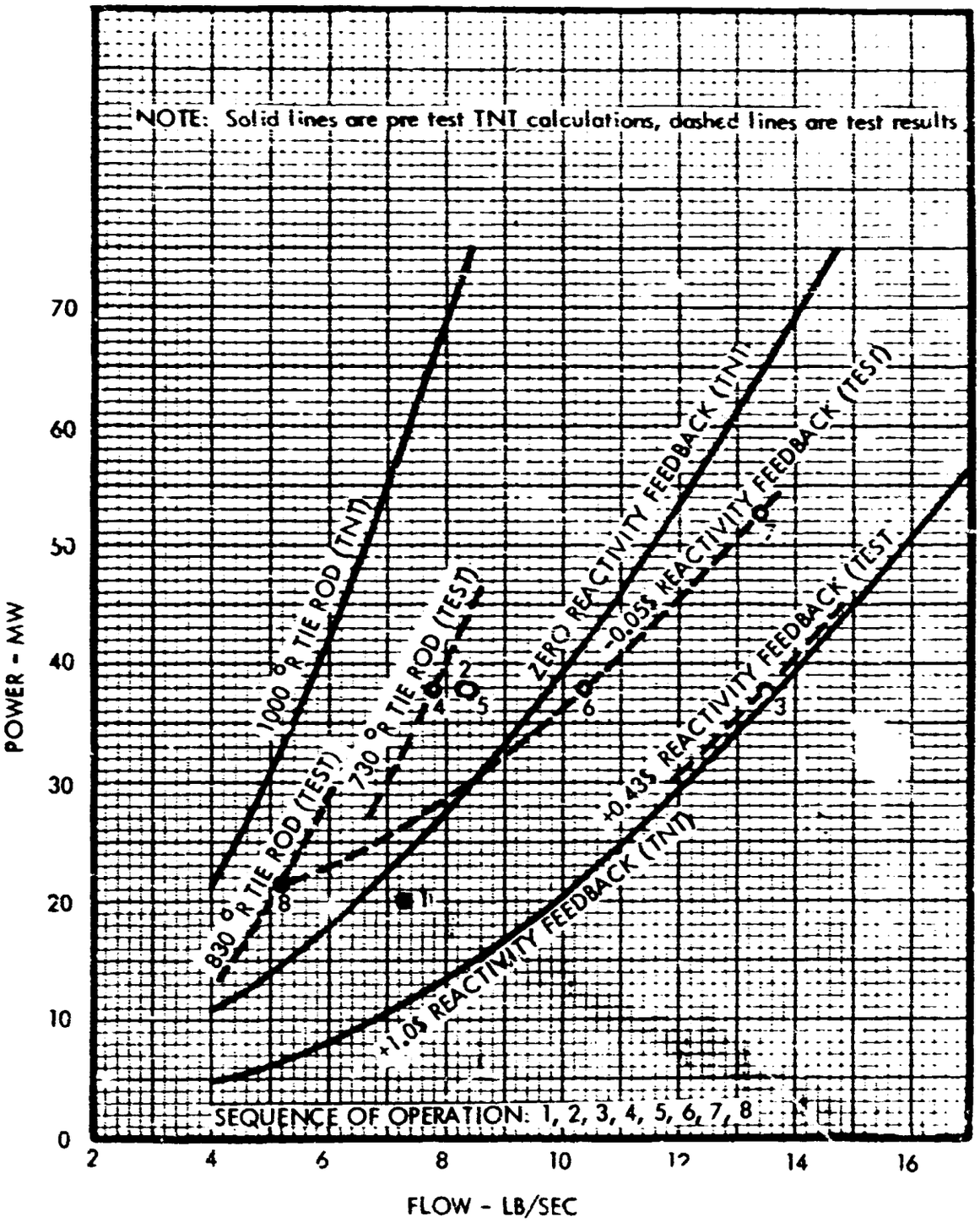

FIGURE 4.1-45 EP-V LOW POWER MAPPING TEST LOW POWER PERFORMANCE MAP

CONFIDENTIAL
RESTRICTED DATA
Atomic Energy Act 1954

map with pre-test(TNT calculation) curves representing 1000°R average tie rod exit temperature, zero reactivity feedback, and $1.00 reactivity feedback. These reactivity feedback lines were calculated with four simplified equations which are based on the detailed nuclear design reactivity calculation method described in Section 4.4. The four simplified equations calculate reactivity feedback as a function of average core hydrogen density, average core material temperature, average inner reflector density, and average outer reflector temperature. These simplified equations are inaccurate in the low power operating region. Conservative reactor operation is possible at any flow-power points that fall between the 1000°R tie rod coolant exit temperature and the +$1.00 feedback reactivity curves. These limits are extremely conservative since the EP-V test was the first attempt to operate in the low power region. For example, the tie rod exit temperatue limitation for normal transients is 1200°R, while the total available shutdown reactivity assuming a 90° control drum position is approximately $4.00. The constant power and flow points that were achieved during the EP-V test are superimposed on the performance map. In addition, test results are used to show the approximate location of lines that represent 730°R tie rod temperature, -$0.05 reactivity feedback, and + $0.43 reactivity feedback. The time variation of power, flow, and control drum bank position starting from the conclusion of the pre-chill is shown on Figure 4.1-46. The constant power and flow points that were achieved during the test are indicated on Figure 4.1-46. In general, the transients during the EP-V test were very slow compared to normal startup and shutdown operation. The entire test from start of pre-chill to reactor scram required approximately 20 minutes.

Astronuclear

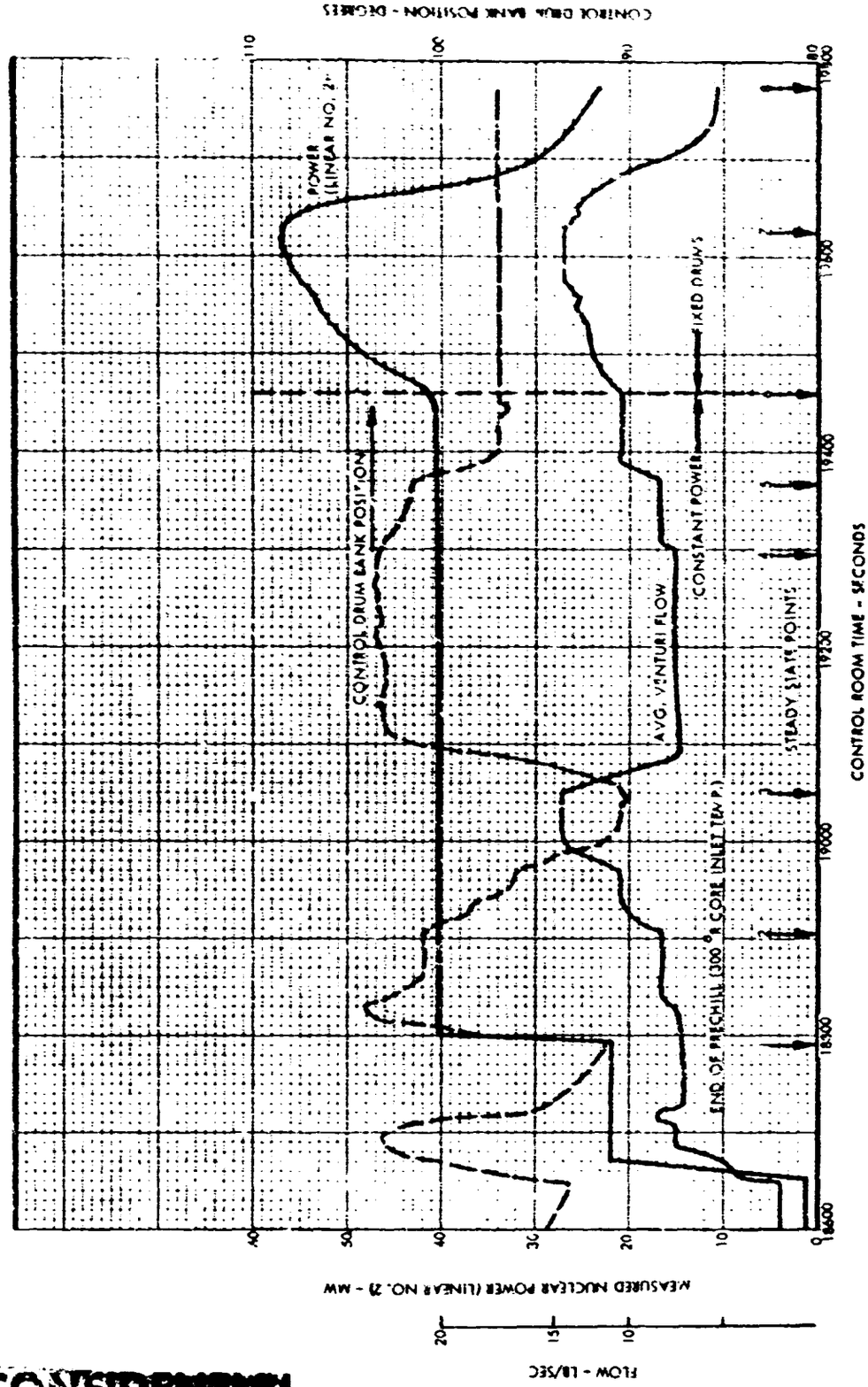

FIGURE 4.1-46 [illegible]

The EP-V test consisted of two parts; one, constant power with flow control, and two, fixed control drum with flow control. On Figure 4.1-45 the constant power part consists of points 2, 3, 4, 5, and 6, and the fixed control drum part consisted of points 6, 7, and 8. The initial part of the test consisted of a pre-chill with approximately 2 lb/sec flow and 1 MW power until the core inlet temperature had decreased to 300°R. At this time, the power was increased to 19.8 MW* with a 2.5 second period, and the flow was increased to 7.3 lb/sec. These conditions of flow and power (point 1) were maintained for approximately 120 seconds, which was not sufficient to establish steady state reactor conditions. Point 1 was required to circumvent the system flow lag which forced the discontinuation of the first attempt to perform the test. At this time the power was increased to 37.7 MW, and the flow to 8.3 lb/sec. The resulting steady state condition (point 2) is the base point for the constant power test. Starting from point 2, steady state reactor operation at constant power with variations in flow was achieved at points 3, 4, and 5. The maximum reactivity feedback equal to +$0.43 occurred at point 3 with 13.5 lb/sec flow. Point 4 with 7.8 lb/sec flow produced the highest apparent tie rod temperature that was observed during the test. Analysis of the test results indicates that this observed tie rod thermocouple was in error, and that the actual tie rod temperature was only approximately 730°R at point 4. The fixed control drum test was initiated from point 4 with 10.5 lb/sec flow, 37.7 MW power, and -$0.05 experimental reactivity feedback. Starting from point 4, the flow was gradually increased to 13.4 lb/sec (maximum flow with 100 psia Test Cell - A dewar pressure) and maintained until

* The best estimate of thermal power, and average venturi flow are specified. These values should correspond exactly with Figure 4.1-45. Figure 4.1-46 shows Linear No. 2 (measured) which is about 9% greater than calculated thermal power.

stable reactor operation at 56.7 MW (point 7) was achieved. From point 7, the flow was slowly decreased to 5.2 lb/sec with a corresponding power decrease to 22.9 MW (point 8). From point 8 an automatic shutdown (reactor scram, discontinuation of liquid hydrogen flow, and initiation of approximately 5 lb/sec of ambient hydrogen) was used to complete the test.

The analysis of the EP-V test are divided into two parts; one, the low power steady state operating conditions and two, reactor operation with fixed control drums. The most significant reactor conditions are compared with TNT calculations using the pre-test TNT reactor model and calculation procedure.

B. Steady State Operating Conditions

1. Thermal and Fluid Flow - Analysis of Data

A major objective of the EP-V test was to obtain steady state data in the low power-low flow operating region. Such data is required to determine the low power operating map. Seven steady state points were achieved during the EP-V test. These steady state points are marked 2-8 on Figure 4.1-45, the low power performance map, and on Figure 4.1-46, the time variation of power, flow, and control drum position. Thermal performance data for these seven steady state points and one intermediate hold during the startup is tabulated in Table 4.1-16. This section will cover the determination of thermal power and the significant reactor performance conditions at these seven low power holds.

The thermal power calculation was based on points 2-6. These points are characterized by constant nuclear power (Linear No. 2 measurement). Calculated nozzle chamber temperature and average venturi flow were

CONFIDENTIAL
RESTRICTED DATA
Atomic Energy Act - 1954

TABLE 4.1-16

EP-V LOW POWER MAPPING: STEADY STATE TEST DATA

Point Designation	Intermediate Hold	Constant Power				Fixed Drums		
Map Point	1	2	3	4	5	6	7	8
CRT Time	18790	18905	19050	19295	19365	19460	19625	19775
Linear No. 2 (test) power - MW	21.4	40.6	40.6	40.6	40.5	41.0	56.7	22.9
Thermal power - MW	19.8	37.7	37.7	37.7	37.7	37.7	52.6	21.3
Flow - lb/sec	7.30	8.32	13.47	7.82	8.40	[illegible]	13.42	5.21
Feed line: T	40	41	38	40	40	39	38	40
P	37	60	64	58	59	61	83	34
Reflector Inlet: T	40	58	47 (TP)	93	52	46 (TP)	49 (TP)	42 (TP)
P	32	52	60	49	52	55	76	30
Core Inlet: T	49	125	47 (TP)	152	140	46 (TP)	59	91
P	31	49	58	46	49	53	73	28
Core Exit: T mixed measured	550	1070	670	1210	1150	880	960	810
T mixed calculated	665	1220	800	1270	1250	1000	1230	980
T Tie rod	—	765	345	730	710	460	560	830
P	23.1	35.7	46.7	34.2	36.5	40.8	58	21.6
Pressure Drops: Nozzle	4.5	7.5	4	9	7.3	6	7.3	4.3
Reflector	12.	3	1.5	3	3	2	2.5	1.5
Shield	nil	nil	nil	nil	nil	nil	nil	nil
Core	7	13	11	12	12	12	15	6
Core Temperatures: Station 8	243	406	339	443	414	363	411	326
Station 20	530	624	577	1022	900	695	743	656
Station 32	646	1140	768	1130	1290	1007	993	834
Station 45	692	1512	915	1627	1543	1218	1428	1213
Reactivity Feedback - $	-0.54	-0.37	+0.43	-0.59	-0.42	-0.05	-0.05	-0.06

Notes: 1. Temperatures - °R, Pressures - psia, pressure drops - psi
2. (TP) designates two phase hydrogen conditions, temperatures shown correspond to pressures.
3. Plenum pressures were changed slightly from test data to correspond to pressure drops.

CONFIDENTIAL
RESTRICTED DATA
Atomic Energy Act - 1954

Astronuclear

used to determine the thermal power. The choked nozzle flow equation using measured nozzle chamber pressure and average venturi flow was used to calculate the nozzle chamber temperature. The calculated nozzle chamber temperature was used in place of the measured temperature due to the inaccuracy of these thermocouples at the relatively low temperatures that occurred during EP-V. Thermal powers for the EP-IV test were determined by multiplying the flow rate times the coolant enthalpy difference between nozzle chamber and reflector inlet plenum. This method was not used for EP-V since the reflector inlet enthalpy could not be determined accurately because two-phase conditions existed and the inaccuracies of plenum temperature measurements near liquid hydrogen temperatures. Therefore, a curve based on TNT prediction calculations which gives chamber temperature as a function of the power to flow ratio was used. This curve which is approximately linear was calculated for flow rates between 7 and 14 lb/sec, and chamber temperatures between 800 and 2000°R. With this curve, the flow to power ratio was found as a function of chamber temperature for points 2-6. The thermal power was then calculated by multiplying the power to flow ratio times the average venturi flow rate. The accuracy of this method is only affected by the accuracy with which the TNT code predicts the nozzle heat pickup. The predicted nozzle heat pickup at these operating conditions is less than 3% of the total reactor coolant enthalpy rise (nozzle torus to nozzle chamber). Therefore with this method, a 50% error in calculating the nozzle heat pickup results in only a 1.5% error in determining total reactor power. For points 2-6, the average calculated thermal power equal to 37.7 MW is approximately 8% lower than the

measured nuclear power (Linear No. 2) of 40.6 MW. The thermal power for points 7 and 8 was determined by multiplying the measured nuclear power times 0.92 which is the ratio of calculated thermal to measured nuclear power for points 2-6. Based on thermal power and average venturi flow, the reactor operated in the range of 21.3 to 52.6 MW power and 5.2 to 13.5 lb/sec flow during the EP-V test.

A conservative reactor operating limitation before the NRX-A2 test was a minimum core inlet temperature equal to 90°R The purpose of this limitation was to assure completely gaseous hydrogen at the core inlet. It was felt that the high densities associated with liquid or two-phase hydrogen could produce excessive and/or unstable positive reactivity feedback which in turn, could produce power oscillations or an uncontrollable power increase. This concern proved to be unfounded by the results of the EP-V test. During the test, the reactor operated stably at two distinct steady state holds (points 3 and 6), with two-phase hydrogen conditions at the core inlet. The plenum temperature measurements were inaccurate at two-phase hydrogen temperatures, and only the existence of two-phase conditions could be established. The two-phase temperatures that are shown in Table 4.1-16 are based on the measured pressures. Stable reactor operation with two-phase hydrogen at the core inlet may be inferred since no power oscillations or other signs of instability occurred. Change in reactivity feedback during constant power operation were accompanied by nearly proportional changes in control drum position. Figure 4.1-46 shows that a smooth inward rotation of the control drums occurred during the transition from point 2 (single-phase at core inlet) to point 3 (two-phase core inlet conditions). This proves that for the test

conditions the transition from single-phase to two-phase does not cause a sudden or abrupt change in reactivity feedback. Therefore, on the basis of EP-V results, the core inlet temperature limitation of 90°R can be eliminated and replaced by a more general positive reactivity criterion which is measured by a change in control drum position from the cold critical position. This will simplify and increase the area of the reactor operating region since only one lower limitation (reactivity feedback) is required.

The tie rod exit gas temperature limitation forms the upper boundary of the low power operating map. For this reason, it is important to locate accurately the tie rod limitation line. Table 4.1-16 shows that tie rod exit gas temperatures (average of T-755 and T-765 measurements) ranged between 345 and 830°R. Tie rod thermocouple T-760 gave unexplainably higher readings than the other two during part of the test. Tie rod thermocouples T-755 and T-765 gave consistent readings during the test with a difference between readings of less than 50°R. On the other hand, at CRT 13900 seconds T-760 read 470°R higher than T-765, and at 19775 seconds T-760 read higher by only 20°R. This unexplained and abnormal behavior may have been caused by the T-760 thermocouple contacting the hotter molybdenum cone during part of the test as discussed in Section 4.3. For this reason T-760 readings were neglected, and the average of T-755 and T-765 is shown in Table 4.1-16. Point 4 was the planned point on the 1000°R tie rod exit gas temperature line (see the low power performance map, Figure 4.1-45); however, by neglecting the T-760 measurement the tie rod temperature at point 4 was only 730°R. The maximum tie rod exit gas temperature of 830°R occurred at point 8. The 55°R difference in tie rod temperatures between points 2 and 5 which have nearly identical power and flow

may be due to transient effects (either point may not be at completely steady state). To summarize, the test results indicate that the predicted 1000°R tie rod curve is approximately correct and thus a considerable operating region exists between conservative tie rod (1000°R) and conservative but arbitrary reactivity feedback (+$1.00) limitations.

The calculated steady state nozzle chamber temperatures using the nozzle compatibility equation ranged between 800 and 1270°R. These are considerably higher than the average of three nozzle chamber temperature measurements. This effect is identical to EP-IV results. Some of the core station temperatures appear higher than would be expected with the corresponding nozzle chamber temperatures. This effect may be due to the inaccuracies of these thermocouples at relatively low temperatures and inaccuracies in data reduction. The pressure drops are relatively low and show no unexpected behavior. The question of temperature asymmetries in the plenums is still under investigation. In general, most pressure and temperature instruments were operating at the low end of their scale, and therefore, are subject to substantial uncertainty.

2. Thermal and Fluid Flow - Comparison with TNT Calculations

This section covers the comparison between test results and TNT predictions. The tabulated comparison of thermal performance at three steady state points is shown on Table 4.1-17 and a graphical comparison of selected performance conditions is illustrated on the low power performance map, Figure 4.1-45. The pre-test reactor model and calculation procedure was used for all TNT comparison calculations. Except for the chamber pressure and

TABLE 4.1-17

EP-V LOW POWER MAPPING TEST COMPARISON BETWEEN TNT PREDICTIONS AND TEST DATA

Point Designation	3		4		7	
CRT Test Time	19050		19295		19625	
	TNT	Test	TNT	Test	TNT	Test
Power, % of 1120 MW	3.37		3.37		4.7	
Flow, lb/sec	13.47		7.82		13.42	
Nozzle Torus:						
Pressure, psia	63	64	53	58	76	53
Temperature, °R	40	38	40	40	41	38
Reflector Inlet:						
Pressure, psia	58	60	46	49	70	76
Temperature, °R	47	47	45	93	49	49
Quality	0.17	--	0.61	1.	0.31	--
Core Inlet:						
Pressure, psia	55	58	44	45	66	73
Temperature, °R	46.5	47	51	152	48	59
Quality	0.47	--	1.00	1	0.75	1
Nozzle Chamber:						
Pressure, psia	46	46.7	35	34.2	54	58
Mixed Temperature, °R	770	800	1345	1270	1086	1230
Tie Rod Exit Temperature	255	345	607	730	349	560
Pressure Drops: (psi)						
Nozzle tube	4.7	4	6.6	9	6.1	7.3
Reflector	2.3	1.5	1.6	3.0	2.6	2.5
Core	9.4	11.0	8.8	12.0	11.5	15.0
Core Material Temperatures:						
Station 8 in.	360	339	463	443	442	411
Station 20 in.	468	577	745	1022	640	747
Station 32 in.	674	768	1124	1430	940	993
Station 45 in.	808	915	1374	1627	130	1428
Reactivity Feedback - $	+0.88	+0.43	-0.37	-0.59	+0.37	-0.05

tie rod temperature measurements, most transducers and thermocouples were operating near the low end of their scale. This reason is probably the major cause for inaccuracies in the test results, and the major reason for discrepancies in the comparison with calculated results.

The three steady state points selected for comparison are the maximum and minimum flow conditions during constant 37.7 MW (thermal) power operation (points 3 and 4) and the maximum power point which occurred during the fixed control drum [illegible]ation (point 7). Good comparison between plenum temperatures (reflector and core inlets) exists for points 3 and 7 where two-phase or near two-phase hydrogen conditions existed during the test. At point 3, the predicted core inlet quality is 0.47 (53% by weight is liquid), which is the maximum predicted liquid percentage at the core inlet for the EP-V test. The TNT results for point 4 show considerably lower plenum temperatures, although the calculation correctly predicts single-phase conditions at the core inlet. The TNT calculation shows considerably lower tie rod temperatures, which is identical to the TNT comparison with the high power test results. Good agreement exists for unfueled element station 8 temperatures. For the other stations, the comparison is only good at a few points.

The low power performance map, Figure 4.1-45, shows a comparison of predicted tie rod temperature and reactivity feedback with test results. Two experimental points with 730°R and 830°R tie rod temperatures compare well with the predicted 1000°R tie rod line. The predicted zero and one dollar reactivity feedback lines are steeper and also closer together than the experimental data indicate. These TNT reactivity calculations are

based on four simplified equations which probably have high uncertainties at these low power and flow operating conditions. The test point with maximum reactivity feedback of 0.43% falls approximately on the $1.00 TNT predicted reactivity feedback curve. This implies that the $1.00 reactivity feedback curve should be further to the right on Figure 4.1-45. To summarize, the conservative and somewhat arbitrary low power operating region based on test results is considerably larger than the pre-test TNT calculated map. The primary reason is that the test $1.00 reactivity feedback line is less restrictive than indicated by the pre-test predictions.

C. Fixed Drum Test Transient Reactor Operation

1. Thermal and Fluid Flow - Comparison of Data with TNT Calculations

The fixed control drum test proved that startup with flow control is feasible. Pre-test calculations showed that with fixed control drums an increase in hydrogen flow adds positive reactivity which increases power until the negative effect of temperature again cancels the positive hydrogen effect. By the same reasoning, a decrease in flow causes a decrease in power. The fixed control drum test proved that this effect happens smoothly for the relatively slow variations in flow that occurred.

The fixed control drum test results were compared with TNT calculations. The pre-test reactor model and calculation procedure was used; however, the detailed nuclear design reactivity feedback calculation method was used in place of the four simplified equations that were used to predict the low power performance map. Figure 4.1-47 shows the averaged venturi flow, measured Linear No. 2 power, and TNT calculated power. A comparison between

CONFIDENTIAL
RESTRICTED DATA
[redacted]

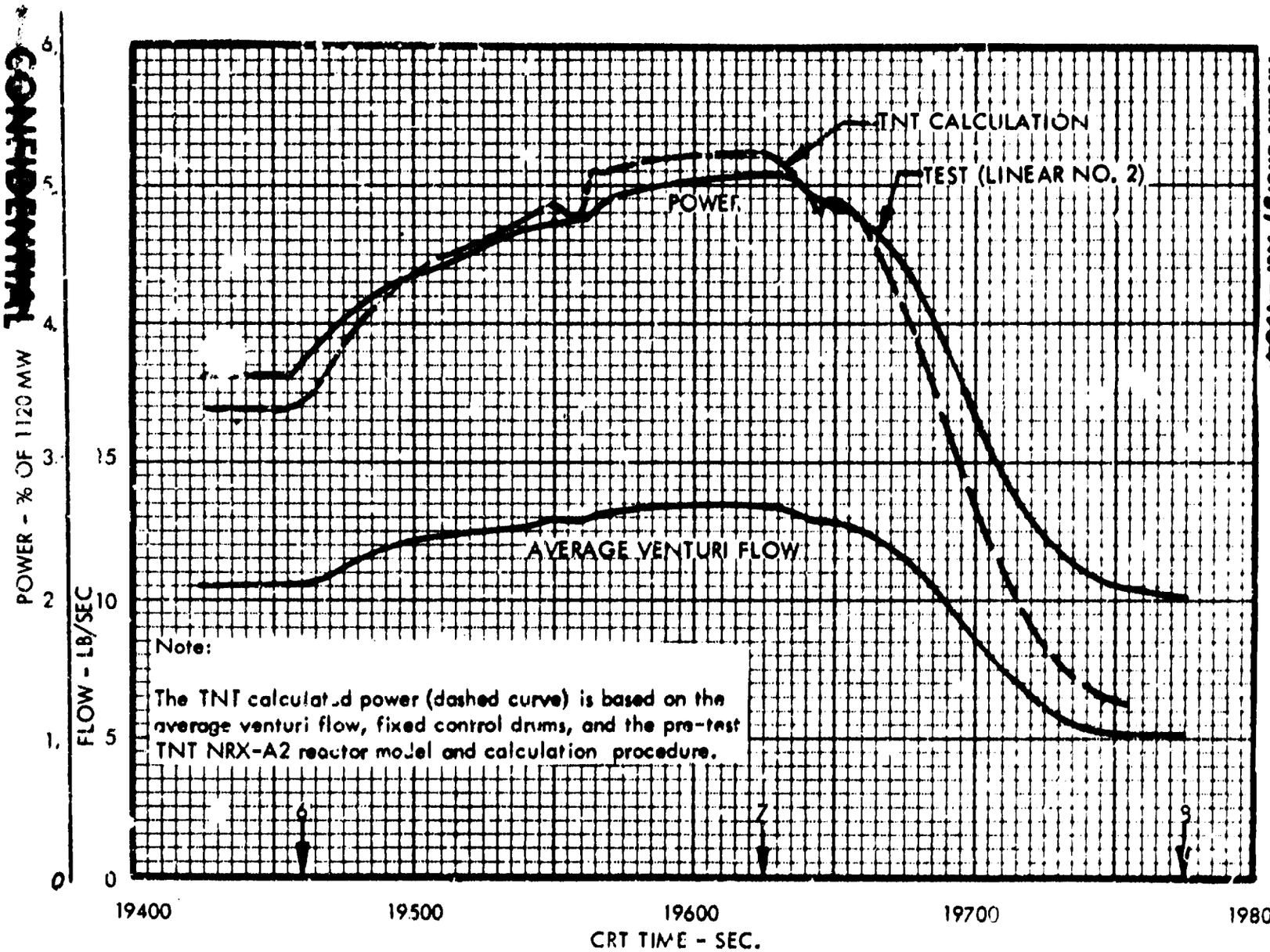

FIGURE 4.1-47 EP-7 LOW POWER MAPPING TEST: FIXED CONTROL DRUMS, POWER AND FLOW

CONFIDENTIAL
RESTRICTED DATA
Atomic Energy Act - 1954

test power and flow shows that every change in flow results in a nearly simultaneous power change in the same direction. In addition, the power curve shows no oscillations or other unexpected results. Using only the average venturi flow as input and the condition of fixed control drum position, the entire fixed control drum test was calculated with the TNT code. The TNT calculated power is shown by the dashed line on Figure 4.1-47. The calculated power shows a greater relative variation than the measured power; however, the response is also stable. The difference between test and calculated power appears to be due to a combination of reactor model, calculation procedure, and uncertainty of test data. Figure 4.1-48 shows tie rod and nozzle chamber temperatures and Figure 4.1-49 shows reactor plenum pressures during the fixed control drum test. On both figures, the corresponding test results at the three steady state holds (points 6, 7, and 8) are indicated. As a result of the difference between test and calculated power, the calculated curves only approximately duplicate the test results. Additional analysis is currently in progress to improve the accuracy with which the TNT code duplicates these test results, both for steady state and transient fixed control drum operation.

CONFIDENTIAL
RESTRICTED DATA
Atomic Energy Act - 1954

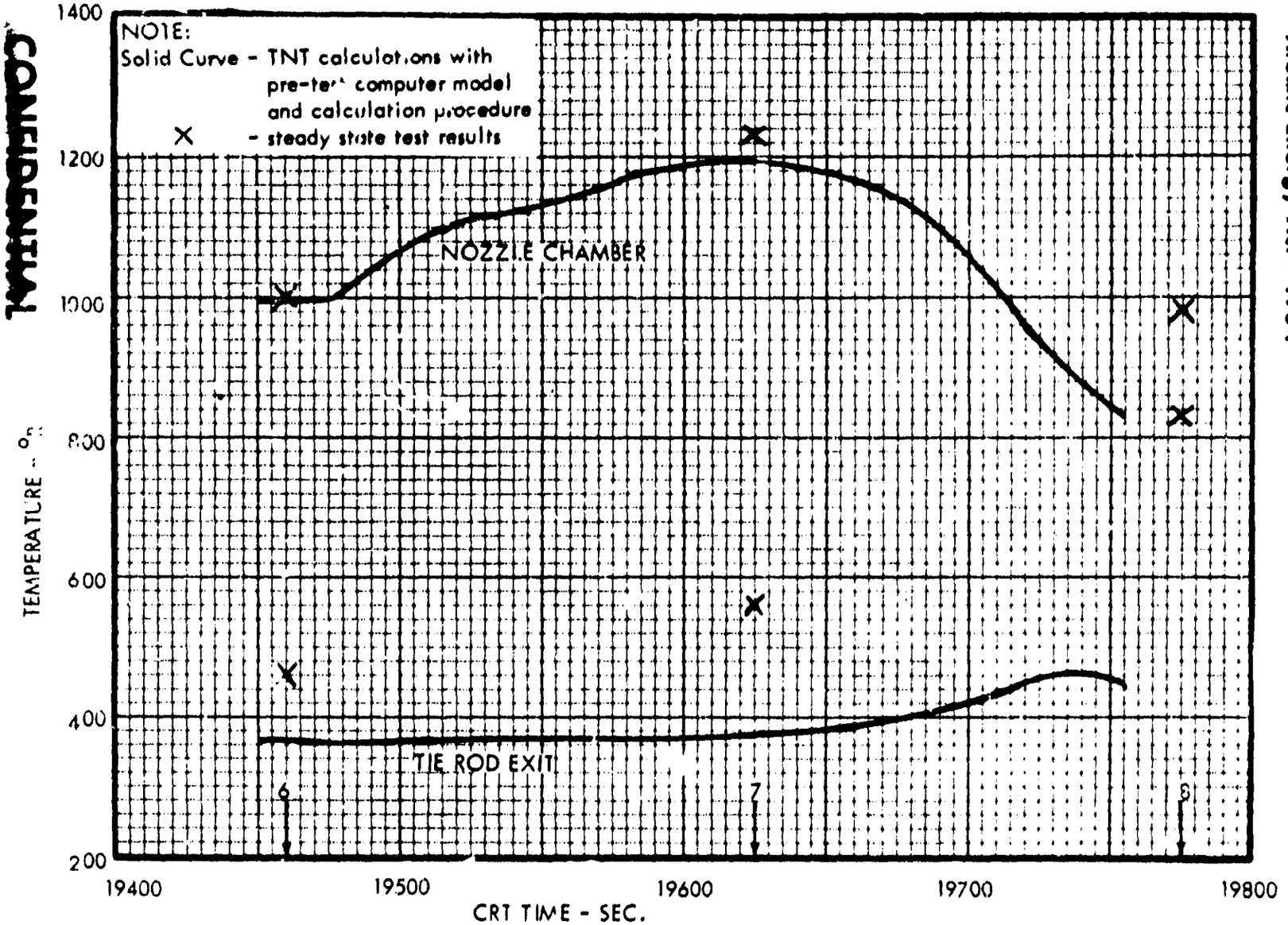

FIGURE 4.1-48 EP-V LOW POWER MAPPING TEST: FIXED CONTROL DRUMS, NOZZLE CHAMBER AND TIE ROD TEMPERATURES

CONFIDENTIAL
RESTRICTED DATA
Atomic Energy Act - 1954

Astronuclear

CONFIDENTIAL
RESTRICTED DATA
Atomic Energy Act - 1954

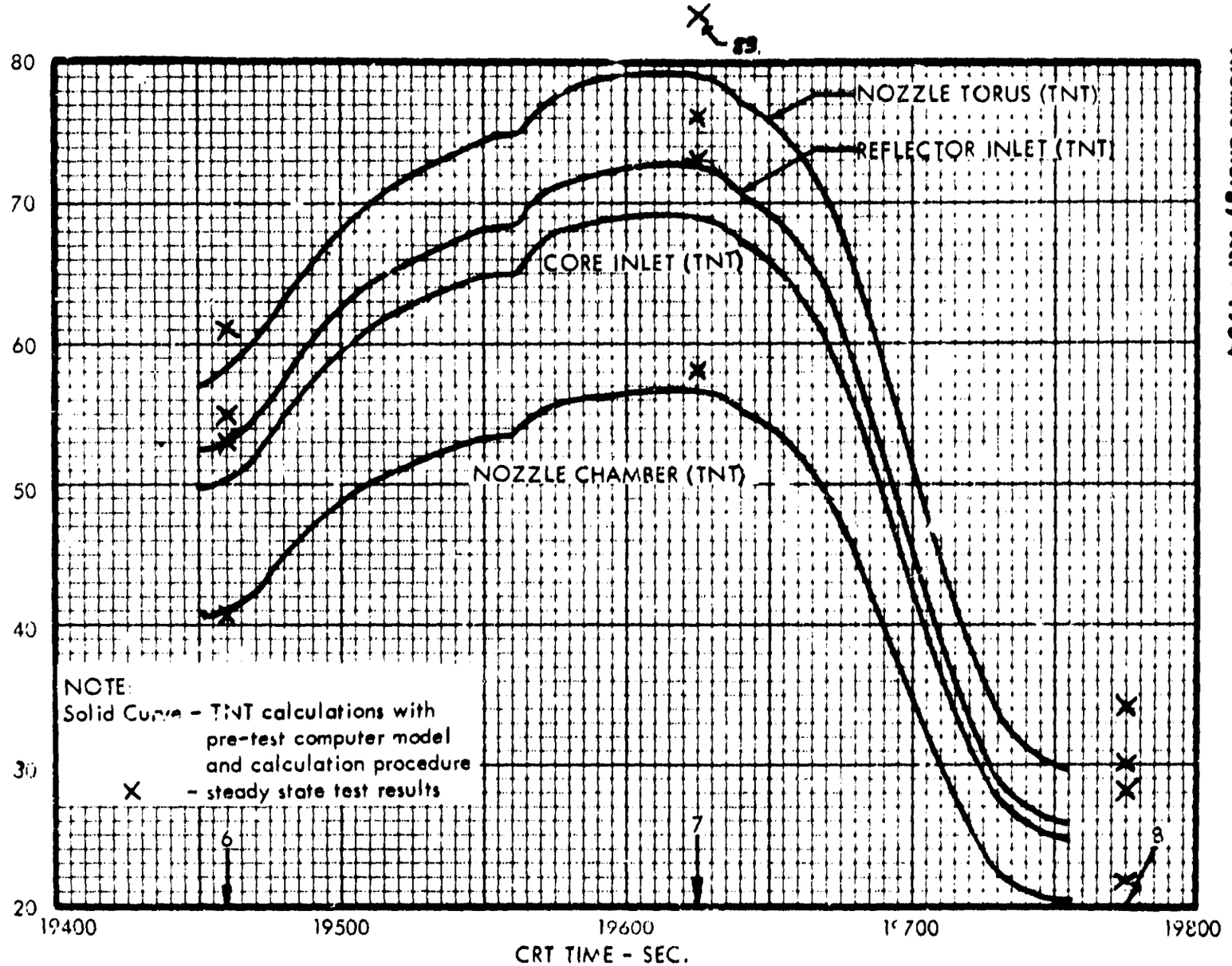

FIGURE 4.1-49 EP-V LOW POWER MAPPING TEST: FIXED CONTROL DRUMS, REACTOR PLENUM PRESSURES

CONFIDENTIAL
RESTRICTED DATA
Atomic Energy Act - 1954

Astronuclear

4.2 FUEL AND OTHER MATERIAL BEHAVIOR

4.2.1 General

This report summarizes NRX-A2 fuel element evaluation studies to date. Aspects of these studies are incomplete including metallographic examination, strength measurements and special property tests. In addition, correlation of observations with radiochemical data have not been made. A formal report on all aspects of fuel element program on NRX-A2 will be issued at later date.

Generally, the material behavior was as expected based on out of reactor corrosion tests and KIWI experience. This behavior, therefore, was demonstrated as adequate for the conditions of the NRX-A2 test.

The most serious corrosion problem occurred along the fuel element flats at the core periphery towards the hot end of the core. This corrosion was the result of hydrogen leaking between filler strips and pyrotiles and contacting fuel at elevated temperatures. In the singular element which had NbC coating on peripheral flats, corrosion of this nature was largely inhibited. It was decided, therefore, to coat the periphery of the NRX-A3 core. In addition, the periphery will be kept cooler by increased flow of coolant using orificing.

The post-operational examinations of NRX-A2 fuel elements at R-MAD* were conducted in two operational phases:

* [illegible] is described in detail in the NRX-A2 Post-Operative Report. [illegible] includes facilities and special handling equipment.

1. Gross visual examination, weighing, and whole body ionization measurement on all the elements in the core.
2. Special examinations on pre-test and post-test selected elements including detailed visual inspections, dimensional measurements, depth of corrosion measurements, incremental electrical resistance measurements, axial sectioning for channel examination, incremental gamma scan and incremental transverse sectioning.

The results of these operations are summarized in the following areas of interest:

I. Surface Corrosion
II. Bore Corrosion
III. Weight Changes
IV. Dimensional Changes
V. Electrical Resistance Changes
VI. Special Element Behavior
VII. Deposits

Throughout Section 4.2 typical photographs and results are given. For a more detailed treatment, reference should be made to the NRX-A2 Fuel Evaluation Report and supplementary reports. The last portion of this section deals with the non-fuel reactor materials.

4.2.2 Surface Corrosion

All of the fuel elements in the NRX-A2 core (1626) were examined visually at the upper disassembly bay, in the R-MAD building. Seventy-eight (78) elements were given a detailed surface examination at higher magnification in the lower bay hot cells. As a result of these examinations, four categories of surface corrosion could be distinguished: (1) At the coated ends, (2) On peripheral element surfaces associated with hydrogen leakage from the pyro-tile joints (hereafter referred to as tile pattern corrosion), (3) Associated with hydrogen leakage from thermocouple installations (hereafter referred to as T/C associated corrosion), and (4) Light streaks and/or sooting on flats between coolant channel positions. The heaviest surface coorosion effects involving significant carbon loss appeared to be associated with tile patterns and thermocouple installations. The distribution of surface corrosion in the core elements is discussed in the following paragraphs:

A. NRX-A2 Elements With Limited Surface Corrosion

While most of the NRX-A2 elements had corrosion at the coated ends (13 were identified as having no end corrosion) there were 270 elements in the core which had no surface corrosion from the dome end to the undercut. A breakdown of these latter elements by sector is as follows:

Sector	Number Without Corrosion
1	91
2	40
3	40
4	27
5	39
6	33

B. Tile Pattern Corrosion

The peripheral elements in NRX-A2 displayed surface corrosion patterns on exterior flats which indicated hydrogen leakage at the pyrotile joints. This corrosion occurred in 10 distinct transverse bands starting at Station 23 with each bank separated axially approximately 3 inches apart as shown in Figure 4.2-1. The upstream edge of these bands was generally sharp with corrosion spreading in a downstream fashion. However, at Stations 26 and beyond, corrosion appeared to spread at the apex edges both in an upstream as well as a downstream direction.

Of the 156 peripheral elements in the NRX-A2 core, 153 had tile pattern corrosion on exterior flats. Two peripheral elements (1J6K and 5J9U) had only light corrosion streaks with no evidence of tile effects. The reason for the lack of corrosion on these latter two is not known. One peripheral element (6J8D) had an NbC coating on the exterior flats which effectively inhibited tile pattern corrosion as shown in Figure 4.2-2. However, there was evidence that the NbC coating at

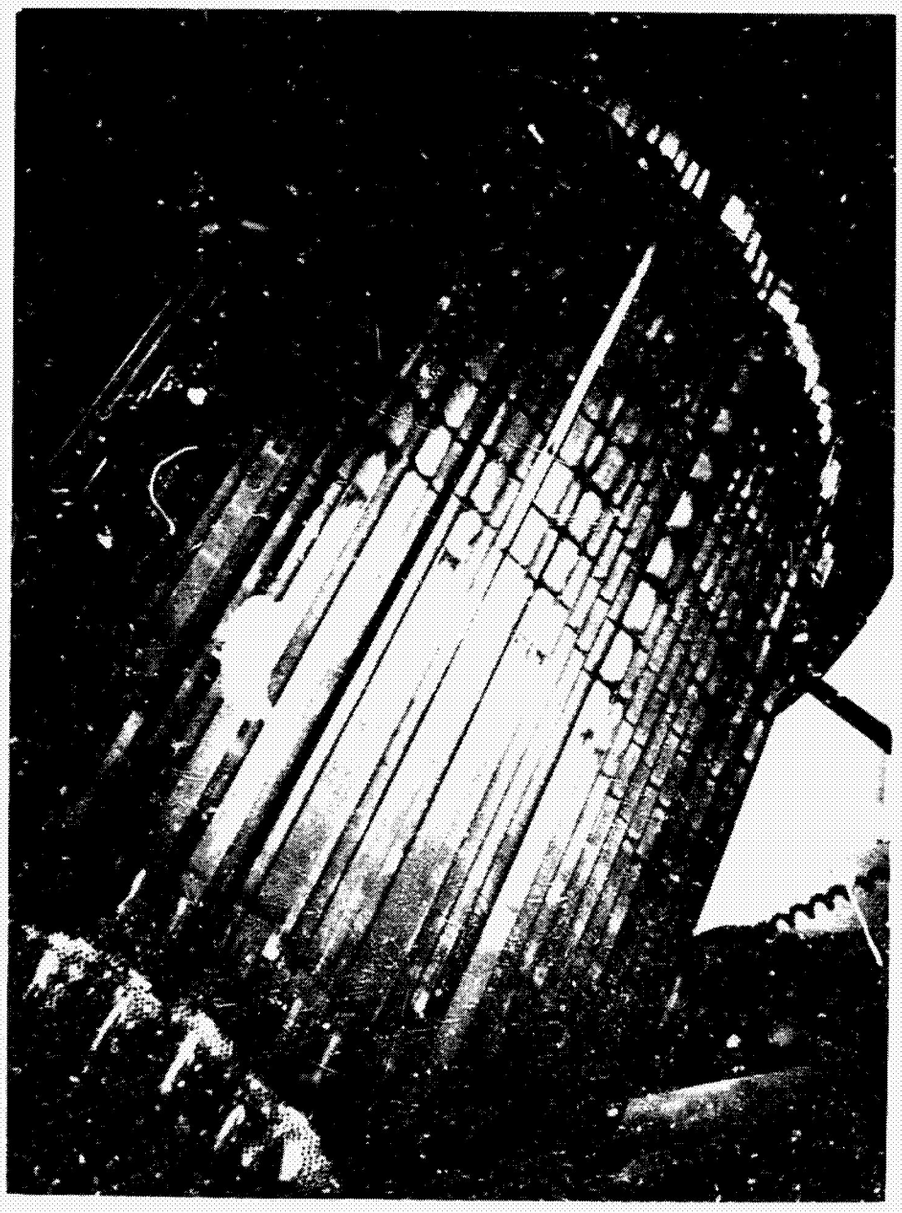

FIGURE 4.2-1 TILE PATTERN CORROSION BANDS ON PERIPHERAL ELEMENTS LOCATED BETWEEN θ = 350° and 75°

FIGURE 4.2-2 PERIPHERAL ELEMENT WITH NbC COATING ON PERIPHERAL FLATS, 39-07639, POSITION 6J8L

Stations 26, 33, and 51 did not completely inhibit tile pattern corrosion. The thickness of the exterior coating on this element is being determined by metallographic procedures.

There were 17 peripheral elements in NRX-A2 in which tile pattern corrosion produced liner exposure. The total axial range of liner exposure occurrence is from Station 40 to 51. A photograph of liner exposure produced by tile pattern corrosion is shown in Figure 4.2-3. Of the 17 peripheral elements which had liner exposure, 6 were in sector 3, 4 in sector 5, 3 in sector 3, 2 in sector 6, and 1 each in sector 2 and 4 indicating that approximately 35% of the liner exposure caused by tile pattern corrosion occurred in sector 3.

C. Thermocouple Associated Corrosion

Thermocouples were installed in the central unfueled elements of several clusters at various axial and radial positions. The examinations of the fuel elements indicated that surface corrosion bands occurred which could be traced to leakage of hydrogen from various thermocouple installations. A breakdown of the associated corrosion by axial thermocouple stations was as follows:

Station	No. of T/C's	No. of Installations Showing Fuel Element Corrosion
8	5	None
20	5	2
32	13	12
45	27	13

FIGURE 4.2-3 LINER EXPOSURE PRODUCED BY TILE PATTERN CORROSION AT STATION 51 ON D FLAT ON ELEMENT 32-11765 POSITION 1J7J

The corrosion effects associated with Stations 20 and 45 thermocouples were observed to be light (one exception, 2J6E, adjacent to a Station 45 couple) with no significant depth and practically no involvement of neighboring elements. In the case of the Station 32 thermocouples, there was considerable surface corrosion not only on an adjacent element but on neighboring element surfaces. Considering the 12 installations showing corrosion, there were 47 associated fuel elements which displayed fairly heavy surface corrosion. Of these latter elements, 19 were corroded to a depth sufficient to produce liner exposure. The corrosion (and liner exposure) occurred in a transverse and longitudinal pattern at axial positions coincident with the T/C stations and extended, in some cases, a considerable distance toward the hot end. A photograph of a corroded element showing the typical effects of T/C associated corrosion is given in Figure 4.2-4. On the element shown in Figure 4.2-4, a depth of corrosion of 11 mils was measured at Station 32 in the center of the d flat. (The six flats of an element were designated a through f.)

D. Corrosion Streaking

Dark streaks were noted on all but 270 of the NRX-A2 fuel elements, occurring on from one to several flats of each element and ranging from Stations 25 to 35 (in several cases the streaks ranged to the hot end). These streaks were typically displayed as two parallel longitudinal dark bands which were located on fuel element flats at positions between the underlying coolant channels. The streaks were

FIGURE 4.2-4 HEAVY CORROSION EFFECT PRODUCED AT STATION 31 ON THE C & D FLATS OF FUEL ELEMENT 89-08407 POSITION 4J6B ADJACENT TO A STATION 32 THERMOCOUPLE INSTALLATION

not always continuous, some being interrupted in the axial direction. A typical example is shown in Figure 4.2-5. Although the exact mechanism for the phenomena is not known, it is believed to be the result of light corrosion by interstitial hydrogen at or above Station 25 with subsequent soot deposition on the hotter downstream portions of the element surface. Results indicate that the major occurrence of streaking is at the axial station of 24 to 33 with very little change in these locations as a function of core radius.

E. End Corrosion

Corrosion was noted on the hot ends of most of the fuel elements in NRX-A2 occurring at the exit face, the end flats and as a corrosion band at the shoulder area of the undercut. In general, the corrosion effect on the exit face and end flats involved liner exposure of varying length and a tapering of the hot end of the elements. The corrosion band at the shoulder appeared in many cases to be independent of the corrosion at the extreme hot end, i.e., there were several elements with light corrosion at the exit face and edge of the end flats which had heavy corrosion bands as shown in Figures 4.2-6 and 4.2-7.

The end corrosion on NRX-A2 fuel elements was rated with respect to the end flats, the exit face and the presence or absence of corrosion bands according to the following conventions:

FIGURE 4.2-5 BLACK STREAKS ON THE C AND D FLATS ELEMENT
89-11877 POSITION 1J5G AT STATION 28

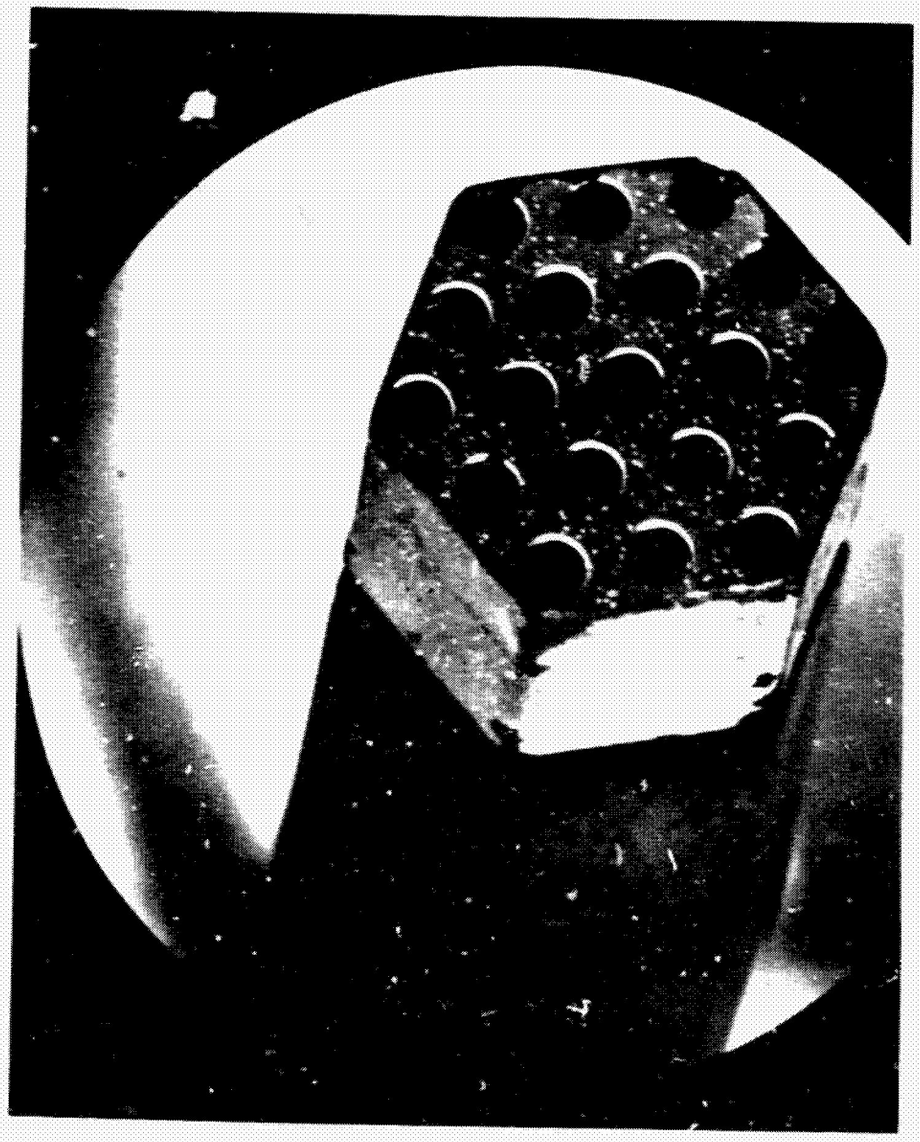

FIGURE 4.2-6 CORROSION BAND AT THE SHOULDER ON ELEMENT WITH VERY LITTLE END CORROSION, ELEMENT 39-11671 POSITION 1J3U AT A AND F FLATS

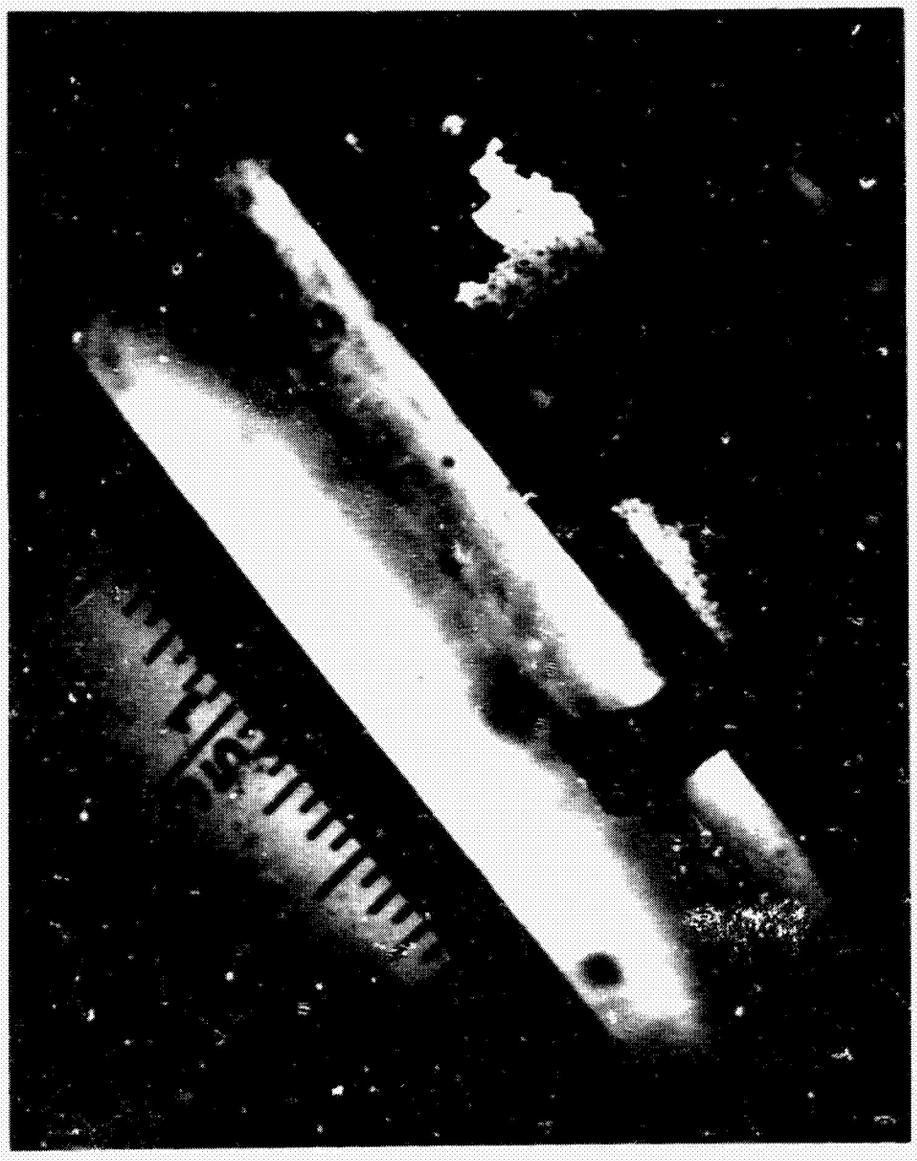

FIGURE 4.2-7 CORROSION BAND AT THE SHOULDER ON ELEMENT 39-11864 POSITION 4J3U ON D, E, AND F FLATS

1. Exit Face

Perfect	No corrosion
Typical	Corrosion at edge of all outer channels with a BAR (bearing area remaining) of approximately 70%.
Better Than Typical	Light corrosion at apex edges with 100% > BAR > 70%.
Worse Than Typical	Corrosion involving more than outer channels with a BAR < 70%.

2. End Flats (All designations may or may not have corrosion band, C.B.)

Perfect	No corrosion on end flats
Typical	Corrosion involving about 1/4 inch of flats from extreme hot end with liner exposure ranging 0 - 1/4 inch from hot end.
Better Than Typical	Corrosion involving less than 1/4 inch of flats from hot end with liner exposure only at extreme hot ends at apex.
Worse Than Typical	Corrosion involving more than 1/4 inch of flats from hot end with liner exposure > 1/4 inch from hot end.

Photographs of NRX-A2 elements illustrating end effects are shown in Figures 4.2-8 through 4.2-12. A comparison of the condition of the coated ends before and after the NRX-A2 test for an internal and peripheral element are shown in Figures 4.2-13 and 4.2-14.

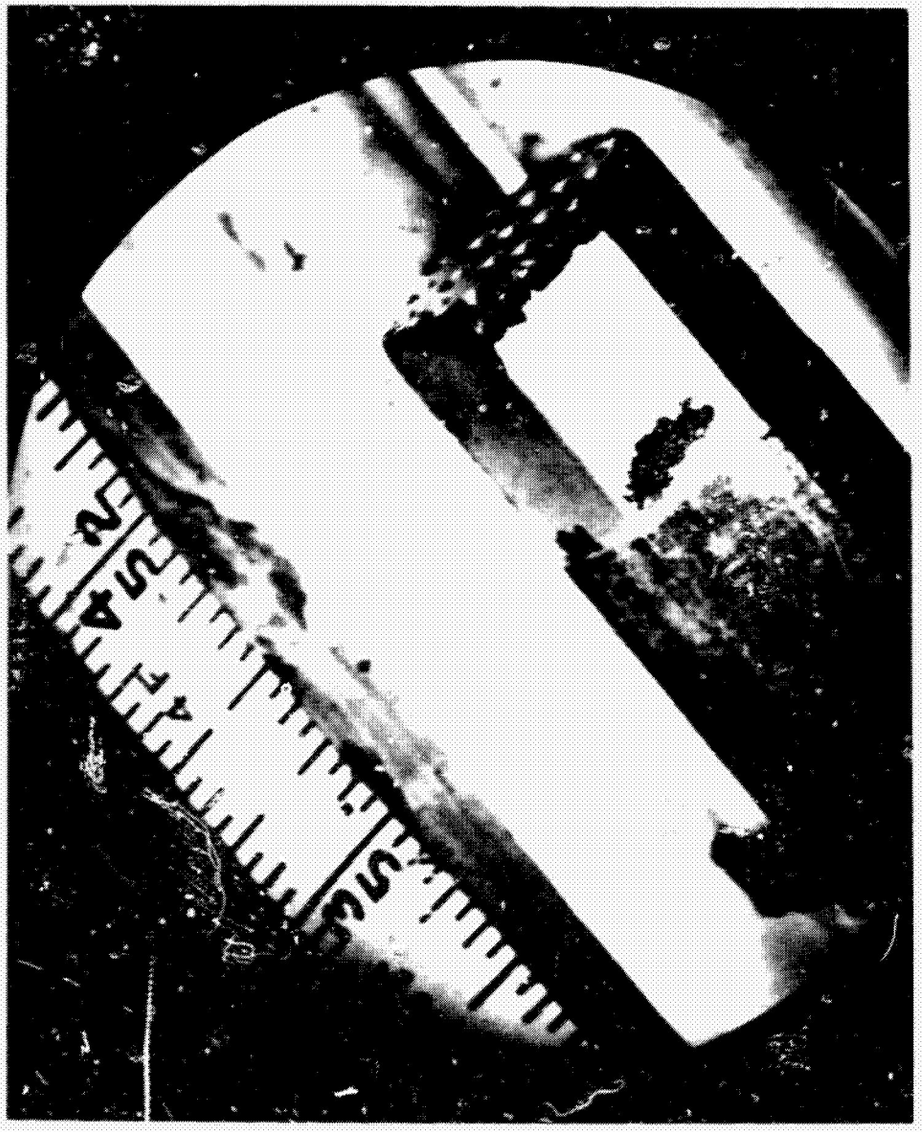

FIGURE 4.2-8 BETTER THAN TYPICAL END FLATS AND EXIT FACE ON ELEMENT 39-07575 C/P 4J4N

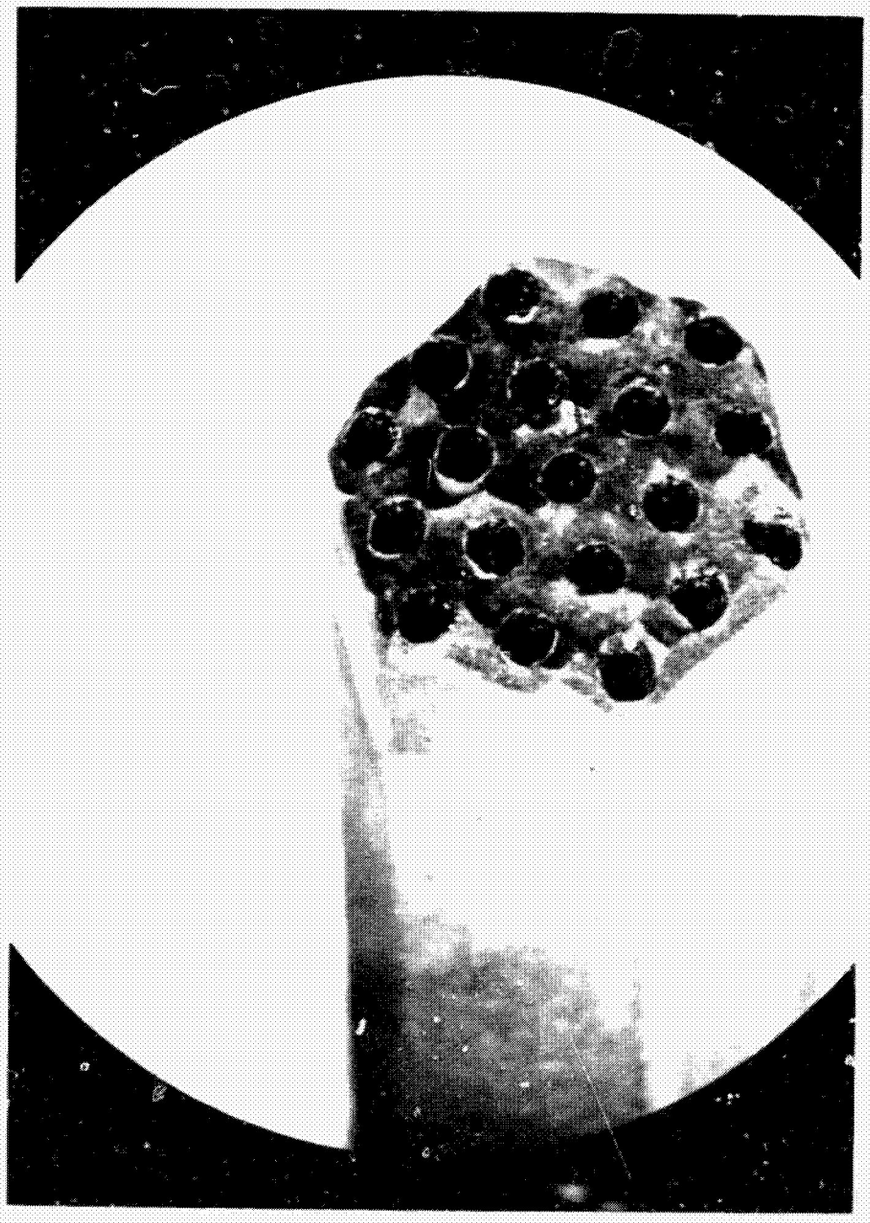

FIGURE 4.2-9 WORSE THAN TYPICAL EXIT FACE CONDITIONS AND TYPICAL END FLAT CONDITION ON ELEMENT 79-11932 C/P 3J9B

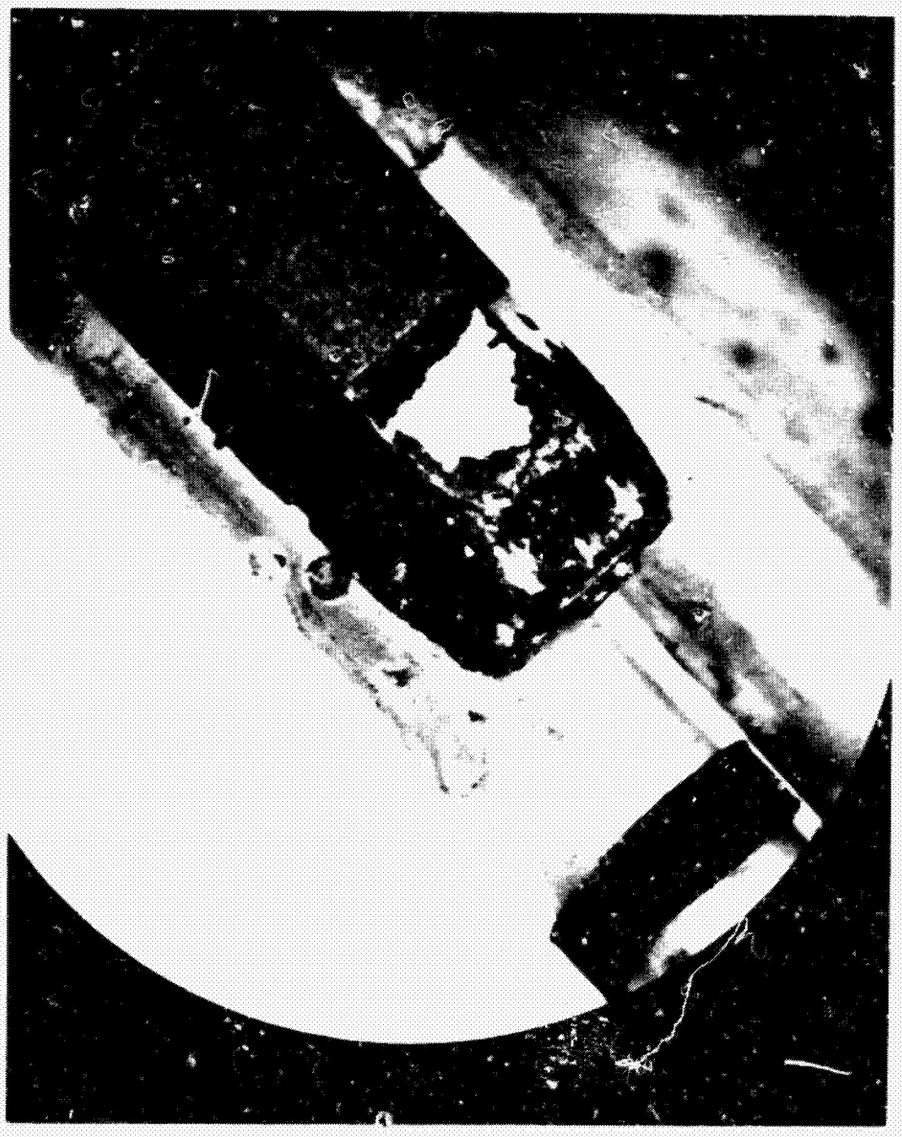

FIGURE 4.2-10 TYPICAL END FLAT CONDITIONS WITH CORROSION BAND AT SHOULDER ON ELEMENT 92-07086 C/P 2A1G

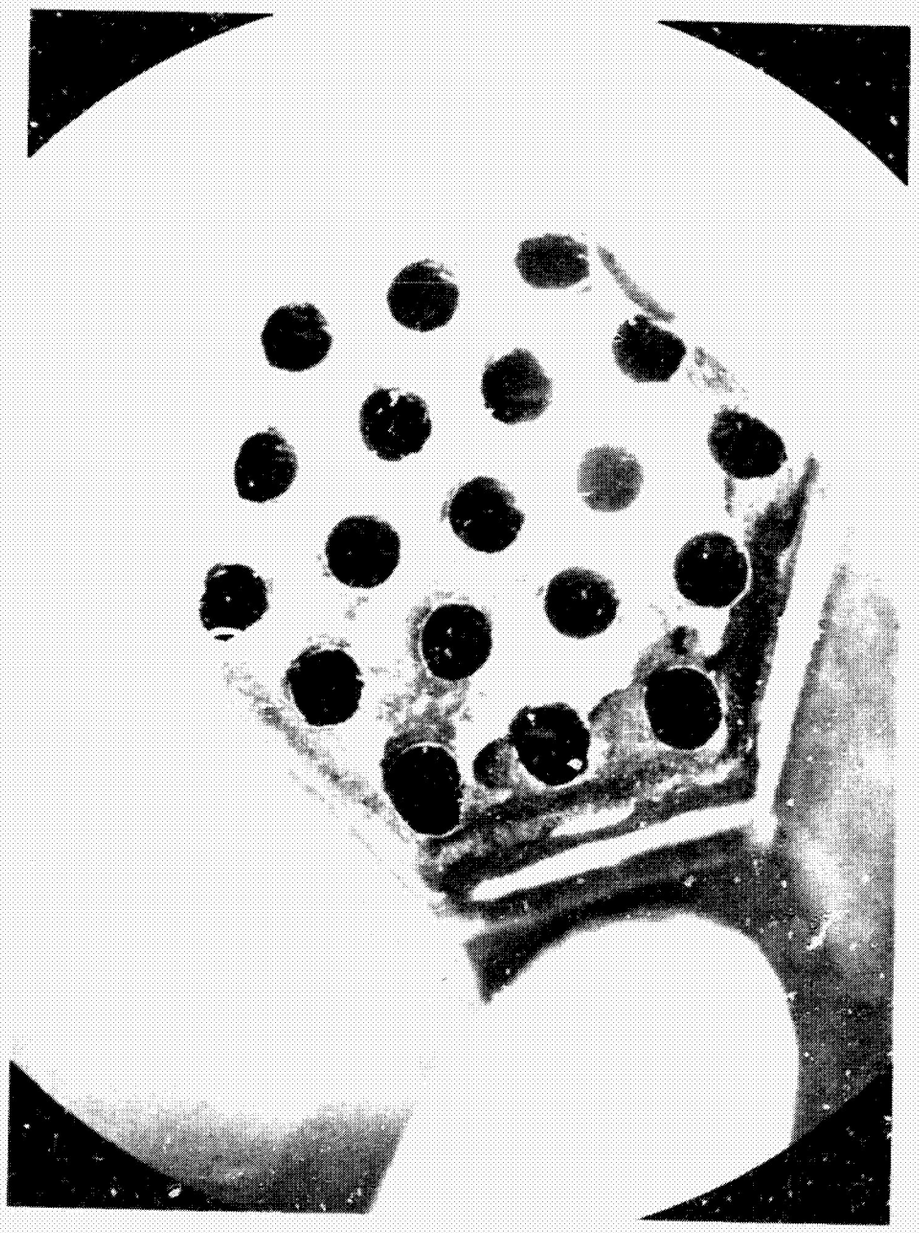

FIGURE 4.2-11 TYPICAL EXIT FACE CONDITION ON ELEMENT 99-09313 C/P 4A1D

FIGURE 4.2-12 WORSE THAN TYPICAL END FLAT ON ELEMENT 39-11681 C/P 6J3N

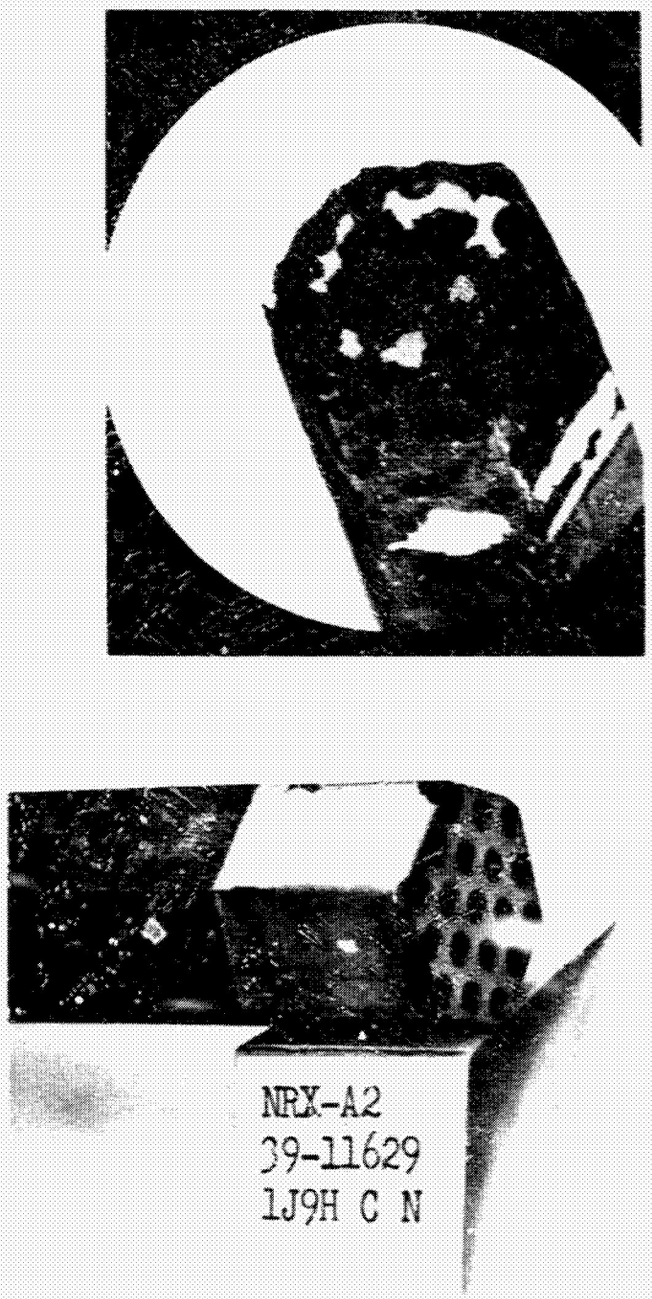

FIGURE 4.2-13 COMPARISON OF THE COATED END ON ELEMENT 39-11629 C/P 1J9H BEFORE AND AFTER REACTOR TEST

FIGURE 4.2-14 COMPARISON OF THE COATED END ON ELEMENT 99-07100 C/P 1F1F BEFORE AND AFTER REACTOR TEST

Of the core fuel elements, there were 13 with no corrosion on the end flats, 17 with no corrosion on the exit faces, and 13 with no corrosion at either position. Nine (9) of those showing no or light end corrosion had been recoated at ORNL. The recoated elements are discussed in Section 4.2-7.

To evaluate the observed end corrosion as a function of the pre-test hydrogen corrosion ratings, (an "A" rating being better than a "C" rating) 1525 fuel elements were analyzed according to the conditions of the exit faces using the conventions described previously. The distribution of exit face corrosion by end rating was as follows:

<u>1156 Elements with "A" End Ratings Analyzed</u>

There were a. 232 (20.1%) with Better Than Typical Exit Face

b. 642 (55.5%) with Typical Exit Faces

c. 282 (24.4%) with Worse Than Typical Exit Face

<u>369 Elements with "C" End Ratings Analyzed</u>

There were a. 86 (23.2%) with Better Than Typical Exit Face

b. 142 (38.5%) with Typical Exit Face

c. 141 (36.2%) with Worse Than Typical Exit Face

These data indicate that the end corrosion on the exit face of the "A" rated elements was somewhat less severe than on the "C" rated elements. A survey of the end corrosion in Sections 1 and 3 as a function of core radius indicated that the end effects do not vary appreciably from the center of the core to the periphery.

F. Liner Exposure

Liner exposure has been discussed with respect to tile pattern corrosion and T/C associated corrosion. The total distribution of this effect is discussed in this section.

Forty-six (46) elements had liner exposure on the body including the shoulder area. Of the 46, forty-one (41) were found to have liner exposure on the body and five (5) were observed to have liner exposure caused by the corrosion band at the shoulder of the undercut. A breakdown of the corrosion effects causing liner exposure in the 46 elements is as follows:

No. Elements with Liner Exposure	Associated With
17	Tile pattern corrosion
19	T/C associated corrosion
1	Missing liner (5F4F)
4	No apparent reason (3C2C, 3C2I, 1J9B, 2H6C)
5	Corrosion band at shoulder (1D3C, 2C2C, 4E3C, 4J4J, 5D1F)

Of the forty-one (41) elements with body corrosion, 12 elements had liner exposure at more than one axial location. Seven (7) of these were due to tile pattern effects, four (4) to T/C associated corrosion and one (1) due to multiple tile pattern - T/C effects (4J4H). Three (3) elements (of the 41) displayed liner exposure on more than one

disconnected flat; all others were exposed only on one flat or at an apex. There were 54 separate occurences of liner exposure in the 41 elements with the length of liner exposure varying approximately as follows:

Length, Inches	No. of Occurences
1	38
1	5
2	6
3	1
4	2
5	1
21	1

The liner exposure noted on 3C2C, 3C2D, 1J9B, 2H6C, and 5F4F cannot be associated strictly with surface corrosion effects and are apparently due to bore corrosion effects. These elements are discussed in the section on special element behavior.

4.2.3 Bore Corrosion (Pinholing, Channel Examinations)

A complete evaluation of the subject of bore corrosion in NRX-A2 fuel elements must await completion of metallographic observations. In general, light bore corrosion effects were produced in the elements as a result of the NRX-A2 test. A preliminary estimate of the effects produced can be made on the basis of visual observations of pinhole occurrence and the channel examinations on axially split fuel elements.

A. Pinhole Occurrence

Fifty-eight (58) NRX-A2 fuel elements developed pinholes. Forty-four (44) of these elements were rated at IAA (or IAC)* and fourteen (14) as ICC (or ICA) by Quality Control hydrogen corrosion testing. Of the fifty-eight (58) elements, thirty (30) had only one pinhole. The greatest number of pinholes were developed in elements from coating batch C94 (ICC). The predominant axial occurrence of pinholes was at stations 25 - 30 and 45 - 50 inches. A photograph of typical pinholes observed on the surface of an element is shown in Figure 4.2-15.

B. Channel Examinations

Thirty (30) fuel elements from NRX-A2 were sectioned axially through channels 8, 9, 10, 11 and 12 and given detailed visual examinations. Five (5) of these elements had visual indications of pinholes on the surface; the most heavily pinholed element being 4E4E from coating batch C94. Fourteen (14) of the elements examined had no observable channel corrosion; the rest showed some evidence of limited liner flaking, light liner undercutting and corrosion pocketing. Typical of the corrosion pocketing conditions which produced pinholes are photographs of the channels of element 4E4E given in Figure 4.2-16. In general, the available data indicate that bore corrosion occurred predominantly at

*The rating IAA indicates an "A" channel and "A" end, IAC indicates an "A" channel and "C" end, etc.

FIGURE 4.2-15 PINHOLES ON THE A FLAT ON ELEMENT 99-07089
C/P 4E4E AT STATIONS 45 TO 48

FIGURE 4.2-16 VIEW OF CHANNELS 8, 9, 10, 11, AND 12, AT STATIONS 47 TO 49 ON ELEMENT 99-07089, C/P 4E4E SHOWING CORROSION POCKETS AND TYPICAL PINHOLE FORMATION IN THE CHANNELS AND THE GRAPHITE MATRIX

Stations 20 - 50. It was noted in several cases that corrosion pocketing occurred previously at positions of NbC liner defects, i.e., small chipped areas ranging from irregular to circular in shape. The defect areas at the hot end of the element did not appear to be different in character from that at the mid length position. The number of elements examined was insufficient to indicate the radial distribution of bore corrosion in the core.

4.2.4 Weight Changes in NRX-A2 Fuel Elements

All of the fuel elements in NRX-A2 were weighed after the test by means of an automatic balance in cell 5 of R-MAD. Inconsistencies in these results made it difficult to interpret true weight changes. Therefore, 340 elements were reweighed manually by means of an Mettler K-7 balance. Based on the reweigh data, the gross average weight loss of the elements with a IA rating was 1.0 grams and of elements with a IC rating was 1.2 grams. The nominal weight loss in NRX-A2 fuel elements which had no significant surface corrosion but varying end corrosion was about 1.0 ±0.3 grams at the center of the core and in the elements in periphery cluster (but not peripheral elements). The average weight loss of elements which had tile pattern corrosion was 4.3 grams. Those with thermocouple associated corrosion lost 4.6 grams, and those with pinholes 1.5 grams.

An estimate of the total weight loss in the NRX-A2 fuel elements can be made assuming there are 153 elements with tile pattern, 48 with T/C associated corrosion, 43 elements that were uniquely pinholed but with no significant surface corrosion, and 1382 elements with a nominal weight loss. On this assumption, the estimated total weight loss in the NRX-A2 elements due to the reactor test is about 175 grams.

The fuel elements in batch C-94 were notable in being prone to pinholing and bore corrosion. There are eleven (11) elements from this batch which were reweighed, with an average weight loss of 1.9 grams. Considering that none had significant surface corrosion but end corrosion (1.0 gram weight loss) there appears to be about a 0.9 gram weight loss in elements of this batch due to bore corrosion effects.

A comparison of the weight loss data on I-C rated elements as a function of pre-test hydrogen corrosion test results was made. Of significance, the weight loss from reactor tested I-C elements which had no significant surface corrosion or bore effects was about half that observed on a batch basis during the hydrogen corrosion test. The pre-test data was obtained for testing at 5 minutes (at maximum surface temperature of 4310°R) and the NRX-A2 test time at temperature was of the order of 3 minutes.

4.2.5 Dimensional Change in NRX-A2 Fuel Elements

Post-test across flats measurements were performed on 34 pre-test measured NRX-A2 fuel elements at four axial stations. Measurements were performed for the three pairs of flats at each station. Considering each station, the gross average across flats change is -0.3 mils at Station 1, -0.6 mils at Station 24, -0.1 mils at Station 48 and -0.1 mils at Station 51. These data indicate no significant change occurred in across flats dimensions.

The results of length change measurements on 35 NRX-A2 fuel elements were tabulated. The pre-test lengths with orifices were estimated to ±4 mils. Based on the pre-test data, there was no significant change in length (-3.5 mils average) except for four elements (6E2C, 2G3C, 4J3W, 6J3N). Three of these showed a length decrease of approximately 30 mils (0.06%) while one showed a length increase of 15 mils (0.03%). The corrosion at the exit face on those showing the 30 mil decrease was not unusually high and all were IE rated elements. It is reasonable to suspect that the large changes are due to error in measurements.

4.2.6 Incremental Electrical Resistance Changes

The electrical resistance at 1 inch increments from Station 2 to 50 was measured on the "a" flat of 74 fuel elements from NRX-A2 and the profiles compared with pre-test data. In general, the profiles indicate an increase in resistance at the cold end believed to be due to radiation effects and a general peaking in ΔR at station 20. This peaking is

believed to be an indication of corrosion effects related to liner defects. By comparison with pinhole occurrence described in a previous section, this region is about 5 inches upstream from the axial location of maximum pinhole occurrence (see 4.2.3 on Bore Corrosion). All of the post-test resistance profiles indicated very little graphitization or fuel migration had occurred in the fuel element. Additionally, the data indicated regular resistance peaks corresponding to tile pattern corrosion bands on the surface of several peripheral elements which were measured. The effect of pinholing was observed as an increase in resistance at the stations affected although the increase was small unless several pinholes had developed. It is believed that considerably more detail could be obtained on these effects if the resistance measurements were performed incrementally every 1/2 inch along the fuel elements length.

A plot of the ΔR for a typical IC rated element which had insignificant surface corrosion is compared with that of a IC element tested under hydrogen corrosion conditions in Figure 4.2-17. The major difference between the element from the reactor and the electrically tested element is the shift of the ΔR peak in the reactor element toward upstream station by about 3 - 4 inches. Both show similar changes at the hotter end. The comparison indicates that the NRX-A2 element probably saw maximum temperature comparable with those of a I-C test (4310°R surface)

Astronuclear

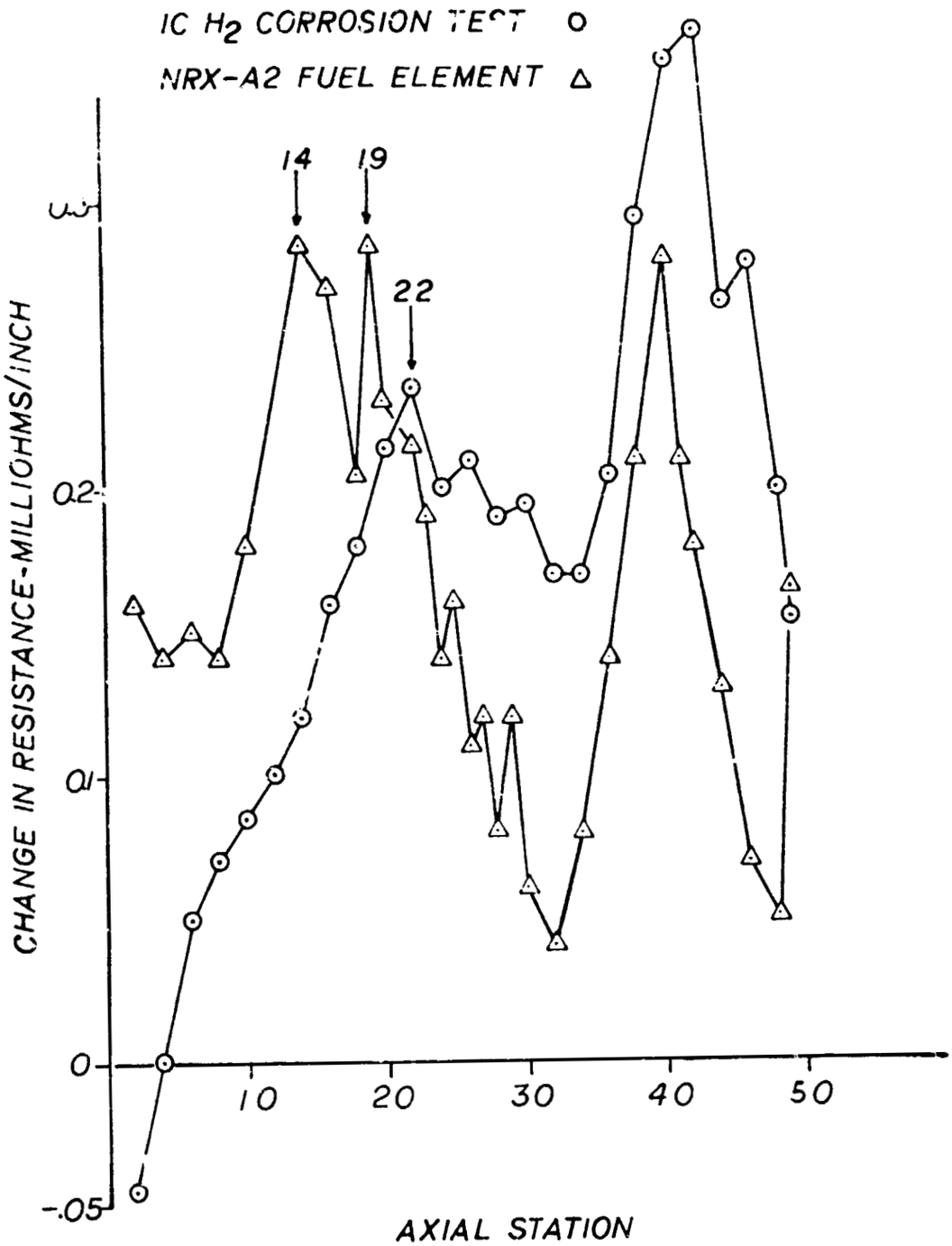

FIGURE 4.2-17 - COMPARISON OF CHANGES IN ELECTRICAL RESISTANCE PROFILES OF ELEMENTS FROM SAME RUN TESTED IN WANL H_2 CORROSION FACILITY AND IN NRX-A2.

but with an axial temperature profile slightly shifted upstream. There were no significant changes observed in the axial position of the upstream ΔR peak nor in the general shape of the post-test resistance profiles as a function of core radius.

4.2.7 Special Element Behavior

This section is included to discuss the behavior of special elements based on pre-test history or on unusual post-test observations.

A. ORNL (Y-12) Recoats

There were nine (9) fuel elements in the NRX-A2 core which had their ends recoated at ORNL. These were characterized by excellent end flat and exit face condition. The results of post-test observations on these elements are given in Table 4.2-1. Six of these elements had no corrosion at the coated end while the other three (3) showed slight corrosion effects mostly at the shoulder area of the undercut. Pinholes were noted in three (3) of the elements occurring at Stations 30 to 36, although these were associated with tile pattern corrosion. On those with tile pattern, the corrosion band at Station 51 was characteristically inhibited by the presence of intact NbC and coatings. A typical exit face condition is shown in Figure 4.2-18. Channel examinations were performed on three of these elements. Two (5H6E and 2J3H) showed some evidence of undercutting corrosion at about the center of the elements (Station 22 to 38) while the third (6J5L)

CONFIDENTIAL
RESTRICTED DATA
Atomic Energy Act - 1954

TABLE 4.2-1

EXAMINATION RESULTS FROM AXIALLY SECTIONED Y12 FUEL ELEMENTS

Position	Serial Number	Coat Rate	Body Corrosion	End Flat Condition	Exit Face Condition	Pre-Test H2 Data ΔW	ΔW	BAR
2J3H	39-11704	F59IA	Tile pattern (cd), soot at 45" on "b"	No corrosion 100% CAR	BAR 100 CAR 99	-2.1*	-2.8	100
4H6E	99-09364	F49IA	OK	No corrosion 99% CAR	BAR 100 CAR 100	(-)	-3.0	100
5H6E	99-09813	F49IA	OK	No corrosion 100% CAR	BAR 100 CAR 100	(-4.0)**	-3.0	100
6H6E	99-10122	F49IA	OK	No corrosion 100% CAR	BAR 100 CAR 100	(-)	-3.0	100
6J3K	32-11632	F59IA	Tile pattern "d", Pinholes 33, 34, on "d"	No corrosion 100% CAR	BAR 100 CAR 95	(-)	-3.0	100
6J4J	32-11734	F59IA	Tile pattern "d" Pinholes 34, 36, apex c-d, pin-holes 30 apex d-e.	Corrosion Band at shoulder, 90% CAR	BAR 100 CAR 100	(-)	-3.0	100
6J5L	32-11735	F59IA	Tile pattern "d" (Corrosion Band 10 stops at shoulder at 51 1/4 due to presence of good coating), Pinholes at 30 on "d" in tile pattern.	Some corrosion at edge of end, 90% CAR	BAR 97 CAR 90	-1.4*	-3.0	100

CONFIDENTIAL
RESTRICTED DATA
Atomic Energy Act - 1954

Astronuclear

CONFIDENTIAL
RESTRICTED DATA
Atomic Energy Act - 1954

TABLE 4.2-1 (Cont)

Position	Serial Number	Coat Rate	Body Corrosion	End Flat Condition	Exit Face Condition	Pre-Test H_2 Data ΔW	ΔV	BAR
6J6H	39-C7697	C73ICC	Tile pattern on "d" (Corrosion band at shoulder at 51 1/4 due to presence of good end coating)	Same corrosion band at shoul- (c, d, e) 95% CAR	BAR 100 CAR 100	(-)	-2.8	100
6J6J	32-11736	F59IA	Tile pattern on "d"	No corrosion 100% CAR	BAR 100 CAR 100	(-)	-3.0	100

*Reweigh data

**Reweigh data indicated a 15 gram weight loss, but the orificed end of the element had been cut-off before weighing. The figure given is an estimate based on a calculated loss due to cutting.

CONFIDENTIAL
RESTRICTED DATA
Atomic Energy Act - 1954

Astronuclear

FIGURE 4.2-18 VIEW OF THE EXIT FACE OF A RECOATED ELEMENT 32-11735 C/P 6J5L

had liner flaking and light corrosion at Station 40 - 45 with a good deal of liner flaking at Stations 32 - 38. The liner in 5H6E displayed a blue discoloration at Stations 32 - 34. There is not enough weight loss data available on these elements to be meaningful.

B. Less Than IC Rated Elements

There were two fuel elements in NRX-A2 which had failed to pass a I-C hydrogen corrosion test (4G5G and 5H7F). Both of these showed no unusual surface corrosion effects or pinholing. Both elements had end corrosion that was worse than typical on the end flats with typical exit face corrosion.

C. Missing Liner Element

The fuel element at position 5F4F (C9t-IA) was observed to have channel 3 exposed by corrosion from Station 28 to 50. An examination of the element indicated that bore corrosion in this channel had actually started at about Station 20 and was due to the absence of NbC liner. The neighboring elements (5F4G and 5F5C) both had apex corrosion varying from Stations 30 to 50 at the corners adjacent to the liner exposure. A weight loss of 15 grams was measured on 5F4F.

D. Liner Exposure Not Associated with Surface Corrosion

Four (4) elements in NRX-A2 had liner exposure which could not be associated with surface corrosion effects. These elements and the exposure are as follows:

Element	Coating Batch	Rating	Liner Exposure Occurrence
3C2C	F44	IA	c-e apex, 48
3C2E	F44	IA	a-f apex, 48
ZH6C	C46	IC	d-e apex, 49.5 - 5[illegible]
LJ9B	L4	IA	a-f apex, 49

All exposure occurred at an apex and all were seen to occur at about the same axial station. Two (3C2C and 3C2E) are related since adjacent edges are involved. The exposure on LJ9B appeared to be partially manipulator aused; however, some corrosion was noted at the hole. It is possible that the exposure was caused by a pinhole occurring at the apex which subsequently was broken open by the hot cell manipulator. The reason for the exposure on ZH6C is not readily apparent other than from bore corrosion.

4.2.8 Deposits

White to shiny appearing deposits were noted on the surface of fuel elements throughout the NRX-A2 core. These deposits were not always identified on the element during initial examinations due to the character of the deposits and lighting deficiencies. The white deposits were noted on 99 elements by axial position. The axial distribution was as follows:

Axial Station of Occurrence	Number of Elements with Deposits
0 - 20	3
21 - 35	87
36 - 51	9

The total range of deposits on the 99 elements was from Station 5 to 51, occurring as patches or isolated spots with some cases of multiple axial occurrence on the same element. The deposits appear to be somewhat heavier on some of the peripheral elements covering a considerable axial length. A photograph of a typical white deposit observed on a peripheral element is shown on Figure 4.2-19. The identity of these deposits have not yet been determined although it is believed that they are some form of pyro-carbon coating.

In addition to the white appearing deposits, a shiny deposit was noted on the surface of several elements typically in areas with heavy surface corrosion as shown in Figure 4.2-20. These deposits appear to be pyro-carbon deposited at fairly high temperature.

4.2.9 Non-Fuel Reactor Materials

This section discusses the post-operative condition of non-fuel components of the NRX-A2 reactor. It is noted that, with the exception of disassembly observations, most of the pertinent data remain

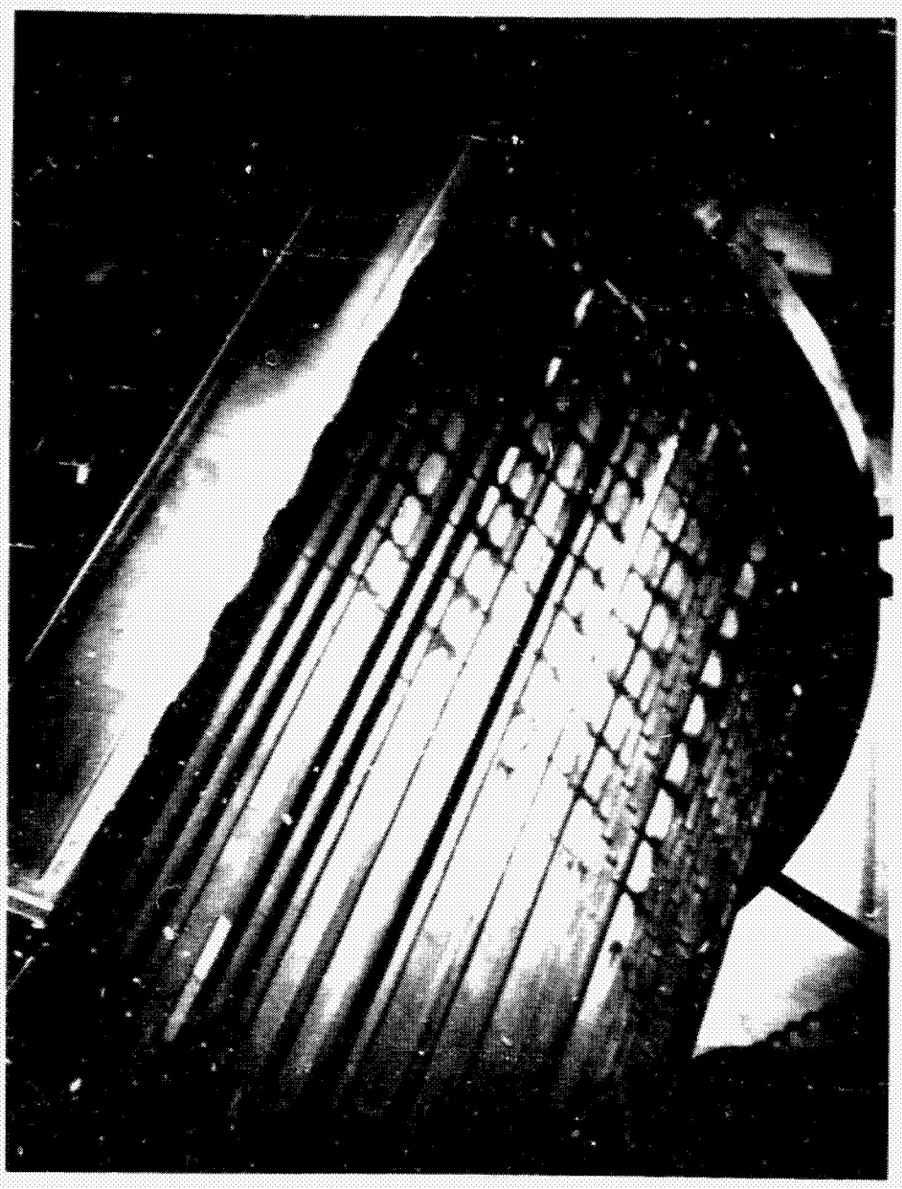

FIGURE 4.2-19 CORE PERIPHERY SHOWING ELEMENTS WITH TILE PATTERN CORROSION AND WHITE DEPOSIT, $\theta = 310° - 75°$

FIGURE 4.2-20 VIEW OF SHINY PYRO CARBON DEPOSITS IN CORRODED AREA OF ELEMENT 39-07575, CORE POSITION 4J4M, AT AXIAL STATION 44 TO 45

to be determined from further examination of samples, currently underway. Results of these examinations will be reported when they have been completed.

From a materials engineering viewpoint, observations of the disassembly produced information of two sorts:

1. They established which components underwent no apparent change as a result of the test.
2. They provided a description of such changes as were evident through visual examination.

It is important to distinguish between damage incurred during disassembly and that which occurred during test (including cooldown and the decay period). Primary concern is with test effects; disassembly damage - through of interest - is of secondary importance. In the following discussion, damage which was observed to occur during disassembly, or which obviously was of that origin, is excluded from consideration.

Damage that occurred during the test runs might conceivably have resulted from (1) inherent material inadequacy not previously revealed, (2) design inadequacy, (3) insufficient quality control, (4) improper test procedures, or (5) some combination of the preceding factors. It may be noted, in passing, that in a test such as the NRX-A2 series, the maximum amount of engineering information is obtained if the severity of the test is sufficient to produce damaging effects, within the limits of safe operation. It is then important to establish

insofar as possible, the nature of the causative factors for each instance of damage so that proper remedial action can be taken. Such a classification of the observed effects will be attempted here, although it is recognized that in some cases considerable overlap occurs.

Components which did not show visual evidence of pre-disassembly damage include the following:

1. Nozzle End Support Ring
2. Dome End Support Ring
3. Tie Bolts
4. Control Drum Assemblies
5. Core Support Ring and Bolts
6. Core Band and Couplings
7. Dome End Seal
8. Core Support Plate
9. Spring Support and Bearing Rings
10. Core Support Barrel
11. Lateral Support Spring Brackets and Bolts
12. Simulated Shield
13. Dome & Nozzle End Bearing Shafts
14. Shield-to-Core Seal
15. Split Tubes and Bushings
16. Orifice Jet Bushings and Centering Bushings
17. Lateral Support Springs
18. Cluster Preload and Positioning Springs

19. Cluster Nuts and Locking Devices
20. Instrumentation Standoffs
21. Flow Screen Assembly
22. Orifice Jets
23. Outer Reflector Sectors
24. Seal Segments and Retainer Segments
25. Plunger Pine
26. Filler Strips and Blocks
27. Insulating Tile (possibly occasional delamination)
28. Insulating and Support Washers
29. Support Cones
30. Inner Reflector
31. Nozzle Interface
32. Tie Rod Nuts

In addition, the following components exhibited some surface markings or discoloration, but did not appear to be damaged:

1. Cluster Plates
2. Stainless Steel Liner Tubes
3. Tie Rods
4. Insulating and Countersunk Sleeves

The causes of the surface markings have not yet been satisfactorily established. In the light of recent experience during NRX-A3 assembly,

it seems possible that chlorides evolved from central elements might be responsible. Measures have been taken to control this in NRX-A3. Until the origin of these markings is determined, it annot be said that they might not constitute a source of damage if present in future tests; therefore, their recurrence should be prevented if possible.

Components showing damage associated with inherent material properties include the following:

1. Central Elements; local corrosion of the center hole at insulating sleeve junctions in most elements, varying from extremely light to moderately severe, depending on axial station; several instances of local corrosion at the shoulder on the hot end faces; two elements broken (most likely during disassembly).
2. Orifice Adhesive; loss of elastromeric properties as expected for the radiation dose sustained, the change being evident by fracture of the adhesive along with graphite chipping during disassembly handling.
3. Support Blocks; small areas showing material transfer from central element (sticking) on some blocks; possible corrosion around one hole of one block at the exit end.

4. Insulating Cups; graphite exposure on exit face of some, without associated corrosion.
5. Instrumentation Potting Compound; all or part of potting missing from most core thermocouple slots at Stations 20, 32, and 45; thermal capsule potting generally cracked but in place; inner reflector potting unaffected.
6. Core Thermocouples; Station 45 couples showed embrittlement and cracking of the external sheath (tantalum with tungsten coating) below about Station 10; some plugs were slightly pushed out of Station 45 thermocouple holes.

Anomalies observed which are not believed to be associated with materials limitations include these:

1. Burnish marks on several axial preload springs.
2. Burnish marks on control drum drive shaft splines.
3. Voids in the cement under at least one element key.

In summary, it may be said that the over-all picture presented by the non-fuel materials was very good; it should also be reiterated that further examination must be completed before the possibility of more subtle effects, or incipient damage, can be assessed. Typical photographs of the components mentioned in this section are given in Section 4.3. Data tables on the post-operational inspection are given in the Appendix.

4.3 MECHANICAL EVALUATION

4.3.1 General

This section evaluates the mechanical performance of the NRX-A2 reactor test. Thermal and flow parameters are not discussed unless they are relevant to the mechanical analysis. Two major areas are considered: 1) Analysis of data, 2) Evaluation of component damage.

The data analysis treats both static (structural) and dynamic (vibrational) responses. Most of the data of interest were generated during EP-IV (the high power run). However, some references are occasionally made to EP-IB, the ambient hydrogen test, and to EP-V, the low power, low flow restart of NRX-A2.

Static data were reduced from transducers monitoring the core/inner reflector cylinder gap changes, tie rod loads, and control drum torques. These data have been corrected for non-linearity and thermal effects wherever experimental calibration information was available.

The instrumentation available for monitoring vibration consisted of the above mentioned tie rod and inner reflector spring transducers (strain gages), as well as dynamic pressure transducers internally, and strain gages and accelerometers externally on the pressure vessel.

---

* G. Downs, P. Stancampiano, and P. C. Warner, NRX-A2 Post-Mortem Analysis, WANL-TME-1075, January, 1965, CRD.

The section on component damage deals with non-corrosive damage only. Corrosion is discussed in Section 4.2. The areas discussed are those in which the evidence strongly suggested that the damage occurred as a result of test environment or inadequate design. In general, NRX-A2 survived all of the tests and disassembly without serious component damage, and it may be assumed that the other reactor components, not specifically mentioned in this section, performed satisfactorily.

4.3.2 Analysis of Data

A. Lateral Support Spring Strains

The method of measuring the lateral support leaf spring strains is shown schematically in Figure 4.3-1. The locations of the plunger pins, whose motions were monitored, are also tabulated in Figure 4.3-1.

The lateral support leaf spring strains were measured relative to the initial preload strain and, therefore were indicative of changes in the gap between the core and inner reflector cylinder that occurred during the NRX-A2 EP-IV power run. The transducer system shown in Figure 4.3-1 is capable of detecting only the relative radial displacements between the core and inner reflector cylinder. Any rotational motion (circumferential slipping) between the plunger pins and seal segments therefore would, be undetected. Lateral displacements between the core and inner reflector cylinder appear up as asymmetric gap changes.

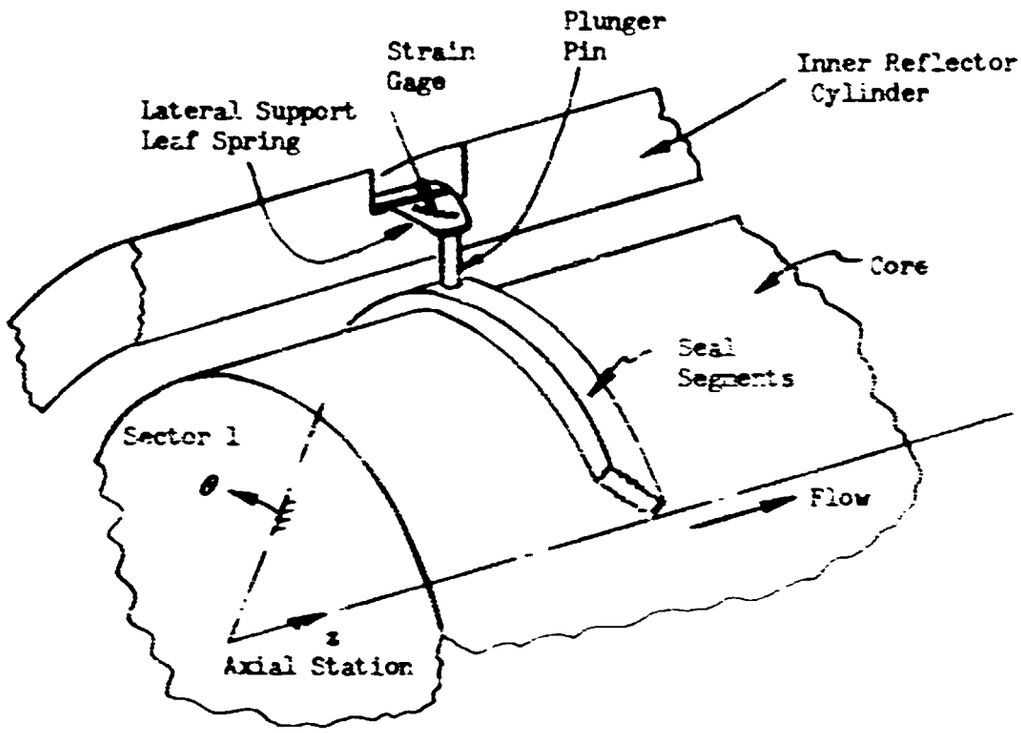

Leaf Spring Strain Gage Channel	Plunger Pin Location Station, In.	Plunger Pin Location θ, degrees
M414	19.810	95°
M418	19.810	215°
M422	19.810	335°
M415	31.058	85°
M419	31.058	205°
M423	31.058	325°
M416	47.930	85°
M420	47.930	205°
M424	47.930	325°

Figure 4.3-1 Schematic of Strain Gage Transducers Measuring Core/ Reflector Cylinder Gap Changes.

Figure 4.3-2 shows typical signal profiles of core temperature, the radial pressure differential across the inner reflector cylinder near the core exit, and leaf spring deflection (strain). It can be seen that the strain gages were responsive to the variations in core temperature and reflector cylinder pressure differential throughout the KF-IV test run.

The lateral support spring strain data obtained from these transducers have been utilized to determine the change in radial gap between the core and inner reflector cylinder, the core thermal expansion, the core centering with respect to the inner reflector cylinder, and the interaction between the plunger pins and plunger pin holes in the inner reflector cylinder. Each of these items is considered in detail in the following paragraphs.

1. Radial Gap Change Between Core and Inner Reflector Cylinder

Prior to the test, calculations were made to determine the change in radial gap between the core and inner reflector cylinder at the aft end. These calculations were based on predicted reactor pressures and temperatures and available material properties. Maximum and minimum gap changes were computed as well as the nominal values. These variations from nominal were based on the following deviations:

a) A $\pm$ 10 percent variation in the modulus of elasticity and coefficient of expansion of the inner reflector cylinder material.

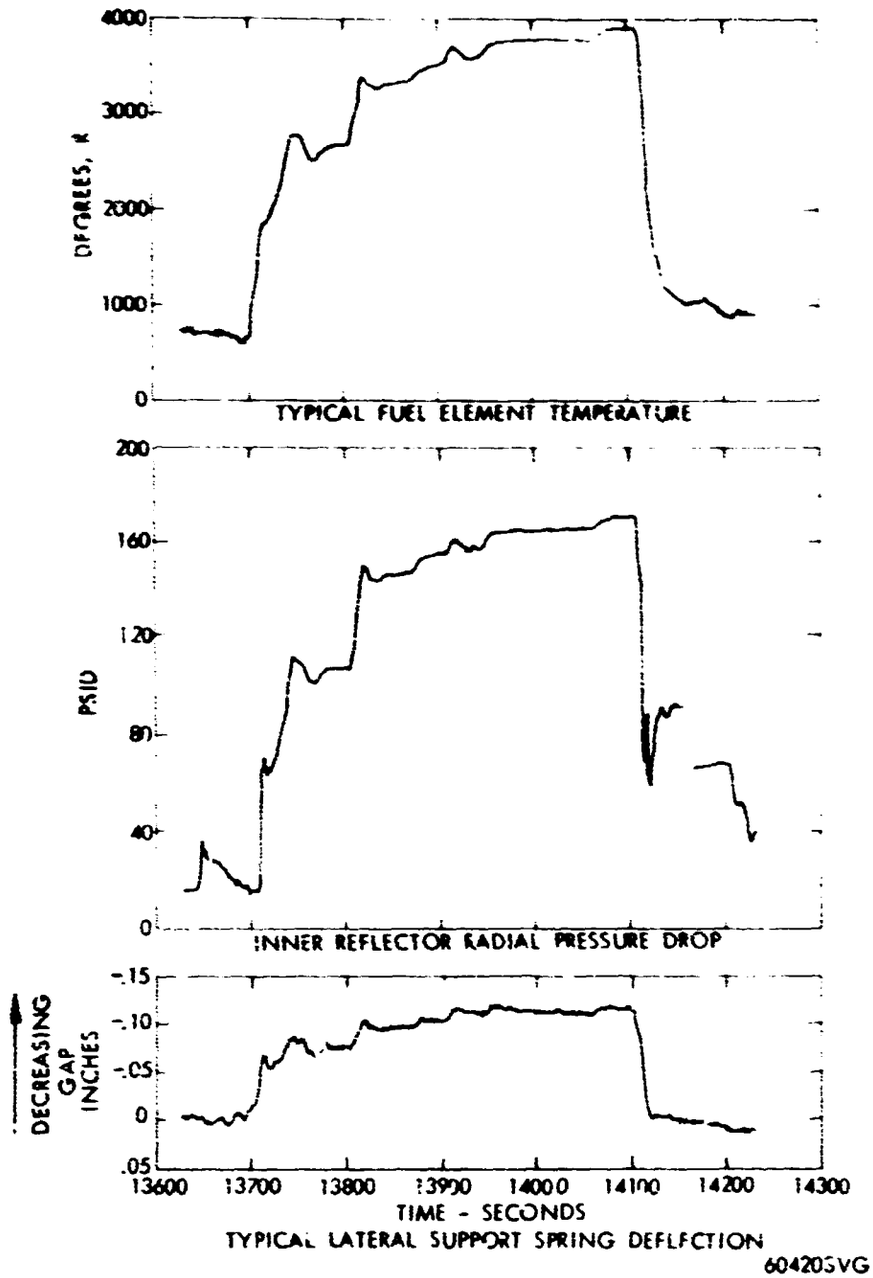

Figure 4.3-2 Typical Signal Profiles of Core/Reflector Cylinder Gap Change and Related Parameters During NRX-A2 EP-IV Power Run.

b) A ± 25 percent variation in the radial pressure drop across the inner reflector cylinder.

c) A ± 10 percent variation in the temperature of the inner reflector cylinder.

d) A ± 250°R variation in the core temperature.

d) A ± .17 $°R^{-1}$ variation in the coefficient of expansion of the fuel element material.

The maximum, nominal, and minimum computed gap changes are plotted in Figure 4.3-3. From this figure, it can be seen that interference between the core and reflector cylinder should result before 100 percent power and 100 percent flow are obtained if parameter deviations tend to favor the upper band limit.

The calculations were repeated after the NRX-A2 test was completed, using the temperatures and pressures measured during the test and nominal material properties. The results of these calculations for the first and last hold periods of the test are plotted as a function of axial core station on Figure 4.3-4, together with the circumferentially averaged test results. Additional test results for the four hold periods are listed in Table 4.3-1.

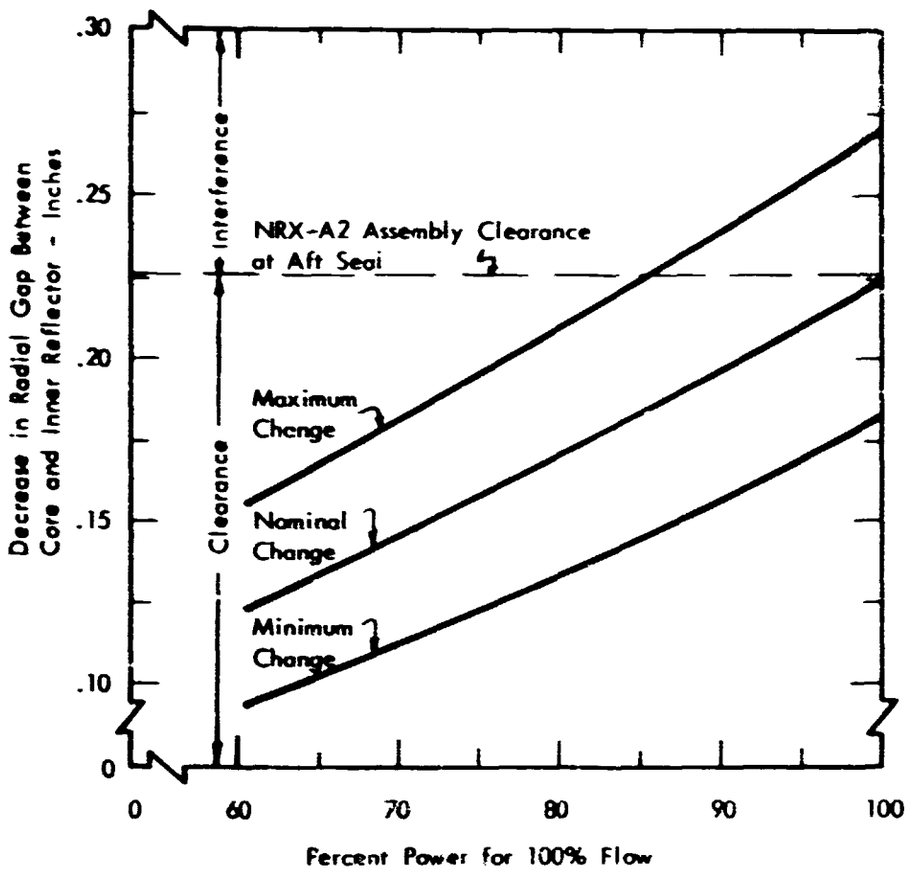

Figure 4.3-3 Predicted Average Decrease in Radial Gap Between Core and Inner Reflector at the Aft End.

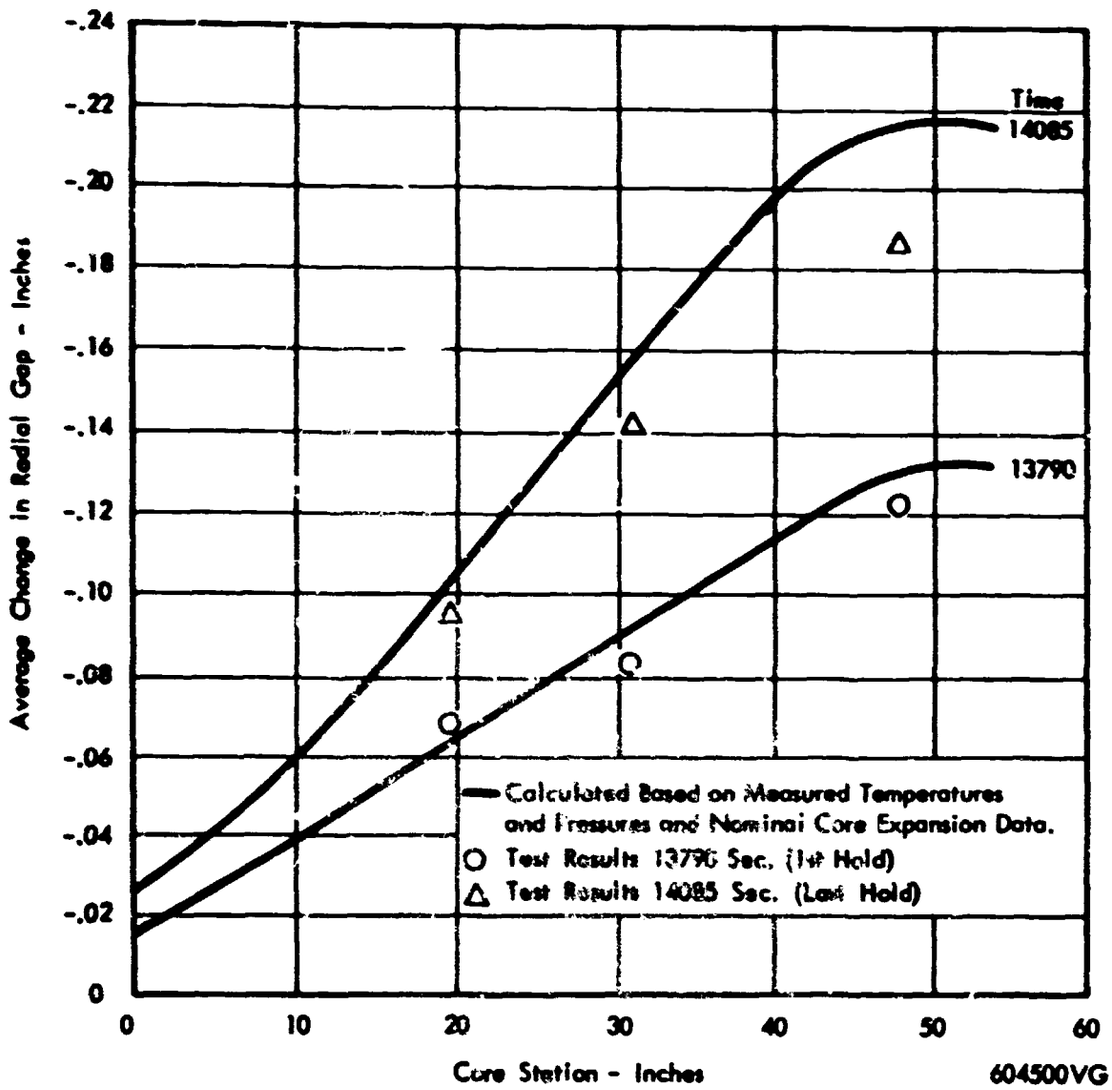

Note: Negative Values Indicate a Decrease in Gap.

Figure 4.3-4 Calculated and Measured Change in Radial Gap Between Core and Inner Reflector.

The test results, in Table 4.3-1 and Figure 4.3-4 have been corrected for non-linearity and temperature effects by using existing calibration data*. It was not possible to correct for any zero shift (drift), that could have occurred during the test, therefore, the test results agree better with computed values at the early hold time. Some of the discrepancies between the computed curves and measured points at high temperatures could be due to uncertainties in the fuel element expansion coefficient.

No contact occurred between the core and inner reflector during EP-IV as can be seen from the gap changes in Table 4.3-1 which were within the NRX-A2 assembly clearance (0.226 in.) at the aft seal.

2. Core Growth

The radial core growth at any position and time is related to the gap change by

$$U_{core} = U_{cyl} - \Delta g \qquad (1)$$

where U_{core} = radial core growth (inches)

U_{cyl} = radial inner reflector cylinder growth (inches)

Δg = increase in gap (inches)

---

* WANL Calibration for NRX-A2, WANL-TME-872, July 2, 1964.

CONFIDENTIAL
RESTRICTED DATA
Atomic Energy Act 1954

TABLE 4.3-1

RADIAL CHANGE IN GAP BETWEEN CORE AND REFLECTOR CYLINDER

DURING NRX-A2 EP IV POWER RUN HOLDS

	Station 19.810				Station 31.058				Station 47.930			
EP IV Time, Seconds	0-95° M414	215° M418	335° M422	Ave.	0-85° M415[3]	205° M419	325° M423	Ave.[3]	0-85° M416	205° M420	325° M424	Ave.
13790	-.063	-.080	-.062	-.068	-.026	-.085	-.062	-.083	-.097	-.126	-.145	-.123
13900	-.087	-.109	-.083	-.093	-.052	-.163	-.112	-.138	-.127	-.163	-.175	-.155
13985	-.088	-.109	-.109	-.102	-.076	-.173	-.121	-.147	-.139	-.193	-.192	-.175
14085	-.092	-.108	-.081	-.094	-.082	-.156	-.126	-.141	-.152	-.207	-.203	-.187

Note: 1. Negative values indicate a decrease in gap relative to the start of EP IV.

2. All the above displacements have been corrected for non-linearity and temperature effects in accordance with the calibration information in Ref. 1.

3. Thermal calibration for channel M415 was questionable, hence the average was computed without M415 data.

4. All displacements in inches.

CONFIDENTIAL
RESTRICTED DATA
Atomic Energy Act 1954

Astronuclear

The core growths for each of the four hold periods were estimated using equation (1), the gap changes in Table 4.3-1, and the calculated inner reflector cylinder displacements. These cylinder displacements were calculated for the pressure and thermal environments experienced by the inner reflector during EP-IV. The calculated cylinder displacements and the resulting estimated core growths for the four hold periods in the EP-IV test run are listed in Table 4.3-2.

The calculated core growths at each of the four hold periods have been computed using the core temperatures measured during theEP-IV test run and the nominal coefficient of expansion of the fuel element material. These calculated growths have been plotted in Figure 4.3-5 which also shows (for comparison) the circumferentially averaged values of core growth estimated from the strain gage results (Table 4.3-2). This comparison shows closer agreement at the first hold period that at the last for the same reasons discussed in previous sub-section on the radial gap change.

3. Core Centering

In prior analytical investigations, the core and inner reflector cylinder have been assumed to be initially concentric, and to remain so during reactor operation. An attempt has been made, utilizing the gap change data, to evaluate this assumption. It should

CONFIDENTIAL
RESTRICTED DATA
Atomic Energy Act 1954

TABLE 4.3-2

ESTIMATED RADIAL CORE GROWTHS DURING

NRX-A2 EP IV POWER RUN HOLDS

	Station 19.810					Station 31.058					Station 47.930				
		U_{core}					U_{core}					U_{core}			
Time, Seconds	U_{cyl}	0=95° M414	215° M418	335° M422	Ave.	U_{cyl}	0=85° M415[2]	205° M419	325° M423	Ave.[2]	U_{cyl}	0=85° M416	205° M420	325° M424	Ave.
13790	-.018	.045	.062	.044	.050	-.020	.006	.065	.062	.063	-.033	.064	.093	.112	.090
13900	-.016	.071	.093	.067	.077	-.021	.031	.142	.091	.117	-.041	.086	.122	.132	.114
13985	-.015	.073	.094	.094	.087	-.020	.056	.153	.101	.127	-.042	.097	.151	.150	.133
14085	-.014	.078	.094	.067	.080	-.020	.062	.136	.106	.121	-.042	.110	.165	.161	.145

Note: 1. The calculated cylinder displacements assume axial symmetry.

2. Thermal calibration of gap data for channel M415 was questionable, hence the average was computed without M415 data.

3. All displacements in inches.

CONFIDENTIAL
RESTRICTED DATA
Atomic Energy Act 1954

Astronuclear

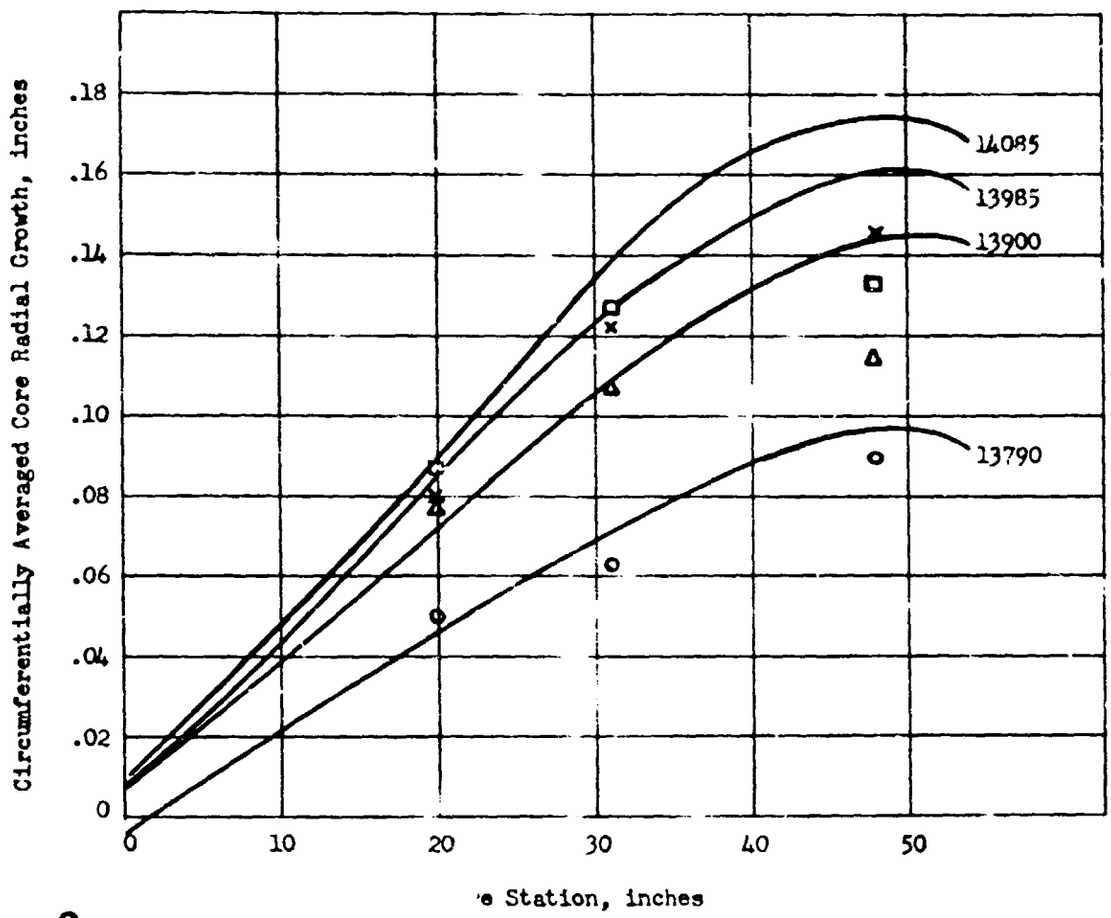

○ Estimated based on strain gage test results @ 13790 sec.

△ Estimated based on strain gage test results @ 13900 sec.

□ Estimated based on strain gage test results @ 13985 sec.

× Estimated based on strain gage test results @ 14085 sec.

——— Calculated using measured temperatures and nominal coefficient of expansion.

Figure 4.3-5 Calculated and Estimated Core Growth

be emphasized that the gap changes are due to the displacements of both the core and inner reflector cylinder. As a result, [illegible] asymmetry that may be present in the gap data could be due to unsymmetrical radial displacements of the inner reflector cylinder and/or the core growths. It is not possible to completely resolve this question with the present transducer system. It is apparent from Table 4.3-2 that the expected (calculated) reflector cylinder radial displacements are much smaller than the core [illegible], and it would be reasonable to assume that much of any asymmetry present is due to the core displacements.

Using a least squares method* and the gap data from Table 4.3-2 a best fit of an expanded core has been applied to the core stations that were monitored for gap changes (19.800, 31.058, and 47.930), and the results are shown in Table 4.3-3.

It can be seen that the estimated displacements of the core center are small particularly near the forward end (station 19.810). This may be due to the relatively greater tie rod restraint to lateral motion at the forward end than at stations 31.058 and 47.930. There also appears to be a tendency for the [illegible] to displace toward the 3rd quadrant ($180° < \theta < 270°$). The core displacements shown in Table 4.3-3 for station 31.058 include the core growths based on the strain gage data from Channel M-415 (Table 4.3-2). The

---

* G. Downs et al, NRX-A2 Post-Morten Analysis, WANL-TME-1075, January, 1965, CRD.

TABLE 4.3-3

ESTIMATED DISPLACEMENT OF CORE CENTER

MRA-A2 BF IV POWER RUN

	Time (sec)	h_c (in.)	θ_c (degrees)
	13790	.006	212°
Station 19.810	13900	.008	207°
	13985	.007	275°
	14085	.008	141°
	13790	.019	241°
Station 31.058	13900	.032	239°
	13985	.027	232°
	14085	.022	242°
	13790	.014	287°
Station 47.930	13900	.014	278°
	13985	.018	264°
	14085	.017	260°

thermal calibration of gap data for this channel was questionable (see note 2., Table 4.3-2) and may be contributing to the asymmetry. It should be re-emphasized that data from only three core/cylinder gap transducers, 120° apart, are not sufficient to establish unquestionably whether or not the asymmetries shown in Table 4.3-3 are real.

4. Interaction of Plunger Pins and Holes

Prior to the NRX-A2 reactor test, an investigation was made into the effect of compressive stresses at the aft end of the inner reflector cylinder on the changes (reductions) in plunger pin hole diameters. These changes, coupled with possibly large pins (tolerance-wise), would result in frictional restriction of pin motion. These restrictions might produce excessive local core bundling forces during thermal expansion of the core or pin binding during thermal contraction. The forces required to move the pins in the holes, when diametrical interference occurred, were determined by component testing.*

During shutdown as the core cools, moving radially inward, any stuck pins would remain fixed relative to the inner reflector cylinder. This could open up gaps between either the plunger pins and seal segments, the seal segments and filler strips, or filler strips and core, Figure 4.3-5. The free body diagram of a filler strip, shown in

---

* W. G. Parker, Plunger Hole Stress Concentration in Building Test, WANL-TME-960, September, 1964.

Astronuclear

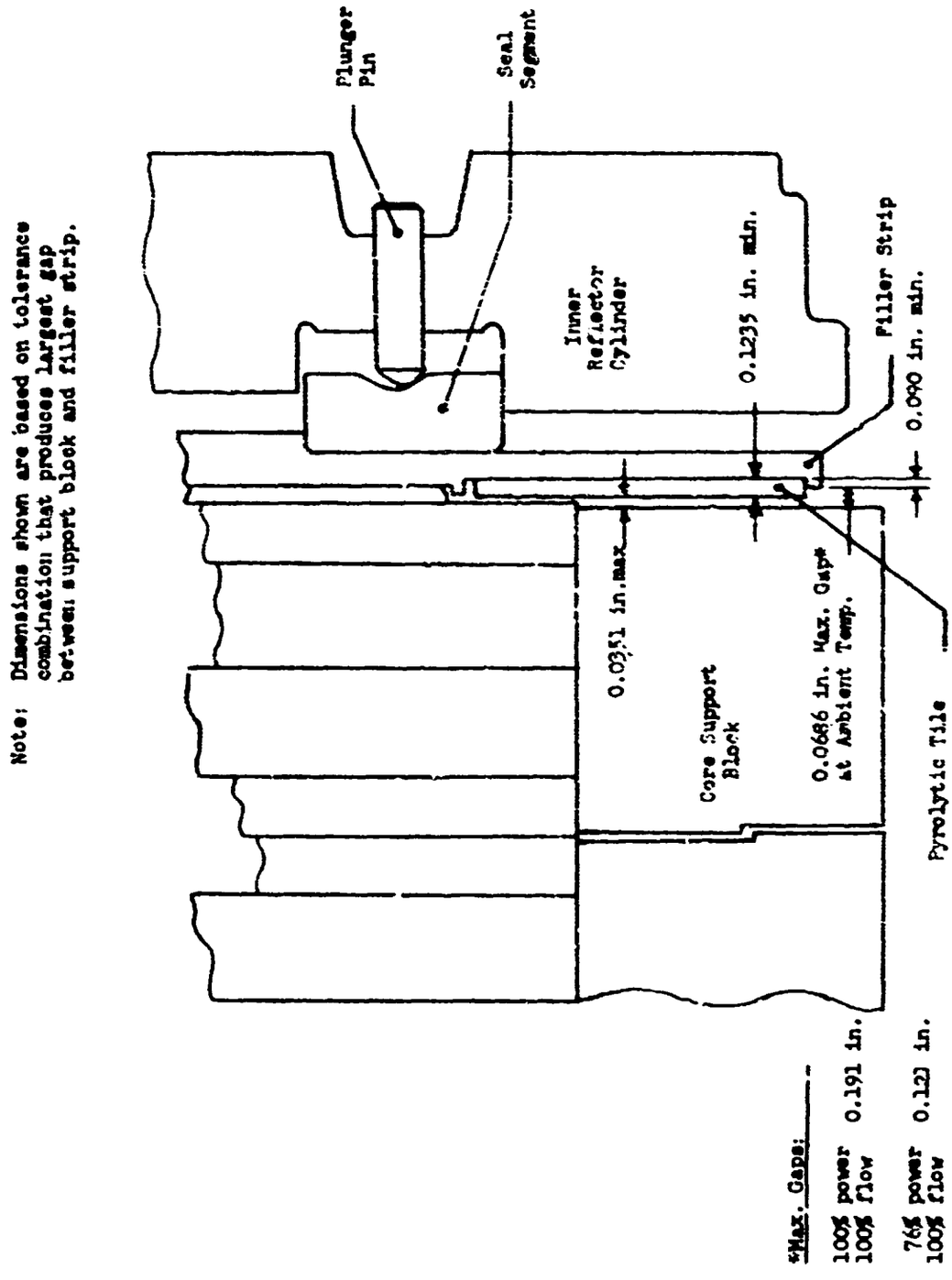

Note: Dimensions shown are based on tolerance combination that produces largest gap between support block and filler strip.

Figure 4.3-7 Schematic of Core Periphery and Inner Reflector Clearances at the Aft End, NRX-A2 Reactor.

Figure 4.3-7, at the time when such gaps might exist illustrates the physical configuration it would assume prior to cooldown due to the relatively greater thermal expansion at the aft end of the core.

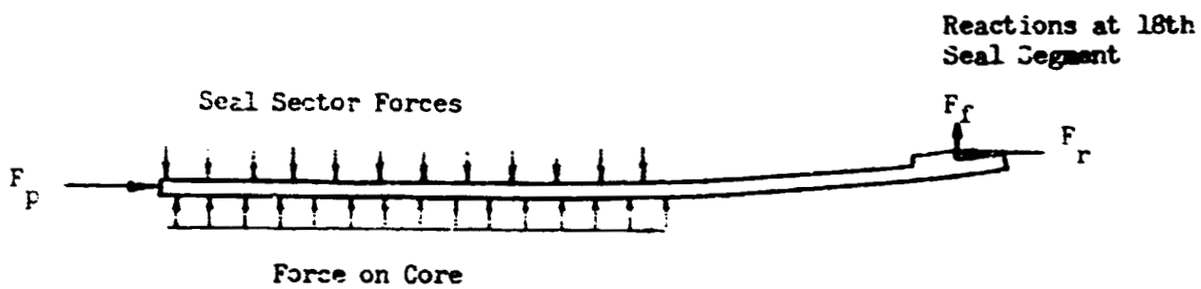

Figure 4.3-7 **Free Body of Filler Strips when Gap Exists.**

Because the line of action of the axial pressure load (F_p) is offset with the seal reaction (F_r), a moment occurs at the aft end of the filler strip tending to bend it outward away from the core. As a consequence, the frictional force (F_f) may be sufficient to cause the filler strip to remain with the eighteenth seal segment rather than straighten and follow the contracting core. Hence it appears more likely to have a gap, should one occur at all, between the filler strips and the core.

The dimensions shown in Figure 4.3-6 are the worst tolerances that might occur at the aft end periphery of the NRX-A2 core. Calculations were made for cooldowns from 100% power-100% flow, and 76% power-100% flow that predicted the maximum gaps between the core and filler strips to be 0.191 and 0.121 inches respectively. Since the minimum tile thickness is 0.1235 inches, there is a possibility that pyrolytic tiles might be ejected from the core for shutdowns from runs above 76% power. However, since each seal segment is loaded by three plunger pins, all three pins would have to stick for a gap to form. Thus the chance that tiles would be ejected as a result of pin hang-up only during a test is extremely small. No tiles were lost during the NRX-A2 power test.

While no tiles were lost in NRX-A2, there was evidence from the lateral support spring strain gage data that one of the three instrumented plunger pins in the seventeenth row (station 47.930) hung-up for a short time during the shutdown phase of the EP-IV power run. The curves in Figure 4.3-8 were reproduced directly from the test tape and are continuous data from channels M-416, M-420, and M-424 in the seventeenth seal row. Figure 4.3-9 is an enlarged plot of the same data except that linearity and temperature calibration corrections have been applied. This figure shows the radially inward plunger movement measured relative to the maximum outward position obtained during the last power hold of EP-IV.

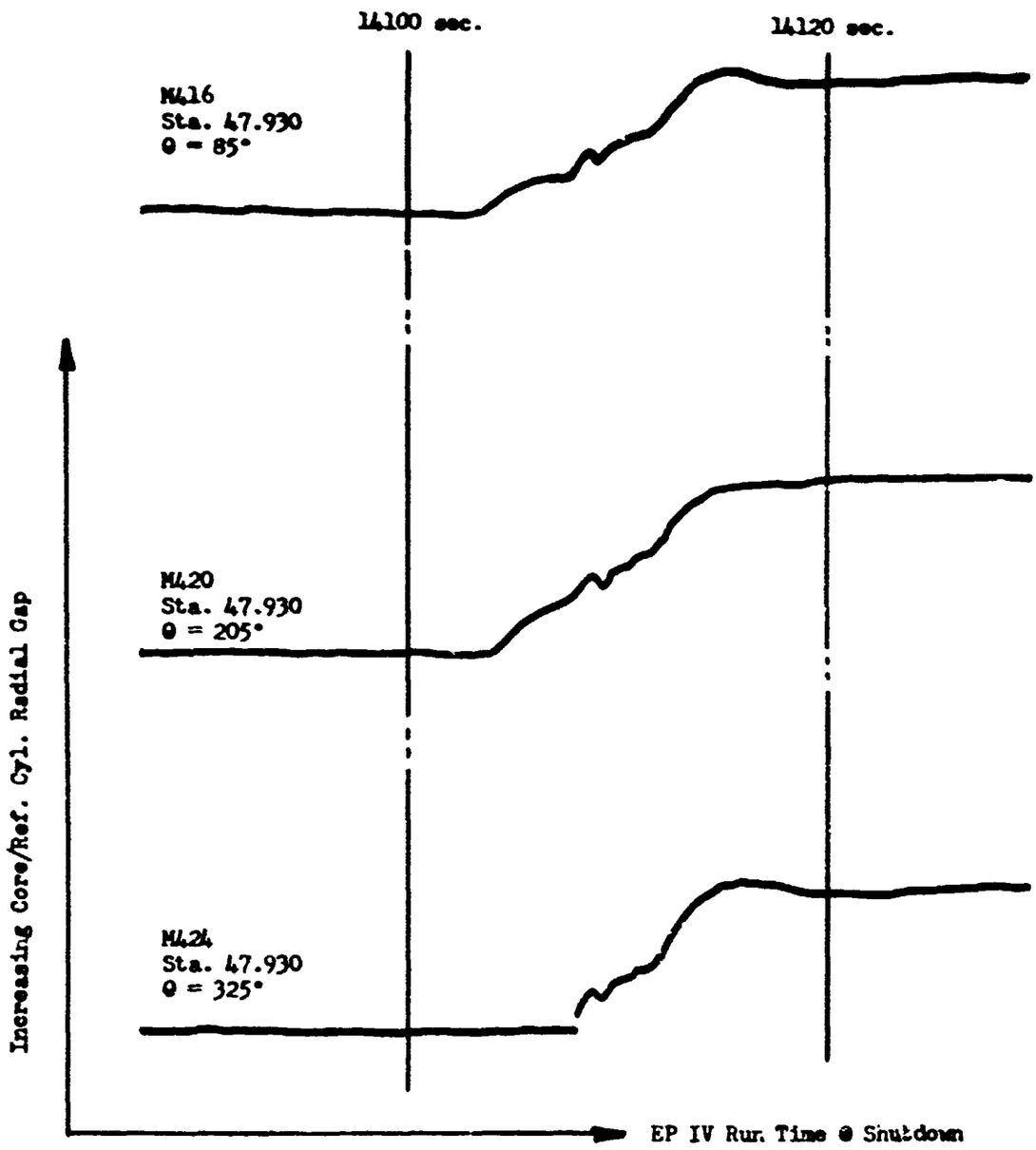

Figure 4.3-8 Continuous Playback of Wide Band Data from Channels M416, M420, and M424 During Shutdown of NRX-A2 EP-IV.

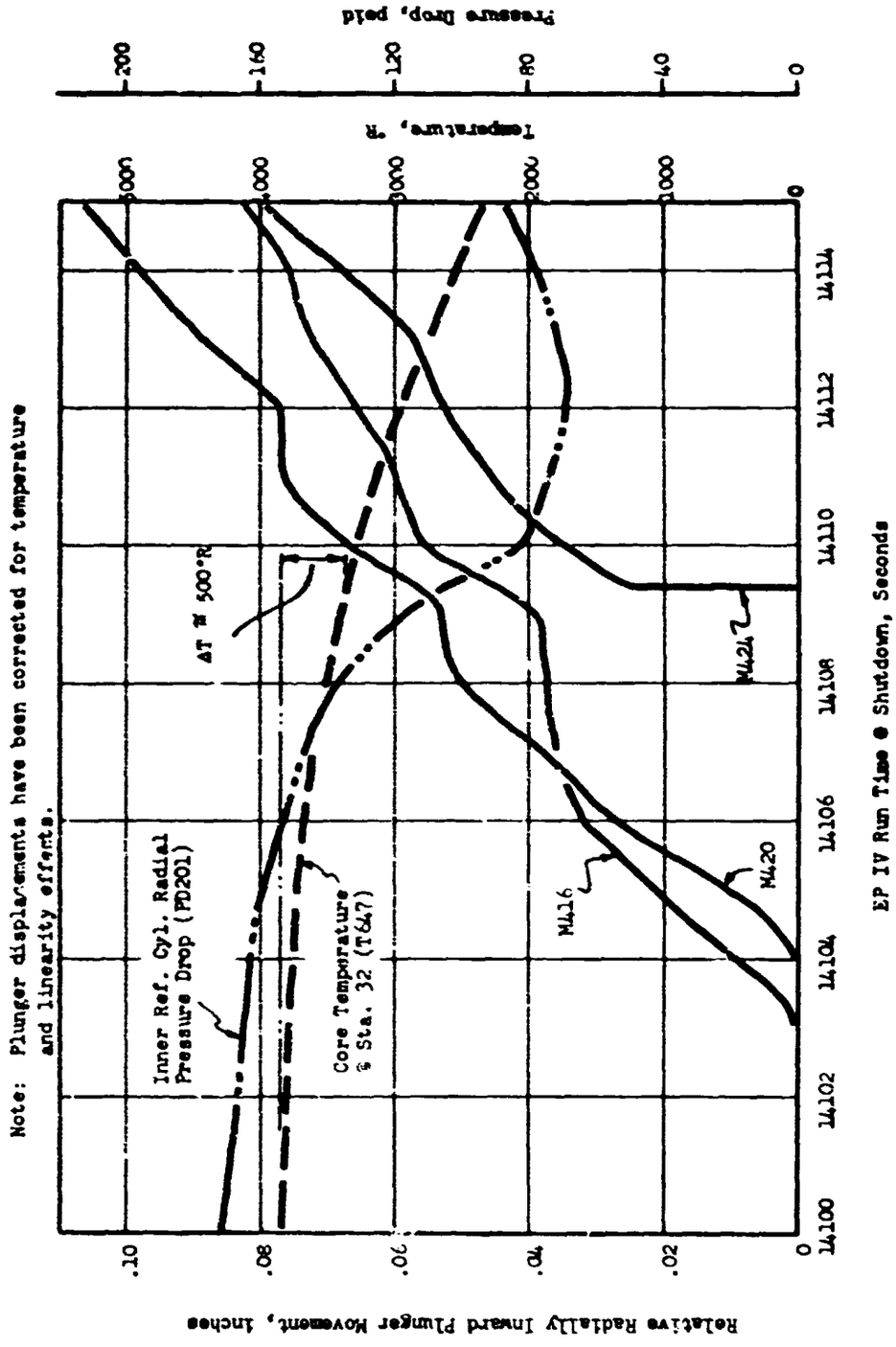

Figure 4.3-9 Relative Radially Inward Plunger Pin Movement from Maximum Outward Position and Related Parameters During NRX-A2 EP-IV Shutdown.

From this figure (and Figure 4.3-8), it can be seen that the pins monitored by M-416 and M-420 started moving approximately 6 seconds before pin M-424 and had actually moved inward approximately 0.045 inch. This is equivalent to a temperature drop of the core of 700 to 800°R. Note that the vertical line on the M-424 curve in Figure 4.3-9 corresponds to the gap in the data reproduction of channel M-424 on Figure 4.3-8. Also plotted in Figure 4.3-9 are the core temperatures at station 32 given by channel T-647 and the radial pressure drop across the exit end of the inner reflector, channel PD-201. These channels indicate that the free plungers (M-416 and M-420) should be moving radially inward, and they do. Also the 500°R core temperature drop at station 32 is in keeping with the expected 700-800°R drop mentioned above at the relatively hotter station 48, where the plungers of Figures 4.3-8 and 4.3-9 were located.

The plunger pin assembly clearance has been increased in the NRX-A3 reactor to eliminate the possibility of plunger pin sticking.

B. Core Tie Rod Strains

The original plan for the NRX-A2 test was to have two strain gages located 180 degrees apart (diametrically opposite each other) on each of the three tie rods in a J9 irregular peripheral cluster. However, one gage was damaged prior to the test, and a second gage (on another tie rod) was found to be faulty during the test. The analysis, therefore, was based on the remaining four gages which were believed to be performing satisfactorily. Figure 4.3-10 locates the tie rods in the cluster and indicates the corresponding strain gages that were operative.

Table 4.3-4 lists the loads on the tie rods as obtained from strain readings and by calculations for each of the four power hold periods. The strain readings were converted to force using calibration data*, and the calculated values are based on the assumption that the support block is a rigid body supported at three points (the tie rods) under axial core pressure drop loading.

There is a close correlation between the measured and computed loads in Table 4.3-4. It can be seen that the total measured load (cluster load) was larger than the direct load from the core pressure drop. This may be due to thermal calibrations which were not available directly for the NRX-A2 tie rod strain gages. The NRX-A3 thermal calibrations indicate that the tie rod strain gages

---

* WANL Calibration for NRX-A2, WANL-TME-872, July 2, 1964, CRD.

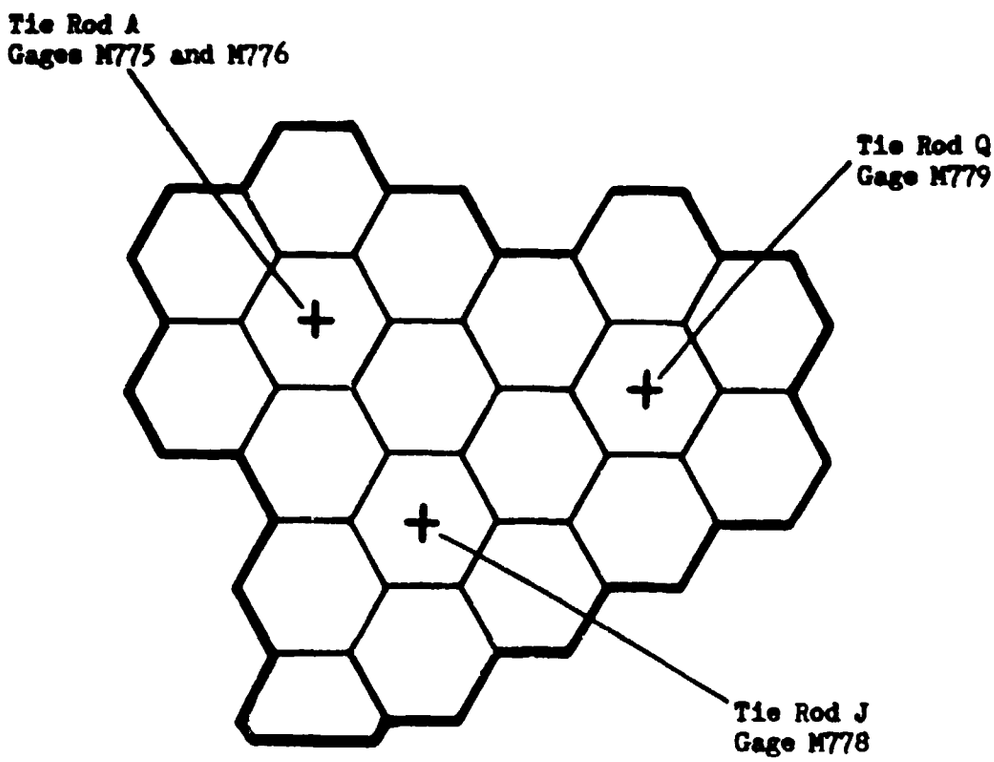

Figure 4.3-10 Location of Instrumented Tie Rods in Cluster J9, Sector 5, NRX-A2 Power Test.

CONFIDENTIAL
RESTRICTED DATA
Atomic Energy Act - 1954

TABLE 4.3-4

MEASURED AND COMPUTED TIE ROD LOADING

NRX-A2 EP IV POWER RUN

	Rod A				Rod J		Rod Q		Cluster J9, Sector 5	
	Measured Load			Computed Load	Measured Load	Computed Load	Measured Load	Computed Load	Measured Load	Computed Load
Time	M775	M776	Ave.		M778		M779			
13790	261	191	226	242	350	287	327	256	903	785
13900	391	386	389	338	467	401	447	358	1303	1097
13985	391	404	398	358	467	426	461	379	1326	1163
14085	407	417	412	366	467	434	461	387	1340	1187

Note: 1. All loads in pounds.

2. All loads have been determined using calibration data in Ref. 1.

3. Cluster load is the sum of the three tie rod loads.

CONFIDENTIAL
RESTRICTED DATA
Atomic Energy Act - 1954

Stronuclear

will read about 10% more strain than expected due to direct tension at cryogenic temperatures. However, some of this increased loading may be read and due to localized bundling (lock up) causing this cluster to pick up additional core pressure drop loading from adjacent clusters. In addition, the peripheral tie rods are nominally cooler than the central rods and were expected to carry more load in a bundled core.*

The ratios of individual tie rod load to the total cluster load are tabulated in Table 4.3-5. This table shows that there seems to have been a redistribution of loading in the cluster between times 13790 and 13900. From Table 4.3-4, there also seems to be relatively more bending in tie rod A initially at time 13790 seconds.

In all cases, the recorded tie rod loads were well within the material strength, and no tie rod damage occurred during the NRX-A2 power test.

---

* G. Downs, Stress Analysis NRX-A Cluster Tie Rod, WANL-TME-568, October, 1963.

TABLE 4.3-5

TIE ROD LOAD DISTRIBUTION

IN CLUSTER -J9, SECTOR 5

Time Sec	Load A/Cluster Load		Load J/Cluster Load		Load Q/Cluster Load	
	Measured	Computed	Measured	Computed	Measured	Computed
13790	.250	.308	.388	.366	.362	.326
13900	.299	.308	.358	.366	.343	.326
13985	.300	.308	.352	.366	.348	.326
14085	.307	.308	.349	.366	.344	.326

C. Control Drum Torque

The results of the NRX-A1 cold flow tests indicated rubbing between the aluminum control drum housing and the beryllium sectors. During these cold flow runs, control drum torque readings as high as 1200 in-lb were recorded.* The sector bores were consequently increased for the NRX-A2 reactor configuration. Examination of the control drum torques during the NRX-A2 power run indicated no rubbing as experienced in the A-1 tests. The torques are small, but peak at the initiation of scram (14109 seconds). These peak values are about ± 90 in-lb. Figure 4.3-11 shows typical reproductions of control drum torque and angular position data taken from the continuous wide band tape recorded during shutdown of the EP-IV test run.

D. Vibration Data Analysis

The instrumentation available for monitoring core vibration consisted of the tie rod and lateral support spring strain gages to measure core motion and dynamic pressure transducers to pick up internal pressure fluctuations. In addition, strain gages and accelerometers mounted externally on the pressure vessel were available for cross correlation. The wide band data from these channels were carefully reviewed and the essential features of the findings are tabulated in Tables 4.3-6, 4.3-7, and 4.3-8 for EP-IB, IV, and V respectively. Figures 4.3-12 to 4.3-23 graphically illustrate the comments in these tables.

---

* C. V. [illegible], Post-Operative Structural Analysis of NRX-A1, August, 1964, CRD.

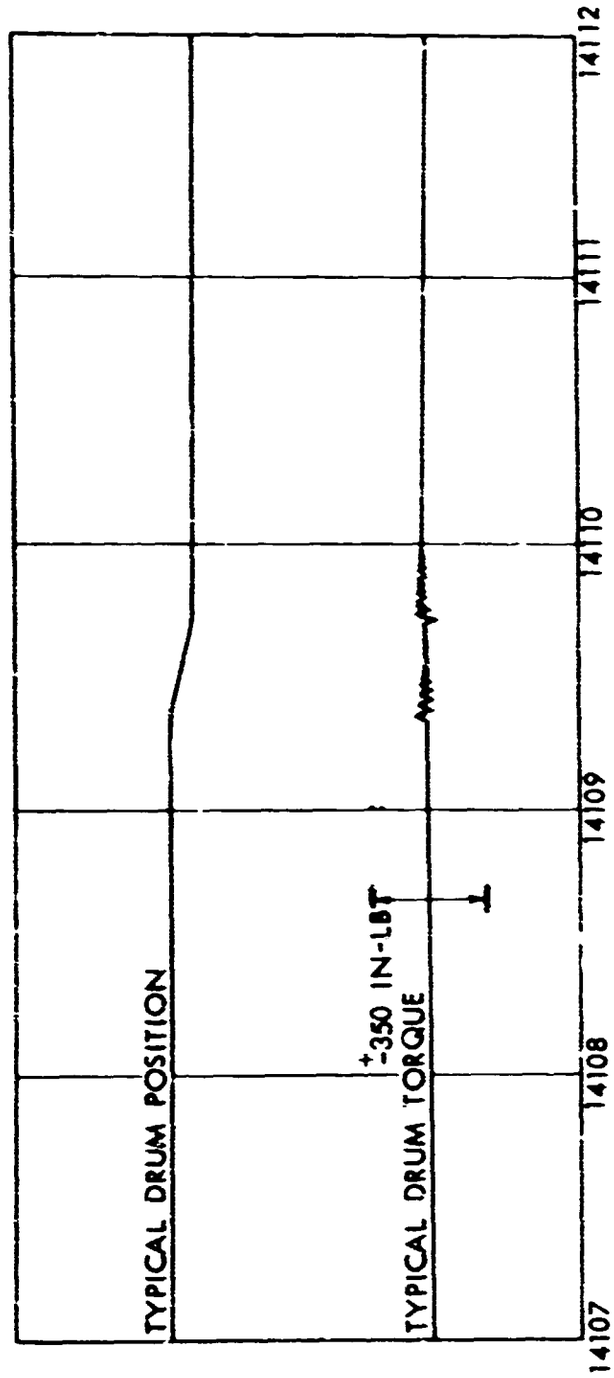

Figure 4.3-11 Typical Wide Band Playbacks of Control Drum Position and Torque During Shutdown of NRX-A2 EP-IV Power Run.

TABLE 4.3-6

DYNAMIC MEASUREMENTS AND COMMENTS FOR NRX-A2 RUN EP 1B

MEAS NUMBER	LOCATION	RANGE	SYS B/W	COMMENT ON CHANNEL STATUS	COMMENTS
H 150Y	Nos Flg	+- 150	750		12607 10 @ 240 cps
H 151Z	Nos Flg	+- 150	750		No Dynamic Data
H 260X	Fwd Flg	+- 150	750		No Dynamic Data
H 261X	Fwd Flg	+- 150	750	? Shield Loose	12610 .60 @ 320 cps (340 cps + 900 cps)
H 262Y	Fwd Flg	+- 150	750		12611 Trace 26654 .30 @ 10 cps
H 263Z	Fwd Flg	+- 150	750	? Noisy Cal	No Dynamic Data
H 805Y	Fwd Flg	+- 250	1K		12605 Bursts of VHF Modulated @ 140 cps (3.5 G's @ 1020 cps)
H 806Z	Fwd Flg	+- 250	1K		No Dynamic Data
M 202X	RPV AFT	+-3.5KU	300		No Dynamic Data
M 203Z	RPV AFT	+-3.5KU	300		No Dynamic Data
M 204X	RPV AFT	+-3.5KU	300		No Dynamic Data
M 205Z	RPV AFT	+-3.5KU	300		No Dynamic Data
M 208X	RPV AFT	+-3.5KU	300		No Dynamic Data
M 209Z	RPV AFT	+-3.5KU	300		No Dynamic Data
M 210X	RPV AFT	+-3.5KU	500		No Dynamic Data
M 211Z	RPV AFT	+-3.5KU	500		No Dynamic Data
M 414	IR SPRING	+-.250IN	500		No Dynamic Data
M 415	IR SPRING	+-.250IN	500		No Dynamic Data
M 415T	IR SPRING	+-.25 IN	500		19710 (Figure 4.3-12) 17.7 cps ±.025 IN, also large 60 cps, not supported by M415.
M 416	IR SPRING	+-.250IN	500		No Dynamic Data
M 416T	IR SPRING	+-.125IN	500		No Dynamic Data
M 418	IR SPRING	+-.250IN	500		No Dynamic Data
M 419	IR SPRING	+-.250IN	500		No Dynamic Data
M 419T	IR SPRING	+-.25 IN	500		No Dynamic Data
M 420	IR SPRING	+-.250IN	500		No Dynamic Data
M 420T	IR SPRING	+-.125IN	500		No Dynamic Data

CONFIDENTIAL
RESTRICTED DATA
Atomic Energy Act - 1954

TABLE 4.3-6 (Cont.)

DYNAMIC MEASUREMENTS AND COMMENTS FOR NEX-A2 RUN EP IB

MEAS NUMBER	LOCATION	RANGE	SYS B/W	COMMENT ON CHANNEL STATUS	COMMENTS
M 422	IR SPRING	+-.250IN	500		No Dynamic Data
M 423	IR SPRING	+-.250IN	500		No Dynamic Data
M 423T	IR SPRING	+-.125IN	500		No Dynamic Data
M 424	IR SPRING	+-.250IN	500		No Dynamic Data
M 424T	IR SPRING	+-.25 IN	500		No Dynamic Data
M 775	Tie Rod	+-4K UIN	1K		No Dynamic Data
M 775T	Tie Rod	+-2000UIN	1K		No Dynamic Data
M 776	Tie Rod	+-4K UIN	1K		± 400 μin/in continuously @ 100 cps until 15597 -- see M776T (No Con., also noisy cal.)
M 776T	Tie Rod	+-2000UIN	1K		No Dynamic Data
M 778	Tie Rod	+-4K UIN	1K		No Dynamic Data
M 778T	Tie Rod	+-2000UIN	1K		No Dynamic Data
M 779	Tie Rod	+-4K UIN	1K		No Dynamic Data
M 779T	Tie Rod	+-2000UIN	1K		No Dynamic Data
M 780	Tie Rod	+-4K UIN	1K	Questionable Bridge	12610 ± 17000 psi, not real
M 780T	Tie Rod	+-2000UIN	1K		[illegible] ±19400 psi (Figure 4.3-[illegible]) [illegible] cps [illegible], Very suspicious looking

CONFIDENTIAL
RESTRICTED DATA
Atomic Energy Act - 1954

Astronuclear

TABLE 4.3-7

DYNAMIC MEASUREMENTS AND COMMENTS FOR NPX-A2 RUN EP 1B

MEAS NUMBER	LOCATION	RANGE	SYS B/W	COMMENT ON CHANNEL STATUS	COMMENTS
H 150Y	Noz Flg	+- 15G	750	Questionable	Large zero drifts (13390,13694 etc.);goes out 13649-13693,(Fig 4.3-14)
H 151Z	Noz Flg	+- 15G	750	Questionable	" " " " " " full scale excursion 13993, (Fig 4.3-15)
H 260X	Fwd Flg	+- 15G	750	Defective Transducer	" " " " " "
H 261X	Fwd Flg	+- 15G	750	Bad charge amp.	" " " " " " noisy 14014,(Fig. 4.3-16)
H 262Y	Fwd Flg	+- 15G	750	Questionable	" " " " " " largest data occurs after power run 14136,(Fig. 4.3-17)
H 263Z	Fwd Flg	+- 15G	750	Bad charge amp.	" " " " " "
H 805Y	Fwd Flg	+- 25G	1K	Questionable Transducer; continuous ~5g @ 1040 CPS, believed to be due to loss of damping gas	
M 202X	RPV AFT	+- 3.5KU	300	Defective gage	
M 203Z	RPV AFT	+- 3.5KU	300	Blown fuse	
M 204X	RPV AFT	+- 3.5KU	300	Defective gage	
M 205Z	RPV AFT	+- 3.5KU	300		No dynamic data
M 208X	RPV AFT	+- 3.5KU	300		No dynamic data
M 209Z	RPV AFT	+- 3.5KU	300		No dynamic data
M 210X	RPV AFT	+- 3.5KU	500	Blown fuse	
M 211Z	RPV AFT	+- 3.5KU	500	Defective gage	
M 414	IR SPRING	+-.250IN	500		No dynamic data
M 415	IR SPRING	+-.250IN	500		No dynamic data
M 415T	IR SPRING	+-.250IN	500	Questionable	60 cps prevalent, low freq. @ 13708, 14109; not confirmed by M 415, (Fig. 4.3-18, 4.3-19)
M 416	IR SPRING	+-.250IN	500		No dynamic data
M 416T	IR S[illegible]	+-.125IN	500		No dynamic data
M 418	IR SPRING	+-.250IN	500		No dynamic data
M 419	IR SPRING	+-.250IN	500		No dynamic data
M 419T	IR SPRING	+-.250IN	500		No dynamic data
M 420	IR SPRING	+-.250IN	500		No dynamic data
M 420T	IR SPRING	+-.125IN	500		No dynamic data

TABLE 4.3-7 (Continued)

DYNAMIC MEASUREMENTS AND COMMENTS FOR NRX-A2 RUN EP IB

MEAS NUMBER	LOCATION	RANGE	SYS B/W	COMMENT ON CHANNEL STATUS	COMMENTS
M 422	IR SPRING	+-.250IN	500		No dynamic data
M 423	IR SPRING	+-.250IN	500		No dynamic data
M 423T	IR SPRING	+-.125IN	500		No dynamic data
M 424	IR SPRING	+-.250IN	500		No dynamic data
M 424T	IR SPRING	+-.250IN	500		No dynamic data
M 775	Tie Rod	+-4K UIN	1K		No dynamic data except slow pulse @ 14109.3
M 775T	Tie Rod	+-2000UIN	1K		No dynamic data
M 776	Tie Rod	+-4K UIN	1K		No dynamic data except slow pulse @ 14109.3
M 776T	Tie Rod	+-2000UIN	1K		60 cps signal, trace of 5-10 cps, some DC not real.
M 778	Tie Rod	+-4K UIN	1K		No dynamic data except slow pulse @ 14109.3
M 778T	Tie Rod	+-2000UIN	1K		No dynamic data
M 779	Tie Rod	+-4K UIN	1K		No dynamic data except slow pulse @ 14109.3
M 779T	Tie Rod	+-2000UIN	1K		No dynamic data
M 780	Tie Rod	+-4K UIN	1K	Questionable	13820 - ~ 8000psi @ several hundred cps - very suspicious looking. (Slow pulse @ 14109.3)
M 780T	Tie Rod	+-2000UIN	1K	Bridge	13820 - ~8000 psi @ several hundred cps - very suspicious looking. Data not confirmed by M779 and M779T, (Fig. 4.3-20)
P 100	Feed Line	0-1K PSIA	400		Slow pressure pulse (drop) of 486 psi followed by several oscillations @ 14109.3*
P 100T	Feed Line	+-36.5	400		Looks unreal throughout
P 110	Noz Torus	0-1K PSI	400		Slow pressure pulse (drop) of 475 psi followed by several oscillations @ 14109.3*
P 120	Noz Cham	0-600 PSI	400	Questionable	Slow pressure pulse (drop) of 475 psi followed by several oscillations @ 14109.3*
P 120T	Noz Cham	+-22.8	400		60 cps throughout; looks bad

Astronuclear

CONFIDENTIAL
RESTRICTED DATA
Atomic Energy Act - 1954

TABLE 4.3-7 (Continued)

DYNAMIC MEASUREMENTS AND COMMENTS FOR NRX-A2 RUN EP IV

MEAS NUMBER	LOCATION	RANGE	SYS B/W	COMMENT ON CHANNEL STATUS	COMMENTS
P 200	Noz T Out	0-750 PSI	400	Questionable	Slow pressure pulse (drop) of 520 psi followed by several oscillations @ 14109.3*
P 306	OR Out PL	0-800 PSI	500	Questionable	Slow pressure pulse (drop) of 500 psi followed by several oscillations @ 14109.3*
P 306T	OR Out PL	+-80 PSA	500		Looks bad throughout, contains some 60 cps also
P 501	Shield PL	0-750 PSI	300	Questionable	Slow pressure pulse (drop) of 640 psi followed by several oscillations @ 14109.3*
P 601	CO IN PL	+-30 PSID	300	Questionable	Signal at 14109.3, but not like any of the others*
P 603	CO IN PL	0-750 PSI	300	Questionable	No pressure pulse @ 14109.3, but channel appears operative; contains steady state data.
P 603T	CO IN FL	+- 27.1	300		Looks very bad at first then straightens out and becomes quiet. Obvious signal at 14109.3, but looks unreal and unlike any others at this time.

*Refer to Table 4.3-11

CONFIDENTIAL
RESTRICTED DATA
Atomic Energy Act - 1954

Astronuclear

CONFIDENTIAL
RESTRICTED DATA
Atomic Energy Act - 1954

TABLE 4.3-8

DYNAMIC MEASUREMENTS AND COMMENTS FOR NRX-A2 EP V

MEAS NUMBER	LOCATION	RANGE	SYS B/W	COMMENT ON CHANNEL STATUS	COMMENTS
H 150Y	Noz Flg	+- 15G	750		No Dynamic Data
H 151Z	Noz Flg	+- 15G	750	Questionable	Data do not appear to be real, (Fig. 4.3-21, 4.3-22)
H 261X	Fwd Flg	+- 15G	750		No Dynamic Data
H 262Y	Fwd Flg	+- 15G	750		No Dynamic Data
M 203Z	RPV AFT	+-3.5KU	300		No Dynamic Data
M 205Z	RPV AFT	+-3.5KU	300		No Dynamic Data, but DC shift.
M 208X	RPV AFT	+-3.5KU	300		18593 full scale spikes, looks unreal, 14123 DC shift.
M 209Z	RPV AFT	+-3.5KU	300		No Dynamic Data, but DC shift.
M 210X	RPV AFT	+-3.5KU	500		Low level, low frequency data.
M 414	IR Spring	+-.250IN	500		No Dynamic Data
M 415	IR Spring	+-.250IN	500		No Dynamic Data
M 415T	IR Spring	+-.25 IN	500		60 CPS everywhere, some DC shift.
M 416	IR Spring	+-.250IN	500		No Dynamic Data, but DC shift.
M 416T	IR Spring	+-.125IN	500		No Dynamic Data
M 418	IR Spring	+-.250IN	500		No Dynamic Data
M 419	IR Spring	+-.250IN	500		No Dynamic Data
M 419T	IR Spring	+-.25 IN	500		No Dynamic Data
M 420	IR Spring	+-.250IN	500		No Dynamic Data
M 420T	IR Spring	+-.125IN	500		No Dynamic Data
M 422	IR Spring	+-.250IN	500		No Dynamic Data
M 423	IR Spring	+-.250IN	500		No Dynamic Data
M 423T	IR Spring	+-.125IN	500		No Dynamic Data
M 424	IR Spring	+-.250IN	500		No Dynamic Data
M 424T	IR Spring	+-.25 IN	500		No Dynamic Data

CONFIDENTIAL
RESTRICTED DATA
Atomic Energy Act - 1954

Astronuclear

CONFIDENTIAL
RESTRICTED DATA
Atomic Energy Act 1954

TABLE 4.3-8 (Continued)

DYNAMIC MEASUREMENTS AND COMMENTS FOR NRX-A2 EP V

MEAS NUMBER	LOCATION	RANGE	SYS B/W	COMMENT ON CHANNEL STATUS	COMMENTS
M 775	Tie Rod	+-4K UIN	1K		No Dynamic Data
M 775T	Tie Rod	+-2K UIN	1K		No Dynamic Data
M 776	Tie Rod	+-4K UIN	1K		No Dynamic Data
M 776T	Tie Rod	+-2K UIN	1K		No Dynamic Data, some 60 CPS
M 778	Tie Rod	+-4K UIN	1K		Low level signals, same as on 2 adjacent channels.
M 778T	Tie Rod	+-2K UIN	1K		No Dynamic Data
M 779	Tie Rod	+-4K UIN	1K		No Dynamic Data, but DC shift.
M 779T	Tie Rod	+-2K UIN	1K		No Dynamic Data
M 780	Tie Rod	+-4K UIN	1K }	Questionable	No Dynamic Data, but DC shift.
M 780T	Tie Rod	+ 2K UIN	1K }	Bridge	No Dynamic Data

CONFIDENTIAL
RESTRICTED DATA
Atomic Energy Act 1954

Astronuclear

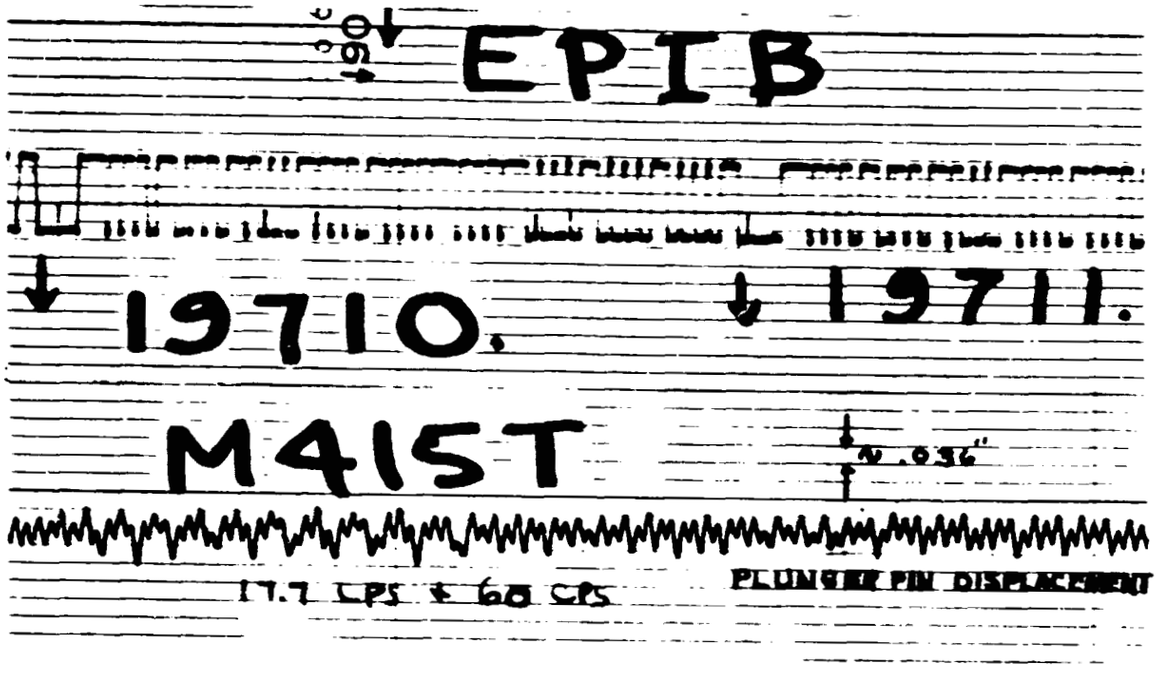

Figure 4.3-12 Continuous Signal of 60 cps with some 17.7 cps on Inner Reflector Spring Strain Gage.

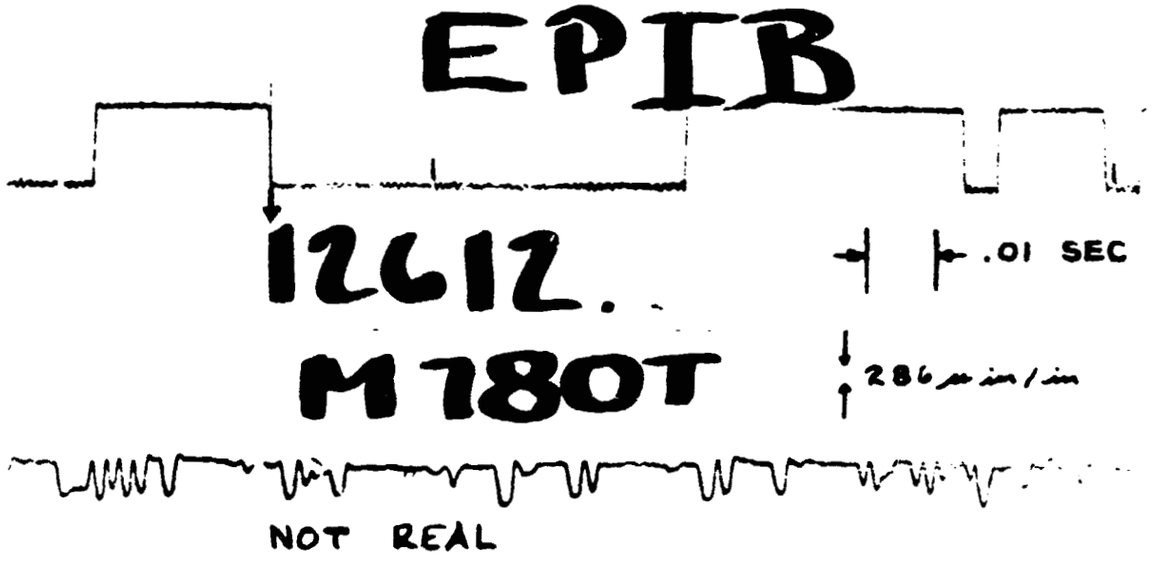

Figure 4.3-13 Hi Speed Playback (40"/sec) of Unreal Signal on Tie Rod Strain Gage.

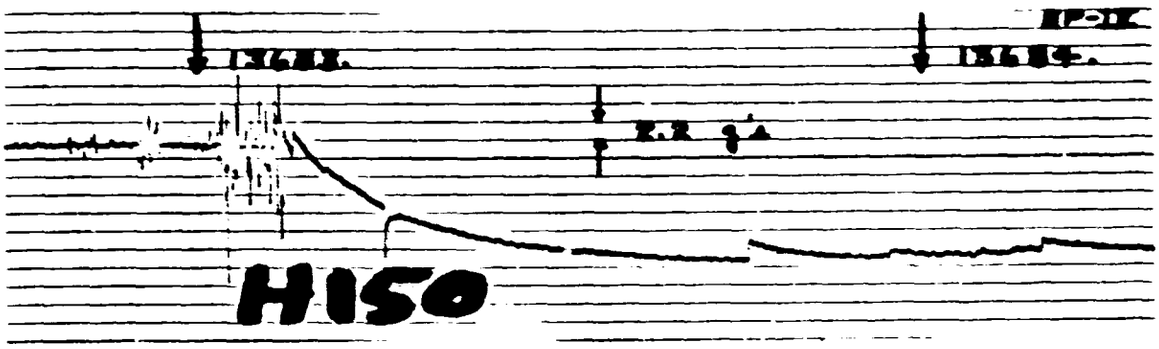

Figure 4.3-14 Nozzle Flange Accelerometer Drift, Seconds Prior to Initial Power Increase.

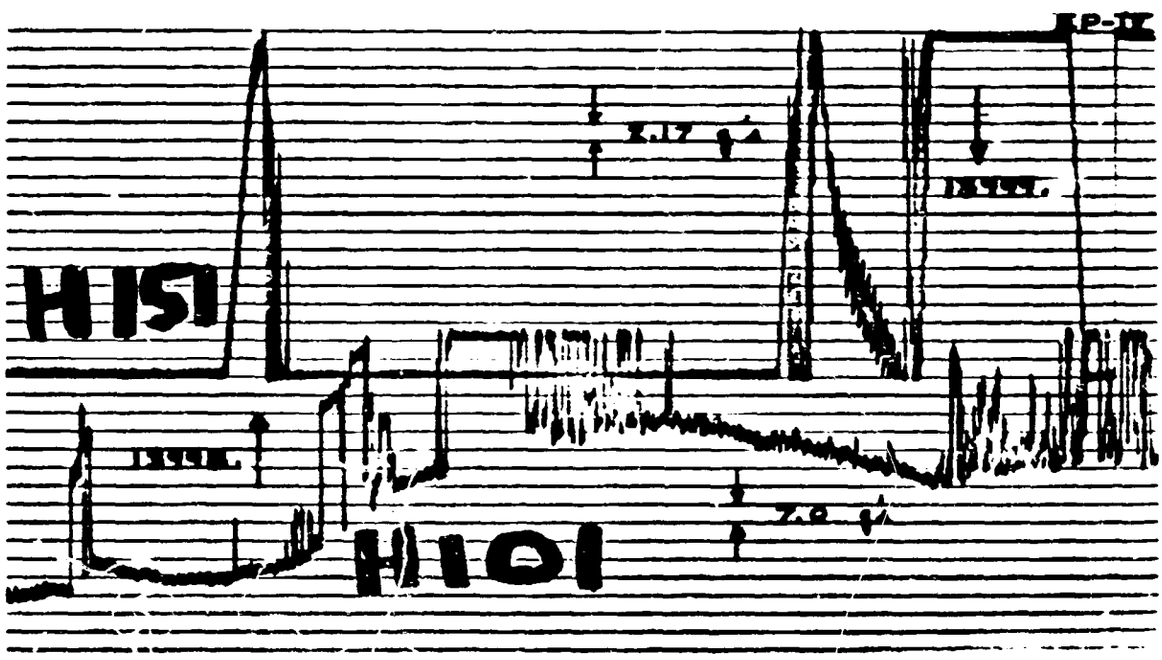

Figure 4.3-15 Nozzle Flange (H151) and Feedline (H101) Accelerometers Displaying Unreal Signals at 3rd Power Hold.

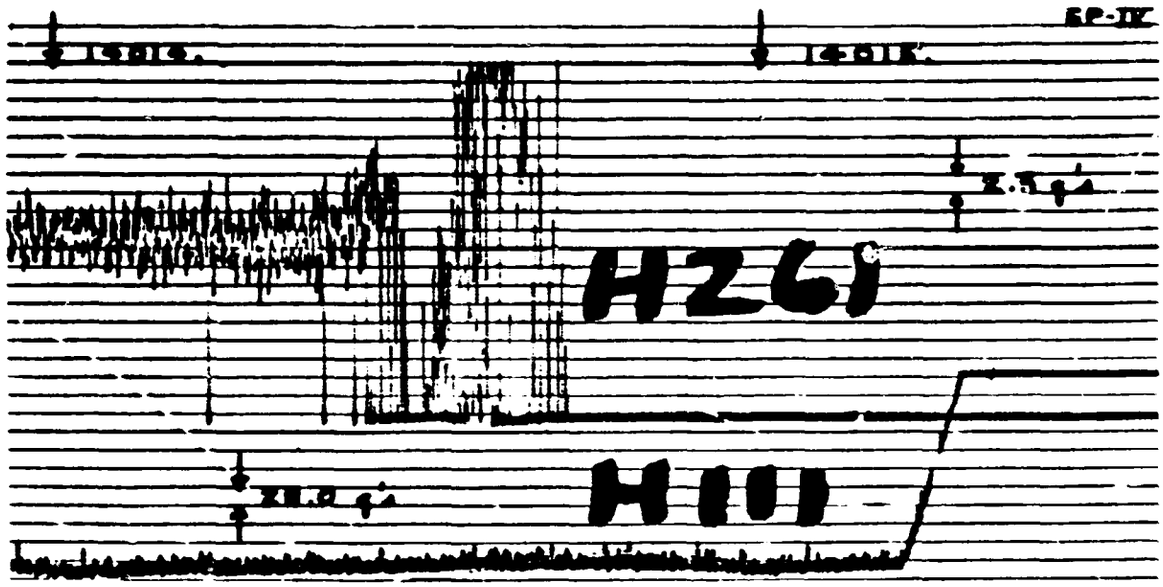

Figure 4.3-16 Forward Flange (H261) and Nozzle (H111) Accelerometer Signals at 3rd Power Hold.

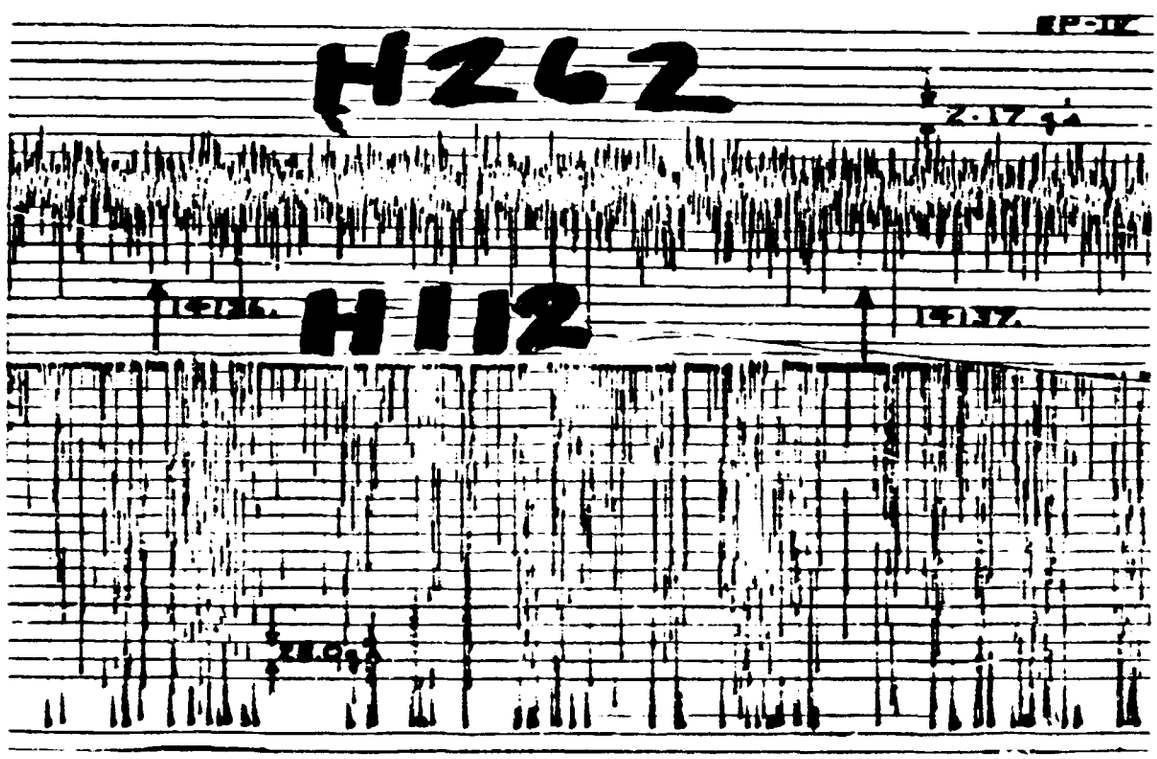

Figure 4.3-17 Forward Flange (H262) and Nozzle (H112) Accelerometer Signals at Cooldown.

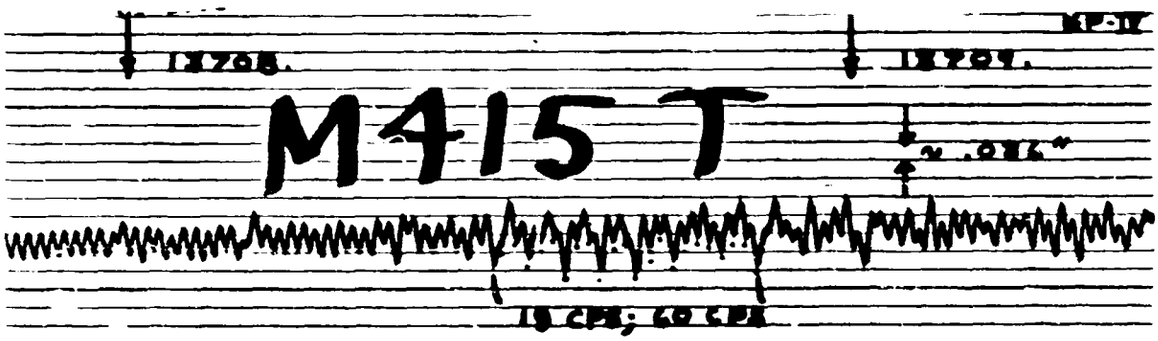

Figure 4.3-18 Inner Reflector Spring Strain Gage Output During Initial Power Ramp.

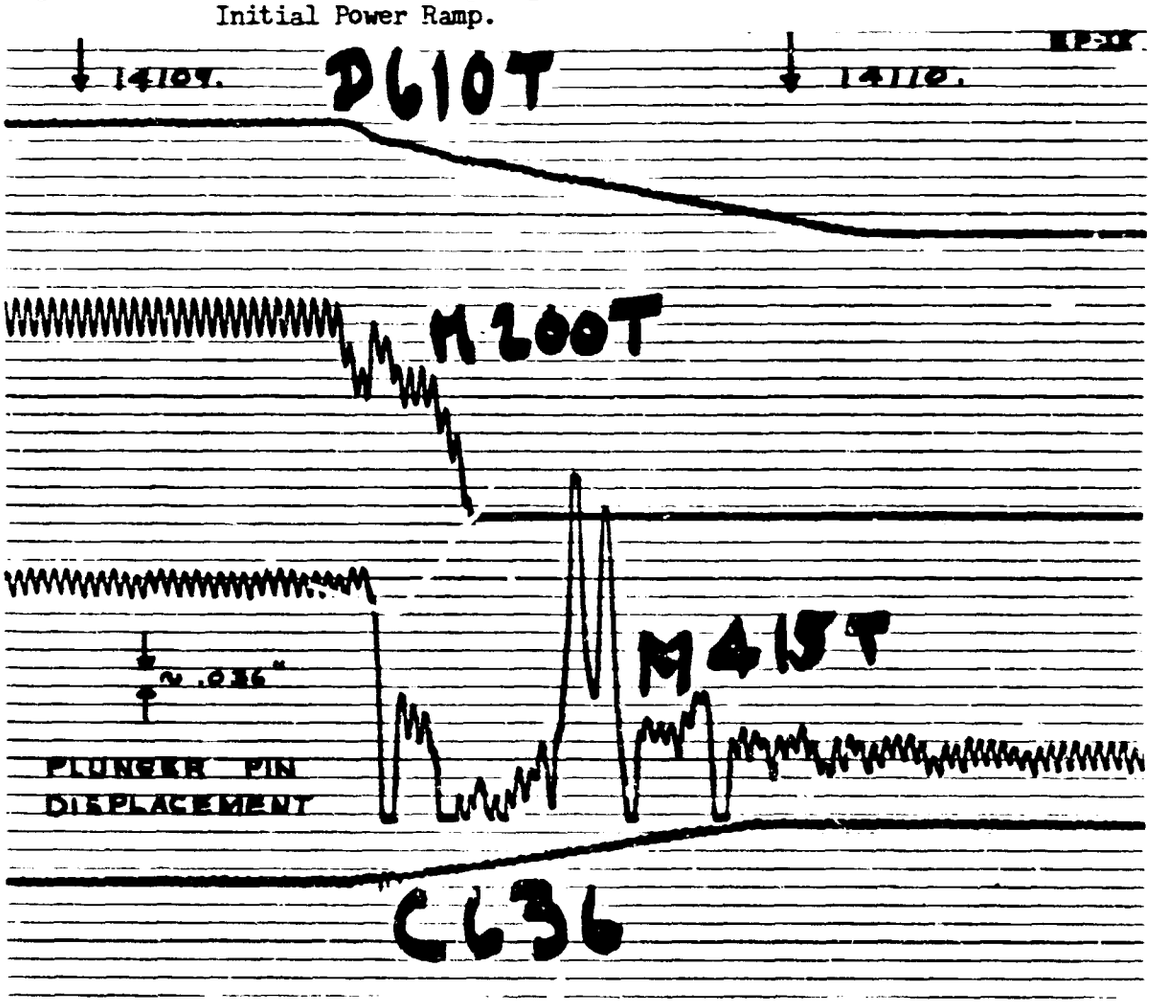

Figure 4.3-19 Various Channel Outputs at Full Power Scram.

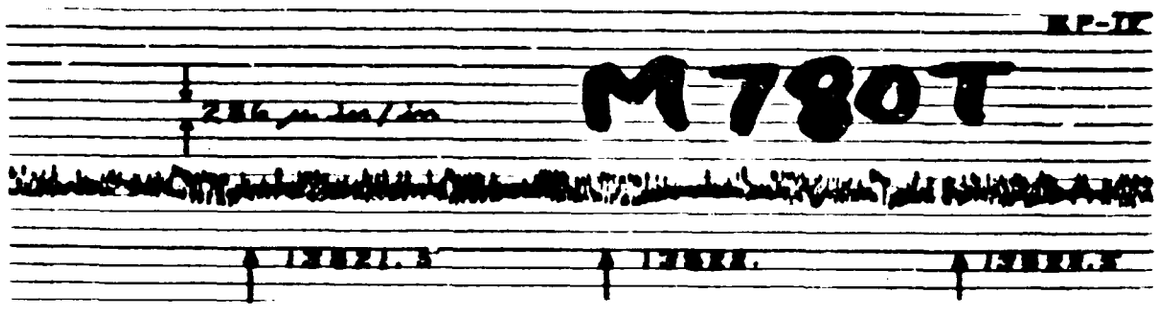

Figure 4.3-20 Tie Rod Strain Signal Observed at Start of 2nd Power Hold.

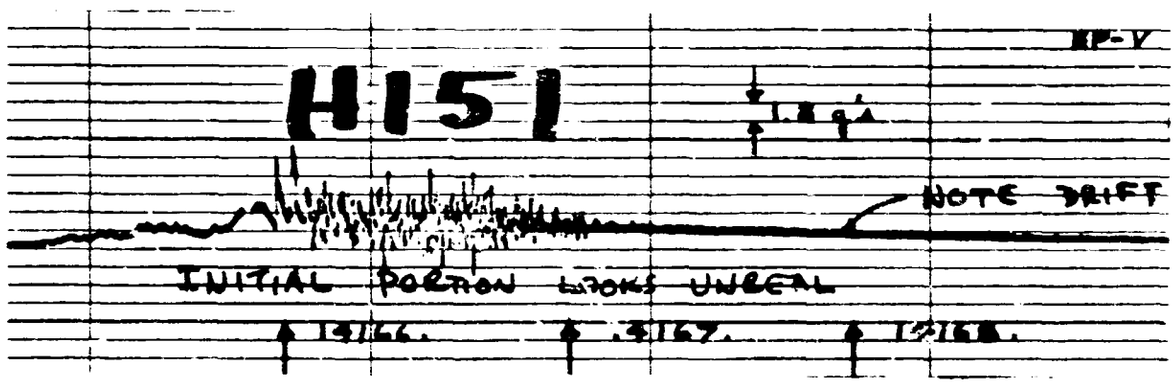

Figure 4.3-21 Nozzle Flange Accelerometer Signal Observed During Low Power Mapping of Restart Test.

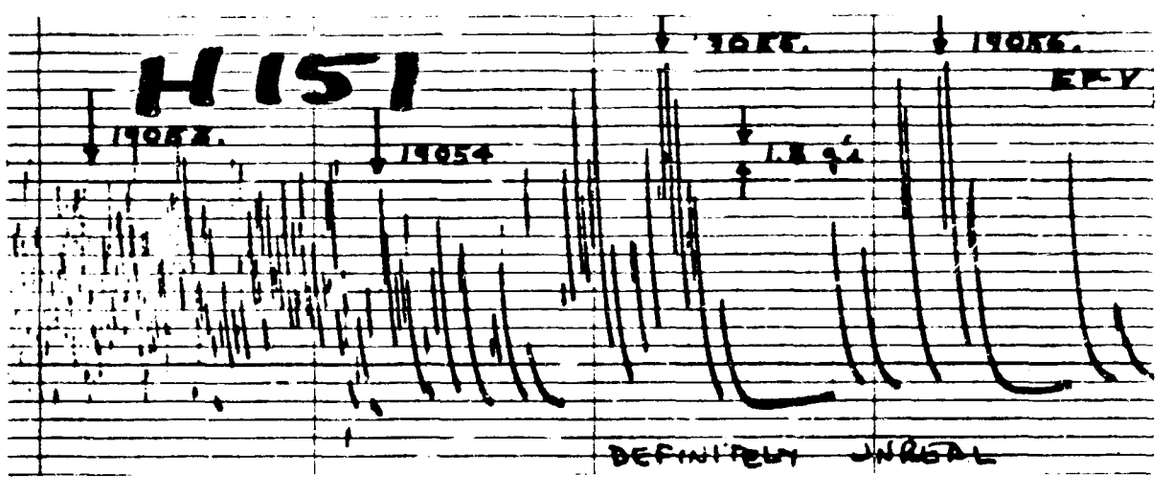

Figure 4.3-22 Nozzle Flange Accelerometer Signal Observed During Low Power Mapping of Restart Test.

Astronuclear

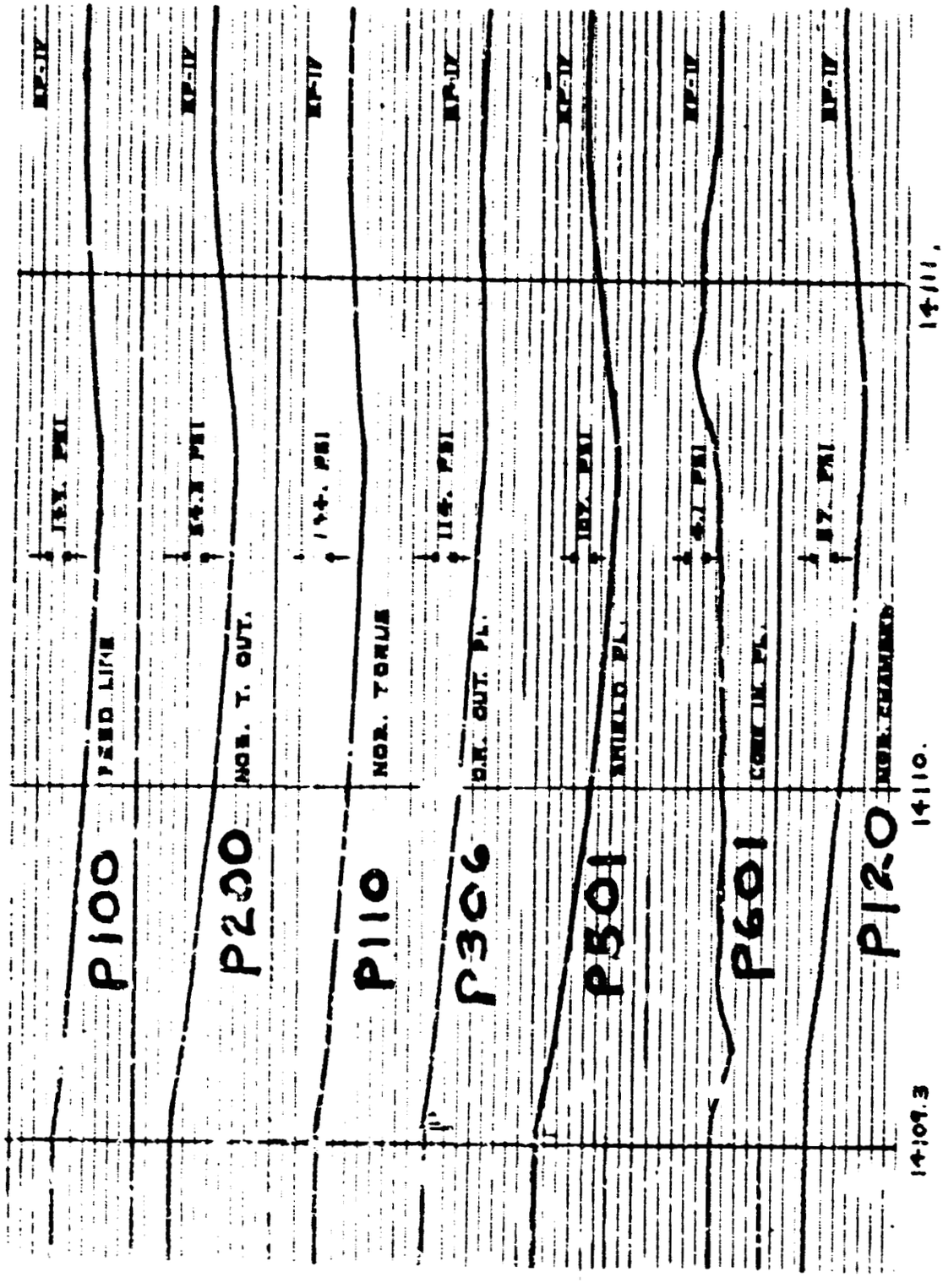

Figure 4.3-23 Various Pressure Profiles at Full Power Scram.

It can be seen from these tables that the channels monitoring core vibration showed essentially no dynamic signals. The problem encountered is one of assuring that the transducer and data channel were operative, hence, there were no dynamic signals recorded because no vibrations were occurring. This assurance was achieved, in general, by the reasonable results from the quasi-static data analyses of these channels reported in sections A and B, and in particular, by observing what happened in a given channel when a known event such as a pressure transient occurred. The pressure transient at time 14109.3 seconds in the shutdown of EP-IV, Figure 4.3-23, is a good example of such a known event. It can be seen from Table 4.3-7 that the tie rod strain gages showed this pulse since they were responsive to changes in the core pressure drop loading.

Another general problem arose in the evaluation of dynamic data. Some of the transducers produced dynamic signals in which it was difficult to differentiate between real and erroneous data. When such signals were judged to be unreal or suspicious, it was generally for the following reasons:

a) Physically impossible vibrations or stress amplitudes - For example, an accelerometer recorded pressure vessel flange vibrations whose amplitude would have been ± 100 inches. An example of D.C. drift implying steady unidirectional velocity over a long period is shown in Figure 4.3-14.

b) Improbable details in the trace - the signals shown in Figure 4.3-15, for example, imply a large amplitude vibration that stops in one cycle. For most mechanical systems (systems with inertia) such motions are highly unlikely. Also, unexplained signals which nearly duplicate those from known defective channels were regarded as suspicious.

c) Cross correlation between transducers - For example, Figure 4.3-20 shows a tie rod strain signal which was considered unreal since the strain gage mounted across the tie rod diameter (0.11 inches) did not produce the same type of signals concurrently.

The overall conclusion from these data is that there is no reliable evidence of large vibrations of the reactor and/or the instrumented components.

4.3.3 Analysis of Component Damage

This section presents a discussion of the component damage that occurred in the NRX-A2 power test. The emphasis is primarily on mechanical damage as opposed to material damage due to corrosion. In general, the NRX-A2 reactor performed extremely well structurally, and survived the power test without serious component damage. Non-corrosive damage was confined to the following: bending of the tabs at the forward end of the aluminum barrel; removal problems with a few of the tie rod holders and cluster nuts during disassembly; two broken, unfueled, 13-hole central elements, pushed out end plugs in most of the station 45 thermocouple elements; and buckling of tie rod coolant gas thermocouples due to differential expansion of the stainless steel central element liners during the EP-V test run.

A. Aluminum Barrel Tab Bending

At disassembly of the NRX-A2 reactor, it was observed that the tabs at the inlet end of the aluminum barrel were bent and had apparently interferred axially with the core support ring (Figure 4.3-24). A schematic of the core support structure is shown in Figure 4.3-25.

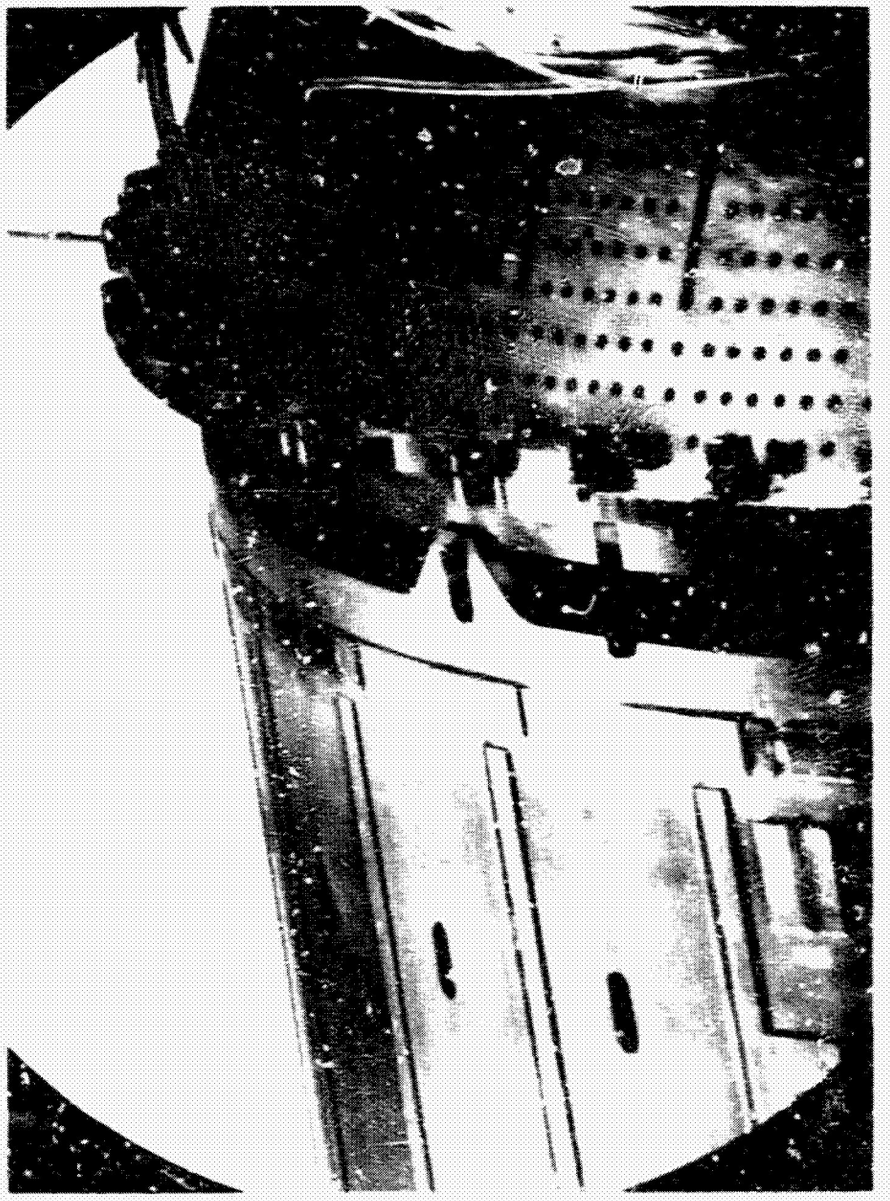

Figure 4.3-24 NRX-A2 Barrel and Support Cone Showing Bent Tabs at Forward End of Barrel.

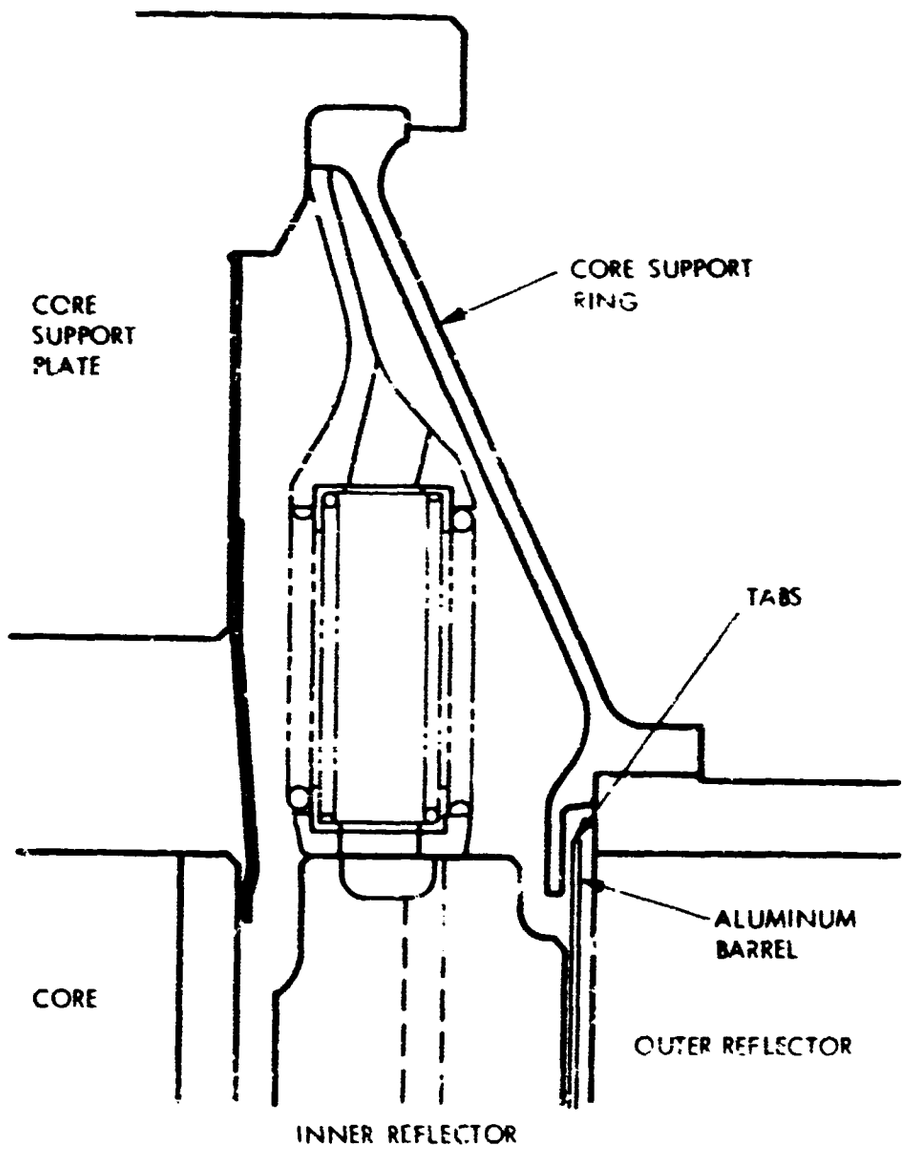

Figure 4.3-[illegible] Schematic of Core Support Structure.

If the aluminum barrel, in the pre-operational condition, was initially displaced forward against the support ring, a possibility of support ring interference exists. This displacement is quite likely because the reactor was inverted for the test. The pre-operation ambient gas flow in the inner/outer reflector annulus would have also tended to assist gravity in moving the barrel axially toward the support ring. At the beginning of any test run, when cryogenic flow is initiated, the aluminum barrel contracts radi y onto the inner reflector. This shrinkage results in a situation where considerable axial force would be required to move the barrel axially relative to the inner reflector. For example, during EP-V, it was estimated that the inner reflector cylinder was displaced toward the forward end approximately 0.25 inches due primarily to pressure vessel axial contraction as it reached about 150°R. (This was considerably more movement that could have occurred in the NRX-A1 cold flow test since the lowest pressure vessel temperature was about 350°R. The aluminum barrel tabs were not bent in NRX-A1.) Such an axial contraction of the pressure vessel in the NRX-A2 reactor would be sufficient to force the barrel tabs against the support ring, assuming the barrel was displaced axially in the direct n as the power test began. The tabs would buckle before sufficient axial force dev oped to slip the barrel relative to the inner r

This condition i [illegible] ore, will not adversely affect the NRX-A3 pow

B. Tie Rod Holder - Cluster Nut Disassembly

Some difficulty was encountered during the remote disassembly of the tie rod holders and cluster nuts. Figures 4.3-26 and 4.3-27 show an exploded view and typical cross-sections respectively of the cluster retention hardware. It is believed that the difficulty was not a result of the reactor environment and power run. The few problems encountered (about 12 out of 289 cluster nuts) may have been due to human factors, since this remote disassembly operation is rather difficult.

In all but one of these 12 cases, it is believed that cluster nut binding in the core support plate may have occurred when torque was applied to the nut. This torque may have been partially transmitted to the locking cup through frictional contact with the socket wrench and/or through the crimps, causing it to turn. If this torque, transmitted to the cup, was sufficiently high as the wrench turned, and if the leg on the locking cup wedged between the cluster nut and support plate, a jammed condition could result. It was not possible, however, to duplicate cluster nut binding with laboratory tests conducted at WANL.

Thread galling (or seizing) apparently occurred in at least one location. This condition resulted in a broken tie rod holder. (A tie rod holder was also broken in the NRX-A1 reactor). Tests conducted by WANL verified that such a failure could only be

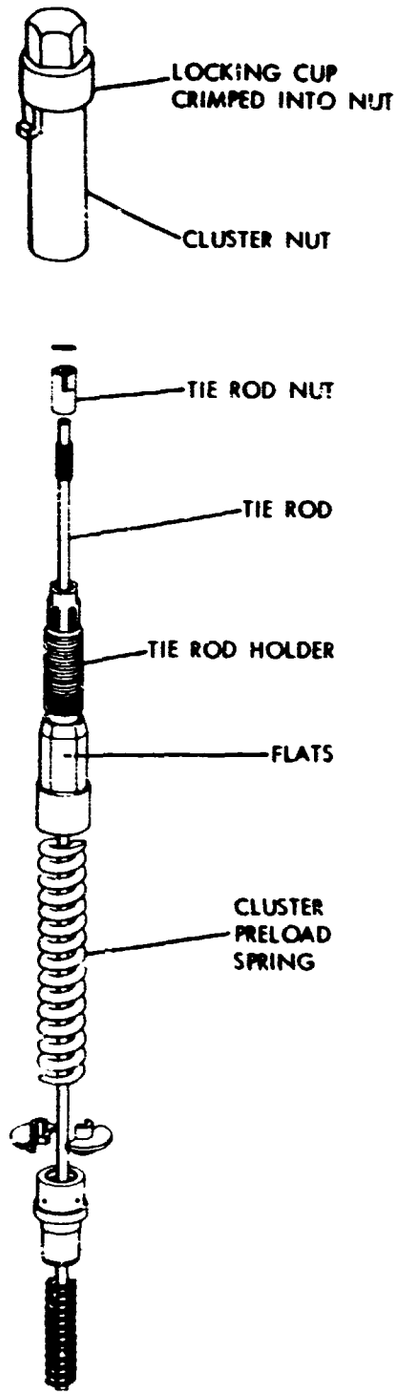

Figure 4.3-26 Exploded View of Cluster Retention Hardware, NRX-A2.

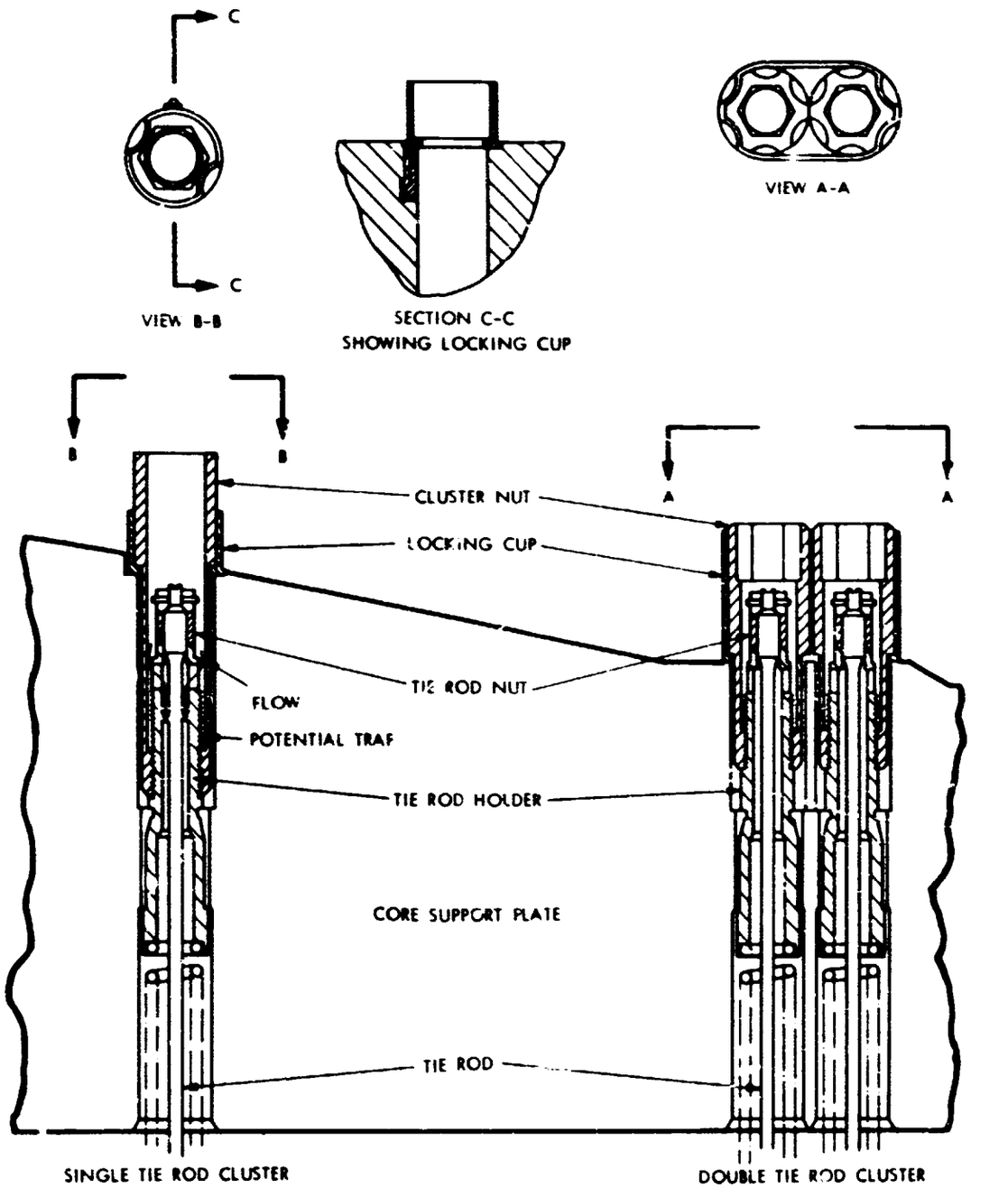

Figure 4.3-27 Typical Cross Sections of Cluster Retention Hardware, NRX-A2.

produced by torsion of the holders, and sufficient torque to cause such a failure in NRX-A2 could only be produced by galled (or seized) threads transmitting wrench torque to the tie rod holder. It is believed that some of the factors that may have contributed to galling (or seizing) are:

a) High bearing pressure on the threads due to the preload torque on the cluster nuts and lateral displacement (loading) of the nut due to misalignment with the socket on disassembly.

b) Entrapment of fine particles that may have been in the propellant flow in the space between the cluster nut and tie rod holder.

c) Greater than necessary number of turns was required for disengagement at many locations, thus increasing the potential for lateral loading (displacement).

Another possible disassembly problem could exist if the cluster nut is not permitted to move forward away from the support plate as it is turned for removal. In this event, the tie rod holder would be forced aft and might disengage the support plate at the mating flats. Should this occur, the cluster nut and tie rod holder would then spin together preventing removal of the cluster nut. A dimensional tolerance study indicated that this could not occur nominally and that all the dimensions would have to combine in the extremes for it to occur at all.

The following design changes have been incorporated in the NRX-A3 reactor in order to minimize potential binding and thread seizure at disassembly:

a) The leg on the locking cup is shortened, and the foot was eliminated.

b) The locking strength of the crimps is reduced by shortening the height of the locking cup.

c) The clearance between the locking cup and the cluster nut is increased.

d) The external bearing surfaces of the cluster nut were flash chrome plated.

e) The preload torque on the cluster nut was reduced.

f) The number of turns required for disassembly is reduced by shortening the cluster nuts. This will also eliminate the possible particle "trap" and flat-to-flat disengagement mentioned above.

C. Element Damage*

There were no broken elements that could be attributed to the NRX-A2 reactor test. The only serious element damage discovered, that could not be conclusively indentified with disassembly handling, was transversely broken, unfueled, instrumented central elements, Figures 4.3-28 and 2.3-29. However, it cannot be definitely inferred that these elements broke during the power run since there was almost no corrosion at the breaks. Figure 4.3-30 shows the location in the core of the broken elements. In each case, the breaks occurred at or near the station 32 thermocouple slot.

The potting material was lost in 12 central elements having such instrumentation at station 32. This loss of material permitted flow to cool the element cross section locally at the instrumented hole by about 500°R at full power and flow, Figure 4.3-31. Because the fuel element is not free to bend, there is a tensile stress around the chill hole of approximately 2100 psi. This unfueled element may also be in tension due to the differential axial expansion between the unfueled element and the adjacent fueled elements. Such additional tension as calculated** could easily be 1000 psi based on a 10% variation in the average coefficient of thermal expansion in the axial direction and a 80°R difference between

---

* This section only deals with non-corrosive damage.

** J. W. Swanson, Stress Analysis: NRX-A Unfueled Elements and Miscellaneous Cluster Compounds, WANL-TME-740, July, 1964.

Figure 4.3-28 Tensile Crack in Element 4A1A.

Figure 4.3-29 Tensile Crack in Element 405A.

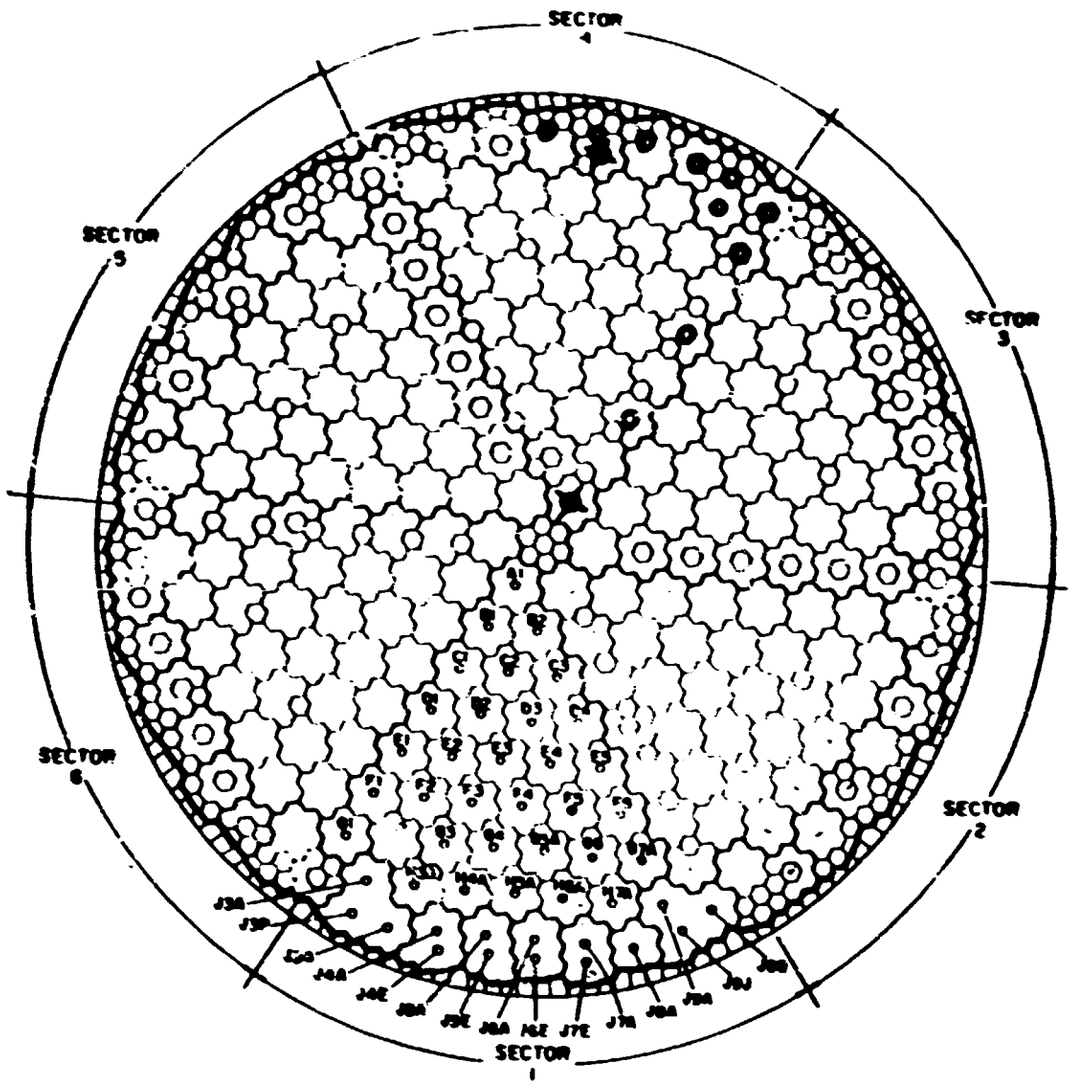

Broken Elements

Unbroken Elements

Figure 4.3-30 Location of Station 32 Thermocouples.

CONFIDENTIAL
RESTRICTED DATA
Atomic Energy Act - 1954

3578	3578	3576														
	3582	3580	3578	3574												
	3585	3584	3582	3579	3575	3572										
	3588	3586	3584	3582	3579	3576	3574									
3590	3588	3586	3585	3583			3573	3572	3572							
3589	3585	3582	3582					3564	3564	3567	3571					
3584	3579	3575						3548	3551	3555	3562	3568	3572			
3577	3570	3563	3555					3524	3532	3540	3550	3560	3568	3572		
3568	3559	3548	3535					3501	3511	3520	3534	3552		3572	3573	3573
3557	3546	3533	3518	3502	3485	3475	3475	3480	3485	3494						3573
3545	3532	3517	3501	3486	3472	3462	3457	3455	3455	3458						3570
			3482	3466	3452	3441	3432	3426	3421	3415						3560
				3442	3427	3414	3403	3394	3386	3375	3357				3513	3545
					3397	3382	3370	3359	3349	3339	3329	3328	3357	3418	3479	3530
						3346	3333	3321	3309	3300	3295	3304	3334	3386	3450	3517
							3292	3280	3266	3253	3246	3253	3284	3340	3417	3502
							3249	3238	3221	3200	3180	3175	3203	3273	3372	3482
							3209	3200	3178	3144	3100				3316	3458
							3178	3172	3146	3096						3437
								3162	3134	3077						3428

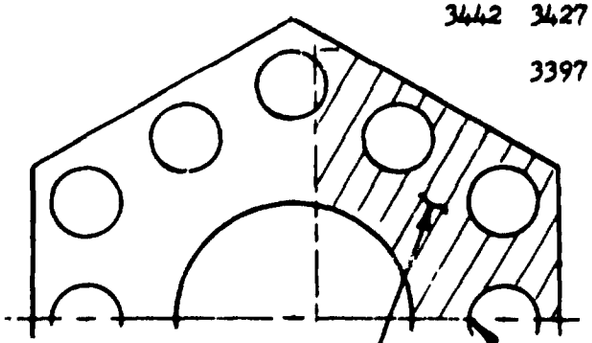

Cooled Hole

3041°R
Minimum Wall
Temperature

Figure 4.3-31 Temperature Distribution in Cooled Unfueled Element.

CONFIDENTIAL
RESTRICTED DATA
Atomic Energy Act - 1954

STORNUCLEAR

the average temperature of the unfueled and surrounding fueled elements. It would, therefore, be reasonable to expect a peak tensile stress of about 3100 psi near the instrumented hole. Tests conducted at WANL indicated a reduction of over 20 percent in the tensile and flexural strengths of these unfueled, slotted, instrumented central elements. Considering these factors, it is not surprising that 2 out of 12 such elements might fail.

The potting was also lost in the station 45 thermocouples, nearer the core exit. Severe local chilling did not occur in this case since these thermocouple probes were larger and impeded the flow of coolant. However, the aft end shim hole plugs in most of these station 45 central element thermocouple installations were pushed out about 0.015 to 0.030 inches as shown schematically in Figure 4.3-32. This probably occurred due to the differential thermal expansion between the tantalum/molybdenum thermocouple probe and the unfueled graphite central element. The thermal expansion of the thermocouple is more than twice as great as the graphite element. Rough calculations show that this expansion would be sufficient to overcome the clearance between the thermocouple tip and rod even if all the potting were lost. Inspection of radiographs of central elements with station 45 thermocouples revealed severe hydriding and binding between the tantalum sheath and graphite element. Apparently this resulting

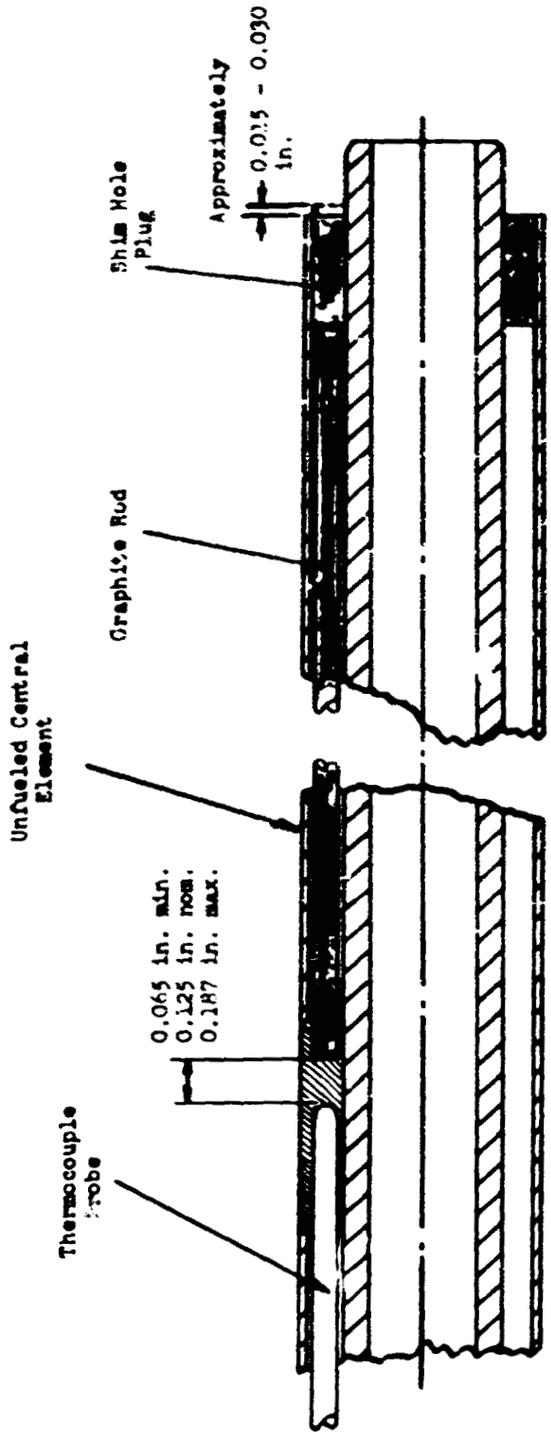

Schematic of Station 45 Thermocouple, NRX-A2.

radial binding was more pronounced near the forward end and forced the axial differential expansion to take place toward the aft end.

The following design modifications have been adopted in NRX-A3:

a) The slotted instrumented central elements are replaced by unslotted elements in as many places as possible.

b) In the remaining places, the slotted elements are rotated in the core, and the instrumentation is located in an unslotted hole such that the position of the instrumentation remained unchanged in the core. The unused slotted holes are then filled with close fitting graphite shim rods, and the slots were potted flush with the element face.

c) All station 45 thermocouples are omitted.

These changes will insure sufficient flow impedance to prevent localized cooling of the central element and corrosion of adjacent elements. Elimination of station 45 thermocouples solves the end plug problem directly.

D. Thermocouple Buckle Due to Liner Expansion

The four thermocouples, measuring tie rod coolant gas exit temperature in the NRX-A2 core, were compressed between the stainless steel liner and the molybdenum cone-tie rod button interface (Figure 4.3-33). The thermocouple sheaths were brazed to the liner

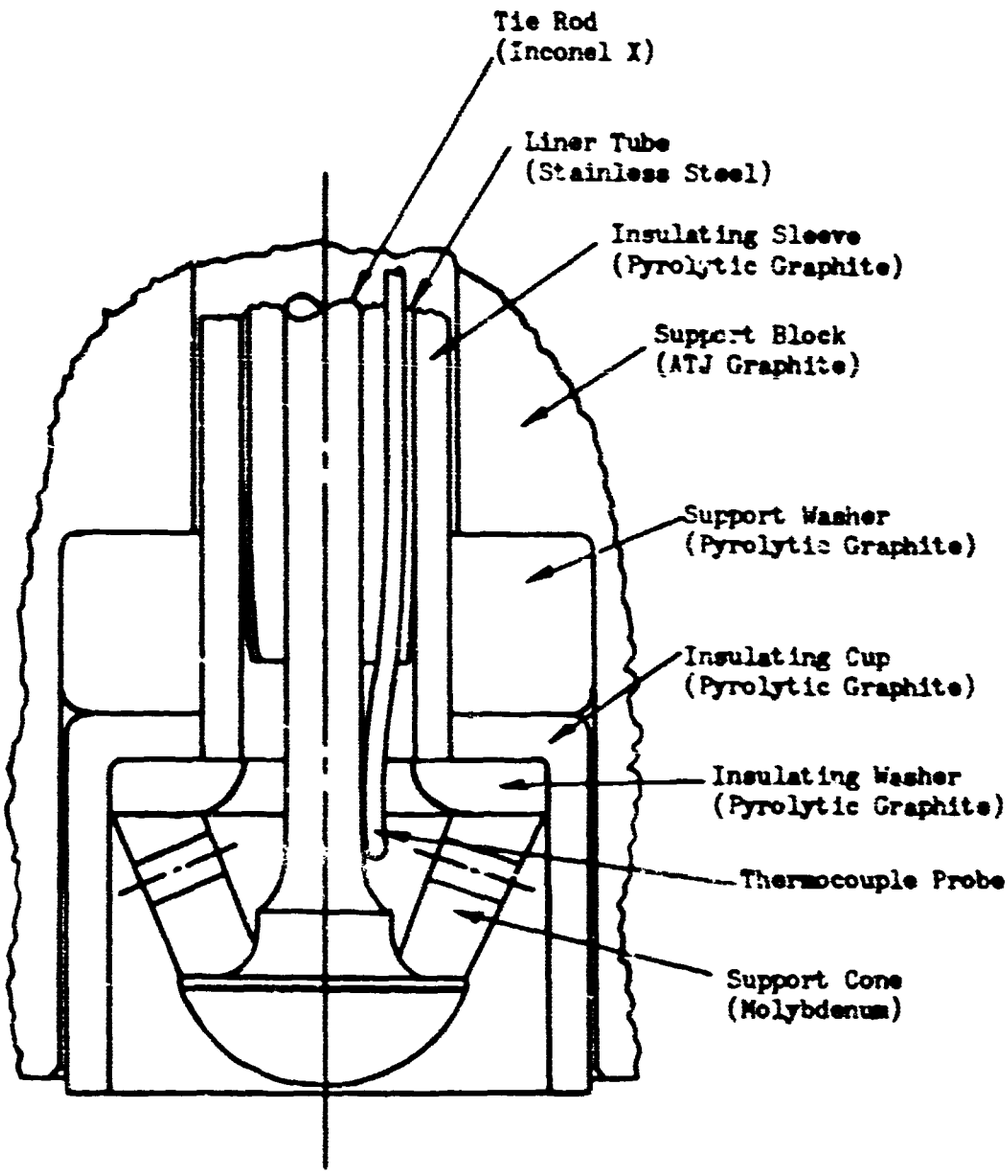

Figure 4.3-33 Sketch of Typical Tie Rod Exit Gas Thermocouple Installation, NRX-A2.

which underwent differential thermal expansion relative to the insulating pyro-sleeves. This differential liner expansion, during a portion of NRX-A2 EP-V, was estimated to be roughly 0.24 in. based on as assumed reasonable temperature distribution in the liner and sleeves. Since the nominal clearance between the tip of the thermocouple and the cone-tie rod button interface was 0.13 in., interference did occur. Figure 4.3-34 shows a typical liner and buckled thermocouple after disassembly. Since these thermocouple tips were in contact with the molybdenum cone and tie rod button interface during at least part of the test, the readings from these channels (T-750, T-755, T-760, T-765) may have been indicating material surface temperatures which are higher than the fluid temperatures.

In NRX-A3 an adapter is used so that under the worst tolerance and eccentricity conditions, the liner expansion could be limited, if necessary, by the insulating washer. Hence, any over expansion of the liner would be taken at the forward end. The thermocouple extension past the liner is also reduced to prevent buckling in NRX-A3.

Figure 4.3-34 Typical Buckled Tie Rod Exit Gas Thermocouple Probe, NRX-A2.

4.4 NUCLEAR ANALYSIS

4.4.1 General

The nuclear characteristics of the NRX-A2 are governed by the configuration of materials with significant nuclear properties, reactor power, and hydrogen flow rate. The materials and their distributions in the NRX-A2 core are shown in Figure 4.4-1. This figure illustrates the reactor core consisting of clusters of six fuel elements surrounding an unfueled fuel module and irregular clusters consisting of up to three unfueled modules and 13 fuel elements. The core contains an enriched uranium inventory of 173.6 kg. The core is surrounded by filler strips, a lateral support system, and a beryllium outer reflector. The beryllium outer reflector contains 12 control drums each of which employ a control vane consisting of boron enriched in the B^{10} isotope dispersed in an aluminum matrix. Table 4.4-1 summarizes the key nuclear component characteristics including all fuel elements, reflector components and control drums.

This section will include the following:

1) The inital criticality and control drum calibration;
2) The reactivity effects and power distribution;
3) The radiation heating and radiation environment.

4.4.2 Criticality and Control Drum Calibrations

The NRX-A2 as shipped from Large, Pennsylvania, to NRDS and installed on the test car contained 6990 poison wires. These poison wires were installed in coolant channels throughout the

CONFIDENTIAL
RESTRICTED DATA
Atomic Energy Act - 1954

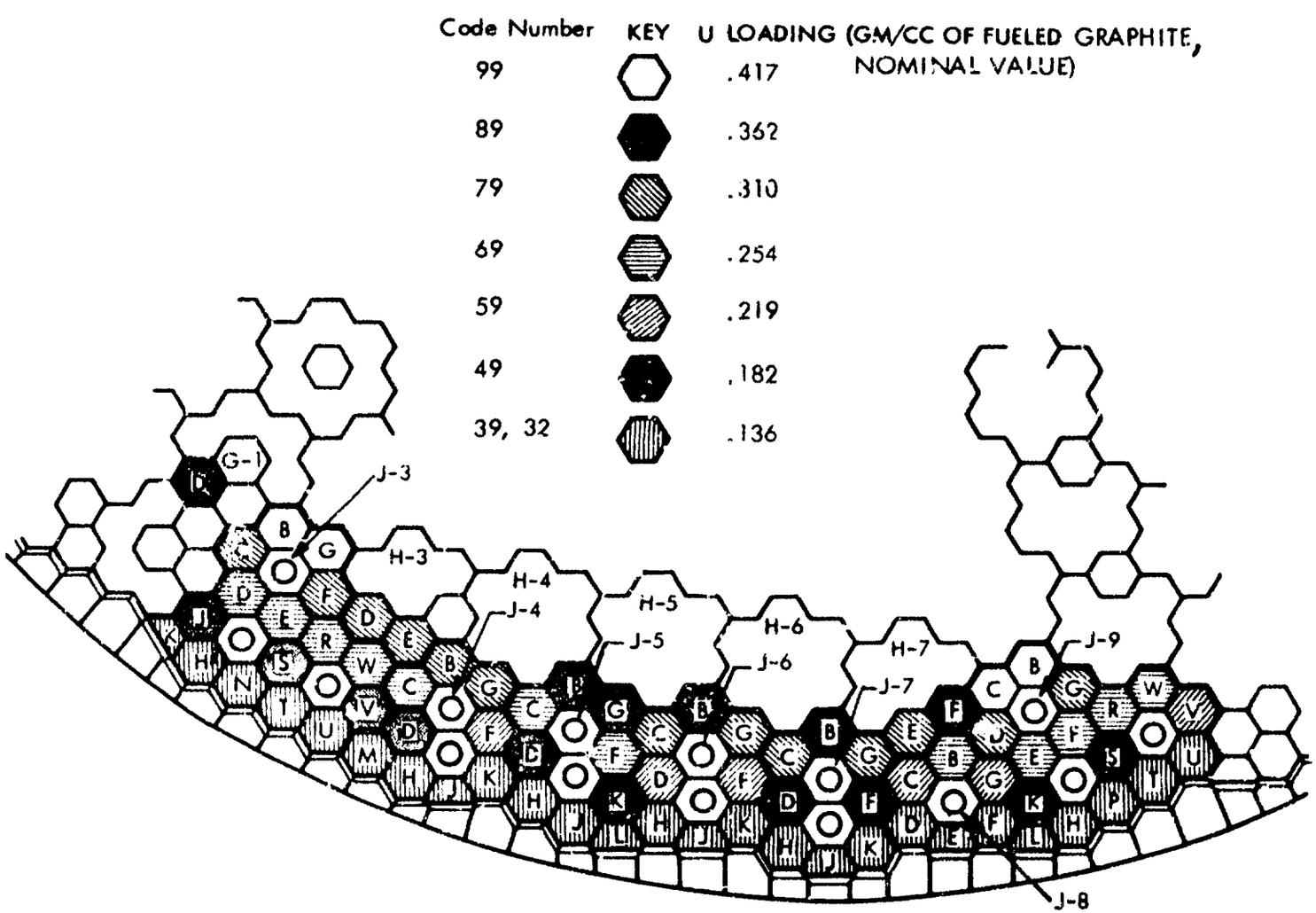

FIGURE 4.4-1 NRX-A2 FUEL LOADING DISTRIBUTION

CONFIDENTIAL
RESTRICTED DATA
Atomic Energy Act - 1954

CONFIDENTIAL
RESTRICTED DATA
Atomic Energy Act of 1954

TABLE 4.4-1

NRX-A2 REACTOR CHARACTERISTICS

COMPONENT MASSES

CORE	
1626 Fuel Elements	1095.0 kilograms
Uranium	173.6
Graphite	855.5
Niobium	66.0
289 Unfueled Elements	
Graphite	198.8
Tantalum	8.6
Inconel - X	19.0
Stainless Steel	8.2
Niobium	0.3
LATERAL SUPPORT (Graphite Reflector)	
Graphite	393.3
Steel	12.1
Aluminum	25.9
Silica	8.0
BERYLLIUM REFLECTOR	
Beryllium	713.
Aluminum	1.[illegible]
Titanium	27.1
CONTROL DRUMS	
Beryllium	208.3
Aluminum	19.8
Boron - Aluminum (vanes)	5.1

COMPONENT DIMENSIONS

CORE		
Average Radius	43.8 centimeters	17.25 inches
Fuel Height	132.1	52.0
Core Height	137.8	54.25
LATERAL SUPPORT (Graphite Reflector)		
Average Inner Radius	43.8	17.25
Average Outer Radius	51.0	20.07
Height	137.8	54.25
BERYLLIUM REFLECTOR		
Inner Radius	51.0	20.07
Outer Radius	62.70	24.68
Height	137.8	54.25
CONTROL DRUMS		
Diameter	10.4	4.1
Total Plate Length	131.8	51.9
Angular Span	120 degrees	
Plate Thickness	0.13	0.050

CONFIDENTIAL
RESTRICTED DATA
Atomic Energy Act of 1954

Astronuclear

reactor and were grouped through the use of cluster cups. Initial criticality was obtained by a step-wise withdrawal of these wires, during which time, inverse multiplication measurements were performed. The nozzle was not installed during these measurements. Initial criticality was obtained with 8 clusters or 336 wires remaining in the core. The critical bank position was 172.9 degrees. These 336 wires were removed step-wise during which time the control drum bank reactivity worth was calibrated. The result of this operation is shown in Figure 4.4-2. This figure illustrates the fact that a movement of 12 drums 6° will introduce 50 cents in reactivity and a movement of 13° will introduce $1 in reactivity. The critical drum angle was 98.6° in configuration with all wires out.

In order to verify the uniformity of the control drum, each drum was bumped from an approximately uniform critical position and a period obtained. Results of this measurement are shown in Figure 4.4-3. This figure illustrates that the measurement indicated an apparent non-uniformity in control drum worth. Analysis of the test indicated the cause of the asymmetry was the variation in the position of the control drum bank position as shown in Figure 4.4-4. The best value of critical drum position with nozzle installed was 97.0 ± 0.5° based on observations during several critical conditions.

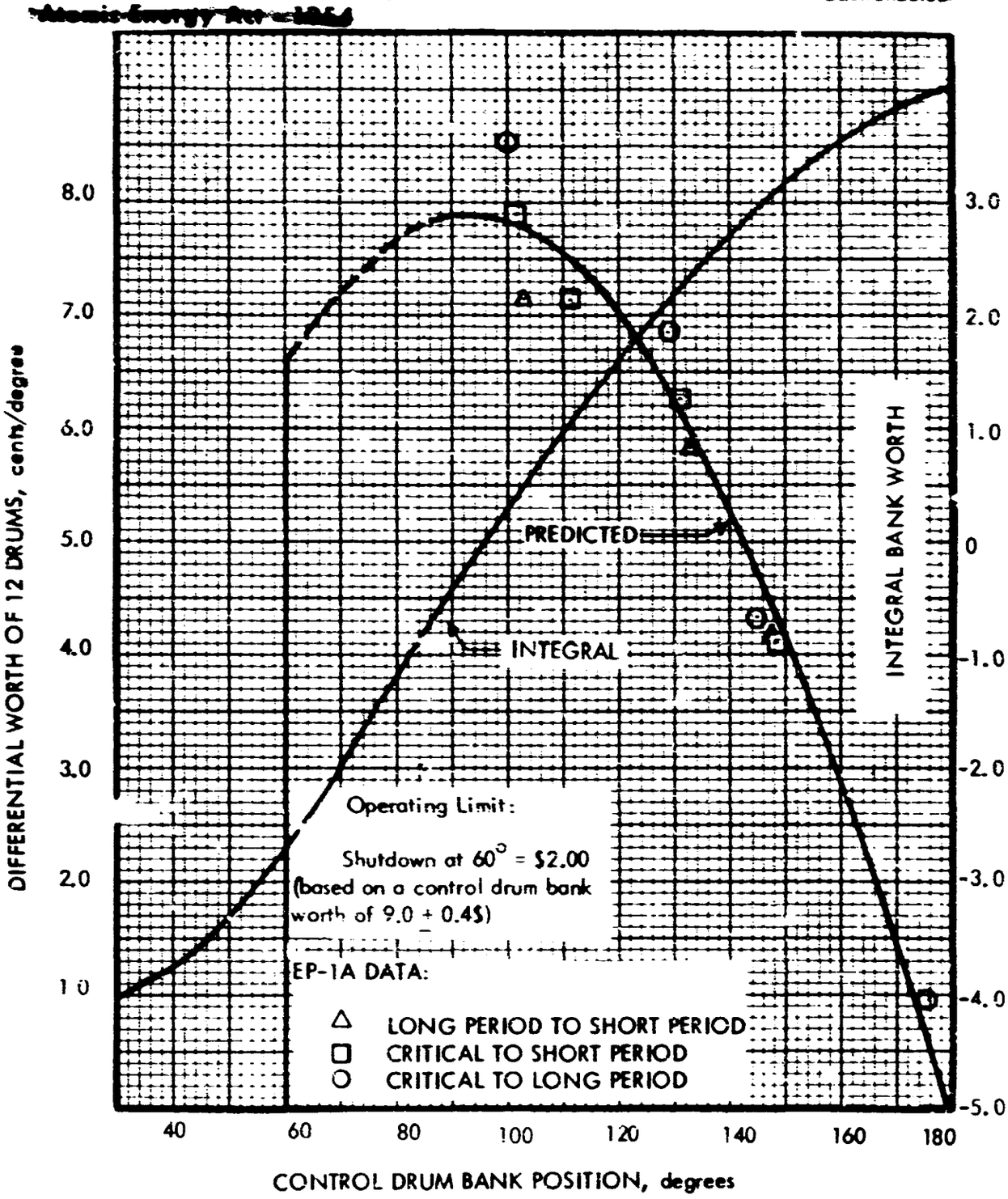

FIGURE 4.4-2 NRX-A2 EP-IA INTEGRAL AND DIFFERENTIAL BANK WORTH

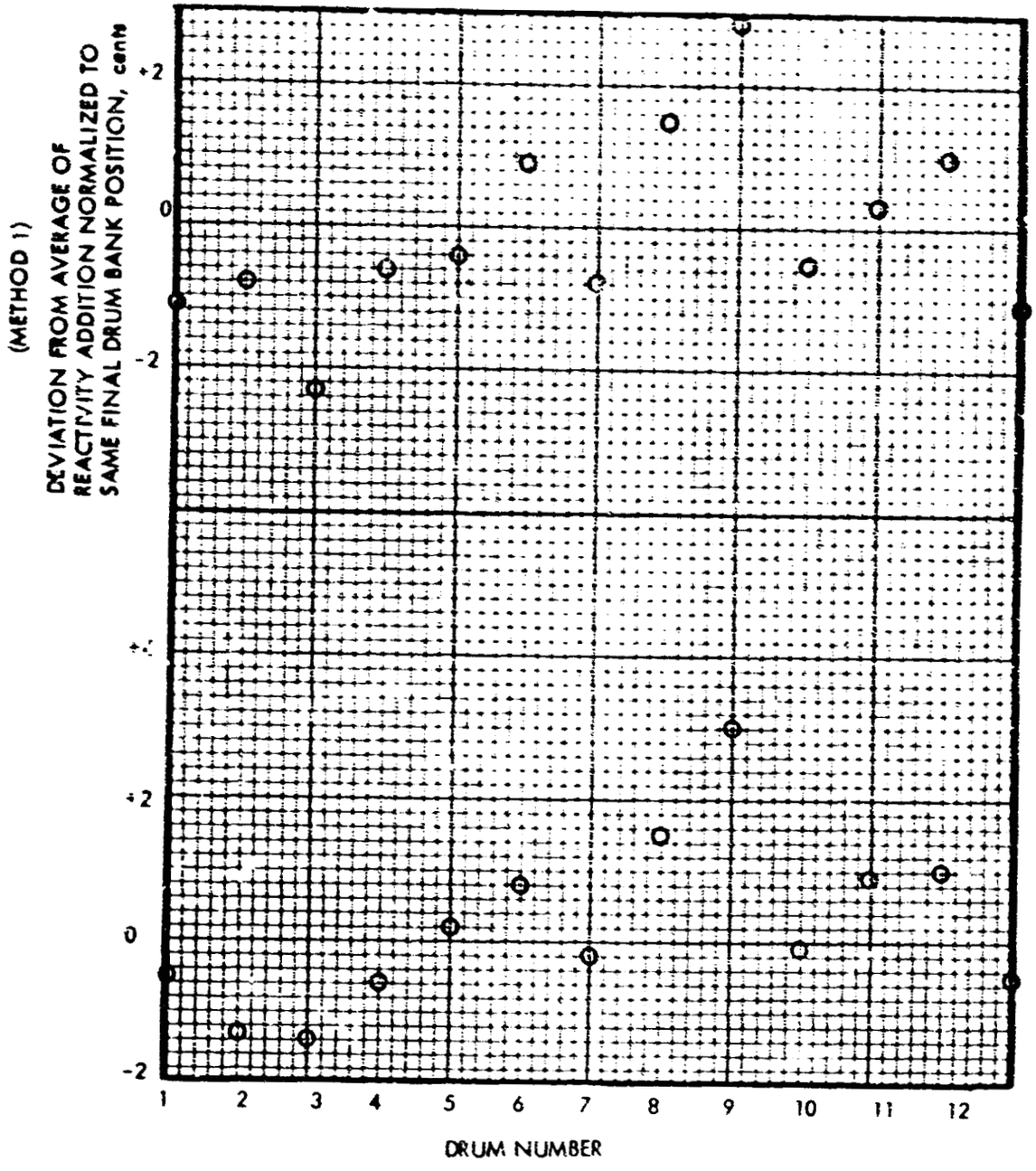

FIGURE 4.4-3 - NRX-A2 EP-IA CONTROL DRUM WORTH REACTIVITY

4.4.3 Reactivity Effects

The NERVA reactor must operate over an extremely wide range of temperatures and propellant density variations. This reactor is sensitive to temperature and hydrogen density within the reactor because it is highly under-moderated and has high leakage. It was therefore, of [illegible] in the NRX-A2 testing to evaluate experimentally the various reactivity contributions.

Steady state operation of the NERVA reactor requires that the net reactivity charge be zero. Figure 4.4-4 illustrates the various factors which contribute to the reactivity of the NERVA reactor. The control drum bank is adjusted to make the reactivity zero to achieve steady state conditions. The principle factors are core hydrogen density, lateral support hydrogen density, outer reflector hydrogen density, core temperature, beryllium temperature, carbon loss, and control drum position.

In order to evaluate separately the various contributions to the reactivity, experiments were devised in which essentially only one or at most two of the significant parameters were varied. In the previous discussion we have seen how the control drum reactivity coefficient was evaluated (Figure 4.4-3).

TABLE 4.4-4

NRX-A2 REACTIVITY EQUATIONS

NRX-A2 Reactivity At Steady-State $= R_D + R_C + R_H + R_T = 0$

Control Drum Position	$R_D = -4.5\ (1 + \cos\theta) + 3.87$
Carbon Loss	$R_C = -5.5\ M_{CL}$
Hydrogen Reactivity Contribution	$R_H = (1 + A)\ (W_C + W_{LS}) + W_{Be}$
Core Worth	$W_C = 4.0\ \bar{\rho}_1 + 10.5\ \bar{\rho}_2 + 4.6\ \bar{\rho}_3$
Lateral Support Worth	$W_{LS} = (0.968 - 10^{-4}\ \bar{T}_C)\ \bar{\rho}_{LS}$
Be Reflector Worth	$W_{Be} = 0.040\ \bar{\rho}_{Be}$
Temperature Reactivity Contribution	$R_T = \left[-1.039\ (\bar{T}_C - 528) + 0.943\ (T_{Be} - 528)\right] \times 10^{-3}$

Where R_i = Reactivity, dollars (is is D, C, H or T)

θ = Control Drum Bank Position, degrees

M_{CL} = Mass of carbon lost, kilograms

A = Fraction of diffused Hydrogen (0.12 used)

$\bar{\rho}_1, \bar{\rho}_2, \bar{\rho}_3$ = Average hydrogen densities in the dome end, middle, and nozzle end thirds of the core, lb/ft^3

$\bar{\rho}_{LS}$ = Average hydrogen density in the lateral support, lb/ft^3

$\bar{\rho}_{Be}$ = Average hydrogen density in the beryllium reflector, lb/ft^3

$\bar{T}_C$ = Average core temperature, °R

T_{Be} = Average beryllium reflector temperature, °R

The first experiment performed to evaluate the various reactivity coefficients required passage of ambient hydrogen through the reactor. The principle parameter that varied during this test was the hydrogen density. Figure 4.4-5 shows the variation in measured drum bank position to make the reactivity zero at each of three hold conditions. The result of the application of the formulas given in Figure 4.4-4 to the calculated variation in hydrogen density in the various components is also shown in Figure 4.4-5. This figure indicates that the hydrogen reactivity coefficients are approximately correct.

The next experiment which can be utilized to evaluate one of the important reactivity effects was a temperature coefficient measurement. Figures 4.4-6 and 4.4-7 depict the variation of average core and beryllium reflector temperature and the measured control drum position versus time during the test. Figure 4.4-7 also shows the result of application of the reactivity formula, and indicates that the reactivity coefficient which takes into account core expansion, thermal base shift and Doppler effect as well as temperature effects in the reflectors is approximately correct.

Another important reactivity effect which was not measured at NRDS but which had been previously measured at WANEF was the effect on reactivity of loss in carbon from the reactor.

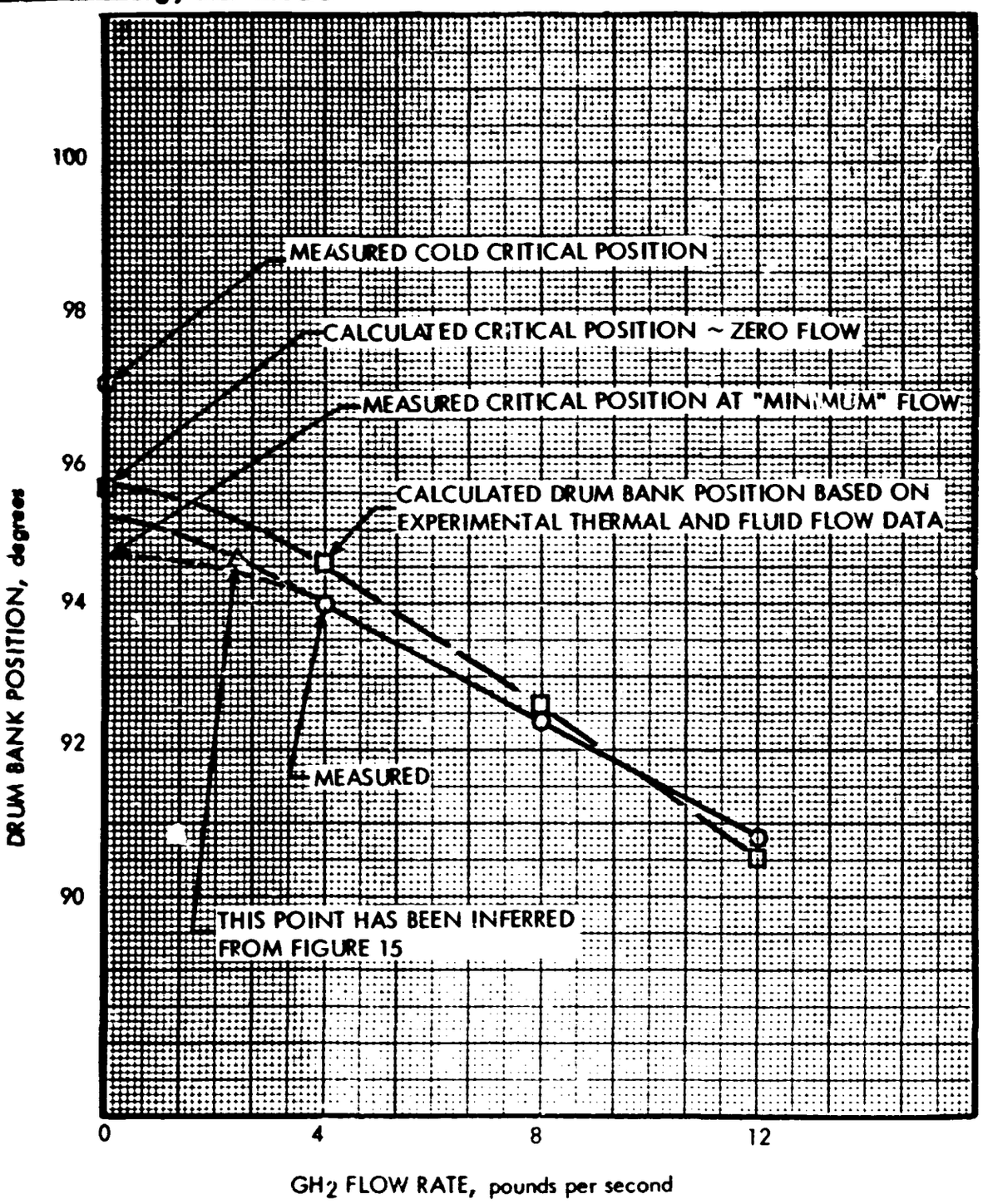

FIGURE 4.4-5 NRX-A2, EF-IB DRUM BANK ROTATION VS. GH_2 MASS FLOW RATE

Astronuclear

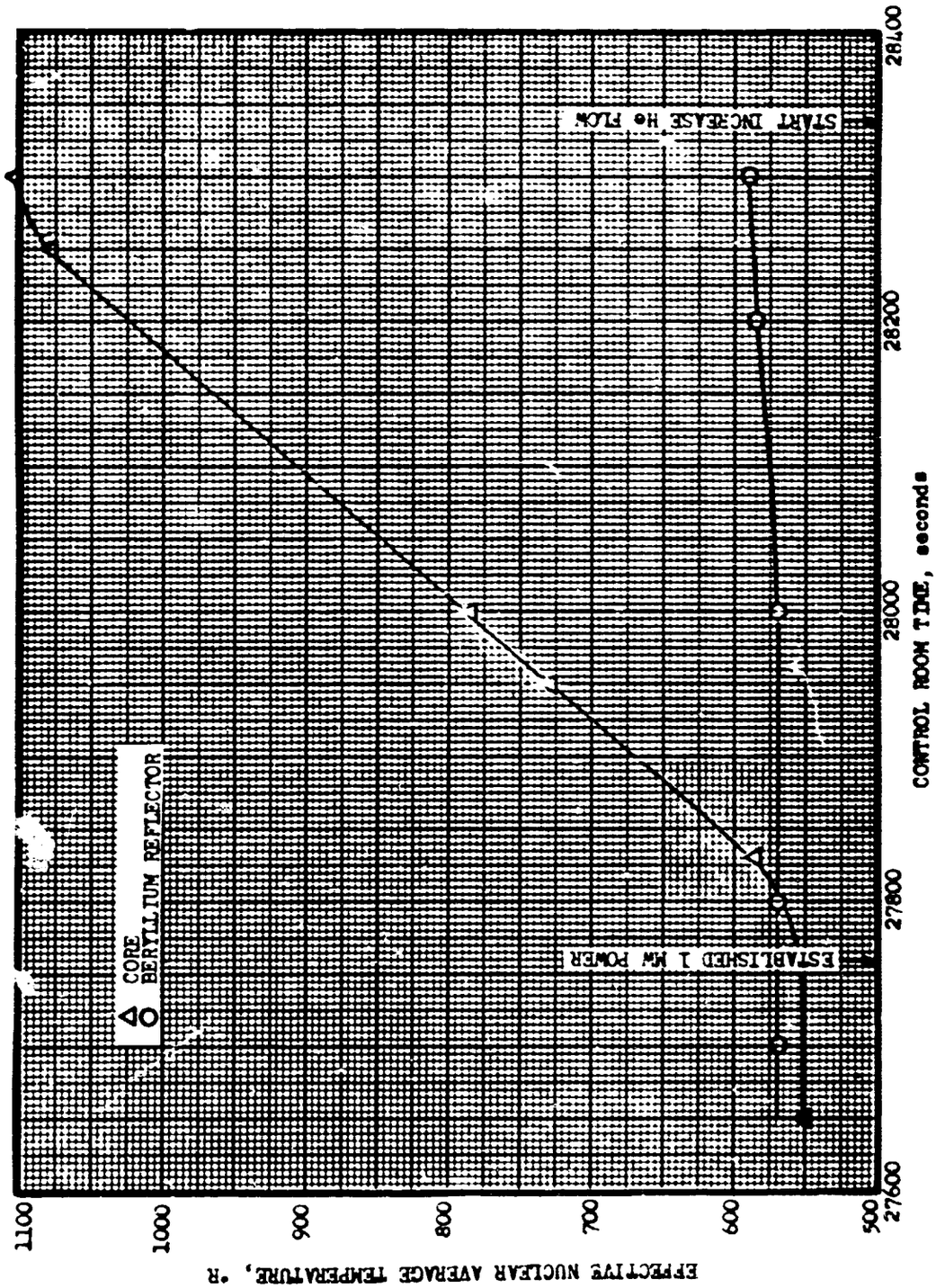

FIGURE 4.4-6 SL-A2, SP-II MEASURED NUCLEAR AVERAGE TEMPERATURE FOR MAJOR COMPONENTS

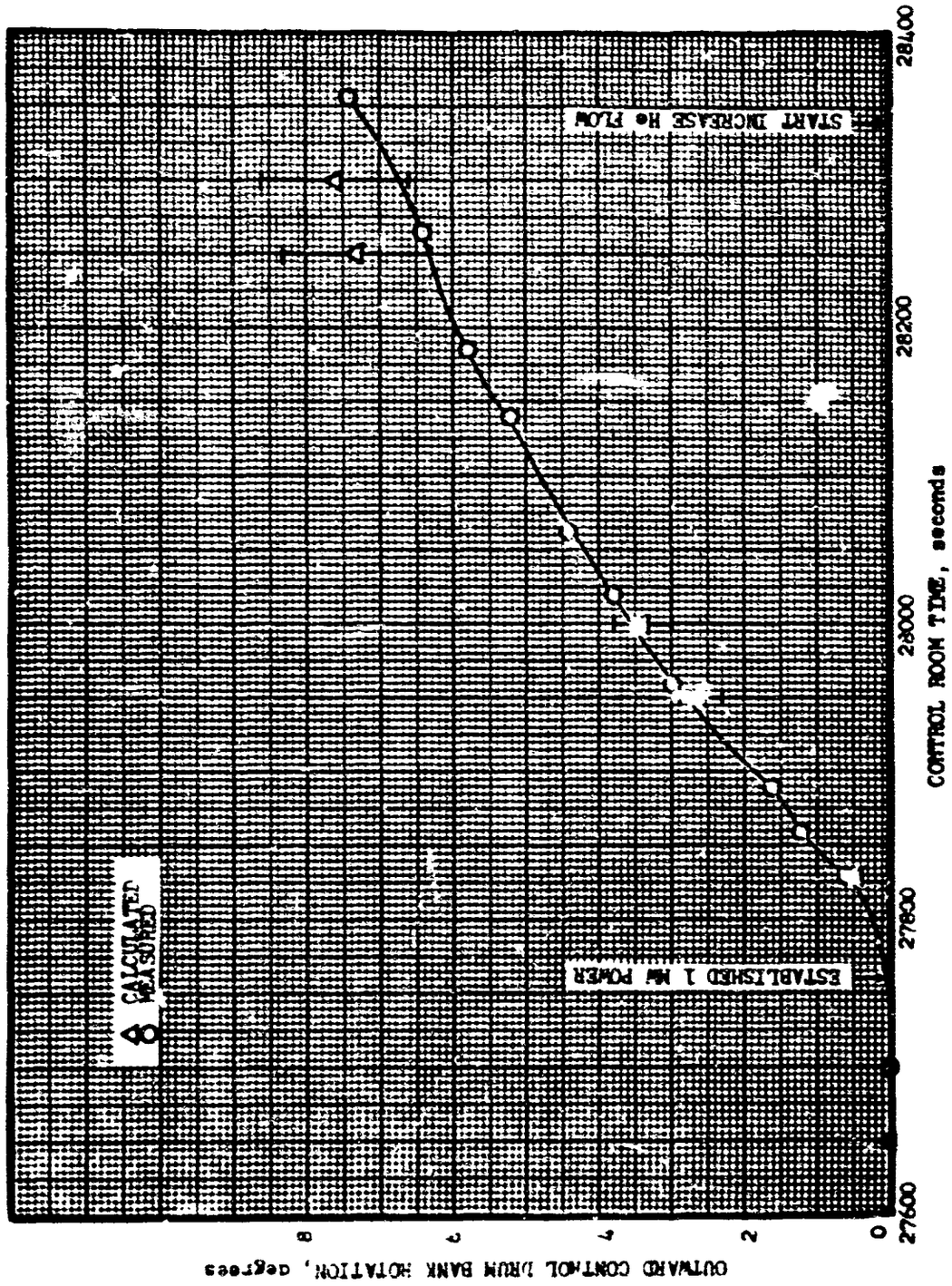

FIGURE 4.4-7 NRX-A2, EP-II CONTROL DRUM BANK ROTATION DURING TEMPERATURE COEFFICIENT TESTS

This effect is important in interpreting the reactivity change experienced during the high power run. Measurements at WANEF on an assembly essentially identical to the NRX-A2 indicated that the uniform loss of carbon from the core result in a reactivity change of 5.5 cents per kilogram. This term is included in Figure 4.4-4.

The interpretation of all the reactivity effects that exist during EP-IV startup, high power operation and shutdown of the NERVA reactor is extermely difficult. Of all the terms appearing in the reactivity equations given in Figure 4.4-4, the only directly measurable one is the control drum angle. The reactivity contribution due to the control drum movement can be determined using the previously developed equation under the assumption that the change in drum worth from room to operating conditions is negligible. Analysis tends to indicate this is the case. Figure 4.4-8 shows the variation of reactor power, hydrogen flow rate and control drum position throughout the high power run (EP-IV). Utilizing the system analysis code TNT and the power and flow from Figure 4.4-8, the densities in the core and reflector have been calculated. These parameters can then be utilized in the equation in Figure 4.4-4 to calculate the drum angle required for criticality. The carbon loss is taken as $0.20 based on critical measurements before and after EP-IV. These results are shown in Figure 4.4-9.

Astronuclear

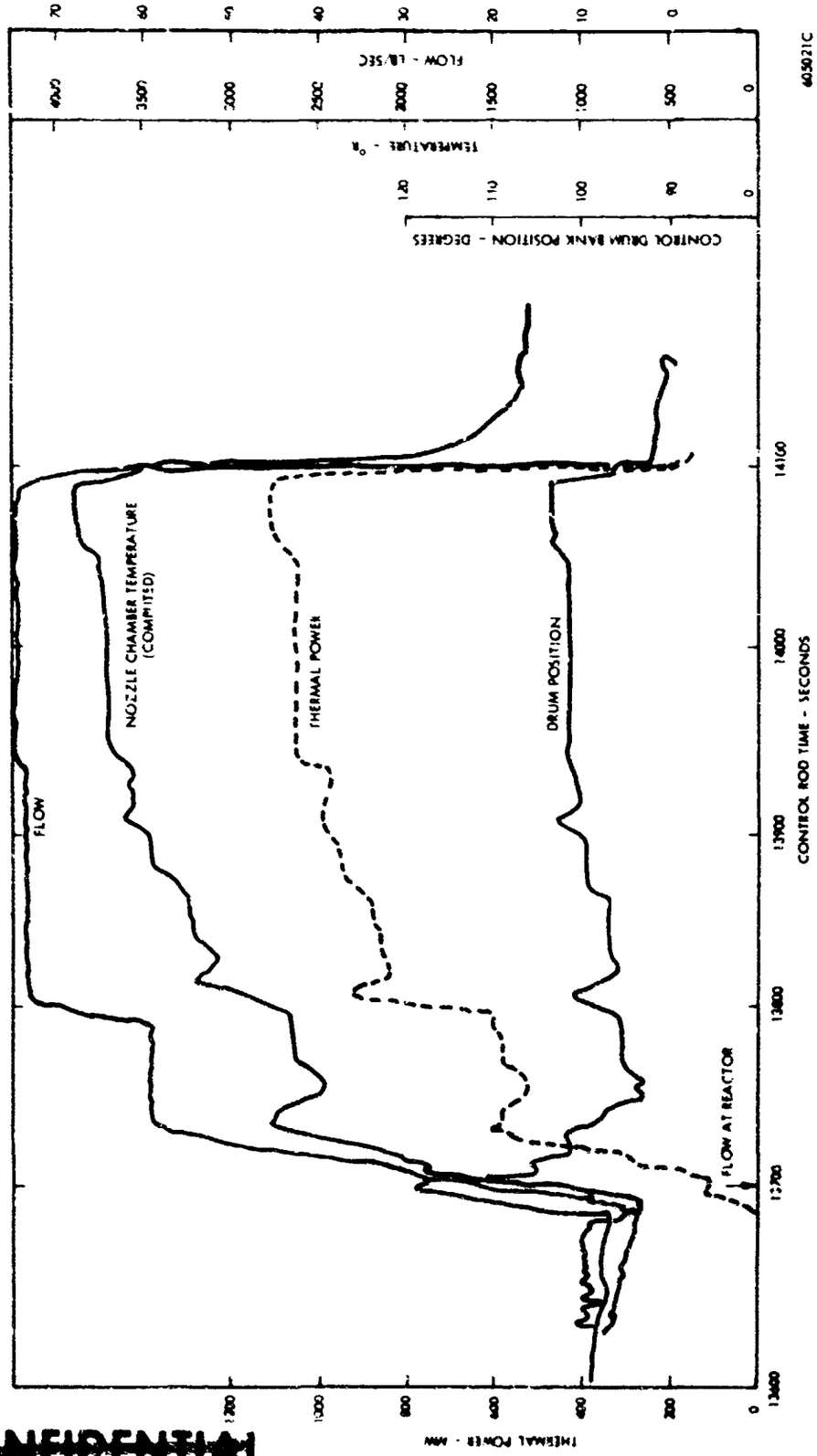

FIGURE 4.4-8 NRX-A2 EP-IV POWER, FLOW, CHAMBER TEMPERATURE AND DRUM POSITION VS TIME

Astronuclear

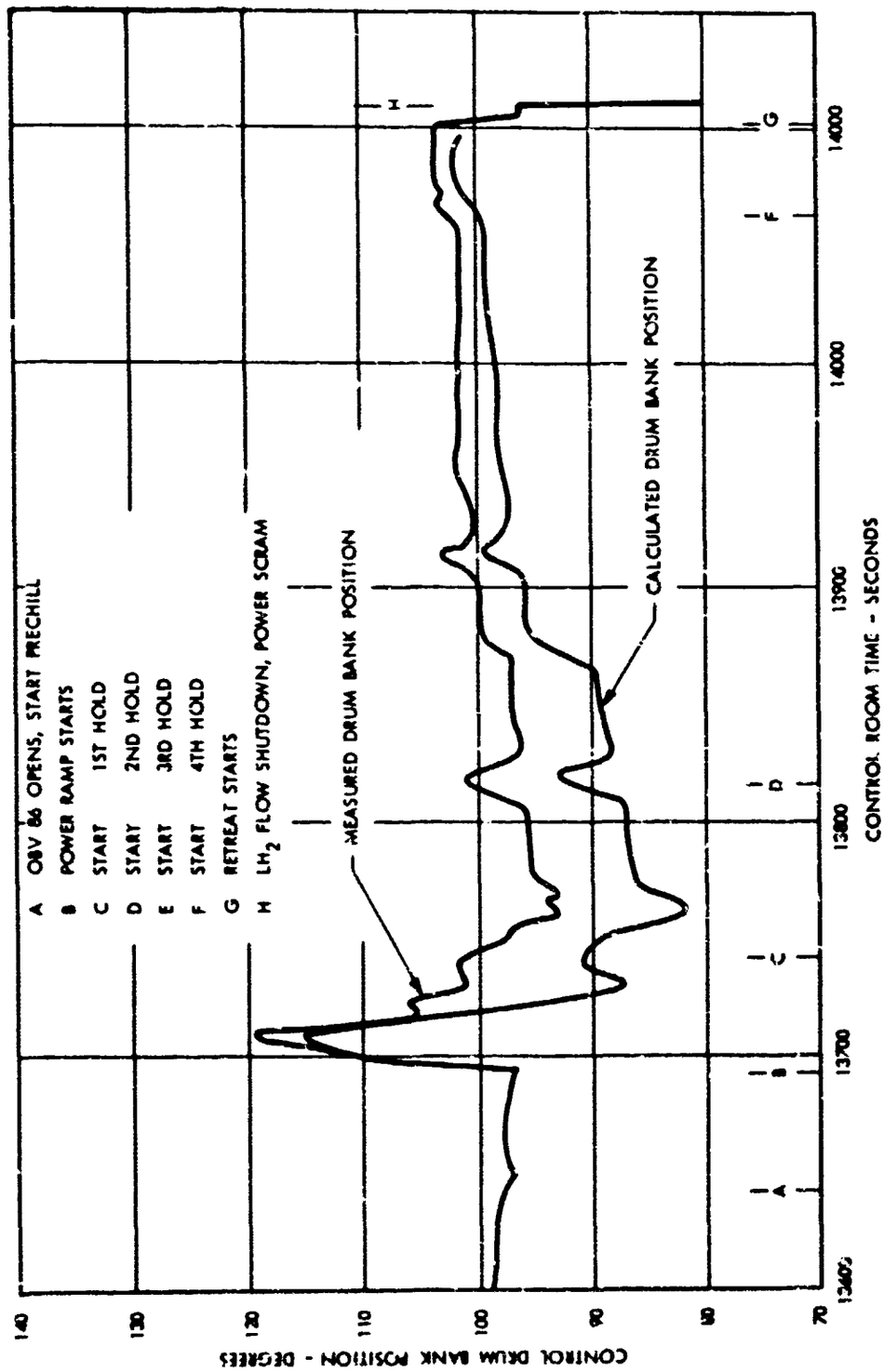

FIGURE 4.4-9 MEX-A2, GP-IV CONTROL DRUM BANK POSITION DURING THE HIGH POWER TEST, MEASURED CALCULATED

The low power mapping performed in EP-V had as one important objective, the evaluation of reactivity effects. These experiments provide an excellent opportunity to evaluate further the general understanding of the reactivity coefficients in the reactor. The operating points on a map of power versus flow have been presented previously in Section 4.1. Figure 4.4-10 shows the variation of power, flow and control drum versus time. The TNT code was utilized with the measured power and flow to calculate the temperatures and densities required in the reactivity equation. The calculated control drum position is also shown in Figure 4.4-9.

The reactivity behavior of the NRX-A2 over the complete power and flow map has been calculated and it is shown in Figure 4.4-11. This figure also shows the lines of constant reactivity that were calculated prior to NRX-A2 operations using equations previously developed. Also shown on this figure are measured values from the high and low power test (EP-IV and EP-V). These results indicate that some adjustments in the coefficients will be necessary to obtain better agreement with all the measurements.

Since these differences decreased with increased power level, a possible explanation for this effect is lower hydrogen diffusion into the fuel at low power than assumed in the prediction equations. This hydrogen diffusion is being investigated experimentally.

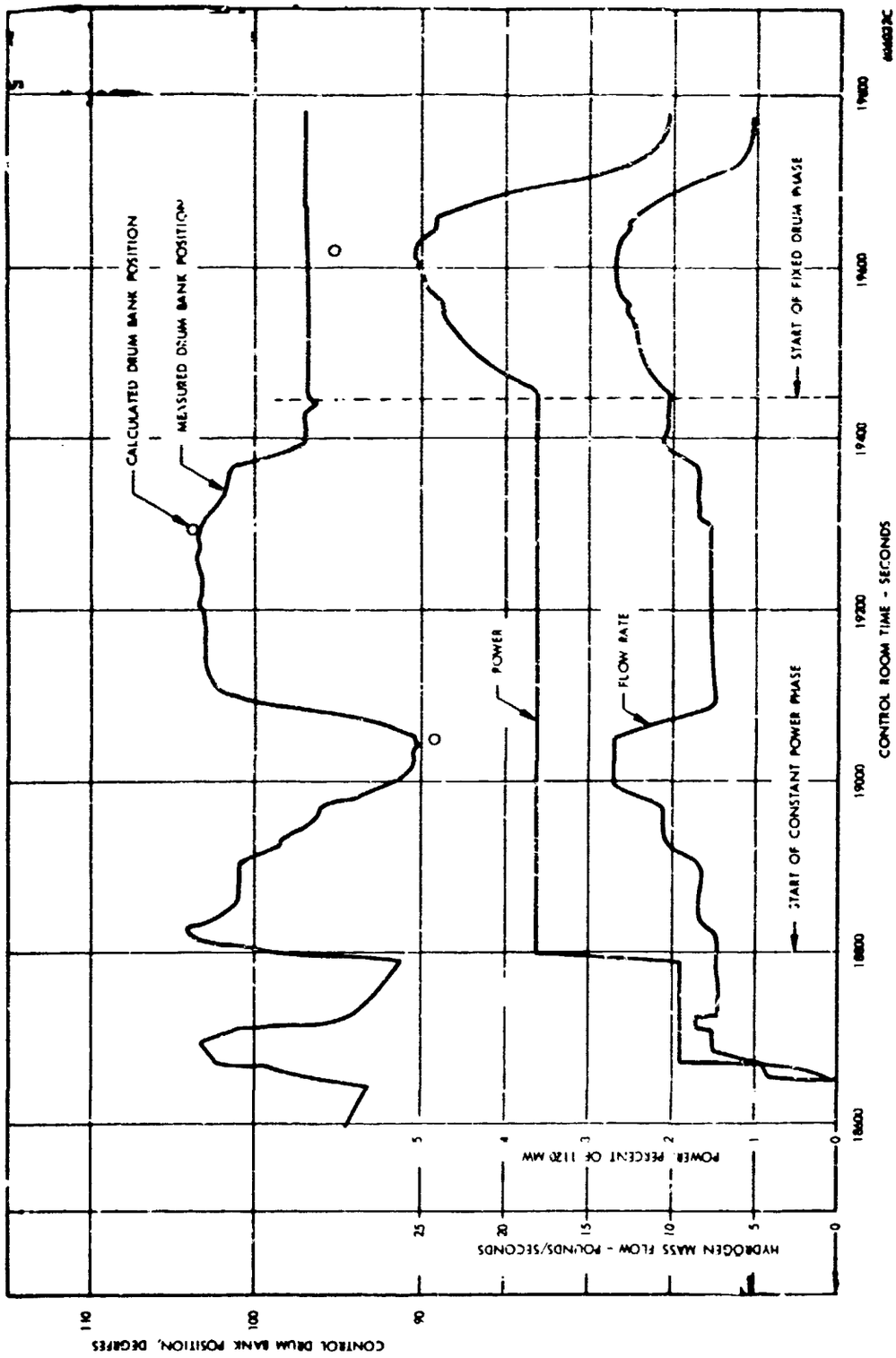

FIGURE 4.4-10 NRX-A2 EP-V LOW POWER MAPPING TEST

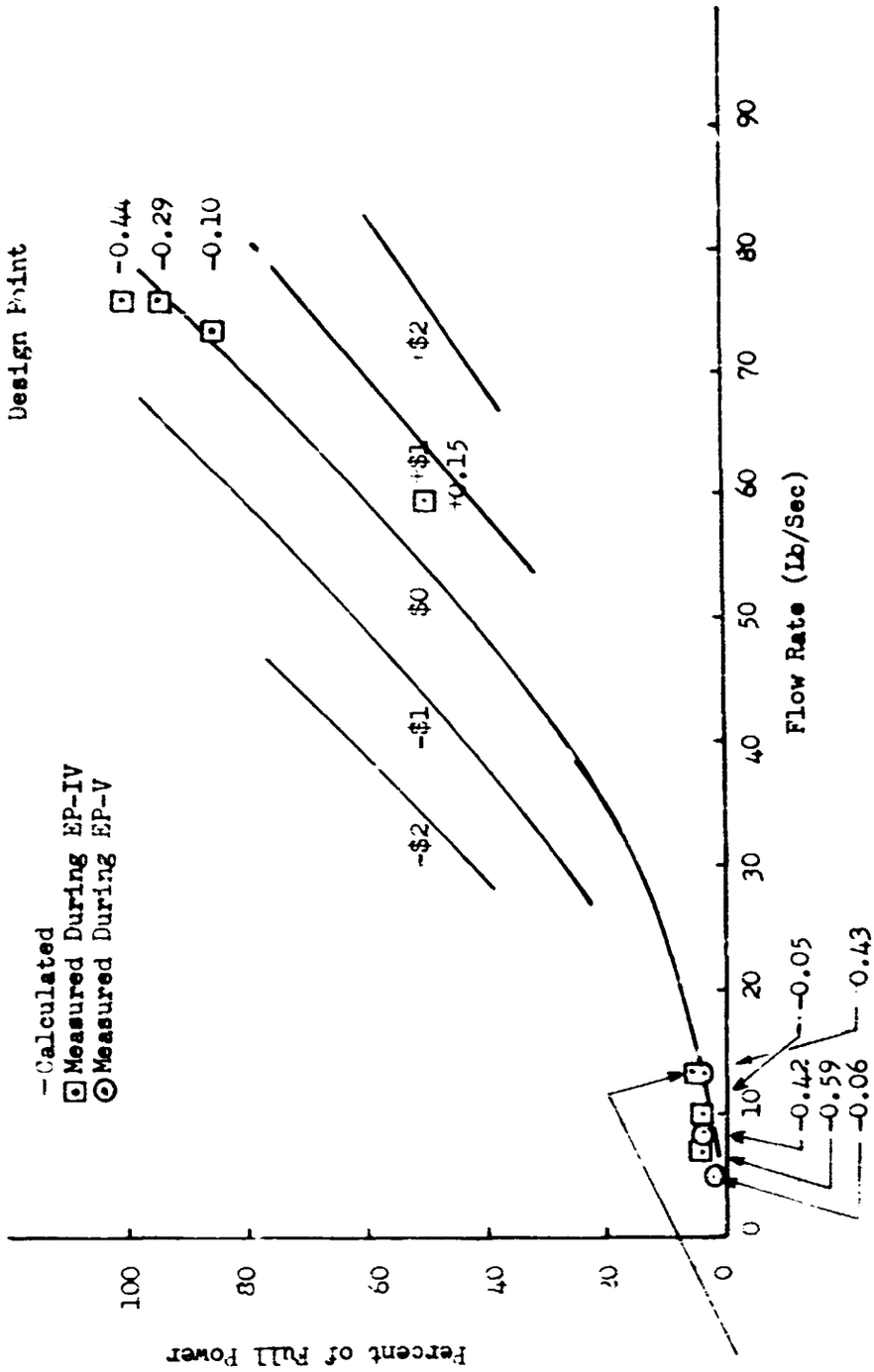

FIGURE 4.4-11 - NRX-A2 OPERATING REACTIVITY MAP

4.4.4 Power Distribution

Radial and axial core power distributions and the power gradient across the flats of peripheral fuel elements were measured during post-operative examinations using gross gamma radiation measurements and radiochemical analysis of fuel elements. Good agreement between measurements and calculated values exist except in the case of power in the peripheral elements.

The radial power distribution was measured (1) by ion chamber gross gamma radiation measurements of all but 18 core elements, and (2) by radiochemical analysis for fission products of 13 elements ground up into 50 gram samples. These measurements were compared with the calculated power distribution at a central drum angle of 99.7 degrees, the power weighted average obtained over the entire series of A2 tests. In the central region of the core the calculated values only differed from measured values by 1 to 2%, but for the peripheral elements the calculated power was approximately 7.2% lower than the measured power. This discrepancy is being studied further.

The axial power distribution was measured by an axial gamma scan of selected fuel elements using a collimated scintillation crystal. Figure 4.4-12 gives axial power distributions from gamma scans of elements 1J3U and 1B1E compared with the corresponding analytical predictions. Each distribution was normalized to an axial peak value of unity.

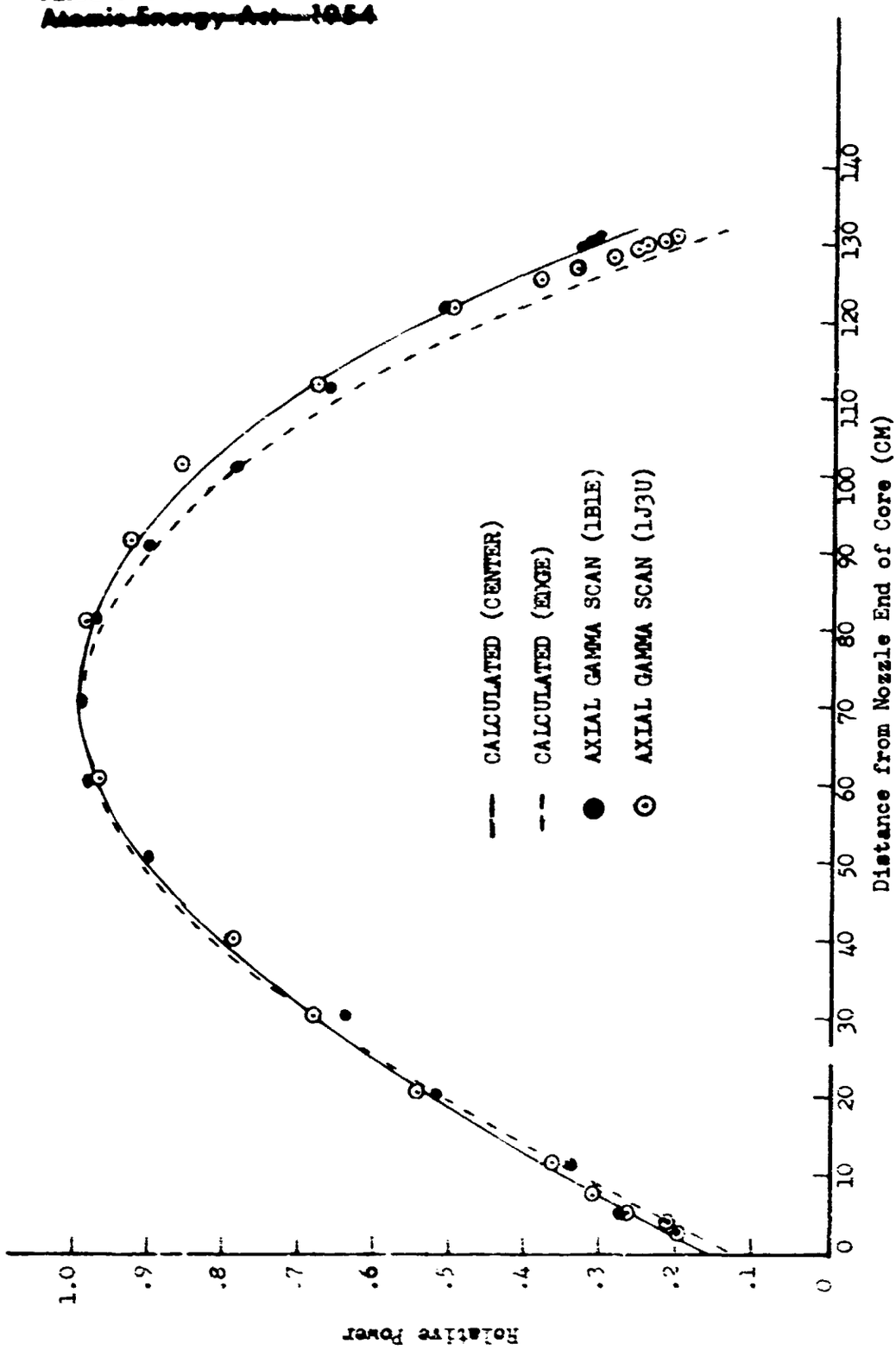

FIGURE 4.4-12 COMPARISON OF THE MEASURED AND PREDICTED AXIAL POWER DISTRIBUTIONS

The power gradients across the flats of peripheral fuel elements was measured (1) by radiochemical analysis of wafers sliced axially from four peripheral fueled element midplane sections, and (2) by wire activation measurements after the NRX-A2 PAX tests at WANEF. The direction of this gradient differs only slightly from the radial direction. Agreement between measured and predicted gradients is within 3%.

4.4.5 Radiation Heating

Of importance in the design of all components, other than fuel elements, is the radiation heating. The best available techniques employing transport theory for neutrons and Monte Carlo theory for gamma rays was employed to investigate the heating in the various components. Even with this detailed analysis, the radiation data was uncertain to $\pm^{50}_{30}$% in the reflector system. Table 4.4-6 shows the calculated heating in these components as a percent of reactor total power for several holds during the run. Also shown in this table are the measured values inferred from the enthalpy rises of fluid together with the uncertainties estimated for this calculation. It is seen that the predicted radiation heating in the inner and outer reflectors was on the average 17% low but still within the estimated uncertainty.

Astronuclear

TABLE 4.4-2

COMPARISON OF MEASURED AND CALCULATED HEATING IN NRX-A2 REFLECTOR

EXPRESSED AS PER CENT OF REACTOR TOTAL POWER

(NRX-A2, EP-IV, POWER RUN)

Control Room Time (Seconds)	Reflector Power / Reactor Power, (%) Measured (Nominal)	Predicted (Nominal)	Predicted / Measured
1379[illegible]	1.93 ±[illegible].8	1.76 $^{+0.93}_{-0.54}$	0.911
139[illegible]	2.20 ±0.66	1.76 $^{+0.93}_{-0.54}$	0.800
13985	2.01 ±0.52	1.76 $^{+0.93}_{-0.54}$	0.876
14085	2.08 ±0.52	1.76 $^{+0.93}_{-0.54}$	0.846
AVERAGE	2.06 ±0.73	1.76 $^{+0.93}_{-0.54}$	0.854

4.4.6 Radiation Environment

Typical of the information on the gamma radiation levels experienced during the NRX-A2 test is shown on Figure 4.4-13 and 14.

Figure 4.4-13 shows a comparison of measured and predicted gamma ray dose rate per operating watt on the reactor midplane as a function of radial distance from the center of the reactor core. These measurements were made during the low and high power runs with various dosimeters (as indicated by the key) at various radial locations. The solid curve shown in this figure drawn through the predicted data was calculated using the point kernel method. Reasonable agreement is shown out to a radius of 50 ft. Beyond 50 ft, the predictions diverge from the measured data due to neglect of the air scattering contribution in the predicted data.

Figure 4.4-14 shows a comparison of measured and predicted gamma ray dose rate per operating watt as a function of polar angle on the meridian ring located five ft. from the center of the core. Reasonable agreement both in shape and magnitude between calculated and measured data is evidenced. The measured dose rates at the dome end ($\theta = 30°$) of the reactor are significantly lower than those observed at the nozzle end due to the presence of an aluminum mockup shield at the dome end of the reactor system.

FIGURE 4.4-13 - EXPERIMENTAL AND CALCULATED GAMMA RAY DOSE RATE (RADS-TISSUE/HR.-WATT) AS A FUNCTION OF DISTANCE FROM REACTOR (FEET)

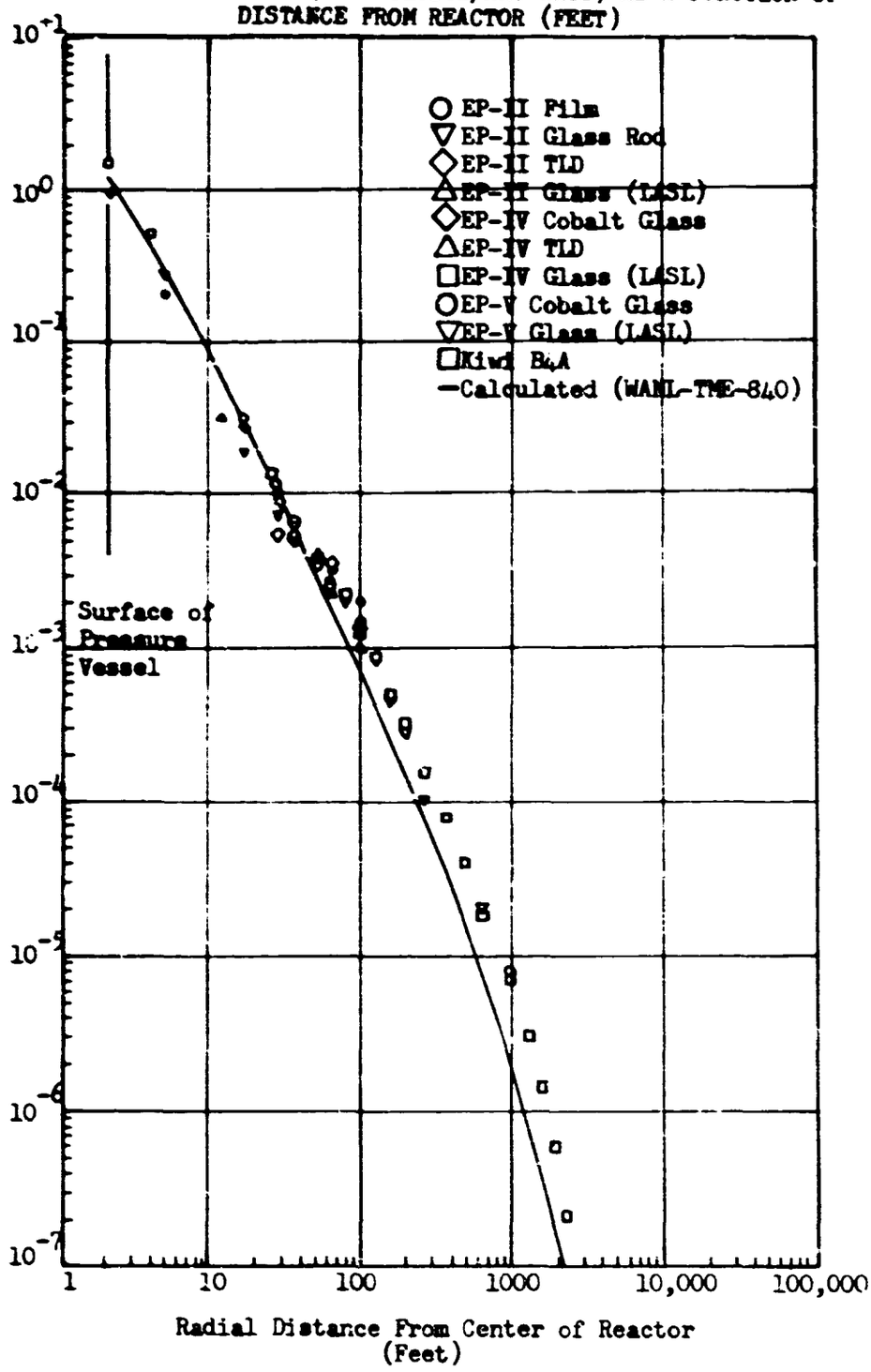

FIGURE 4.4-14 - EXPERIMENTAL AND CALCULATED GAMMA RAY DOSE RATE (RADS-TISSUE/HR.-WATT) ON THE MERIDIAN RING AS A FUNCTION OF REACTOR POLAR ANGLE

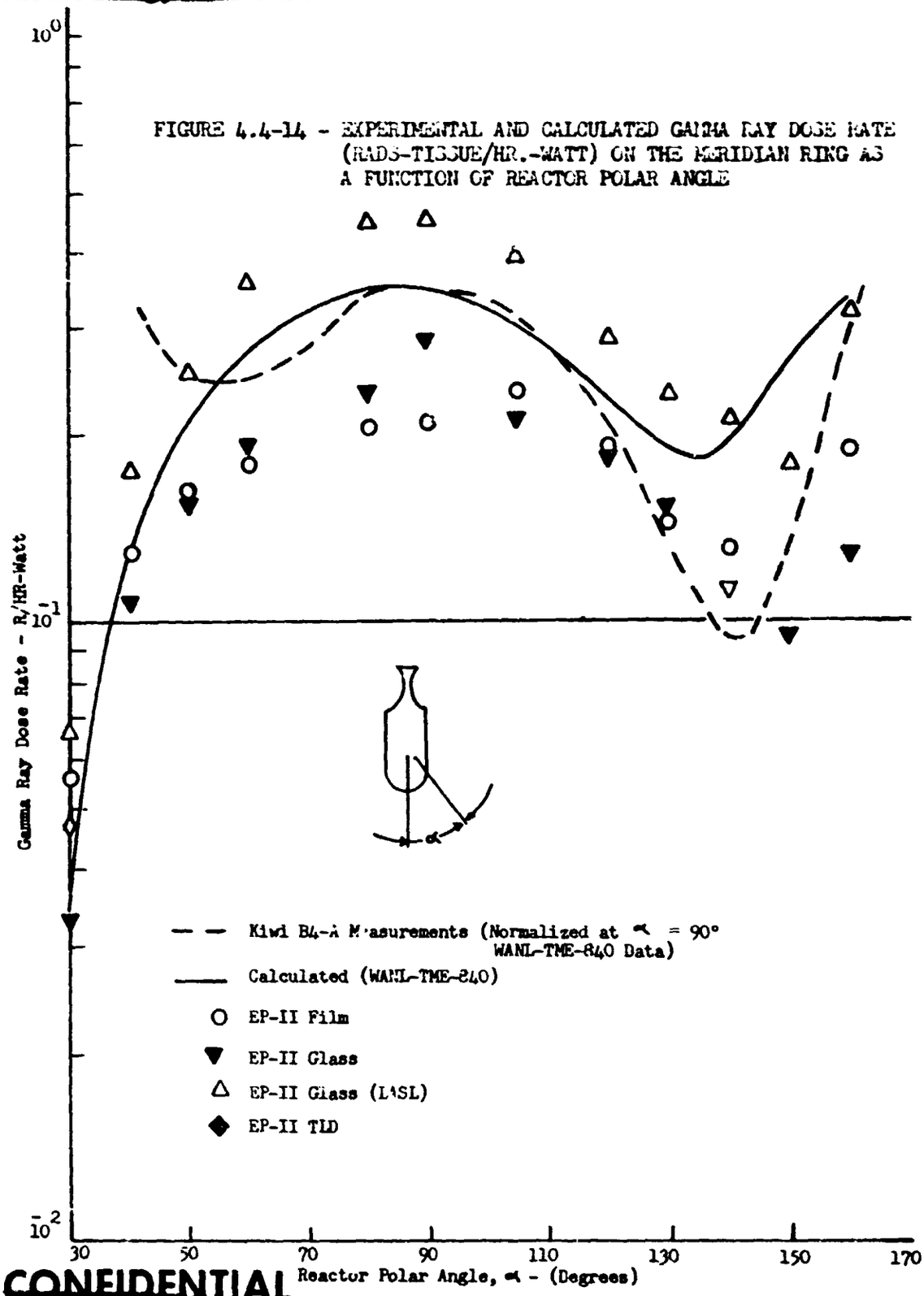

The total fissions experienced by the NRX-A2 reactor during the test series was 1.3×10^{22}. Based on this value and the radiation levels on a per fission basis presented in WANL-TME-840*, the maximum integrated radiation exposures for neutrons ($E > 1.0$ Mev) and gamma rays were computed for the major reactor components. The data are presented in Table 4.4-3. Figure 4.4-15 is a sketch of where the major reactor components tabulated are located. Since experimental radiation levels on major components were not obtained during the tests, the data in the table still contain uncertainties associated with radiation analysis and are probably accurate to within $\pm$ 50%.

---

* "Reactor Analysis Data Book", WANL-TME-840, Reactor Analysis Staff, July 31, 1964.

TABLE 4.4-3

NRX-A2 MAJOR COMPONENT NEUTRON AND GAMMA RADIATION EXPOSURE AS A RESULT OF EP-IV-A AND EP-V

Region No.	Region Description	Maximum Radiation Exposure* Neutron NVT E > 1.0 Mev n/cm	Gamma Ergs/Gm-carbon
1	Core Support Blocks	2.3×10^{17}	5.1×10^{10}
2	Active Core Region	1.5×10^{18}	3.6×10^{11}
3	Filler Strips	6.0×10^{17}	1.9×10^{11}
4	Lateral Support (Inner Reflector)	5.1×10^{17}	1.6×10^{11}
5	Beryllium Reflector	2.1×10^{17}	5.7×10^{10}
6	Pressure Vessel Cylinder	1.6×10^{16}	1.6×10^{10}
7	Reflector-Nozzle Interface Region	4.1×10^{16}	2.5×10^{10}
8	Reflector Support Structure (Nozzle End)	2.2×10^{16}	1.3×10^{10}
9	Cluster Plate Region	3.3×10^{17}	8.3×10^{10}
10	Core Support Plate	2.7×10^{17}	7.2×10^{10}
11	Core Support Ring, Etc.	1.2×10^{17}	4.8×10^{10}
12	Dome End Support Ring	5.4×10^{16}	1.8×10^{10}
13	Drum Drive Shaft Region	4.9×10^{16}	1.7×10^{10}
14	Flow Screen and Support	4.0×10^{16}	1.3×10^{10}
15	Aluminum Mockup Shield	3.8×10^{16}	1.2×10^{10}
16	Pressure Vessel Shield	1.8×10^{15}	6.0×10^{8}

*Exposures are based on the EP-IV-A and EP-V reactor runs for NRX-A2. Gamma exposures include gamma rays liberated after shutdown due to fission fragment decay. Total fissions for EP-IV-A and EP-V = 1.3×10^{22} fissions.

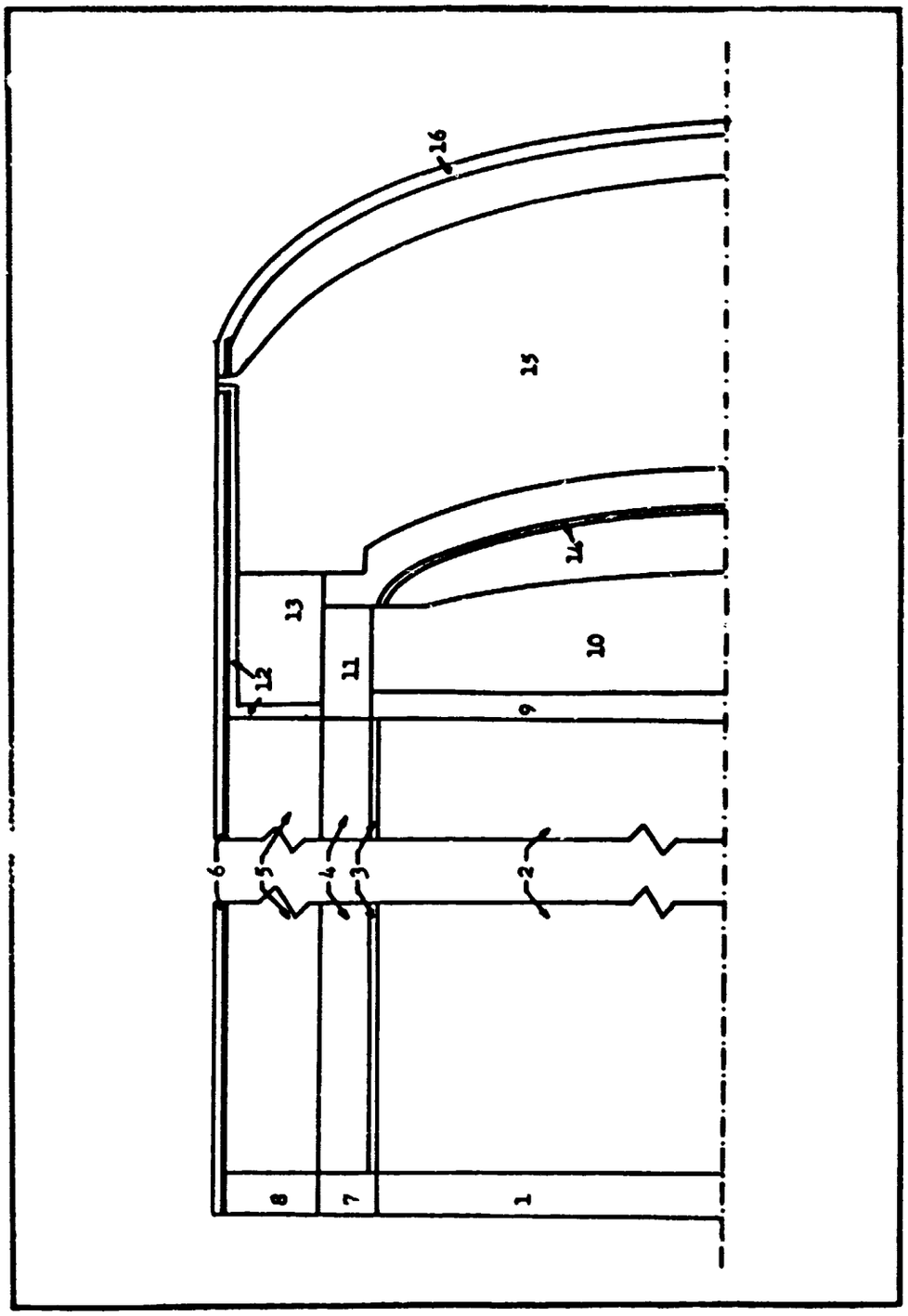

FIGURE 4.4-15 - NRX-A2 REGION DESCRIPTION SHOWING MAJOR COMPONENTS

4.5 INSTRUMENTATION, CONTROL AND DATA SYSTEM PERFORMANCE

This section deals primarily with sensor performance and the utilization of data for control and analysis.

From a total of 196 NRX-A2 WANL diagnostic channels, 97.4% were operating prior to tests and 76.5% were operating at the end of the test with 91.5% of these remaining operative through all testing. A list of** channel results is summarized below and shown in Figure 4.5.1. Specific channel numbers are tabulated in Table 6.2.1 in the Appendix.

Channels operating at the start of each EP test.

Installed	EP-I	EP-II	EP-III	EP-IV	EP-V	End of Test
196	191	188	188	183	153	150
100%	97.4%	96.0	96.0	93.3%	78.0%	76.5%

Channels failing during an EP test. These channels are in addition to those listed above, but were repaired or corrected prior to the start of the next EP test.

EP-I	EP-II	EP-III	EP-IV	EP-V
13	5	None	8	None
*6.8%	2.7%	0%	4.4%	0%

*Percent of channel failure from total number of channels operating at start of each EP test.

**The conclusions reached were based upon the following documents:

1. Data Discrepancy Report, NTO-R-0010, November 2, 1964
2. NTO Data Log Sheets
3. Instrumentation Disassembly and Post Operative Report, WANL-TME-1079, January 25, 1965.

FIGURE 4.5-1

PERCENTAGE OF VALID DATA DURING EACH PHASE OF TESTING

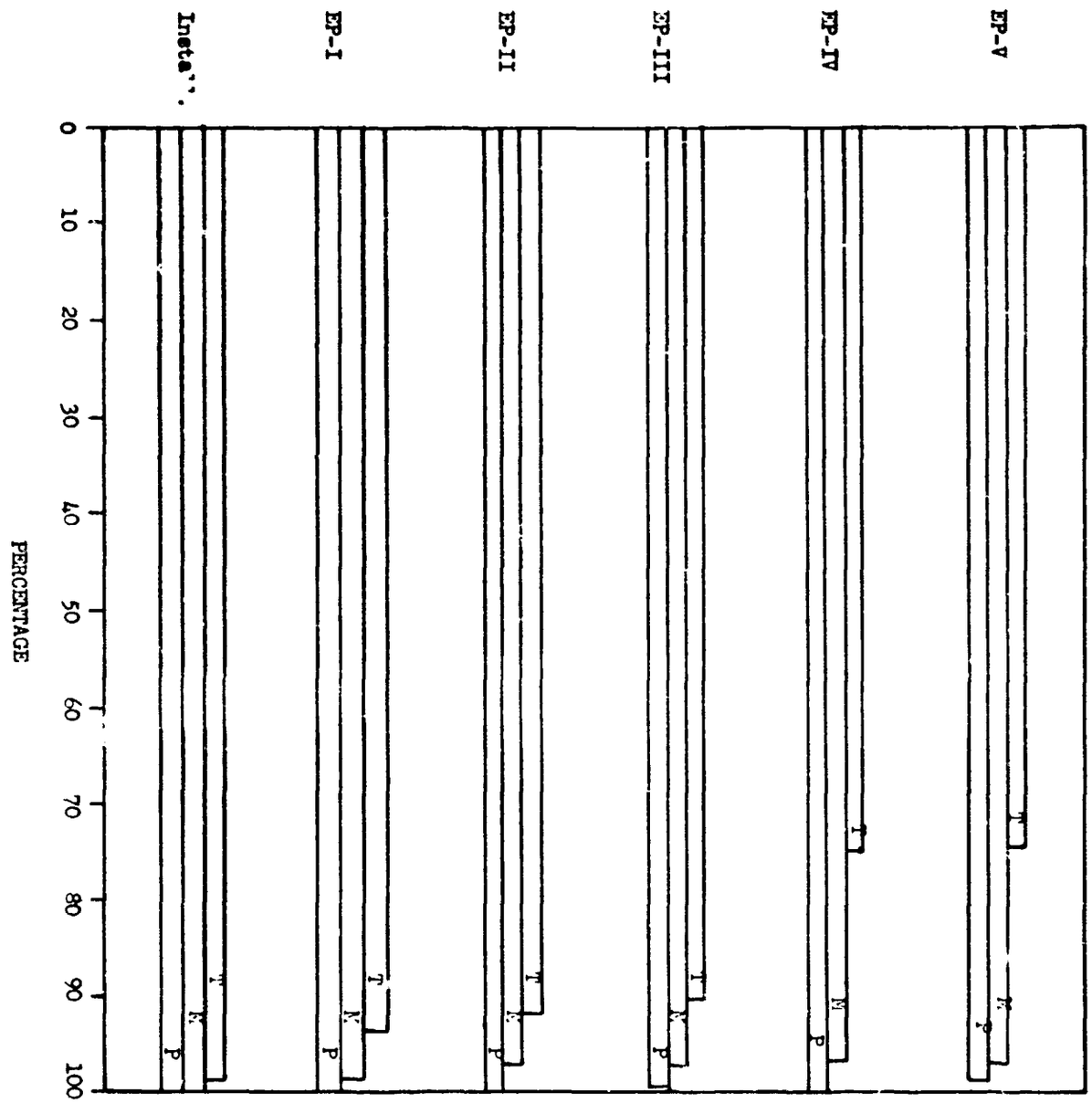

Total No. Transducers	
Temperatures (T)	146
Pressure (P)	25
Strain Gages (M)	25

Mode of failure for channels for all EP tests and assembly with percentage failure of total (196) WANL diagnostic channels are:

**Mode of Failure	No. of Channels	Percentage
Installation Design	22	11.2
Installation Assembly	10	5.1
Data Acquisition	7*	3.6
Sensor Design	4	2.0
Wiring	2	1.0
Reactor Overpower	2*	1.0

*Includes one transducer (P 501) not operating properly during EP-I through EP-IV but was operating satisfactory at start of EP-V.

**The following is a description of the different modes of failure.

Data Acquisition:

Channel failure between the Electronics Room (ELR) at Test Cell "A" and the Control Point (CP), i.e., equipment failure.

Installation Assembly:

Channel failure where the transducer was observed during disassembly of the test article and found to be improperly installed or handled during assembly at WANL or NRDS.

Installation Design:

Channel failures where the installation design of the transducer was observed during disassembly of the test article and found to be inadequate for the environment, i.e., potting failures.

Sensor Design

Channel failures where the transducer was observed during disassembly and found to be inadequate when subjected to its expected environment.

4.5.1 Temperature Measurements

A. Low and Intermediate Temperature Measurements

For low temperature measurements, copper-constantan grounded junction thermocouples proved very effective. These thermocouples were for measuring beryllium, boral, titanium, aluminum and stainless steel material temperatures in a radiation field. This type thermocouple was also very effective in measuring fluid temperature conditions in low temperature areas such as the core inlet. Copper-constantan exposed junction thermocouples functioned well in measuring fluid temperature conditions in various low temperature plenums in the reactor. Of a total of 64 copper-constantan thermocouples installed, only one failed during tests due to a defect occurring in the sensor. It appears this defect was not due to the design of the sensor but was brought on by excessive handling during assembly.

For intermediate temperature measurements throughout the reactor, chromel-alumel thermocouples proved effective. The grounded

---

Footnote continued from previous page

Transducer Wiring:

Channel failures where the wire condition was measured during disassembly operations and found to have shorted or open leads at terminal boards or cable transitions.

Low Parameter Prediction

Channels where the transducer failure was due to the measured parameter attaining a higher value than originally planned.

junction type measured fluid temperatures at the tie rod exit and in the seal chambers. Out of a total of 25 chromel-alumel thermocouples installed, four failed during tests but each failure appears to be the result of an installation problem and not the sensor itself.

B. High Temperature Measurements

In this section emphasis is placed on the in-core thermocouple performance because of the primary significance in controlling and evaluating the test power level. The in-core thermocouples used in NRX-A2 were an extension of early tungsten-tungsten rhenium molybdenum-sheathed thermocouples used in KIWI. Early testing disclosed a carbon eutectic problem preventing operation above 4300°R. Development work increased the range and lifetime of sheath materials by the addition of tantalum and later tungsten coated tantalum and tungsten coated molybdenum. The station 32 thermocouples were required to operate near the eutectic temperature of molybdenum. For this reason a tungsten coating was designed to cover the operation in this critical region.

In July 1964, the results of full length thermocouple tests in fuel elements were evaluated. At that time error due to insulation breakdown was reviewed for station 32 and 45 thermocouples. The NRX-A2 test plans and power levels, at that time, presented no problem in the application of these thermocouples.

Additional tests were conducted in September, 1964 on station 32 thermocouples in view of later NRX-A2 test plan changes. Tests of repeatability on up and down and repeat time temperature testing were conducted. These tests were reported in NAA-TRD-1007 and are summarized as follows:

1. Calibrations below 3400°R reproduced on cycling after exposure to high temperature for 10 minutes or longer.
2. Thermocouples operated satisfactorily after two time exposures greater than 10 minutes at greater than expected NRX-A2 temperatures. (Up to 4200°R.)
3. Hydrogen appeared to give the effect of drift in error at constant temperature holds above 4000°R (where insulator breakdown produced errors).

The NRX-A2 reactor core was fitted with 5 thermocouples for measurement of axial and radial temperature gradients. The sensors had junctions grounded to the metal sheaths which protruded into an unfueled element shim hole up to the station level. The thermocouple sensing end was secured to the element with graphite potting cement, which was applied in a slot in the element, to ensure proper heat transfer, reduce the effects of gamma heating and stop gas flow through the shim hole.

Virtually, all core thermocouples produced good data up to the 5 % power hold in EP-IV. The axial temperature profile of the NRX-A2 core at the 5 percent power hold indicated reasonable agreement with the analytical predictions and measurement data. A spread in temperature was indicated at this power level due to radial power distribution as well as normal hot channel deviations. This spread in temperature confirmed the expected radial temperature distribution at the low power holds. The axial temperature distribution at the 50 percent power hold also confirmed the computed axial temperature distribution pattern with reasonable agreement.

After the 5 % power hold, all but one (T647) of the station 32 thermocouples diverged from the expected rise during rise to second hold and indicated temperatures up to 12[illegible]°R low. The low readings of the station 32 thermocouple in NRX-A2 EP-IV test were not anticipated. Twelve thermocouples of the type used in NRX-A2 were tested in unfueled elements at LASL prior to the NRX-A2 test. There was no evidence of any effects in these tests similar to those observed in the NRX-A2 data. This testing closely simulated the NRX-A2 temperatures and pressure environments. The explanation for the abnormality in NRX-A2 was failure of the potting material. This material was found eroded away permitting coolant gas to cool the thermocouples. The post-mortem examination of the NRX-A2 instrumented central elements in which station 32 thermocouples were installed showed

complete or partial erosion of the potting compound on all elements except the one station 32 thermocouple (7647). There was also evidence of corrosion of adjacent fuel elements, apparently due to the hydrogen flow through the thermocouple installation slots.

During the reactor operation the inside of the fuel element essentially sees core inlet pressure down to the potting compound. The interstitial pressure between the elements is essentially the core exit pressure. The potting cement was therefore subjected to pressure and transient temperature conditions which dislodged it and cooled the thermocouple junction.

A conjecture that breaking or some other failure mechanism occurred was eliminated in the post-mortem examination of the NRX-A2 thermocouples removed. The station 32 thermocouples removed were in excellent condition.

The saturation condition for NRX-A2 station 32 thermocouples was also well above the expected A-2 temperature (Figure 4.5.2). The data and subsequent testing indicated that no operating problem was expected even at the 85 percent power level of the final A-2 test plan. This factor and the successful operation of KIWI-B4E on station 26 thermocouple control prompted the selection of station 32 thermocouples for NRX-A2 control.

At the 95 percent power hold, the station 45 thermocouples were in a state of saturation and indicated below the computed temperature. The saturated condition of the station 45 thermocouples during EP-IV was

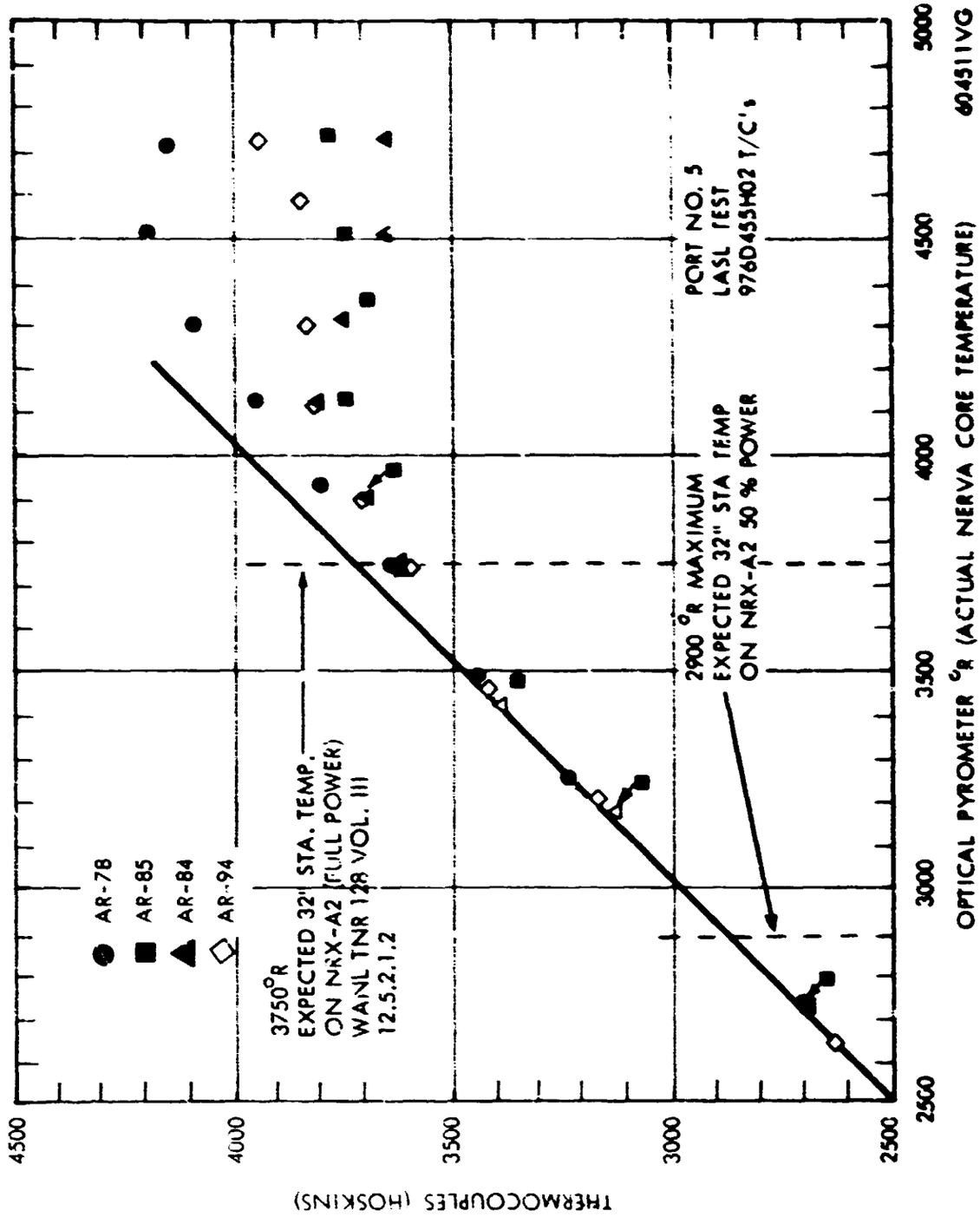
AR-78
AR-85
AR-84
AR-94
3750°R
EXPECTED 32" STA. TEMP.
ON NRX-A2 (FULL POWER)
WANL TNR 128 VOL. III
12.5.2.1.2
2900 °R MAXIMUM
EXPECTED 32" STA TEMP
ON NRX-A2 50 % POWER
PORT NO. 5
LASL TEST
976D455H02 T/C's
4500
4000
3500
3000
2500
THERMOCOUPLES (HOSKINS)
2500
3000
3500
4000
4500
5000
OPTICAL PYROMETER °R (ACTUAL NERVA CORE TEMPERATURE)
604511VG

FIGURE 4.5-2

an expected condition and caused the low readings at temperatures above 35[illegible]°R. This saturation is caused by a high temperature breakdown od the BeO insulators. This characteristic is indicated in Figure 4.5.3 and was reported in July 1964 (NAML-TME-9[illegible]1, page V-6). No problem was expected with the NRX-A2 test as planned at that time. The increased power of the final A-2 test moved the operating temperature into the margin of the saturated region (about 4200°R).

At reactor disassembly the tungsten coated tantalum sheath for the station 45 sensors was found to be fractured. It appears that hydriding caused this condition. Although this sheath was damaged, it accomplished its purpose in protecting the molybdenum sheaths which were found to be in excellent condition at disassembly.

Another apparent problem became evident immediately on reactor shutdown. Station 45 thermocouples primarily on the periphery of the core indicated an apparent increase in temperature. A typical case is illustrated in Figure 4.5.4. No evidence of actual increase in temperature can be found, however, one possible explanation for the indication is: As indicated, the thermocouples were reading a temperature below the actual temperature due to insulation degradation. The amount of this thermocouple error is a function of sheath length subjected to high temperature. It is known that the periphery of the reactor cooled faster than locations within the core. As the sheath cooled the error reduced and the indicated temperature

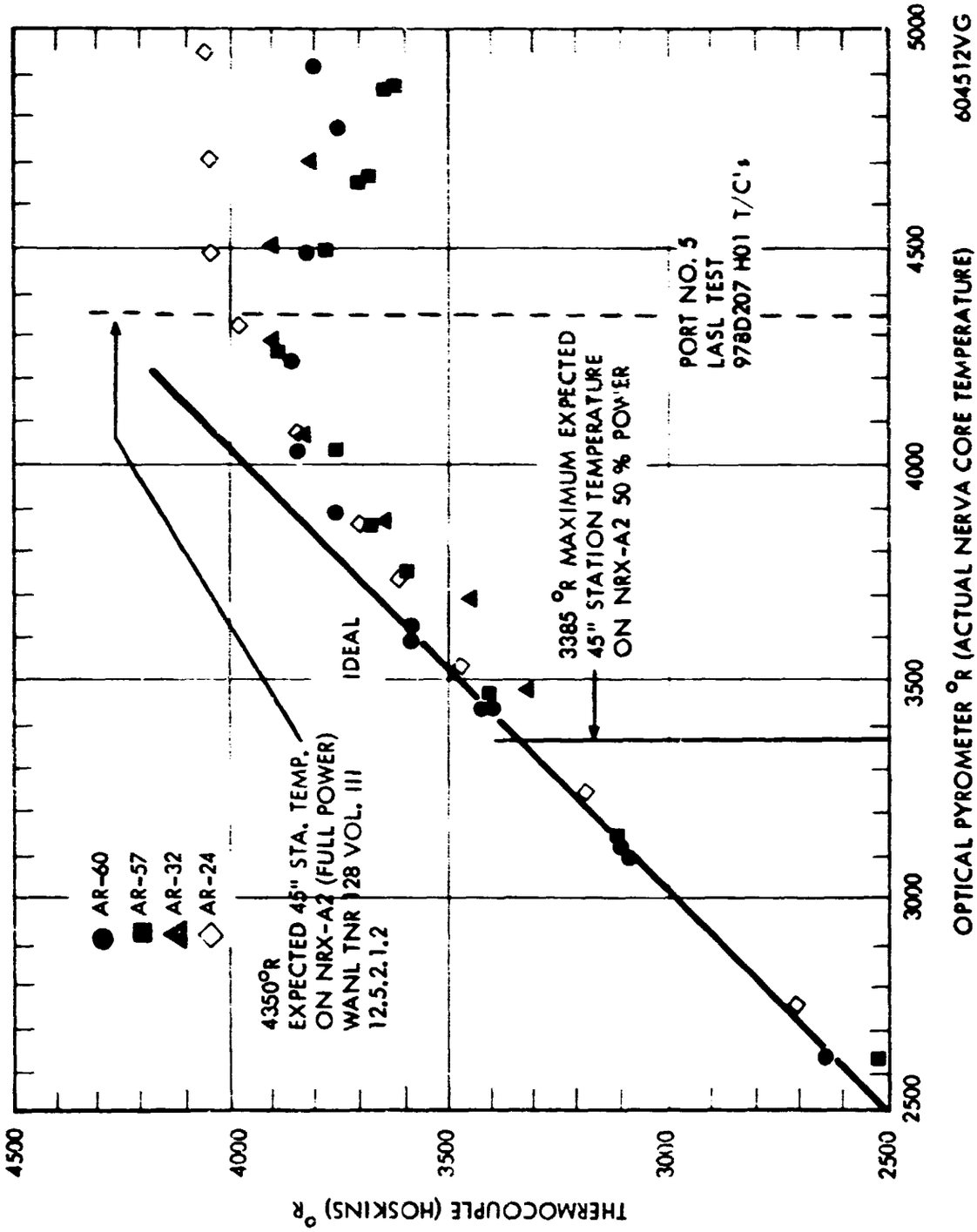
AR-60
AR-57
AR-32
AR-24
4350°R
EXPECTED 45" STA. TEMP.
ON NRX-A2 (FULL POWER)
WANL TNR 128 VOL. III
12.5.2.1.2
IDEAL
3385 °R MAXIMUM EXPECTED
45" STATION TEMPERATURE
ON NRX-A2 50 % POWER
PORT NO. 5
LASL TEST
978D207 H01 T/C's
THERMOCOUPLE (HOSKINS) °R
OPTICAL PYROMETER °R (ACTUAL NERVA CORE TEMPERATURE)
4500
4000
3500
3000
2500
2500
3000
3500
4000
4500
5000
604512VG

FIGURE 4.5-3

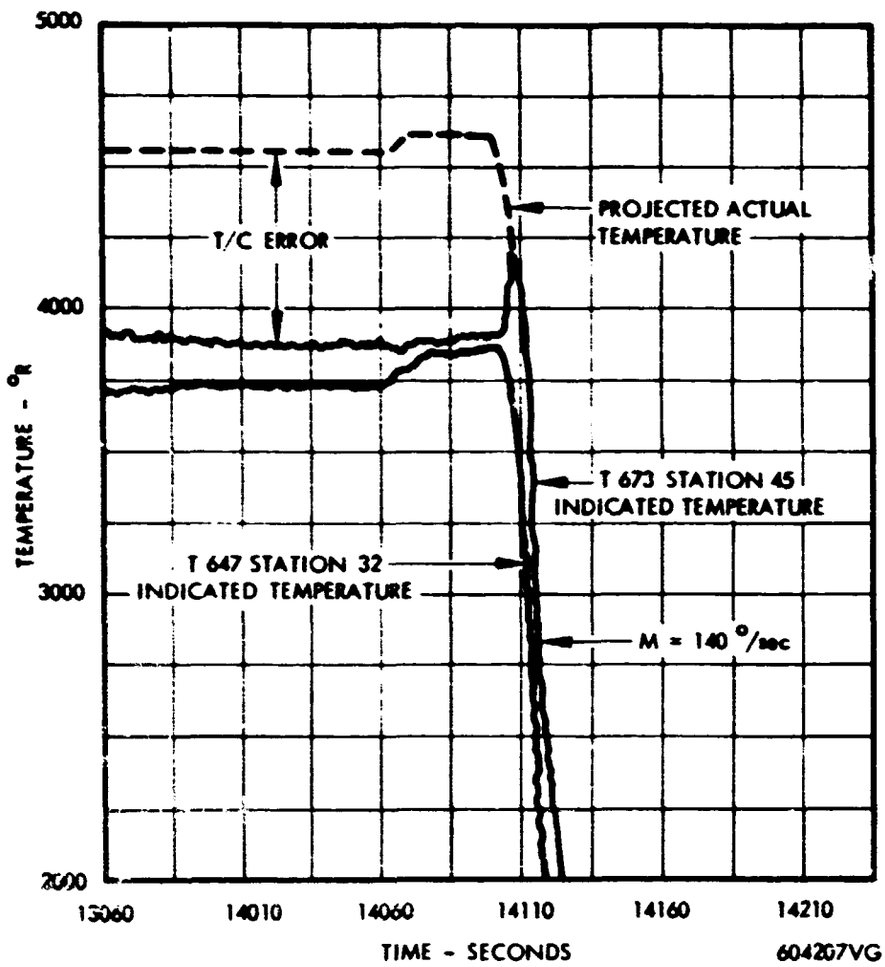

INDICATION OF TEMPERATURE PEAKING EP IV

FIGURE 4.5-4

approached the actual temperature. The net result was an improvement in the thermocouple performance and indicated temperature approached actual temperatures as the thermocouple error reduced.

The scram cooldown appears to have uncovered an additional problem of thermal shock. The peripheral cooldown rate exceeded 200°F per second. Four thermocouples open circuited due to this rapid decrease in temperature which exceeded normally expected rates. An increase in material tolerance has been allowed in new thermocouple designs to increase the thermal shock resistance.

In summary, NRX-A2 tests revealed three basic problems for in-core temperature measurements with the type of sensors used. These problems are:

1. Reliable installation design.
2. Corrosion of sheath materials.
3. Resistance to thermal shock.

The thermocouple installation procedure for NRX-A3 has been changed eliminating both the potting and the slot in the element. Tests have been conducted to establish the performance of the new installation with good results. Analysis of possible error due to radiation heating in the new installation have been conducted and the error indication is less than 50 degrees. This work has been recently reported in NAA-TM-1019.

A survey of methods of temperature measurement, other than thermocouples, was conducted with the conclusion that benefits from efforts along these lines would be two to three years away at the earliest. Further, the materials problems with these systems are similar. The determination of a suitable material for temperature probes is a basic problem of in-core temperature measurement. A sheath material developed for thermocouples could be adapted at a later date to alternate measurement systems.

Emphasis in development is being placed therefore on those in-core measurements which may be called upon for control purposes. In order to establish a design insight into the interaction of hydrogen, graphite and thermocouple materials, a compatability study is being conducted. This study is not completed as yet; however, present indications are that tungsten coated molybdenum (or tungsten) is a more promising sheath material.

Considerable effort has been directed toward improving thermocouple and/or instrumented assembly testing methods. Tests have recently been conducted wherein the interstitial pressure drop has been simulated. This type test was implemented by the utilization of flow down the tie rod hole of a central element to develop the (interstitial) differential pressure. This was accomplished in a WANL fuel element corrosion furnace adapted with a radiant heater tube.

More exact simulated testing of instrumented assemblies is required to assure adequacy of in-core temperature measurement systems. This becomes of prime importance for the longer duration and higher temperatures of future NRX reactors.

4.5.2 Pressure Measurements

For pressure measurements within the reactor, all 21 of the variable reluctance pressure transducers mounted externally operated as expected. There were minor abnormalities. For example, one channel P315, was set up improperly for EP-IV and saturated the amplifier before the 50 percent power level was reached. P315 was calibrated properly and operated satisfactorily during the EP-V run. Pressure measurement precision during all NRX-A2 tests was considered excellent based on comparisons of transducers sensing the same pressure.

Two of the four transducers located internal to the reactor were mounted on the outer reflector dome end support ring. These sensors were both LVDT types, one being a differential and the other an absolute. During the EP-IV test, one transducer (P603) operated well up to the 50% power hold but data beyond that point was questionable. The other transducer (P601) was reported as functioning properly until EP-V when the data saturated full scale.

The other two transducers located internal to the reactor were mounted on the shield (one on the forward end and the other aft) and were both variable reluctance absolute transducers. One of these transducers (P501) was not set up properly for EP-IV. This unit was

set up properly for EP-V. The data for the other transducer (P603) was reported to have gone offscale during the 83% (nominal) power hold.

4.5.3 Strain Measurements

The nine sensors selected for determining the lateral displacement of the core at various axial locations and the displacement of the inner reflector springs were weldable strain gages resistance welded to the inner diameter of the lateral support springs. Of these nine gages, only one has been reported as having a discrepancy, however, this problem was in the data system. The remaining eight gages have yielded displacement data which are within the range of the predicted values.

Six weldable strain gages were located on three tie rods supporting one of the fuel element clusters. The gages were arranged on the tie rods so as to measure both tension and bending strains. One of the six gages was damaged during reactor assembly due to an inadvertent application of 110 AC across the gage leads. The remaining five gages appear to have operated normally during testing with the exception of one gage which was reported to have failed during EP-IV. This was not a sensor problem and was corrected for prior to EP-V. Valuable information was obtained from the tie rod gages.

The ten sensors selected for determining stresses induced in the support stand legs and adapter ring were weldable strain gages resistance welded to the legs and adapter ring. One gage was damaged during installation at NRDS assembly and two channels were canceled after EP-I due to an open

circuit occurring in the data acquisition system. The remaining gages appeared to have worked normally, however, during EP-IV-A, they were greatly over-scaled for the readings that they were actually giving (approximately 100 μ in/in on a scale of $\pm$3000 μ in/in).

4.5.4 Nuclear Heating Measurements

Six calorimeters were installed in the NRX-A2 test to observe the gamma heating effects on beryllium, stainless steel, and aluminum. One calorimeter for each of these three materials was mounted on the center line of the core on the instrument boom to measure radial gamma flux leakage. A similar set was mounted on the rabbit gun boom to measure axial gamma flux leakage.

The calorimeters mounted on the instrumentation boom operated as expected in the NRX-A2 test. The observed heating rates were in reasonable agreement with the expected heating rates. Of the calorimeters mounted on the rabbit gun boom the resistance temperature element failed on two units. The third unit gave data throughout the test but indicated noisy operation coincident with operation of the rabbit gun. Excessive vibration during operation of the rabbit gun apparently caused the failure in the other two probes. Inasmuch as the measurement in the calorimeter is an integrated measurement, the noise did not jeopardize the data. The heating rate is indicated by the slope of the output data and this slope indicated data

in accordance with predictions. The calorimeters as expected went off scale toward the end of the run. This is to be expected as they were reading integrated heating from which heating rate was calculated. (Over-temperature occurs at approximately 1000 watt-sec.)

In summary, the calorimeters performed well within expectations in the NRX-A2 test. The location of these transducers on the rabbit gun boom was a late change resulting from concern over possible vibration of the propellant coolant lines. The vibration of this rabbit gun was not anticipated. A different installation is planned for future tests.

The data on the calorimeter mounted on the instrument boom gave an indication that was 10 to 20 percent below the calculation. This, however, may be the result of self-shielding and gamma energy level. The heating rate level on the rabbit boom location indicates the expected factor of two relative to the instrument boom location. This has been determined to a large extent by observation of the thermocouple measurement on the inner shield of the calorimeter due to the noise reported above on the resistance temperature detectors.

4.5.5 Control System Performance During EP-4

Reactor control subsequent to startup was accomplished using time based programs of the controllable parameters (i.e., Log Power, LH_2 Flow, and Temperature). Station 32 thermocouples were chosen as the prime temperature control parameter, with exit gas as a backup. To evaluate the control system operation during the power run, a summary of the basic controls used is helpful.

Reactivity is varied by means of rotating the control drums about the critical position. The position demand for these drums is generated by the power controller based on the comparison of the measured Log Power with the resultant sum of the Log Power demand, the Man Power Trim Signal, and the Temperature Correction (or trim) signal. The Manual Power Trim can provide a correction to the power demand of from 0.5 to 2.0, whereas the extent of temperature correction is from 0.5 to 1.15. The temperature correction is essentially proportional to the integral of the error between the demanded and measured temperatures and thereby within its controllable limits is the overriding factor in power control.

In the initial portion of the run, the temperature demand exceeded the measured temperature, resulting in the temperature controller going to its +15% limit. As the measured temperature caught up, the controller began to correct the power program controlling the rate of temperature rise and at the 50 per cent hold the proper temperature was maintained.

At this point the operator adjusted the manual power trim from a zero correction to 1.6 to bring the output of the temperature controller to zero. This effectively corrects any errors in the measured or demanded log power signals based on the temperature signal. During the power rise from 50 to 76 per cent, the controllers functioned normally and temperature was maintained during the first half of this hold. Approximately half way through this hold, the indicated station 32 temperature began to reduce and continued to degrade for the remainder of the run. The temperature controller went to its -15 per cent limit and remained there for the balance of the test. The rise to the 93 per cent hold was accomplished with the flux loop being the only effective control. Upon leveling off at this power, the operator inserted a manual power increase in an attempt to bring the indicated exit gas temperature up to the predicted level for this hold.

In regard to the control system the following was concluded:

1. The overall control system performed properly at all times during the test within the limitations of the input signals.
2. During the period in which the station 32 temperatures were indicating properly, the temperature controller corrected the power demand to properly control the reactor heat power output.

3. The manual trim of 0.6 at the 50 per cent hold was required due to inaccuracies in the time based log power demand output. A 3 per cent error in the log scale results in approximately 40 per cent linear power error. This error was due to the use of a low accuracy Simpson Voltmeter for setup of the time based programmer. Subsequent testing using a differential volt meter verified the existance of this error.

4. Although the use of station 32 Thermocouples results in loss of temperature control during the run, it is of interest to note that regardless of the choice of prime temperature control parameters, the final power level would have been the same. The use of exit gas would have resulted in automatically balancing exit temperature demand to the indicated value, instead of the operator manually adjusting to this point. Also, if station 45 had been used, the saturation effect that occurred in their output at high power was predictable from calibration data (Reference Figure 4.5-3) and the controller would have properly controlled the reactor temperature.

4.5.6 Data System Performance

This section on the Data System Performance covers the data acquisition and reduction systems, channel operation, and that portion of sensor performance wherein channel performance was affected.

A. System Description

To understand the over-all data system picture, the NRX-A2 Data Acquisition and Reduction System is described. The two types of acquisition systems used are the PAM/FM Narrow Band and the FM/FM Wide Band.

Figure 4.5-4A is a simplified high level narrow band system. The narrow band system records frequencies from zero (DC) to 5 cps.

The transducers (for temperature, pressure, strain, acceleration, drum torque and position) mounted on the reactor and test car provide analog signals and are connected through the plug on the test car. From this plug they are wired to terminal boards in the Electronic Room and then to the signal conditioners.

The signal conditioners provide excitation voltages, bias voltages, zero shift correction, and a calibration means from a precision programmable power supply. The signal conditioner provides no amplification.

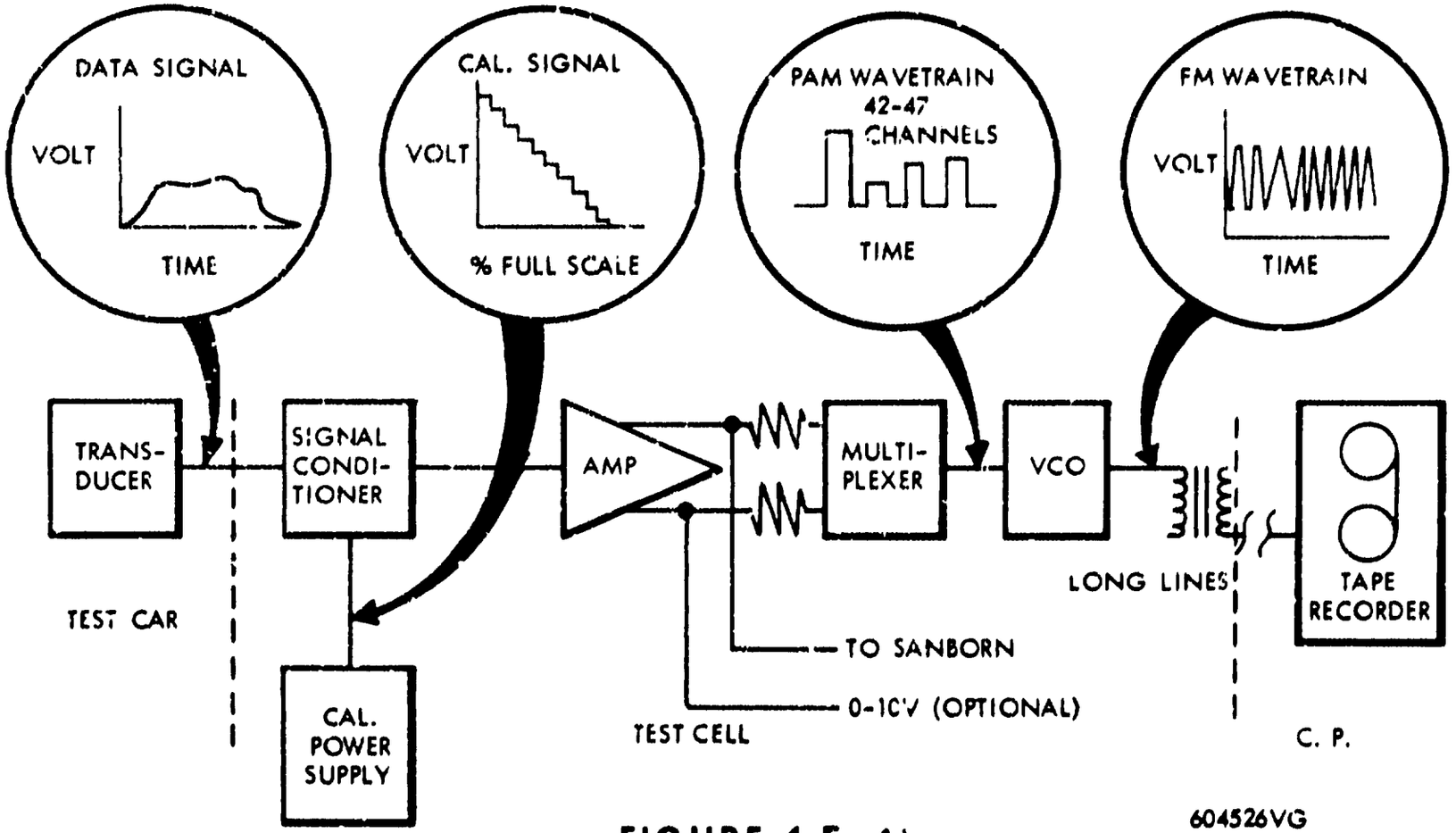

FIGURE 4.5-4A
SIMPLIFIED NARROW BAND DATA ACQUISITION

Astronuclear

The output of the signal conditioner in the high level system is the input to an Offner Amplifier #19.A which provides a dual output of 5 volts to the multiplexer and 10 volts for the quick-look Sanborn. In the low level system the signal conditioner output of 10, 20, or 40 mv is the input directly to the multiplexer; and then to the Dynamics #3557 amplifier which provides a 5 volt signal to the VCO.

There are two types of multiplexers, mechanical (10 samples/sec.) and solid state (40 samples/sec.). In this high level system diagram the solid state is used, and there are 47 channels available per multiplexer for data. The conversion from analog to Pulse Amplitude Modulated (PAM) signals is accomplished by the multiplexer. The multiplexer takes many analog input signals, samples each for a finite period of time while locking out all others, and then combines this information for transmission over a single carrier channel.

The PAM wave train then enters the voltage controlled oscillator (VCO), a voltage sensitive device which changes frequency in a given ratio to the applied PAM wave train voltages. Here, the data is changed from PAM signals to FM. Each PAM signal applied to the VCO causes a frequency change which is essentially a burst of a frequency for a finite time during the application of the pulse to the VCO. From the VCO the FM

signal goes to a line matching transformer for impedance matching and isolation; then over the long lines to the Control Point for recording on tape or visual display.

Figure 4.5-5 depicts the narrow band data processing. The FM tape records of the PAM/FM narrow band system are converted to digital values by a CDC 160A computer processing system at NRDS. A tape reader output is connected to a discriminator which changes the frequency modulated pulses back to a PAM signal similar to the output of the multiplexers. The PAM signal is decommutated and filtered before entering the analog-to-digital converter and format control units where the analog signal is converted into digital values in binary format. The binary data is then recorded on digital tape for future data reduction.

The IBM 704 computer performs a system calibration analysis on each data channel and reduces the data to a useful form. The IBM 704 also performs a correction to each data channel using the transducer calibration values.

The data from the IBM 704 is then converted to engineering units by application of the calibration information recorded with the data. A binary tape is prepared containing detailed instructions to the CDC-160A as to how to position the plotters for plotting the outputs in engineering units vs time.

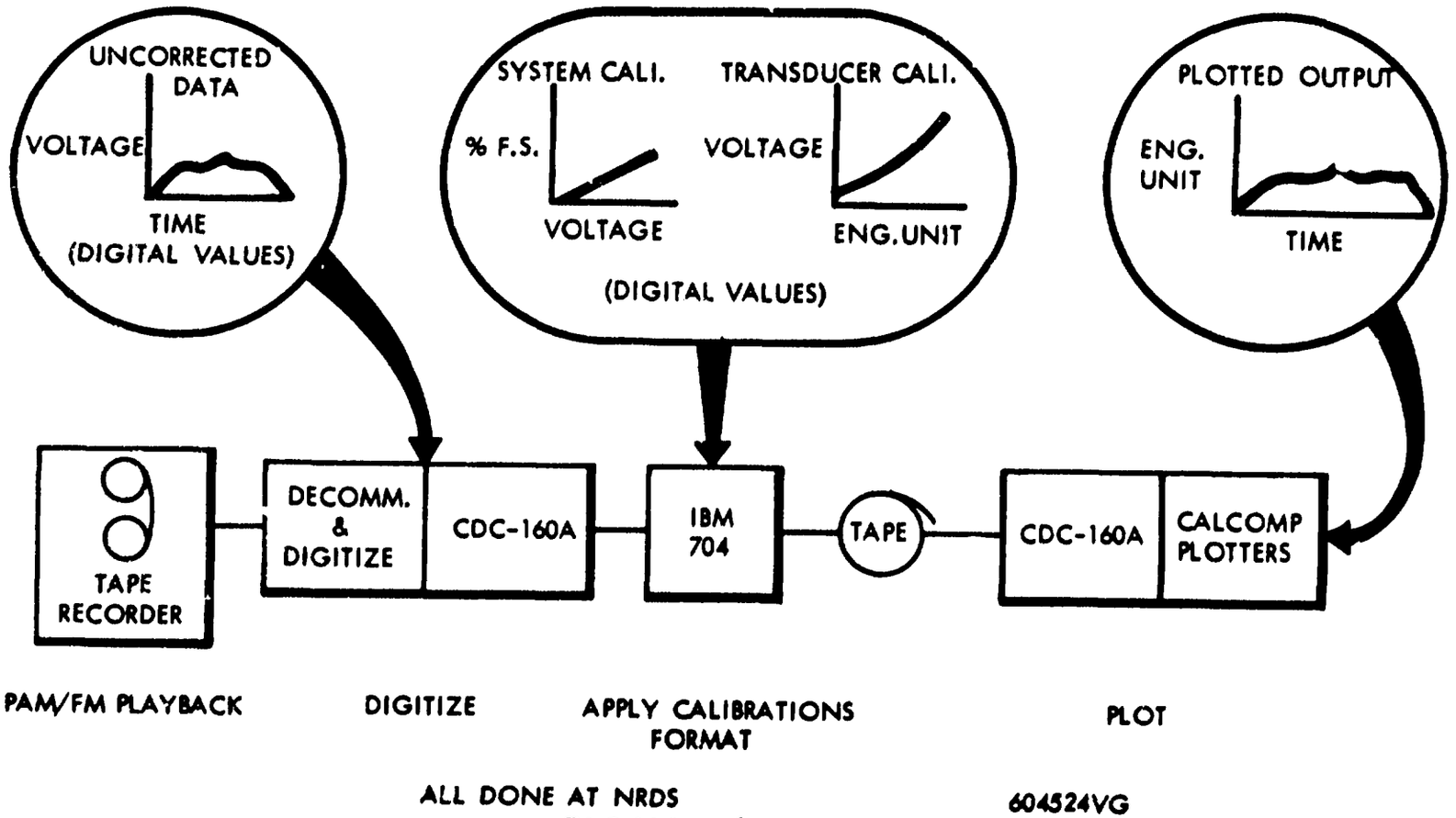

FIGURE 4.5-5
SIMPLIFIED NARROW BAND DATA PROCESSING

Astronuclear

Figure 4.5-6 depicts the simplified wide band data acquisition. All signals with primary frequency variations in excess of 10 cps, but below 1000 cps (specifically in the ranges of 300, 400, 500, 750, and 1000 cps) are handled by the wide band system. The signal conditioning is the same as previously described; however, all signal conditioners are directly wired into wide band amplifiers; then to VCO's, the outputs of which are mixed, 5 signals per multiplex. These signals are then recorded on one track of a wide band tape recorder at the Control Point. The signals themselves must be between 10 mv and 1 volt in amplitude.

The significant difference between the wide and narrow band systems is that the PAM/FM system is a sampled data (time multiplexed) system, whereas the FM/FM system is parallel type recording system (FM multiplexed) and the data is continuously recorded.

Figure 4.5-7 depicts the simplified wide band data reduction. The tape records of the FM/FM wide band system are sent to WAIL, Large, Pa., for analog-to-digital conversion. The wide band conversion system accepts its inputs from the analog tapes and converts them to a digital form suitable for use by the IBM 7094 computer.

The output from the tape playback is an FM composite signal, time versus voltage. It is discriminated and filtered, can go both to the GTC oscillographic recorder and to the analog-to-digital converter.

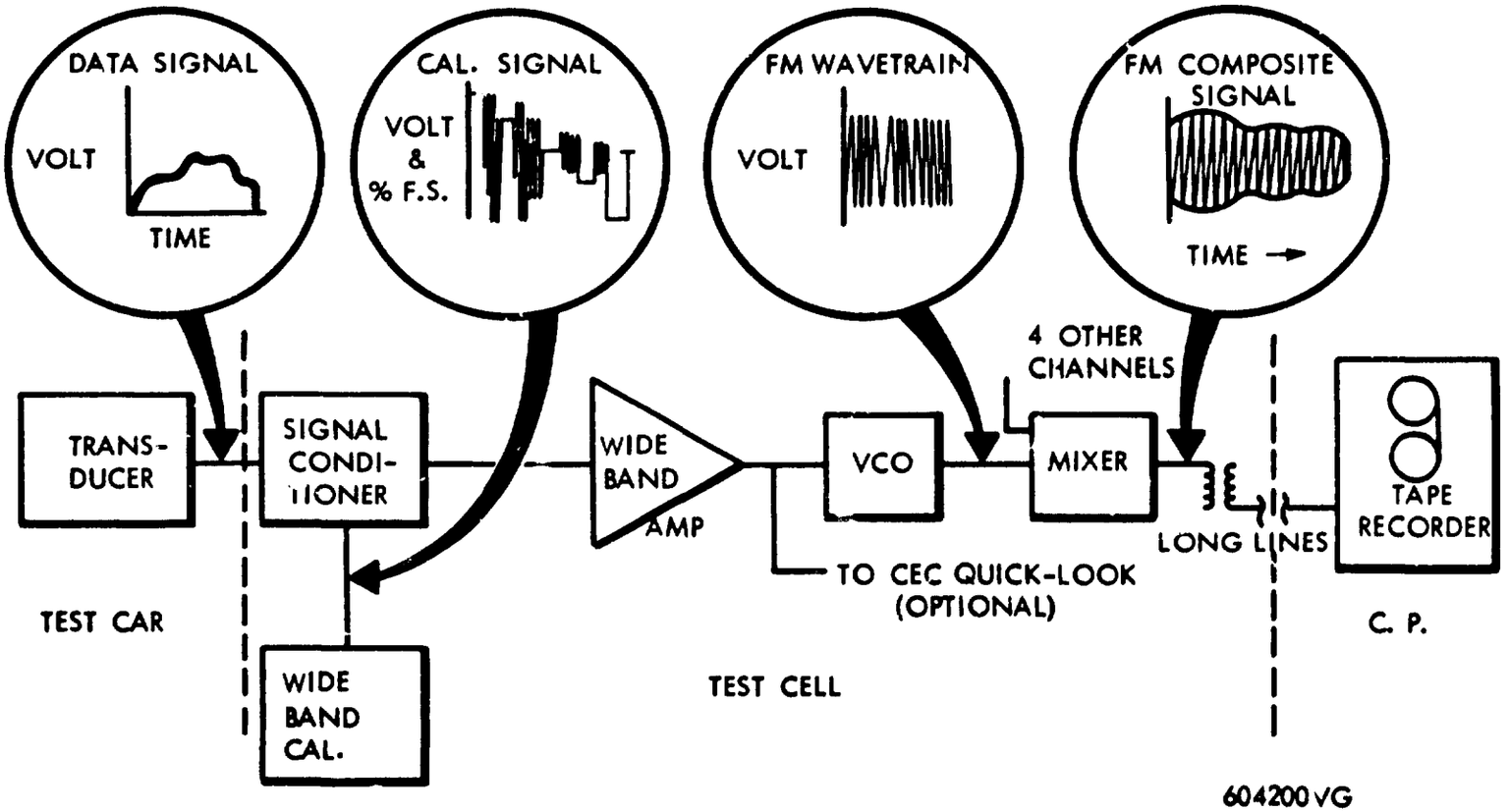

FIGURE 4.5-6
SIMPLIFIED WIDE BAND DATA ACQUISITION

Astronuclear

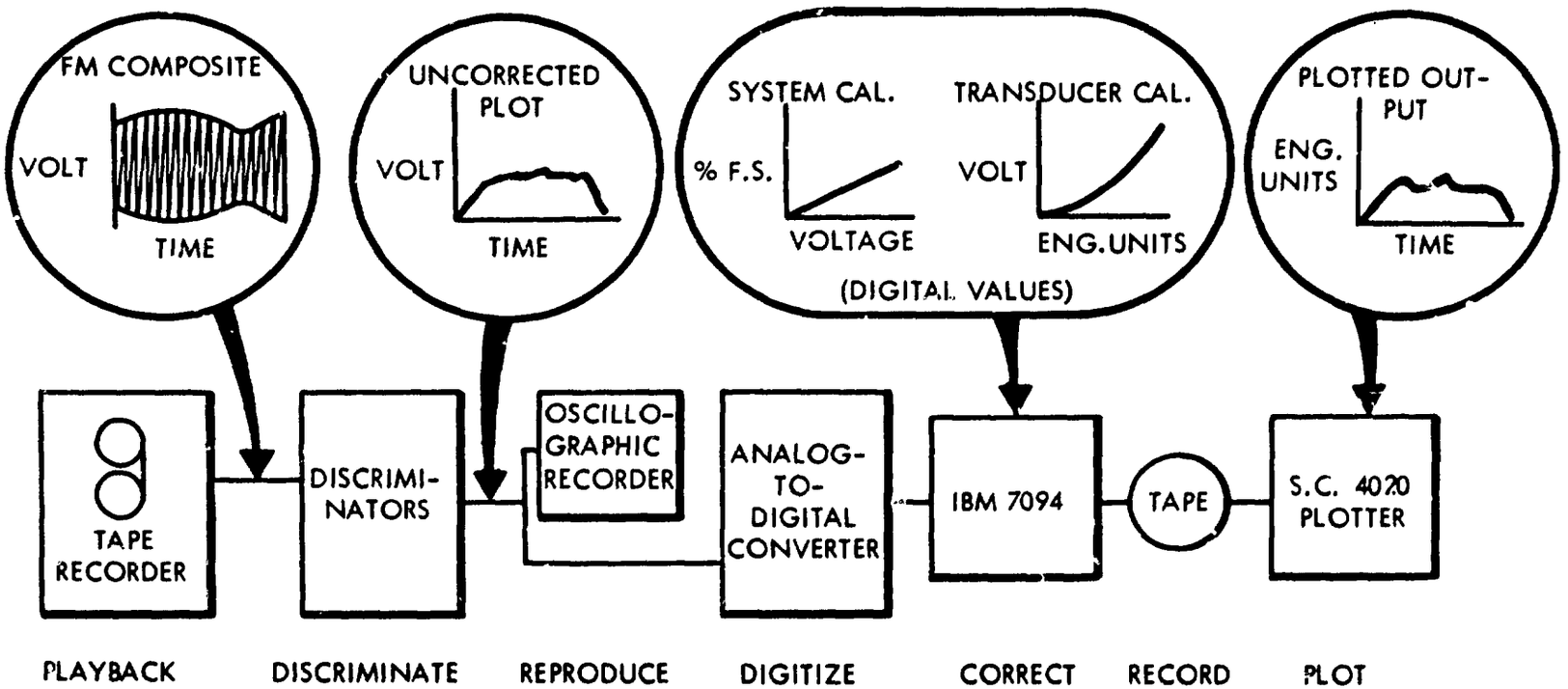

ALL WORK EXCEPT FINAL PLOT DONE AT WANL

604525VG

FIGURE 4.5-7
SIMPLIFIED WIDE BAND DATA REDUCTION

Astronuclear

After conversion, the IBM 7094 computer applies channel calibration and transducer corrections; converting data to physical quantities recorded on a working tape. Plotting tapes are produced and sent to an SC-4020 service center where the required curves are plotted.* These plots are returned to WANL for distribution.

B. Performance Summary

Figure 4.5-8, NRX-A2 Channel Anomaly Analysis, shows a bar graph tabulation of data channel performance. The probable causes of the discrepancies for the five test runs is indicated, plotted against the percentage of the total 379 channels which existed at the start of the test series.

These discrepancies have been classified as follows:

1.	Data Reduction	2.64%
2.	Data Acquisition (excluding wiring problems)	3.70%
3.	Wiring or Wrong Set-up	5.28%
4.	Anomalies Under Investigation	13.50%
5.	Transducer and Test Car Wiring Failures	14.00%

A definition for each classification is covered later in the section on the causes of cancelled channels.

---

*For further discussion, see NRX-A2 Twelve Week Data Processing Report, WANL-TME-1074, January, 1965.

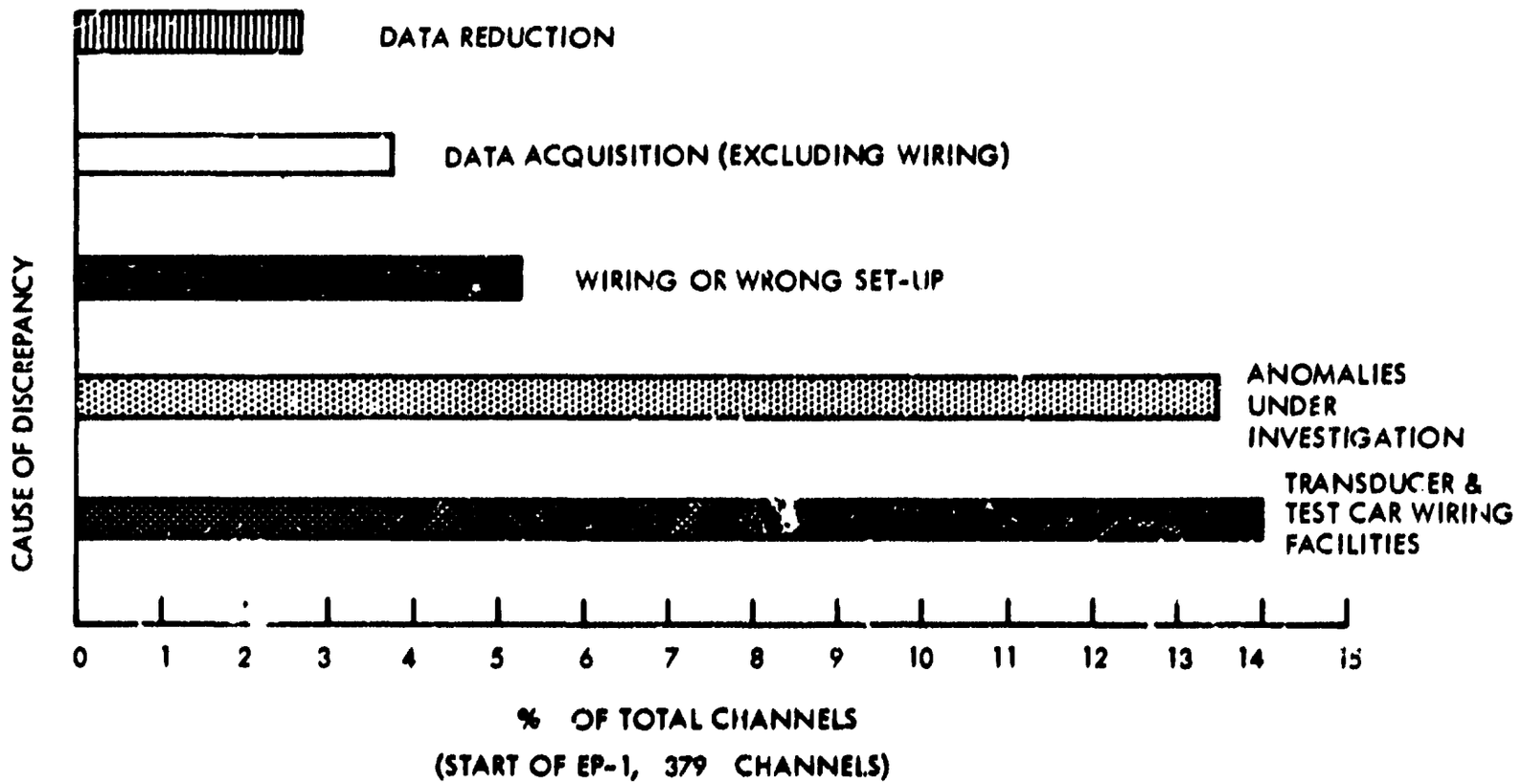

4.5-8 NRX-A2 CHANNEL ANOMALY ANALYSIS

604522VG

Figure 4.5-9 of WRM-A2 Channel Anomaly Analysis is also a bar graph type tabulation. This plot classifies the channel failure by channel designation. For each TP the number of channel failures is plotted vs the percent of total channels of each measured parameter at the start of TP-1. For the purpose of the bar graphs, a failure was defined as any channel from which useful data could not be obtained.

With the exception of the accelerometers in TP-1, the largest channel loss was the thermocouple measurements in TP-IV. Strain gage losses in TP-1 and IV were next highest. The remaining channel losses were 13% and under. With respect to the previous figure (4.5), 13.5% of these channels are presently under investigation.

The channel designation and totals used for this plot are as follows:

1.	T - Temperature, T/C and resistance type	225
2.	S - Strain gage	53
3.	A - Accelerometers	16
4.	P - Pressure, absolute and differential	55
5.	T - Drum torque	10
6.	- Drum position (Not shown on plot)	19
	Total Channels	379

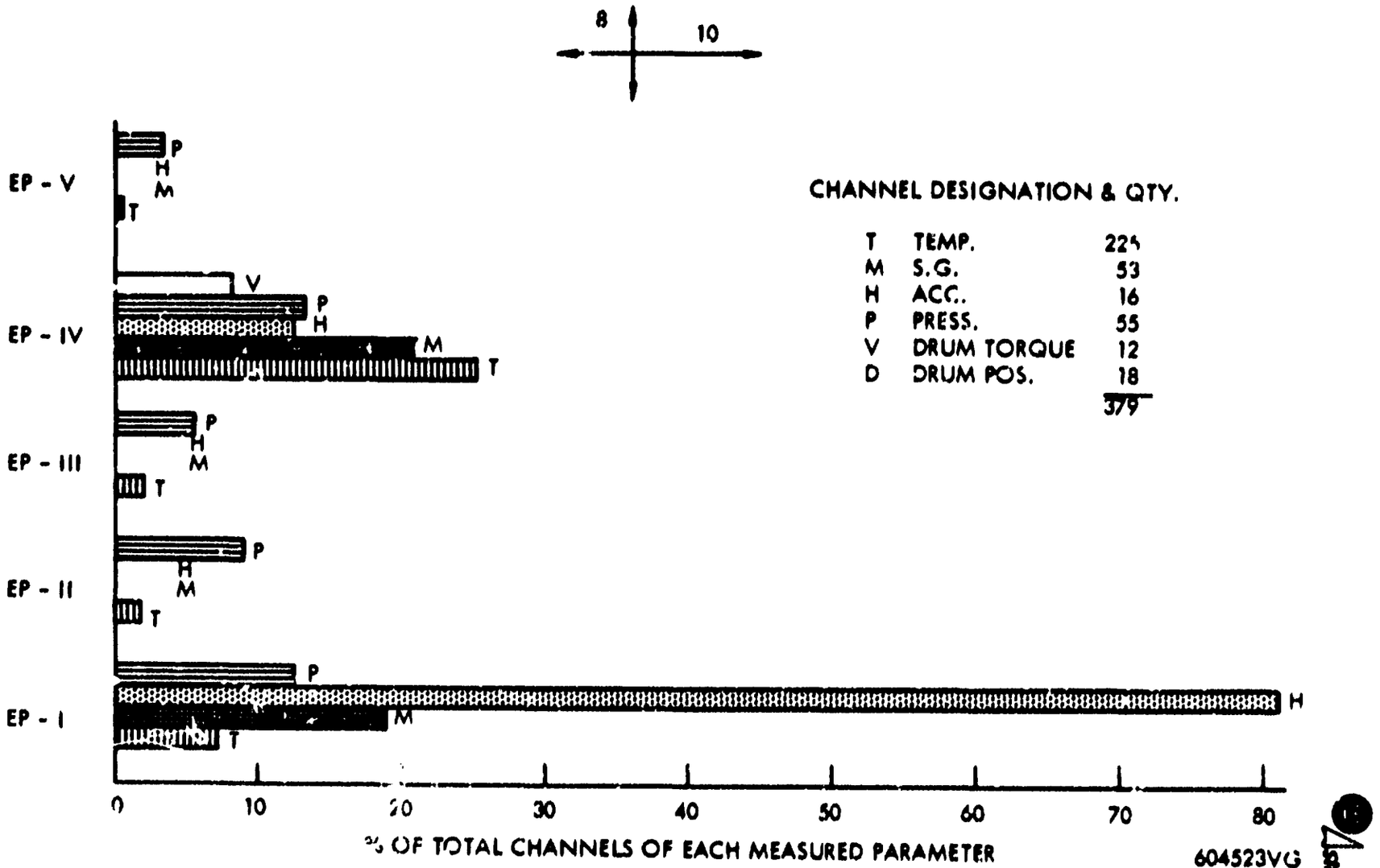

4.5-9 NRX-A2 CHANNEL ANOMALY ANALYSIS

c. Summary of Accountability for Defective Channels

1. Cancelled Channel Causes

To understand how the discrepancies were classified for Figure 4.5-8, it is important to know that the discrepancies were defined as follows:

a. Data Reduction - includes such causes as:

1) Noise due to improper magnetic tape erasure.

2) Low readings - normal malfunctions were checked out, but no anomalies found; to be further investigated.

3) Digital converter malfunction - Narrow band digitizer dropping bits causing displacement of parts of curve.

4) Playback of channel data without tape speed compensation

b. Data Acquisition - includes such causes as:

1) Incorrect ranging

2) Defective charge amplifier operation

3) Loss of excitation due to blown fuses

c. Wiring or Wrong Set-up

1) Study of channel setup indicates error from requested setup.

2) Wrong wire hook-up due to reversal in wire colors.

3) Thermocouple had reversed polarity.

d. Anomalies under investigation includes cases such as:

1) No dynamic output; yet transducer check and channel check show both to be functioning in good order.

2) Data appears to be scaled 10% low; yet a recheck shows no scaling errors.

3) Readings low; each transducer and its channel was checked through to the recording end without malfunction showing up that could account for these discrepancies.

4) Spurious and Noisy Data; Many of the data channels which appeared on the quick-look oscillograph showed data traces which were played back from the recorded magnetic tape. This is a problem that is still being investigated.

e. <u>Transducer and Test Car Wiring Failures</u> - A check is made from the first termination point in the Test Cell, showing:

1) Open transducers. readings "pegged" negative.

2) Bridge resistance changes over 100%.

2. Difficulties with channel data due to non-instrument problems.

a) Mis-Scaled Data

Data can become mis-scaled through any of the following:

1) Use of wrong calibration scale on Sanborns or CalComps.

2) Use of wrong resistance dividers in signal conditioners.

3) Improper set-up of transducer channel.

During the NRX-A2 test series, most of the errors connected with this category were committed by using the wrong scale on the Sanborn charts; when this error was detected on CalComp plots, they were re-plotted and re-issued.

b) Noise Problems

After EP-IV-A Power Test, the wideband system was played back onto oscillographic reporducers for one-site analysis. There were many reports of noisy channels on these playbacks; however, the playback center at NRDS is equipped with only one channel of compensation during playback. All channels which were reproduced with the use of this tape speed compensation (at WANL) demonstrated that most of the noise disappeared from the trace.

Some cases of noisy channels are traceable to re-used tapes on which the background noise had not fully been eliminated. It is possible that if both sides of the tape were not processed through the desausser that noise could still be present on the tape.

Another cause of noisy channels was uncovered after EP-V by resistance checks made in the test cell by R-MAD Building personnel. These checks showed that the shields on some transducer cables were shorted to ground. Grounding of cable shield in more than one place introduces a ground current in the shield and appears as noise on the data signals transmitted through this cable.

c. Unchanging and Intermittent Data

Discrepancies in this cateogry include those channels which showed no data except for a trace that remained unchanged throughout the test or which intermittently showed data traces that appeared valid for some time intervals during the test.

Many data channels were reported as discrepancies because the data trace on playback showed no change in position all through a particular test; the trace remained at zero or "pegged" negative or positive. Zero traces occurred when transducers lost their excitation voltage through blown fuses, broken or burned leads or faulty signal conditioners or amplifiers. Loss of excitation voltage could cause those channels which had negative nulling voltages applied to them to peg negative.

Intermittent data could have occurred through intermittently shorted or open lead wires caused by environment or vibration of the cables on the test assembly. There is a third possibility that the high neutron flux levels encountered during the power run could have changed the physical properties of transducer materials and as a result, the output of the transducer was affected and produced an unvarying or erratic trace.

D. Accuracy Evaluation of Data System

In January 1964, a study was conducted at NRDS to determine the overall accuracy and short term drift of the Test Cell "A" Data Acquisition System. A report entitled "Evaluation of Test Cell "A" Data Acquisition System", dated 20 March 1964, was issued covering the results of this te The study was performed to evaluate the static accuracy of both the wide band and narrow band systems from the signal conditioner through the recording and data reduction processes. Fourty-five channels were tested, 15 wide band channels, 15 low level narrow band channels, and 15 high level narrow band channels. The results of the tests are as follows:

1. Narrow Band High Level System: The average system error for 15 high level channels was 1.54% and the maximum error was 1.95%. The average system noise was 0.43%; the maximum noise was 1.0%. The average and maximum drifts were 0.46% and 1.0% respectively.

2. Narrow Band Low Level Systems: The average system error for the 15 low level channels was 0.92% and the maximum error was 1.56%. The average drift was 0.61% and the maximum recorded value was 10%.

The results of the wide band system are not presently available. The records are being evaluated at WANL-Large.

E. Recommended Improvements

The following is in progress to future test data:

1. Modification of the present temperature reference system to provide better temperature referencing.
2. Purchase and installation of 100 data acquisition amplifiers and eight multiplexers to replace equipment which is in poor condition.
3. A new data reduction code is being written to eliminate the errors and speed up the old code. This should provide a closer fit on the calibration curves and will prevent dropping bits in the narrow band digitizer.
4. An analysis of the wide band data acquisition and reduction system will be performed.
5. Transducer test equipment for testing transducer both in receiving inspection and when wired in the system

at the test cell is being completed. This should help to improve those channel losses due to wiring errors, amounting to 5% shown in Figure 4.5-8. Also, a data channel checker (scheduled to be completed in September) should further correct possible data acquisition discrepancies.

6. It should be noted that the improvements which were completed between the NRX-A1 and NRX-A2 tests have performed satisfactorily. For example: 1) the Sanborn and CEC long lines have been isolated from the wide band primary data channels; and, 2) reduction of cross talk on the CEC recorder long lines to less than 1% over the bandwidth of DC to 5 KC.

5.0 CONCLUSIONS

The major conclusions are summarized in this section. For more detailed discussions reference should be made to the section of this report treating that aspect of the test or to the separate report referenced in the text on a particular topic. All the conclusions but the final one listed generally apply to the high power run.

5.1 Overall

On the basis of a review and analysis of the NRX-A2 test data and observations, it is concluded that the test was successful in meeting its objectives as well as confirming the nuclear, thermal, flow, and mechanical design analysis methods. The reactor operated at sufficient power levels and duration to demonstrate mechanical, thermal and fuel performance.

The NRX-A2 power test has provided a sound basis and increased confidence for proceeding to the more stringent endurance and transient testing in NRX-A3.

5.2 Modifications Resulting from NRX-A1

The design and operational changes in NRX-A2 which resulted from experience with NRX-A1 were all successful. These changes included the increased clearance between the control drum and outer reflector sector for

NRX-A2 which limited the maximum control drum torques to low values with acceptable peaks of ±90 in/lb at the initiation of scram.

Design changes in the nozzle end spigot of the outer reflector sectors eliminated cracking in this component. In addition the increased clearance instituted for NRX-A2 eliminated the pressure vessel interference with the nozzle end support ring.

The flow lag experienced in NRX-A1 led to a flow profile modification for the power test having acceptable characteristics during startup. As predicted, flow choking observed at the orifices in NRX-A1 were not significant in NRX-A2.

5.3 Fuel Element Behavior

Generally the fuel behavior and weight losses observed were as expected, based on out of reactor corrosion tests and KIWI experience. The fuel manufacturing process and element design therefore were demonstrated as adequate for the conditions of the NRX-A2 test.

The most serious corrosion problem occurred along the fuel element flats adjacent to the pyrolytic graphite tile at the core periphery towards the hot end of the core. This corrosion was the result of hydrogen leaking in through filler strips and the large axial gaps between the pyro-tiles and contacting fuel at elevated temperature. In the single peripheral element where NbC coating was present on peripheral flats, corrosion was eliminated or reduced. It was decided therefore to coat the periphery of the NRX-A3 core with NbC. Modification of the pyro-tile installation

on the filler strip was also made to eliminate plenums and reduce hydrogen flow between tiles. In addition the periphery fuel will be kept approximately 300°R cooler by increased flow of coolant using appropriate orificing.

The hot end of fuel elements exhibited corrosion which was a function of the quality of the NbC coating present. The highest quality coated hot ends exhibited nearly perfect final conditions. This enhances the confidence in the unfueled coated tip concept, which will give a high quality coating, and provide corrosion resistance for the longer reactor tests, such as NRX-A3.

5.4 Power Level and Duration

Approximately six minutes were spent in the range of 50 - 100% of design power*. The most accurate estimate of power level is believed to be that based on a calculated nozzle chamber temperature and reactor enthalpy balance using the observed nozzle constants, nozzle chamber pressure and flow rate, in the calculations. This method is preferred to the direct measurement since it is reasonably certain that the nozzle chamber thermocouples were not measuring the mixed mean chamber temperature nor were other temperature measuring devices indicating accurately, as explained in the following section.

5.5 Instrumentation

In addition to not obtaining representative mixed mean nozzle chamber temperature, anomalies were also observed for station 32 core material

---

*112 MW

thermocouples, which were used for control. These thermocouples generally were indicating temperatures below that of the potting compound used. This failure, which was confirmed in the post-operational examination, permitted flow of cool gas around the thermocouple and explains the low temperature indication.

For the NRX-A3 test, one nozzle chamber thermocouple is inserted deeper into the flow stream to see if the probability of obtaining the mixed mean temperature can be impr For power control it is planned to use station 26 thermocouples, which run cooler than station 32, with a redesigned thermocouple installation not requiring potting compound. In addition multiple graphite ocks are used in the thermocouple channel in addition to an exit plug for flow blockage, and the thermocouples are not in peripheral locations as in NRX-A2 where they may have been sensitive to control drum position.

5.6 Control and Data Processing

The startup system, power control system, and temperature trim system performed as expected. The temperature trim was limited by the problems with the station 32 thermocouples. In the data processing system there were some minor problems associated with strain gauge data calibration, data offset and sign inversion which were resolved.

5.7 Nuclear Analysis

This analysis is concerned primarily with core power distribution, reactivity effects, heating rates of non-nuclear components, and radiation environment. The power distribution appears to be generally in agreement

with predictions as inferred from data on total fuel element radioactivity, and radial and axial temperature measurements. Based on the radial temperature profile, some discrepancy exists between the predicted and measured temperatures near the core periphery.

Reactivity effects of fuel and reflector temperature, hydrogen density and control drum position were predicted well. An apparent non-uniformity in individual control drum worth was observed but it has been shown that this was caused by variation in the critical drum band position during the time the individual measurement was made. After allowing for this variation, it was concluded that the reactivity worth of individual drums is approximately uniform.

In the power holds a difference was noticed between measured and calculated drum bank position. This difference decreased with time. A possible explanation of this effect is a time dependent hydrogen diffusion into the fuel material micropores. The off-design drum band position contributed to the non-flat radial temperature distribution at power.

Generally the observed heating rates in the reflector and radiation environment were within the range of prediction accuracy.

5.8 Mechanical Design Evaluation

Consideration of both static and dynamic responses, indicated that the core grew as a result of thermal effects slightly less than would be expected from calculations based on measured temperatures and nominal

material thermal expansion properties. It was evident that the core did not contact the inner reflector and remained essentially concentric with respect to it. There was strong evidence that at least one of the station 46 plunger pins stuck in the inner reflector cylinder during power reduction. Larger clearances and better fit procedures have been specified for NRX-A3 to eliminate this sticking. The measured tie rod loads agreed reasonably well with predictions. There was no evidence of high vibration levels of the reactor or its components.

In general, the NRX-A2 reactor performed extremely well structurally and survived the power test without serious mechanical damage. The following component damage occurred; bending of the aluminum barrel tabs at the forward end; removal problems with a few of the tie rod holders and cluster nuts at disassembly; two broken, unfueled, 13-hole instrumented central elements (believed to be broken during disassembly); and buckling of the tie rod coolant gas thermocouple probes. Design modifications have been made in NRX-A3 to eliminate or minimize these problems.

5.9 Thermal and Fluid Flow Analysis

Good agreement was obtained between measured and predicted values for the core pressure drop, core temperatures, reflector power, reflector material temperature, nozzle tube pressure drop, nozzle tube pressure drop, nozzle chamber pressure, and lat[illegible] support seal sy[illegible]m pressure distribution. After using a corrected value for annulus flow between the inner and outer reflector in post test calculations, agreement was obtained

between the test results and calculated reflector pressure drop. Fluid temperatures predicted by TMT were generally lower than measured at the core inlet and reflector inlet. Improved flow models are needed in these areas for more accurate predictions.

Higher temperatures than expected (200°R higher at maximum power hold) were measured for the tie rod coolant at the exit. Position of the thermocouples close to a solid surface is the most likely of a number of possible explanations for this observation.

The radial temperature distribution was not as flat as desired. This deviation resulted from the off-design control drum angle at power and off design core inlet temperature. These off design conditions have been analyzed and modifications have been instituted to obtain the desired radial temperature distribution in NRX-A3.

5.10 Low Power-Low Flow Mapping Test

This run demonstrated the stability of the system in the low power-low flow region. This stability was obtained under constant power (3.4% of design) for the flow range from 8.3 to 13.5 lb/sec, and for fixed control drum position (approximately 96.8°) with flow and power varying (5.2 - 13.5 lb/sec, 2 - 4.7%).

During these runs a maximum positive reactivity feedback condition of $ .43 was produced at 13.5 lb/sec and 3.4% of design power. At this condition it is significant to note that the core inlet temperature was

47°R at a pressure of 59 psia, indicating a two phase coolant at the core inlet without instability. This proves that for the test conditions the transition from single phase hydrogen to two phase does not cause a sudden or abrupt change in reactivity feedback. Therefore on the basis of these results, the core inlet temperature limitation of 90°R can be eliminated and replaced by a more general positive reactivity criterion. This change will simplify and increase the area of the reactor operating region since only a reactivity feedback limitation is required.

It is also significant that during the fixed control drum position runs, operation with little or no reactivity feedback compensation was demonstrated.

The successful attainment of the objectives of the low flow-low power run are very important to the effective and timely future planning of NRX, NRX/EST, and NERVA engine testing, and reactor shutdown cooling using liquid hydrogen.

6.0 APPENDIX

The Appendix consists of the following three sections:

6.1 Bibliography

6.2 Post-Operative Examination Summary Tables

6.3 Pre-Operational Preparation and Special Tests

CONFIDENTIAL
RESTRICTED DATA
Atomic Energy Act 1954

Astronuclear

6.1 BIBLIOGRAPHY

A. Test Description and Background

1. NRX-A2 Test Prediction Report, WANL-TME-887, July, 1964, CRD.
2. NRX-A2 Test Specification (revised to include Test Specification and Procedu Review Board and Test Review Board modifications), WANL-TNR-153 May, 1964, CRD.
3. NRX-A2 Site Test Report, NTO-R-0008, November 20, 1964, CRD.
4. NRX-A1 Test Final Report, WANL-TNR-176, September, 1964, CRD.

B. Nuclear, Thermal, and Fluid Flow

1. NRX-A2 Reactor Performance, WANL-TNR-199, February, 1965, CRD.

C. Mechanical Design

1. G. Downs, P. Stancampiano, P. C. Warner, NRX-A2 Post-Mortem Analysis, WANL-TME-1075, January, 1965, CRD.

D. Instrumentation, Control, and Data Processing

1. Instrumentation Review Meeting Minutes (of meeting held at SNPO, Cleveland 12/1-2/64) IC-3737, January 26, 1965, CRD.
2. M. W. [illegible]el. NRX-A2 Twelve-Week Data Processing Report,

CO[illegible]
RE[illegible]
Atomic [illegible]

3. G. M. Chambers, "NRX-A2 Instrumentation Final Disassembly and Post Operative Report", WANL-TME-1079, January 1965.

4. G. M. Chambers, "NRX-A2 Sensor Selection and Performance", WANL-TME-1117, March 1965.

E. Post-Operative Evaluation

1. J. Karbowski, NRX-A2 Post-Operative Mechanical Component Evaluation, WANL-TME-1071, February, 1965, CRD.

2. M. A. Vogel, C. R. Simmons, NRX-A2 Fuel Element Evaluation Report, WANL-TME-1122, February, 1965, CRD.

3. G. M. Chambers, NRX-A2 Instrumentation Disassembly and Post-Operative Report, WANL-TME-1079, January 8, 1965, CRD.

4. NRX-A2 Post-Test Report, NTO-R-0018, February 5, 1965, CRD.

F. AGC Reports (In Preparation)

1. An Analysis of System Data from NRX-A2, RN-S-0208, April, 1965.

2. Instrumentation Evaluation, NRX-A2 Test, RN-S-0193, April, 1965.

3. NRX-A2 Test Summary of Engineering Evaluation of S/N 009 Nozzle, RN-TM-0172, April, 1965.

4. Evaluation of the NRX-A2 Pressure Vessel and Propellant Inlet Line, RN-TM-0171, April, 1965.

Astronuclear

6.2 POST-OPERATIVE EXAMINATION SUMMARY TABLES

TABLE 6.2.1

Chart A

List of channels not operating at the start of each EP test and its mode of failure. Channels listed under each EP test are in addition to the channels listed in the previous EP test.

EP-I	EP-II	EP-III	EP-IV	EP-V	End of Test
Instal. Assy	Data Acquisition	None	Instal.Design	Sensor Design	Low Parameter Prediction
M 777	M 803		T 638	T 617	P 601
M 805	M 807		T 640	T 627	P 501*
T 327	P 501*		T 681	T 634	Data Acquisition
T 623			T 750	T 680	T 609
T 637			Instal. Assy	Instal. Assy	
			T 317	T 438	
				T 440	
				T 441	
				T 442	
				Instal. Design	
				T 619	
				T 622	
				T 625	
				T 632	
				T 663	
				T 642	
				T 646	
				T 643	
				T 648	
				T 649	
				T 650	
				T 651	
				T 673	
				T 678	
				T 751	

*This channel was not operating properly during EP-I through EP-IV but was operating satisfactory at start of EP-V.

Astronuclear

TABLE 6.2.1 (Cont)

Chart A

EP-I	EP-II	EP-III	EP-IV	EP-V	End of Test
				T 852 T 854 T 665 Data Acquisition P 306 T 313 T 757 Wiring T 606 T 773	

CONFIDENTIAL
RESTRICTED DATA
Atomic Energy Act 1954

Astronuclear

TABLE 6.2.1 (Cont)

Chart B

List of channels failed during EP tests. These channels are in addition to those listed in Chart A and were repaired or corrected prior to the start of the next EP test. The mode of failure for these channels was Data Acquisition.

EP-I	EP-II	EP-III	EP-IV	EP-V
M 776	M 415	None	P 603	None
M 801	T 642		M 422	
P 603	T 750		M 780	
T 313	T 784		T 315	
T 317	T 791		T 339	
T 333			T 386	
T 382			T 607	
T 537			T 612	
T 850				
T 851				
T 853				
T 857				
T 859				

Chart C

List of channels noted in Data Discrepancy Report having valid data for each EP test.

EP-I	EP-II	EP-III	EP-IV	EP-V
T 609	None	None	P 315*	None
T 613			P 423*	
T 882			P 601	
T 883			P 614*	
			T 613	
			T 616	
			T 784	

*These channels were scaled for EP-III and the data was as expected for EP-IV.

CONFIDENTIAL
RESTRICTED DATA
Atomic Energy Act 1954

TABLE 6.2-2

POST-OPERATIVE EXAMINATION SUMMARY, OUTER REFLECTOR ASSEMBLY, DOME END, AND CORE SUPPORT COMPONENTS

COMPONENT	REFERENCE DRAWING	NO. IN TEST ASSY.		VISUAL	DIMENSIONAL	PHOTOGRAPHY	RADIATION	BOW MEAS.	HIGH MAG.	DYE PENETRANT	SPECIMENS CUT	FLATNESS MEASUREMENTS	DISTORTION MEASUREMENT	DEFECTS	DESCRIPTION OF DEFECTS
Outer Reflector Assembly	WANL 937J118	1	Exam. Performed	x		x	x							No	
			No. on which performed	1		1	1								
Outer Reflector Sectors	WANL 909E533	12	Exam. Performed	x	x		x	x		x				No	
			No. on which performed	12	2		1	12		12					
Nozzle End Support	WANL 937J075	1	Exam. Performed	x			x						x	No	
			No. on which performed	1			1						1		
Dome End Support	WANL 937J077	1	Exam. Performed	x			x						x	No	
			No. on which performed	1			1						1		
Split Tube	WANL 944C906	12	Exam. Performed	x			x							No	
			No. on which performed	12			1								
Tie Bolts	WANL 978D319	36	Exam. Performed	x	x	x	x		x		x			No	One tie bolt was cut during disassembly.
			No. on which performed	36	4	4	1		4		4				
Tie Bolt Bushing and Nuts	WANL 944C905 963B333	36	Exam. Performed	x										Yes	Two nuts slightly galled. Thought to be result of disassy. ops
			No. on which performed	36											
Core Support Plate	WANL 937J212	1	Exam. Performed	x		x	x					x		No	Damaged during disassy. removal of cluster nuts.
			No. on which performed	1		1	1					1			
Dome End Seal	WANL 909E668	1	Exam. Performed	x			x				x			No	Seal "finger" showed no distortion.
			No. on which performed	1			1				1				
Support Ring & Support Ring Pin	WANL 934J696	1	Exam. Performed	x			x		x				x	No	
			No. on which performed	1			1		1				1		
Nozzle End Seal	WANL 909E431	1	Exam. Performed	x	x	x	x		x		x			No	
			No. on which performed	1	1	1	1		1		1				
Support Ring Bolts	WANL 9[illegible]C213	48	Exam. Performed	X					X					Yes	Last two threads on each bolt examd. were galled, thought to be due to disassy. ops.
			No. on which performed	48					18						
Control Drum Assemblies	WANL 937J090	12	Exam. Performed	x	x	x	x	x						No	
			No. on which performed	12	2	2	1	2							
Beryllium Cylinder	WANL 909E534	12	Exam. Performed	x	x	x		x	x	x				No	Slight discoloration.
			No. on which performed	2	2	2		2	2	1					
Boral Plates	WANL 977D791	36	Exam. Performed	x			x		x	x				No	
			No. on which performed	6			3		6	3					
Spring Retaining Bolts	WANL 945C476		Exam. Performed	x					x					No	
			No. on which performed	All					2						

CONFIDENTIAL
RESTRICTED DATA
Atomic Energy Act 1954

Aeronuclear

TABLE 6.2-2 (Cont)

COMPONENT	REFERENCE DRAWING	NO. IN TEST ASSY.		VISUAL	DIMENSIONAL	PHOTOGRAPHY	RADIATION	SOUND MEAS.	SLIP RING	TIE PERFORMANCE	STRAINING TIE	FLATNESS MEASUREMENTS	DISTORTION MEASUREMENTS	DEFECTS	DESCRIPTION OF DEFECTS
Nozzle End Bearing Retainer Nut	WANL [illegible]	12	Exam. Performed	X			X		X					Yes	Inboard end of nut.
			No. on which performed	12			12		12						
Outer Springs	WANL [illegible]	12	Exam. Performed	X		X	X		X	X				No	
			No. on which performed	12		2	2		2	2					
Inner Springs	WANL [illegible]	12	Exam. Performed	X			X		X					No	
			No. on which performed	2			2		2						
Control Drum Coupling	WANL [illegible]	12	Exam. Performed	X		X	X		X					Yes	No. 2 coupling had several pulled teeth.
			No. on which performed	12		2	2		2						
Dome End Bearing Housing	WANL [illegible]	12	Exam. Performed	X		X	X		X					Yes	Distortion around exterior bolt hole retaining sleeves.
			No. on which performed	12		2	2		2						
Dome End Bearing Retaining Nuts	WANL [illegible]	12	Exam. Performed	X		X	X		X					No	
			No. on which performed	12		2	2		2						
Bearings	WANL [illegible]	24	Exam. Performed	X			X		X					Yes	Inner race slightly scored by retainers slightly discolored.
			No. on which performed	24		2	2		2						
Dome End Spring Seat	WANL [illegible]	[illegible]	Exam. Performed	X		X	X	X						Yes	Localized nicks.
			No. on which performed	[illegible]		2	2	2							
Flow Screen	WANL [illegible]	1	Exam. Performed	X		X	X	X						No	Slight amount of foreign material found to be due to lingering.
			No. on which performed	1		1	1	1							
Simulated Shield	WANL 93/J080	1	Exam. Performed	X		X	X							No	
			No. on which performed	1		1	1								

CONFIDENTIAL
RESTRICTED DATA
Atomic Energy Act - 1954

TABLE 6.2-3

POST-OPERATIVE EXAMINATION SUMMARY, NON-NUCLEAR HARDWARE

COMPONENT	REFERENCE DRAWING	ASSEMBLY		VISUAL	DIMENSIONAL	PHOTOGRAPHY	TENSILE	ELECTRICAL	DEFECTS	DESCRIPTION OF DEFECTS
Nozzle Clamp Assembly	3-510119-00	1	Exam.	X					No	
			Perf.							
			No.	1						
Nozzle	AGC 285950-19	1	Exam.	X		X			No	
			Perf.							
			No.	2		2				
Nozzle Seal	AGC 702154	1	Exam.	X		X			Yes	Seal surface oxide
			Perf.							
			No.	1		1				
Nozzle Bolts	AGC 265233-9	96	Exam.	X	X	X	X		No	
			Perf.							
			No.	96	12	12	12			
Pressure Vessel	AGC 298238-IM	1	Exam.	X		X			No	
			Perf.							
			No.	2		2				
Forward Closure	AGC 703887-3B	1	Exam.	X		X			No	Port "A" seal seated improperly
			Perf.							
			No.	2		2				
Forward Closure Bolts	AGC 286664-3	120	Exam.	X		X	X		No	
			Perf.							
			No.	120		6	6			
Forward Closure Bolt Washers	AGC W-39969-WC22	120	Exam.	X		X			No	
			Perf.							
			No.	20		6				
Guide Tubes	-----	12	Exam.	X		X			No	
			Perf.							
			No.	12		12				
Drive Shafts	WANL 976D098	12	Exam.	X		X			No	
			Perf.							
			No.	12		12				
Cable Assemblies	AGC 706507	4	Exam.	X		X		X	Yes	"B" film on one showed slight discoloration
			Perf.							
			No.	4		1		4		
Cable Assemblies	AGC 706724	7	Exam.	X		X		X	Yes	*
			Perf.							
			No.	7		1		7		
Cable Assemblies	AGC 701679	4	Exam.	X		X		X	Yes	*
			Perf.							
			No.	4		1		4		
Cable Assemblies	AGC 299767	7	Exam.	X		X		X	Yes	*
			Perf.							
			No.	4		1		3		
Cable Assemblies	AGC 700286	22	Exam.	X		X			No	
			Perf.							
			No.	8		1				
Cable Assemblies	AGC 706725	4	Exam.	X		X			No	
			Perf.							
			No.	4		1				
Cable Assemblies	AGC 701238	25	Exam.	X		X			Yes	*
			Perf.							
			No.	14		1				
LVDT Mounting Hardware		4	Exam.							No examination.
			Perf.							
			No.							
Accelerometer Mounting Hardware		16	Exam.	X		X			Yes	Discoloration of coolant gens.
			Perf.							
			No.	13		1				
Tube Assembly	AGC 700090-79		Exam.	X		X			Yes	Slight discoloration.
			Perf.							
			No.	1		1				
Clevite Accelerometers	AGC 701565		Exam.	X		X		X	No	*
			Perf.							
			No.	12		9		12		
Forward Closure Seal	AGC 286766	1	Exam.	X		X			Yes	Seal surface oxide. (Specimen taken.)
			Perf.							
			No.	2		2				

*Further details are given in NRX-A2 Post Test Report, NTO-R-[illegible]18, February 5, 1965 - CRD

CONFIDENTIAL
RESTRICTED DATA
Atomic Energy Act - 1954

ASTRONUCLEAR

CONFIDENTIAL
RESTRICTED DATA
Atomic Energy Act - 1954

Astronuclear

TABLE 6.2-4

POST-OPERATIVE EXAMINATION SUMMARY, CORE REGION COMPONENTS

COMPONENT	REFERENCE DRAWING		VISUAL	DIMENSIONAL	PHOTOGRAPHY	SPECTOGRAMS	TEST DEFECTS	DESCRIPTION OF DEFECTS
Aluminum Barrel	WANL 937J279	Examinations Perf.	x		x		No	
		No.	2		2			
Core Barrel Screws	WANL 945D685	Examinations Perf.						Not removed.
		No.						
Inner Reflector Cylinder	WANL 936J568	Examinations Perf.	x	x	x	x	Yes	Discoloration.
		No.	2	1	2	1		
Plungers	963B764 963B761	Examinations Perf.	x	x	x		No	
		No.	60	44	20			
Lateral Segments		Examinations Perf.	x		x		No	
		No.	20		6			
Filler Strips, Blocks, Tile		Examinations Perf.	x		x		Yes	Slight corrosion, see Section 4.3
		No.	20		-			
Axial Spring Rings	936J482 909B446	Examinations Perf.	x		x		No	
		No.	2		2			
Axial Preload Springs	964B150 WANL	Examinations Perf.	x	x	x		No	See text.
		No.	8	8	8			
Axial Preload Springs	WANL 964B151	Examinations Perf.	x	x	x		No	See text.
		No.	8	8	8			
Cluster Nuts	WANL 945C Series	Examinations Perf.	x		x		Yes	Thread galled. See Section 4.3
		No.	20		10			
Tie Rod Holders	WANL 977D774	Examinations Perf.	x		x		Yes	Threads galled. See text.
		No.	20		10			
Cluster Plates	976D Series	Examinations Perf.	x		x		No	Color varied.
		No.	All		25			
Cluster Support Blocks		Examinations Perf.	x		x	x	Yes	Bore corrosion. See text.
		No.	All		25	1		
Tie Rods	WANL 944C732	Examinations Perf.	x	x	x		No	
		No.	All		10			
Tie Rod Nuts		Examinations Perf.	x		x		No	
		No.	All		10			
Cluster Springs	946C053 963B434	Examinations Perf.	x				No	
		No.	All					
Cups, Washers, Spacers		Examinations Perf.	x		x		No	Flaking, disass. ops. damage.
		No.	All		10			
Support Cones	WANL 976D449	Examinations Perf.	x	x	x		No	
		No.	All		10			
Center Unfueled Elements		Examinations Perf.	x	x	x	x		See Section 4.3
		No.						
Liner Tubes		Examinations Perf.	x		x	x		See Section 4.3
		No.						
Insulating Tile		Examinations Perf.	x		x			See Section 4.3
		No.						

CONFIDENTIAL
RESTRICTED DATA
Atomic Energy Act - 1954

6.3 PRE-OPERATIONAL PREPARATION AND SPECIAL TESTS

6.3.1 NRX-A2 ASSEMBLY AND PRE-TEST OPERATIONS

The NRX-A2 Test Assembly was prepared for testing during the months of July and August of 1964. Assembly operation started on July 2, 1964, at the R-MAD area with the unloading of the reactor from its shipping container. Transfer of the Test Assembly to Test Cell A was carried out on July 23, 1964; the nozzle had not been installed. Scheduling problems of the RN-5 nozzle (specified up to that time as the prime nozzle for the NRX-A2 Test Assembly) and a re-evaluation of the AGC stainless steel nozzle resulted in using the AGC nozzle for the NRX-A2 Test Assembly. The nozzle was subsequently installed prior to EP-IE. A more detailed discussion of operations associated with the NRX-A2 Assembly and preparation for testing can be found in the NRX-A2 Assembly Report.*

A. Receiving and Inspection

All components for the NRX-A2 Test Assembly were inspected at the R-MAD Building for evidence of shipping damage, inventory and possible interference problems during assembly.

---

*NRX-A2 Assembly and Preparation for Testing, NTO-R-0007, October 16, 1964.

The Pressure Vessel and Forward Closure were transferred to the R-MAD Building on June 23, 1964, approximately two weeks after arrival at the site. This delay was the result of the R-MAD Clean Room not being finished on schedule.

The KRX-A2 Reactor/Pressure Vessel Assembly was assembled in a clean room to reduce the possibility of entry of foreign material into the assembly which could block the reactor flow screen or fuel element orifices. Since the KIWI reactor was being assembled in the R-MAD Clear Assembly Bay, a temporary plywood enclosure was built in the Test Car Assembly Bay for use as a Clean Room during KRX-A2 assembly.

The Pressure Vessel/Forward Closure Assembly was moved to the Clean Room, placed in the Trunnion Fixture, and the Forward Closure removed. The inspection of the non-nuclear hardware revealed that there were approximately ten areas of slight damage on the Pressure Vessel Forward Closure Flange, that the Forward Closure Guide Tube seal surfaces required re-work, and that the entire assembly required extensive cleaning. In general, the corrective action required was carried out prior to the reactor arrival on June 30, 1964 from MARL.

The Control Drum Actuators were received and the Receiving Inspection Procedure performed.

The Simulated Shield arrived from WANL on June 24 and was inspected. The inspection revealed that approximately half the flow holes were burred and that the shield surface and flow holes required cleaning.

The special train from WANL-Large, with the reactor assembly, arrieved in Las Vegas on June 30, 1964*, with arrival at NRDS on the same day. The removal of the inner shipping container from outer shipping container, and the removal of the reactor assembly from the inner container were accomplished. The reactor was moved directly from the inner container to the Clean Room and installed in the pressure vessel on July 2. Results of the reactor inspection revealed pieces of gold plating from instrumentation leads on the flow screen.

The AGC stainless steel nozzle was received at NRDS on August 8 and was not inspected as originally planned because of a prior inspection by NTO Quality Control at AGC. The polyethylene covering around the nozzle was only removed on the sides to allow for instrumentation installation.

B. Assembly Operations

1. Assembly of Components Into Pressuve Vessel

The assembly of components into the pressure vessel started on July 2 with the installation of the reactor. After removing the control

---

*R. D. Davis, NRX-A2 Reactor Shipping Report, GSE-1200, (in preparation).

drum shipping locks and performing the required control drum torque checks, the shipping clamps were removed from the flow screen. In order to reduce the possibility of foreign material entering the fuel element orifices, the flow screen was shipped in place and not removed at NRDS.

The Simulated Shield was mated in the Pressure Vessel without incident. During this installation of the instrumentation hardware in the shield, the nut on the Port B galled on the sleeve. Since the nut could not be removed, an ETO fabricated split bushing was installed between the nut and the shield sleeve.

Final inspection of the Pressure Vessel Forward Closure Omega Seal just prior to mating the Forward Closure to the vessel, revealed a scratch in the seal. The seal was replaced and the Forward Closure installed.

During bolting down of the Forward Closure, it was found that the Pressure Vessel Forward Closure Flange Bolt Hole #32 (counter clockwise from $\theta = 0°$) would not accept a bolt. The bolt hole threads seemed to be scored. The #32 bolt was inserted and torqued to the required value after tapping the hole.

Following installation of the instrumentation port hardware, the control drum drive shafts were inserted through the Forward Closure and coupled to the control drums. This was followed by the installation of the guide tubes which were torqued to 60 $\pm$20 ft/lbs.

The leak check closure was installed on the nozzle end of the vessel, following rotation, and the pressure check of the assembly initiated. Upon initial pressurization, it was found that all guide tube K seals were leaking. The Test Specification and Procedure Review Board approved increasing the torque to 120 ft/lbs. A 15 psig pressure check revealed that all guide tubes were still leaking. Subsequent operations, including replacement of the K seals and the use of Dupont Slip Spray, resulted in sealing nine guide tubes with the application of 160 ft/lbs torque. The remaining tubes were torqued at values up to the maximum allowable value of 240 ft/lbs. A 100 psig helium leak check was then carried out with no leakage observed. It should be pointed out that the problem of sealing the guide tubes was also experienced during NRX-A1 assembly operation.

2. Privy Plug Installation

The Reactor/Vessel Assembly was placed on the Reactor Support Stand on July 11, 1964. The Reactor Support Stand had previously been installed with the Privy Plug on the Privy Plug Stand. The routing of the instrumentation leads on to the Privy Plug was completed and preparations were made to mate the Reactor/Vessel Assembly to the Test Car.

3. Installation of Reactor/Vessel Assembly on Test Car

The Reactor/Vessel Assembly was placed on the privy roof of the Test Car on July 13, 1964.

Upon completion of this operation, actuator installation and instrumentation hook-up and checkout started. Because the NRX-A2 nozzle had not yet been delivered to the site, the planned sequence of operations could not be carried out and was modified accordingly.

The propellant inlet line to be used with the RE-6 nozzle was cleaned, and insulated with one-inch thick cork. The inlet assembly was then installed on the Test Car.

On July 23, 1964, the Test Assembly was given final preparation for transfer to Test Cell A. The condition of the Test Assembly at this time was as follows:

a. The leak check closure plate was still in place.

b. All poison wires were still in the core.

c. The NRX-A2 nozzle was not yet installed.

d. The propellant inlet line assembly (for RE-6 nozzle) was installed.

e. The Pressure Check Piping Assembly was installed.

f. All instrumentation (except for that on the nozzle) had been installed, hooked up and checked out from the front of the Test Car.

C. Test Car/Test Cell Mate-Up

The transfer of the NRX-A2 Test Assembly to Test Cell A was accomplished on July 23 (Figure 6.3-1). Upon arrival at the Test Cell A, problems were encountered in pushing the Test Car onto the outrigger and in aligning the test cell jacks to the jack retainers on the Test Car. The T-6 Test Car (used for the NRX-A2 assembly) had not been trial fitted at Test Cell A during Test Car Build-up. The jacking operation of the mate-up procedure was accomplished the morning of July 24. Work then commenced on the following operations:

1. Connection of all service lines between the Test Car and the Test Cell.
2. Leak checks of the interface piping connections of the service lines.
3. Performance of resistance checks from the first test cell termination point through the master plugs to the transducers.

On July 30, a LN_2 pressure check of the propellant inlet line assembly, purge line and feed line was stated. When word was received that the AGC stainless steel S/N 9 nozzle was to be used, all work on the pressure checking was terminated and the RN-6 propellant feed line assembly was removed and transferred to the R-MAD Building. The following operations were than completed:

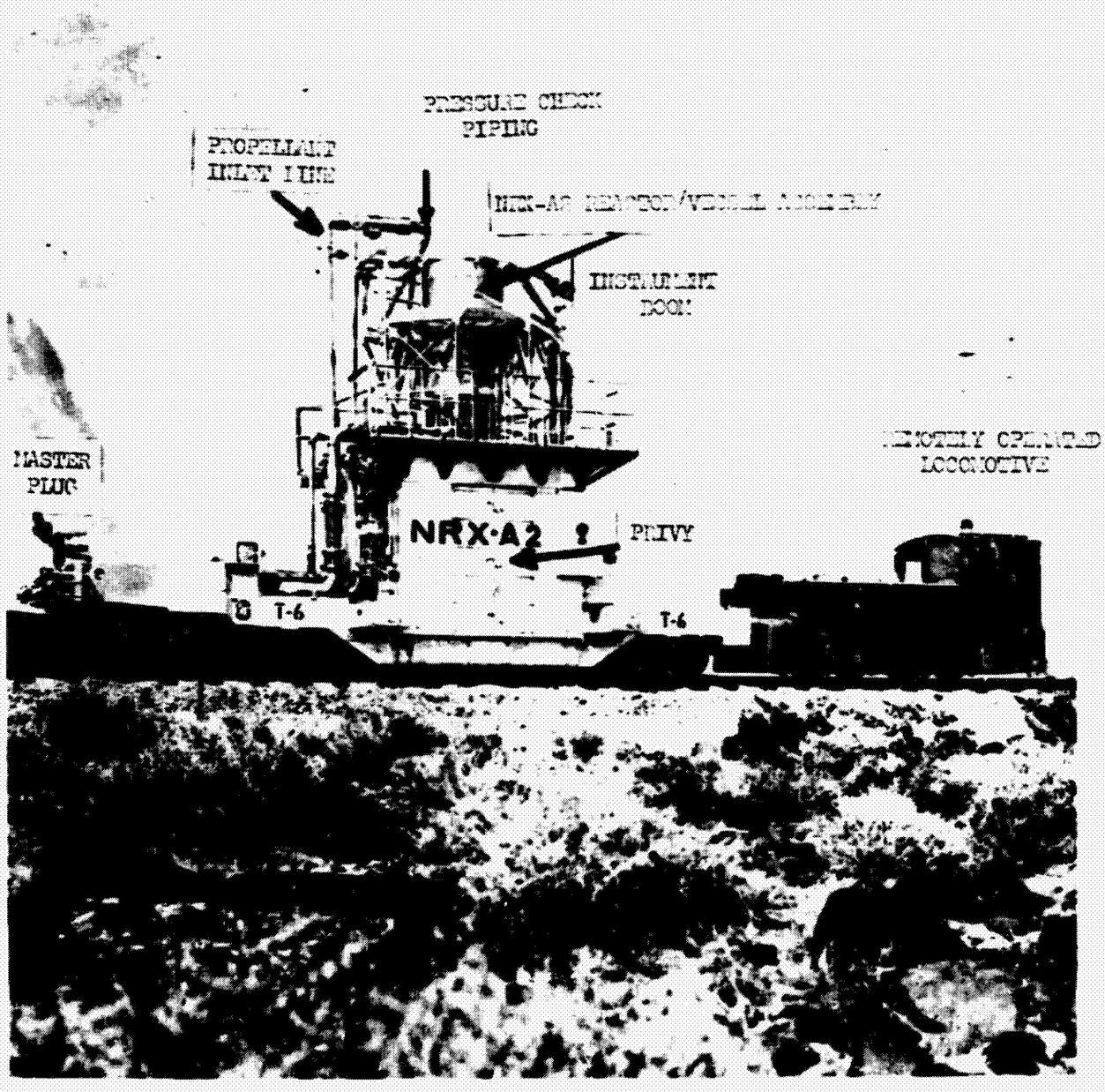

FIGURE 6.3-1
NRX-A2 TEST ASSEMBLY ON
WAY TO TEST CELL "A"

1. Cleaning of the propellant inlet riser for the AGC nozzle.
2. Insulation of the AGC propellant inlet riser (one-inch thickness of cork).
3. Installation of the propellant inlet riser onto the Test Car.
4. Installation and checkout of the propellant line instrumentation.

After the propellant inlet line assembly installation onto the Test Car, the Pressure Check Piping Assembly was again installed.

On August 3, the cryogenic leak check of the propellant line was started. The test resulted in over-pressurization of the line during the ambient gas phase of the test. The over-pressurization was 50 psi above the vendor check pressure on the same line and a subsequent visual inspection of the propellant line revealed no apparent damage. The test consisted of the following.

a. A GN_2 pressure test to 1250 psig.
b. A LN_2 test to 1000 psig.
c. A LN_2 test to a steady state of 1000 psig for 10 minutes. In obtaining a steady state condition, a pressure of 1100 psig was obtained.
d. Following the cryogenic pressure test normal test cell connections were completed and were pressure checked to 80[illegible] psig with helium.

In preparation for the Test Car Plumbing Checkout run on August 8, the instrumentation checkout was completed, the privy leak check carried out and the OBV-86 checkout performed.

D. Peripheral Poison Wire Removal

Peripheral poison wire removal operations were completed at Test Cell A on August 10 and 11, 1964. For this operation, a polyethylene tent was designed and fabricated. The tent was placed over the Reactor/Vessel Assembly and allowed personnel to work at the reactor top in a clean room condition. The operation was completed in approximately 8 hours.

Three men, stationed on the reactor catwalk, located, pulled and identified the specific poison wire clusters. One man, located on the privy roof platform, moved the wires from the reactor catwalk, out of the Clean Tent, to Quality Control on the Test Cell Pad. Quality Control inspected the wires for defects and verified the actual number of wires removed. The poison wires were monitored for contamination. Further data on poison wires is given in the site report* and in Section 4.4

6.3.2 NRX-A2 VIBRATION TESTS

The NRX-A2 Vibration Tests were completed between EP-IA and EP-IB during the period August 21 to August 25. These tests were completed to

*NRX-A2 Site Test Report, NTO-R-0008, November 20, 1964, CRD

satisfy the requirements of Appendix E of the NRX-A2 Test Specification. This Specification was an addition to the original Test Specification.

The objectives of the vibration tests were as follows:

a. To determine the resonant frequencies, mode shapes and amplifications of the nozzle and the propellant line.

b. To determine the coupling between the propellant line and nozzle and the nozzle and pressure vessel.

Vibration testing was initiated following installation of the nozzle at the completion of EP-IA. A total of thirty-six accelerometers were mounted on the propellant line, nozzle pressure vessel and reactor support stand for this test. They were removed prior to the EP-IB test.

The accelerometers were of the crystal type and were accurate up to 2000 cps. The tests were performed by inducing vibratory forces to the Test Assembly using a seismically mounted exciter. Output of the exciter could be controlled continuously over the ranges of 0 to 50 lbs force and 15 to 2000 cps frequency.

Two data acquisition systems were employed during these tests. These systems were not a part of the normal NRX-A2 data system. A quick-look data system was used to identify the resonant frequencies. This system provided continuous dynamic response information from 12 transducers; eight of these channels were recorded on tape. The second data

system was used to obtain data to define the wave shapes of the resonant frequencies. A digital printer data acquisition system recorded 24 channels of information during the discrete frequency testing.

Four tests were performed as follows:

Test I - Excitation at the propellant line-nozzle torus junction in a horizontal plane perpendicular to the propellant line, i.e., tangent to the nozzle torus.

Test II - Excitation at the nozzle torus $\theta = 300°$ in a horizontal plane and a radial direction.

Test III - Excitation at the nozzle torus at $\theta = 75°$ in a horizontal plane and a radial direction.

Test IV - Same location as Test III except that excitation was in a vertical plane.

The excitation points and accelerometer mounting locations are shown in Figures 6.3-2 and 6.3-3, respectively. A similar test was completed during NRX-A1 testing. For the NRX-A1 Tests, the maximum excitation force was 2250 lb and the frequency range was from 5 to 75 cps. Results from the NRX-A1 Test were reported previously.*

---

*NRX-A1 Thirty-Six Day Test Report, NRX-A1-R-5, May 22, 1964 - NRX-A1 Test, Final Report, WANL-TNR-176, September, 1964 - CRD.

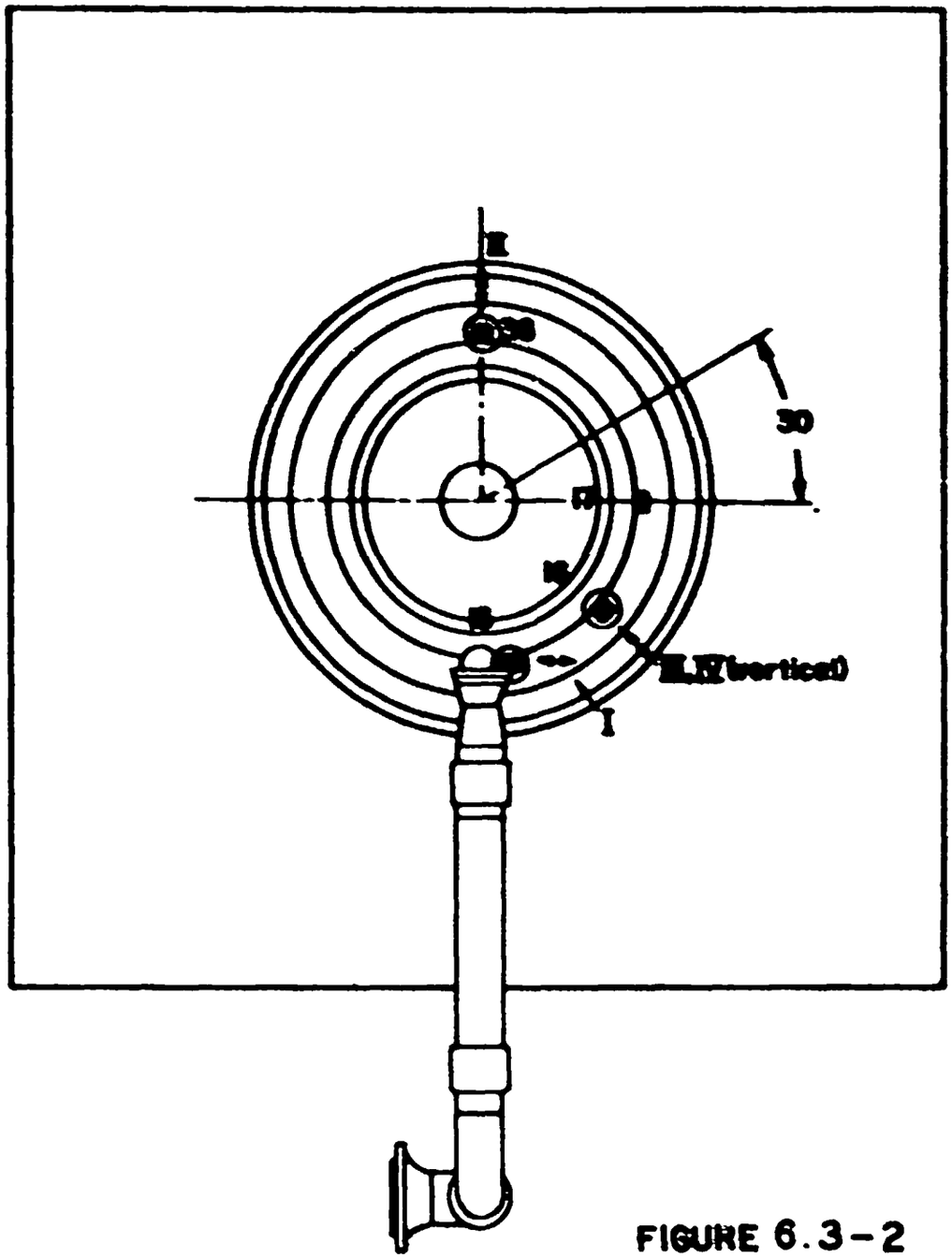

FIGURE 6.3-2
NRX-A2 VIBRATION TEST
EXCITATION POINT AND
ACCELEROMETER LOCATIONS
PLAN VIEW

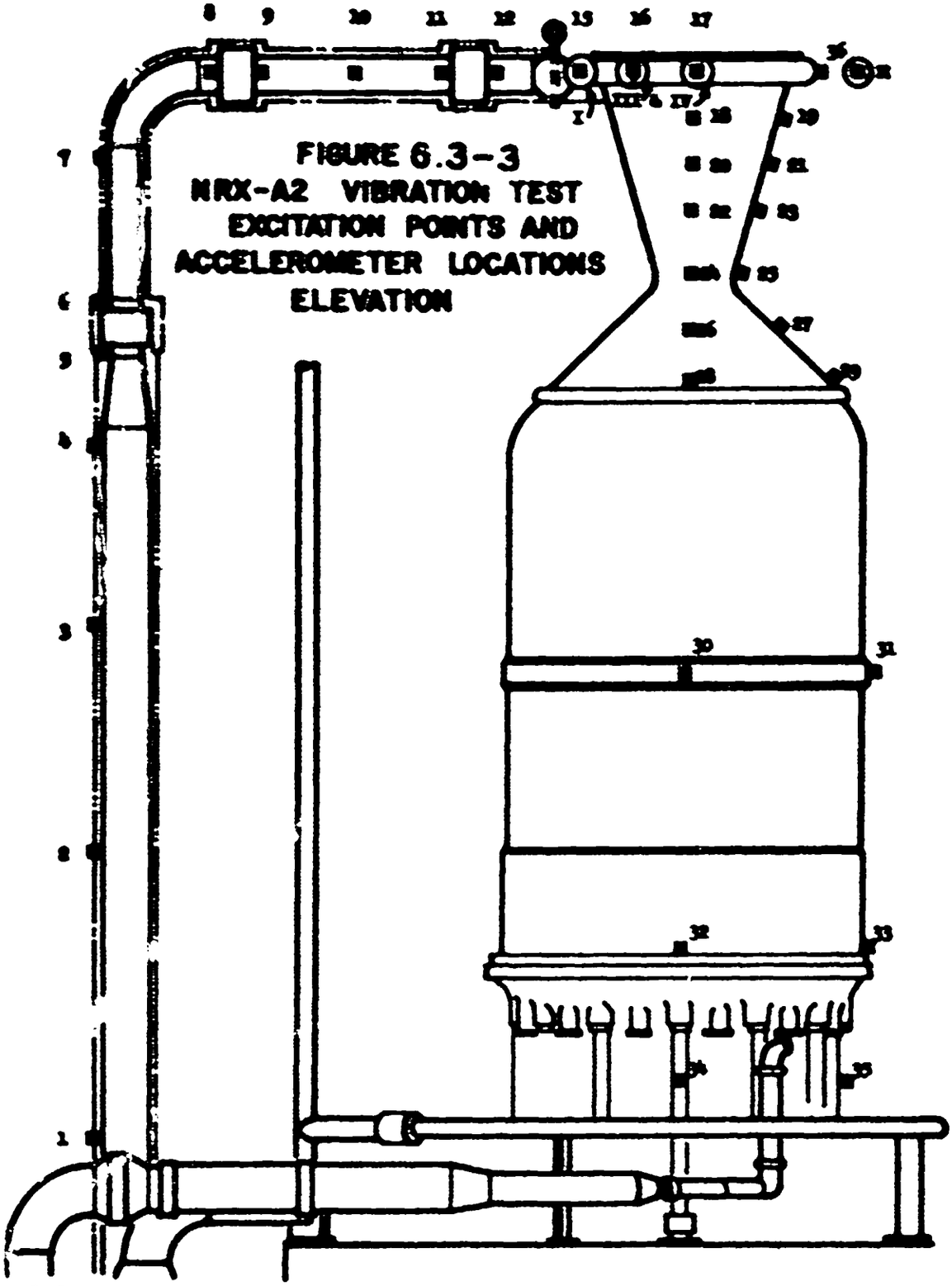

FIGURE 6.3-3
NRX-A2 VIBRATION TEST
EXCITATION POINTS AND
ACCELEROMETER LOCATIONS
ELEVATION

The tests were performed by setting the force input at a constant level, selected to give good readings on the accelerometers, and then sweeping from 1500 to 15 cps. Discrete frequency runs were made following each sweep at the most significant resonant frequencies detected. In completing the tests, the maximum output of the exciter never exceeded 50 lbs, nor did the accelerometers give readings in excess of 5 G's or 0.125-inch single peak displacement.

The tests indicated that the most significant resonance to be 239 cps. Center frequencies of other resonances were 171, 245, 319, 1350, and 1478 cps. The 239 cps resonance involved motion in the four quarters of the nozzle, with longitudinal mode lines at the propellant line-nozzle torus junction downward to the nozzle throat and at 90°, 180°, and 270° from this position. This mode had a magnification factor of 72, which is relatively high for mechanical systems. This mode was easily detected by touch when dwelling at this frequency. Since the 239 cps frequency was so predominant, the other frequencies were not explored in as much detail.

These test results were confirmed by the analysis of spectrum data of the NRX-A1 EP-IB, GH_2 run. This NRX-A1 run showed the 239 cps frequency to be a strongly excited mode under gas flow excitation. After critical analysis* of all the data it was concluded that gas flow excited vibration at 239 cps would not be harmful to the nozzle during the duration of the NRX-A2 run.

---

*G. T. Bove, NRX-A2 Vibration Survey, EHL-55, WANL-TME-979, September, 1964 - CRD.